FEASIBILITY STUDY FINAL REPORT

GEODETIC ORBITAL PHOTOGRAPHIC SATELLITE SYSTEM

VOLUME 4 DATA PROCESSING, PART 2

JUNE 1966

Notice of Missing Page(s)

Pages ii, iv, xiv, xvi, xviii, 4-14, 4-16, 4-18, 4-22, 4-38, 4-48, 4-58, 4-64, and 4-224 of the original document were blank and unnumbered.

SECRET [redacted]

[redacted]
Copy No. [redacted]

FEASIBILITY STUDY FINAL REPORT

GEODETIC ORBITAL PHOTOGRAPHIC SATELLITE SYSTEM

VOLUME 4 DATA PROCESSING, PART 2

JUNE 1966

Itek

ITEK CORPORATION LEXINGTON 73, MASS[redacted]ETTS

[redacted]
AF4 1
Vol 4
Cy [redacted]

SECRET [redacted]

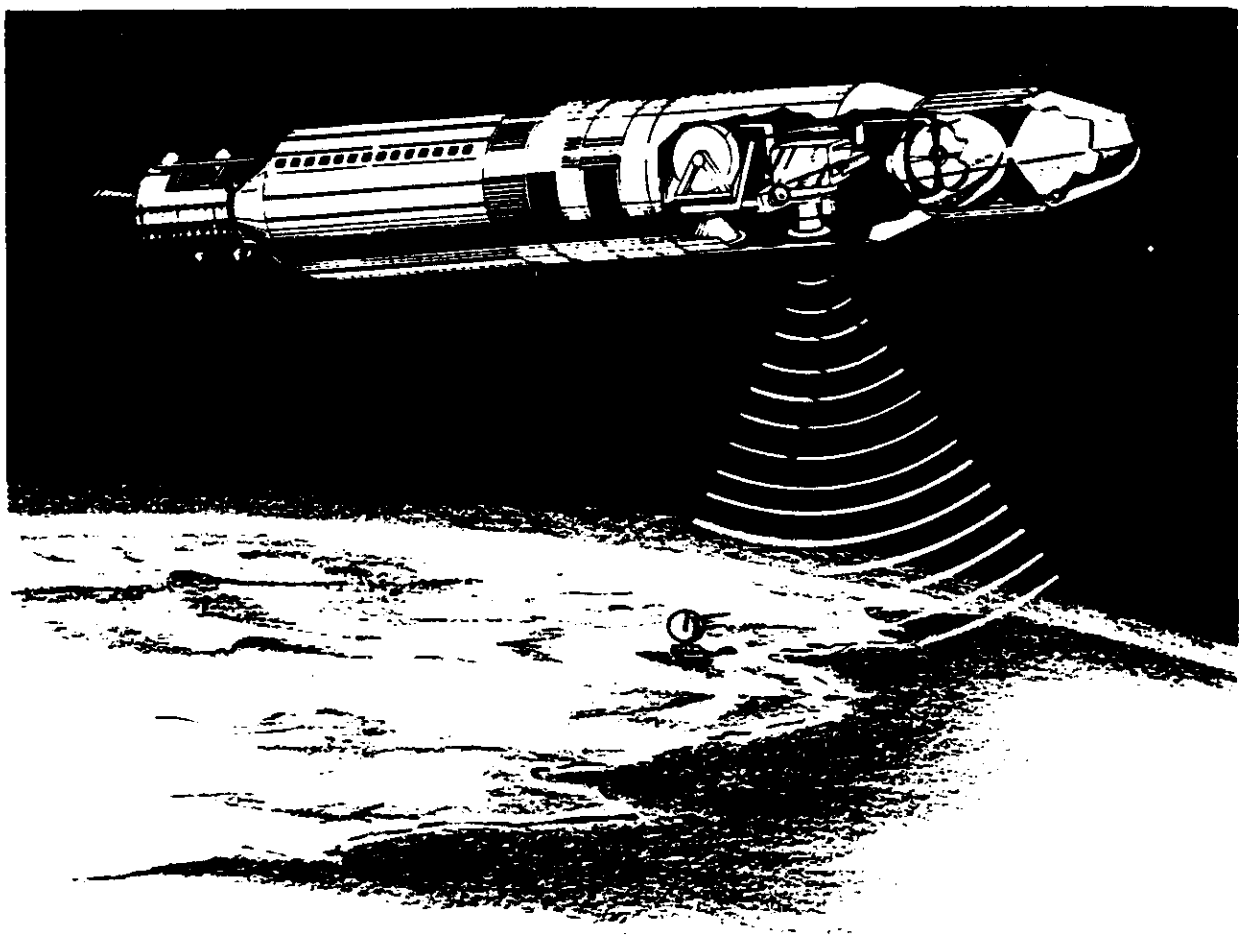

Geodetic Orbital Photographic Satellite System

CONTENTS

FIGURES

Page

Page

Page

TABLES

PREFACE

The objective of the Geodetic Orbital Photographic Satellite System (GOPSS) is to accurately determine the location of landmarks widely distributed over the earth's surface and provide better information concerning the geophysical parameters which affect this system and other systems operating at similar altitudes. The means chosen to accomplish this objective is to orbit a series of data acquisition systems supported by ground-based instrumentation. The data gathered by this system is incorporated into a sophisticated data reduction scheme which determines the geodynamic parameters and landmark locations.

Detailed studies were conducted to determine the feasibility of the GOPSS. The study period was designated as Phase I, and the results of these studies have been compiled into five volumes for reader convenience.

This volume discusses orbital considerations affecting the feasibility of the GOPSS. Physical models and computational procedures are reviewed and error studies involving typical sensor and model inaccuracies are described. Based on these studies, recommendations are made for tracking networks, auxiliary on-board sensors, and detailed orbit plans. In addition, the data reduction procedure, whereby the acquired data are simultaneously located to yield geodynamic parameters and landmark locations, is considered.

The division of the remaining volumes and their content are now briefly described for information and reference purposes.

Volume 1, Program Compendium and Conclusions, was prepared to provide briefly the details essential to a comprehensive understanding of the effort conducted during Phase I of the GOPSS feasibility study. System concept and objectives are described plus conclusions which concern the attainment or modification of the initial objectives, along with recommendations for a system configuration and a solution of the attendant data handling problems.

Volume 2, Data Collection Systems, describes the effort for implementation of the data acquisition requirements for the GOPSS program. This volume presents the preliminary design which defines and describes the various sensors, considers their functional interdependencies, and shows their evolvement into an integrated GOPSS.

Volume 3, Data Processing, Part 1, considers the photogrammetric data subject to constraints imposed by orbital and auxiliary data, and the mapping capabilities of the system, and ground handling of mission photography.

Volume 5, Phase II-V Program Plan, describes the planning activity as it has been programmed through Phases II to V for the engineering, fabrication and operational support for the delivery of five systems. Continuing studies which are required are also defined in this volume.

SUMMARY

Orbital considerations affecting the feasibility of accomplishing the objectives of the Geodetic Orbiting Photographic Satellite System (GOPSS) have been investigated. The goals of the GOPSS program are found to be realistic and the accomplishment of these goals is within the capabilities of present orbital positioning techniques.

The objectives of the GOPSS have been listed and the approaches taken to investigate these objectives are discussed. The physical models and computational procedures needed to calculate accurate orbital positions and reduce the data are reviewed. The applications of auxiliary sensors or concepts such as accelerometers, zero-g satellites, and passive attitude control systems are investigated.

A number of parametric orbital position covariance and ephemeris-differencing calculations for various uncertainties in observational quantities and model quantities have been performed and are reported. Limitations in the available computer program prevented complete analyses; however, a sufficient number of calculations were performed to substantiate the conclusions. The results of these calculations are discussed. Orbit planning for orbits to accomplish the objectives of the GOPSS is presented. Based on the previous discussions, conclusions are drawn and recommendations are made. Recommendations are made for a tracking network consisting of the TRANSIT and photogrammetric data, and the inclusion of on-board accelerometers. Data reduction is discussed, and recommendations for a final data reduction scheme are included.

4.1 INTRODUCTION

4.1.1 General

The mission of the Geodetic Orbiting Photographic Satellite System (GOPSS) is to locate landmarks over the earth's surface to high accuracies from data collected by an orbiting vehicle and the simultaneous accurate evaluation of the geodynamic parameters which influence the motion of the orbiting vehicle. The principal data gathering system for landmark location is photogrammetric, and consists of a set of cameras, one to photograph the earth's surface and two stellar cameras to define orientations. Orbit position is defined by typical tracking networks, reenforced by selective photogrammetric data. Accurate time in orbit is recorded and auxilary on-board sensors will be employed.

The GOPSS program can be treated as two independent calculating schemes. The first is the utilization of tracking data as the prime input to determine the orbit; the second is the use of this orbit to position the camera stations from which the location of ground points is obtained. In this positioning task, the camera is considered as the prime sensor, so that the production of a landmark catalog is approached as if it were a photogrammetric problem alone.

An approach which treats each of the data types according to independent data reduction schemes, could result in complications, since functional relationships exist between the various types of data, despite the fact that they are independently acquired. For example, ground tracking data are most suited for the determination of orbital parameters, yet these parameters can be weakly determined from the photogrammetric solution. The independent reduction of ground tracking data and the photographic records is theoretically unsound, since these two sets should be consistent with each other through the common factors, namely, the orbital parameters. An integrated approach involving the collective reduction of all observational data is therefore to be desired. However, investigating the feasibility of the GOPSS concept using such an integrated treatment requires the complete data reduction scheme that will be necessary to finally reduce the data from the GOPSS. This data reduction program is not completely available at this time and it is apparent that only partially integrated analyses can be performed in this study. If, by proceeding with partially separated calculating schemes, such as mentioned above, we conclude that meeting the specification is feasible, then the final data reduction involving complete integration would more strongly reenforce this conclusion. The following analyses are based on such an approach.

4.1.2 Orbital Analyses

This volume deals with the considerations, particularly in the field of orbital analysis, associated with accomplishing the objectives of the GOPSS program. These objectives and our approach to the necessary orbital analyses are discussed in Section 4.2 of this volume. Succeeding sections discuss: (1) the state of knowledge of forces acting on the satellite which are important

in accomplishing the orbital analyses (Section 4.3), (2) data processing and computational techniques (Section 4.4), (3) a few selected possible auxiliary techniques and instrumentations required to better define or remove uncertainties in the force models (Section 4.5, 4.6, and 4.7), (4) computations and the results of computations made to investigate the feasibility of the program objectives (Sections 4.8 and 4.9), and (5) orbit planning for the GOPSS mission (Section 4.10). Finally, Section 4.11 contains a summary of the preceding sections, conclusions drawn from them and recommendations for accomplishing the GOPSS program objectives as well as for further analyses.

In addition, several conceptual questions are partially or completely considered in the following sections. Some of these questions involve, for example, such considerations as:

1. To what extent can the objectives of the GOPSS be satisfied without recourse to subsidiary data-taking systems or previous measurements, (except, perhaps, for the initial phases) in an iterative "bootstrapping" process?

2. Data reduction concepts: What are the relative values or merits in considering analyses for specialized purposed utilizing very short orbital arcs (i.e., of the order of 1000 miles or less), short arcs (of the order of 4 revolutions), long arcs (up to 7 to 15 days) and very long arcs (greater than 15 days)? To what extent should orbital determination and landmark determination be integrated? Are there advantages to considering orbital determination as partially independent, that is, as only a fixed constraint on the photogrammetry, if auxiliary sensors can accurately define the orbit?

3. Which of the many alternative choices are recommended as efficient, economical, and accurate computational procedures for the required data reductions?

These questions are partially discussed in Sections 4.9 and 4.11.

Section D

ORBIT ANALYSIS

4.2 APPROACH TO ORBITAL ANALYSIS

4.2.1 Objectives

The objectives of the orbital analysis conducted for this feasibility study are:

1. Satellite Positioning. To determine the feasibility of determining satellite orbital positions for the proposed satellite and satellite orbits to accuracies consistent with the landmark location specifications (200 feet horizontally and 40 feet in elevation), using realistically attainable data obtained during the period of observation comprising the mission-flight time.

2. Tests of Calculational Techniques and Adequacy of Physical Models Using 6-Hour Orbit Position Prediction Test Criterion. To determine the adequacy of calculational techniques and physical models using as a test criterion the prediction of satellite orbital positions for the proposed satellite and satellite orbits. The positions are to be determined to within accuracies consistent with landmark location specifications for a period of up to 6 hours after the cessation of the recording of observations following an extended period of observations using realistically obtainable data.

3. Evaluation of Geodynamic Parameters. To determine the feasibility of evaluating the geodynamic parameters of the earth (including the undulation of the geoid) that are used in the various physical models used in the above orbital calculations to within accuracies consistent with the required accuracies of the orbital calculations. These geodynamic parameters are to be determined from realistically attainable observational data.

4. Datum Ties and Station Locations. To determine the feasibility of improving datum ties and the location of specific stations on the ground to within specified accuracies.

5. Input Data Requirements. To determine the types, geographical distributions, density, and accuracies of the observations required to provide the minimum input to the above calculations necessary to make feasible the calculations to the desired accuracies.

6. Evaluate Physical Models and Computational Techniques. To investiage the adequacy of the available physical models and computational technqiues to accomplish the above objectives.

7. Recommended Sensor Configuration. To recommend additional sensors or instrumentation and model and/or computational program development as needed to accomplish the above objectives.

8. Prepare an Optimized Orbit Plan. To produce a set of optimized orbit plans for the proposed five satellites to optimize the mission objectives.

4.2.2 General Approach

4.2.2.1 Introduction and Comments

The general approach to investigating the feasibility of attaining the objectives cited above is to conduct parametric investigations for each of the cited objectives. Calculations of the pertinent residuals or variances of the orbital coordinates are made for an input range which brackets the expected parametric variations. These calculations are performed using the Aerospace TRACE A and D programs which are typical of one type of highly flexible and refined orbital calculational program.

The adequacy of any proposed calculational framework to reflect all of the pertinent physical phenomena of importance into an orbital position prediction scheme can be evaluated only a posteriori, by comparisons of the predictions made with such a model with observational data. The adjustments of the coefficients or other variable parameters of the model to give a best computed fit to observational data, and the techniques for improving the accuracy and reducing the computational time to achieve such best fitting, are subjects for research in numerical analysis. Ultimately, however, the adequacy of any model is judged on the basis of the magnitude of the residuals in the "computed minus observed" sense for comparisons between computed predictions and observations taken during the prediction period but not used to evaluate model or orbit parameters.

The computation of residuals requires that actual observational data be available with which computed results can be compared. When such data are available, the calculation of residuals as discussed above is to be preferred. In the absence of such data, however, and for system planning purposes, it is desirable that statistical error analyses (covariance analyses) be performed as aids aids in determining the effect of system changes or proposed modifications and errors in the system parameters. Caution must be exercised in interpreting the results of such analyses, however, inasmuch as the usual assumptions of statistical independence and randomness of errors must be invoked and, even more important, assumptions must be made for the physical models and parameters to be employed in the analyses. Thus, for example, the extent of the ill-conditioning of data for various global configurations of observational data sensors can be fairly well treated by covariance analyses, but no conclusions on the validity of the models or physical assumptions can be drawn.

Another useful analytical technique involves the differencing of orbital ephemerides for variations in orbital models or observational parameters. Such differencing techniques are useful in evaluating the degree to which off-nominal variations affect calculated orbital positions. They also lend to valuable insights into physical model effects, and the effects of biases in station locations or observational parameters. Some of these effects are further discussed in Section 4.9. Root-mean-square values of the difference between ephemerides evaluated for the entire mission period should be used for model evolution. This type of calculation is sometimes called "Monte Carlo" by analogy, since statistics on the variation in nominal orbital positions can be accumulated by repeating the ephemeris differencing process for random combinations of variations in the tested parameters.

In assessing models it is therefore necessary to rely upon the observational data taken for orbiting vehicles and on the experience of groups of investigators who have attempted to reduce the residuals from such observations. Most of such attempts have been made for satellites orbiting at altitudes of 500 miles or more, where the effects of air drag and orbit perturbations due to high degree terms in the spherical harmonic expansion of the geopotential are smaller than at the altitudes of interest here (e.g., the results of the Smithsonian Astrophysical Observatory and Kaula at NASA on Baker-Nunn data analysis for Anna, Echo, etc., and especially the

work of Johns Hopkins University Applied Physics Laboratory and Naval Weapons Laboratory on the TRANSIT satellites). Some data have been taken for orbiting vehicles in essentially circular orbits at lower altitudes of the order of 150 miles, but this data was reduced using a truncated spherical harmonic model (e.g., the joint Aerospace-Aeronutronics effort using the TRACE 44 program).

An analysis of the errors due to "observational" contributions for the TRANSIT satellites is given by Newton, Guier, and Weiffenbach.[1*] A distinction is drawn between "observational" errors which contain all of the factors affecting the quantity and quality of the raw data fed into the analytic program and "analytical" contributions. The postional errors due to observational contributions are found to be less than 5 meters for colocated satellite passes. "Analytical" contributions are defined as including phenomena which would affect the analytic results but which are not included in the analysis. Included in this group are such effects as neglected gravity components in the estimates of the gravity field, improperly treated air-drag phenomena, and undocumented vehicle originating forces. It was asserted in this report that the neglected components of the gravity field gave rise to the largest "analytic" errors at the TRANSIT satellite altitudes, and that this situation could be remedied by obtaining and treating more observational data.

The results of past analyses have indicated that, with a reasonable geographical distribution of data stations, satellite orbits with low eccentricity and altitudes of 500 miles or higher may be fitted by calculated orbits with residuals of 50 meters or less along-track using a model incorporating zonal harmonics out to about J_{10}, nonzonal harmonics out to J_{88}, and selected resonance terms of higher degrees. The continued activity in these areas together with the extension and elaboration of the existing models and computational programs, and consideration of the much increased coverage and distribution of data from the photographic systems and auxiliary onboard sensors aboard the GOPSS, tend to give confidence that expanded spherical harmonic expansion models utilizing a sufficient number of resonance coefficients will be adequate to produce the desired residuals, even at the reduced altitudes, if the perturbations due to nongravitational effects can be accurately predicted or measured.

It appears that, of the nongravitional perturbations, air drag and vehicle originating forces may have sufficient uncertainties associated with them for the present satellite and satellite orbit as to suggest the desirability of the inclusion of at least a one-axis along-track accelerometer.

4.2.2.2 Discussion of Approaches

4.2.2.2.1 Satellite Positioning

Orbital computations are usually accomplished by using physical models for the forces acting on the satellite to establish its equations of motion. By comparison with observation, parameters in the model are adjusted so as to obtain a "best fit," usually through a least squares procedure that minimizes residuals. The solutions so obtained are iterated until no further reduction in residuals is obtained. Positioning capabilities are thus investigated by an examination of the residuals resulting from the orbital calculations for a proposed physical model, using orbital

*References are listed in Section 4.2.5.

position observational data obtained from as many sensors as possible for as many different satellites and orbits as possible over as long a period of orbiting as possible. As discussed in Section 4.2.2.1 the accuracy of the orbital position may be tested by computing residuals for observations which have not been used in the least-squares procedure. Additional tests may be performed by ephemeris differencing orbits computed for physical models which differ slightly from one another, within the bounds of knowledge of physical model behavior (Monte Carlo technique).

Thus positioning can only be investigated by utilizing real data for actual flights, since the calculation of "residuals" and model coefficients requires actual observational data. Very few data of sufficient accuracy and proper distribution were available for the observational networks and satellite altitudes of interest here. An example using the available data for a low altitude satellite observed by the SCF network was investigated, as is discussed in Section 4.8. However, by noting the growth of variances for a complete range of simulated input orbital parameters and simulated data, the adequacy of the calculational procedure (not the physical models, or the data processing procedures) and the adequacy of the observational network to satisfy this objective for a given physical model were considered. The capabilities of the computer program to accomplish these calculations is described in Section 4.2.3 and also in the next section. Typical results of satellite position calculations are discussed in Sections 4.8 and 4.9.

4.2.2.2.2 Six-Hour Orbit Position Prediction Test Criterion

The ability to predict orbital position into the future accurately, using observations made in the past, is considered to be a sensitive test of the adequacy of the physical models and calculational procedures used to define the orbit.

The orbital prediction feasibility was investigated by performing the computations described in Section 4.2.2.1, but continuing the orbital computations beyond some termination time for inserting observational data. The "predicted" orbit was then compared either with observational data taken during this prediction period time (but not included in the orbit calculation) to obtain residuals, or the orbital position covariance matrix was computed from an error analysis. The first method was preferred when data were available. Ephemeris differencing calculations were made for several cases (Monte Carol techniques) for small changes in input model parameters.

In the absence of real observational data, simulated observational data were used. The Aerospace Corporation TRACE program contains the provision for computing simulated data for almost any type of sensor (see Section 4.2.3 and 4.2.4). For a given set of physical model parameters, initial orbit conditions, sensor locations and sensor characteristics, the program will compute simulated data for any period of orbiting. The model parameters to be used are taken from the best values available in the literature and from previous experience, initial conditions are estimated for each parametric orbit to be investigated, and sensor locations and characteristics are taken from survey measurements and manufacturers' data and quotations.

The error analysis section of the TRACE program has provision for computing covariance matrices for orbital position (i.e., for estimating the potential accuracy attainable for a given set of physical models and observational network) given the observational station locations, data type, rates and quality uncertainties in the model parameters, station locations, and the specifications of the nominal orbit (see Section 4.2.3). In addition, an estimate of the potential accuracy attainable in solving for station locations (given the uncertainties in other quantities) or several other parameters is available.

The prediction "feasibility" is then investigated by considering the accuracies required in observational data, station locations, etc. for a given set of orbital initial conditions and observation network using covariance matrices for the simulated observational data, covariance matrices for the station locations, biases, etc. The calculational program computes the covariance matrix for the initial conditions for the orbit fitted to the observational data. This covariance matrix is then updated for later times, assuming any desired period for data taking. This allows prediction to be made after any prescribed period of observations.

The results for one example of this type of calculation are shown in the figure on the following page. Simulated data were computed for the seven station SGLS radar net for one day of orbiting in a circular polar orbit at about 150 nautical miles. Standard deviations of 60 feet in range, 0.05 degree in angle, and 0.1 foot per second in range rate were assigned for all of the observations. Data were accumulated out to t = 1440 minutes and the covariance matrix for the initial conditions for the best fitted orbit was computed at t = 0. This matrix was then updated as a function of time so as to give the covariance matrix for orbital position as a function of time. In Figure 4-6, in-track standard deviations are also shown for the case where the station coordinates are assumed to be uncertain by 100 feet in the horizontal directions. This curve indicates the importance of having accurately known reference points from which to make observations or, more realistically, illustrates the need for solving for station locations in the final data reduction program for orbital positions and landmark locations. It also shows the typical reduction in variance toward the center of the data-taking period and the rapid growth of the variance during the "prediction" period following the taking of observational data. In this case, the "prediction" period was for 6 hours following one full day of observation. Other calculations are discussed in Sections 4.8 and 4.9.

4.2.2.2.3 Evaluation of Geodynamic Parameters

The determination of geodynamic parameters from observational data is usually accomplished in the course of minimizing the residuals in a differential orbit improvement program. The parameters enter the calculation through the physical models and therefore the comments made dealing with the determination of the adequacy of physical models, also apply here. When the residuals are minimized, then the geodynamic parameters which have entered into this calculation, will also be determined as accurately as the adequacy of the physical model and the observational data allow.

It should be pointed out that there are strong correlations among some of the coefficients describing the geodynamic parameters, especially among coefficients in the spherical harmonic expansion for the gravity potential themselves and among some of these coefficients and air-drag coefficients (if only short observational arcs are used). Much of this correlation can be removed by having observational data for as long as possible from satellites in orbits with appreciably different inclinations. At least four of such inclinations are required, at a minimum, to separate out the various terms from an expansion extending up to J_{88}, and the determination of the zonal harmonics will require even more.

The zonal harmonics of the earth's gravitational field produce a fundamentally different effect on the orbit of a close satellite than do the tesseral or sectoral harmonics. The even-degree zonals produce secular variations in ω, Ω, and M, while the odd-degree zonals produce extremely long-period periodic variations in all elements except the semimajor axis. These long-period variations, completing one cycle in approximately 100 days, would hardly be separable from secular variations during the expected lifetime of 15 days. Therefore, the zonal harmonics

which are best determined from observations over a period of several months, should not be parametrized in this solution. Instead, the very best available values for the zonal harmonic coefficients should be imposed upon the solution.

Many critical selected geodynamic parameters will be best determinable from the data collected in this program. For the few remaining parameters, notably the zonal harmonics, the best adjusted values will be taken from the results of other programs. In particular, some of the resonance coefficients and air-drag coefficients which are peculiar to the altitudes being used here should be better defined by this program, as well as some of the higher harmonic terms in the gravity potential, (see Section 4.3.1). Aliasing considerations make difficult the extrapolation of gravity potential coefficients determined at low altitudes to higher altitude orbits. On the other hand, although the low altitude use of such coefficients determined from high altitude data is more valid, the accuracy of determination of high frequency (high degree) terms is reduced at the higher altitudes. In the course of this investigation data has been compiled which could be used to determine the sensitivity of gravitational harmonic coefficient determination to orbital inclinations.

By using the error analysis feature of the TRACE A program, the covariance matrix for any of the coefficients in the TRACE A physical gravity model may be investigated. These include zonal harmonics out to J_5 and tesserals out to J_{44}. The effect of uncertainties in simulated observational data computed with the full TRACE D model, which includes zonals to J_9 and tesserals to J_{66} or uncertainties in any of a number of other parameters in the covariance matrix for the TRACE A gravity coefficients, may be computed. Conversely, the effect of an uncertainty in a gravity model parameter on orbital position uncertainty, can be computed, and tolerances on the allowable uncertainties in these parameters established. By combining both of these types of calculations we may determine the adequacy of any given observational network for the determination of the geodynamic parameters up to at least J_{44}.

Unfortunately, practical numerical difficulties involving the propagation of roundoff errors preclude a complete analysis made in this fashion. It was found, experimentally, that due to these numerical roundoff errors, many of the calculations of uncertainty in orbit postion for uncertainties in gravity model parameters were not well behaved, as was also the case for the calculations of uncertainties in gravity model parameter determination due to uncertainty in the observational data. Some results on the effect of variations in geodynamic parameters on orbital position have been obtained by ephemeris differencing (Monte Carlo) of orbits calculated using different values for the geodynamic parameters. These calculations are reported and discussed in Sections 4.8 and 4.9.

4.2.2.2.4 Datum Ties and Station Location

The evaluation of the accuracy of landmark location must, of course, take into account the interaction and overlap between orbital and photogrammetric analyses. In one extreme case, when the orbit is well defined by observations taken by auxiliary sensors, it can be used as a fixed constraint on the photogrammetry. In the other extreme, when the photogrammetric control is very strong, the photogrammetric measurement can be used to adjust the orbit. In the intermediate situation an integrated analysis of orbital parameters and landmark locations must be used. In particular, when extensive photographic redundancy from a given satellite mission or other satellite missions (especially at other inclinations) is present, both orbit determination and landmark location are considerably strengthened by an integrated, or at least partially integrated analysis. This subject is discussed elsewhere in these reports (see Volume 3 which deals with both the photogrammetric analyses and the data reduction concepts).

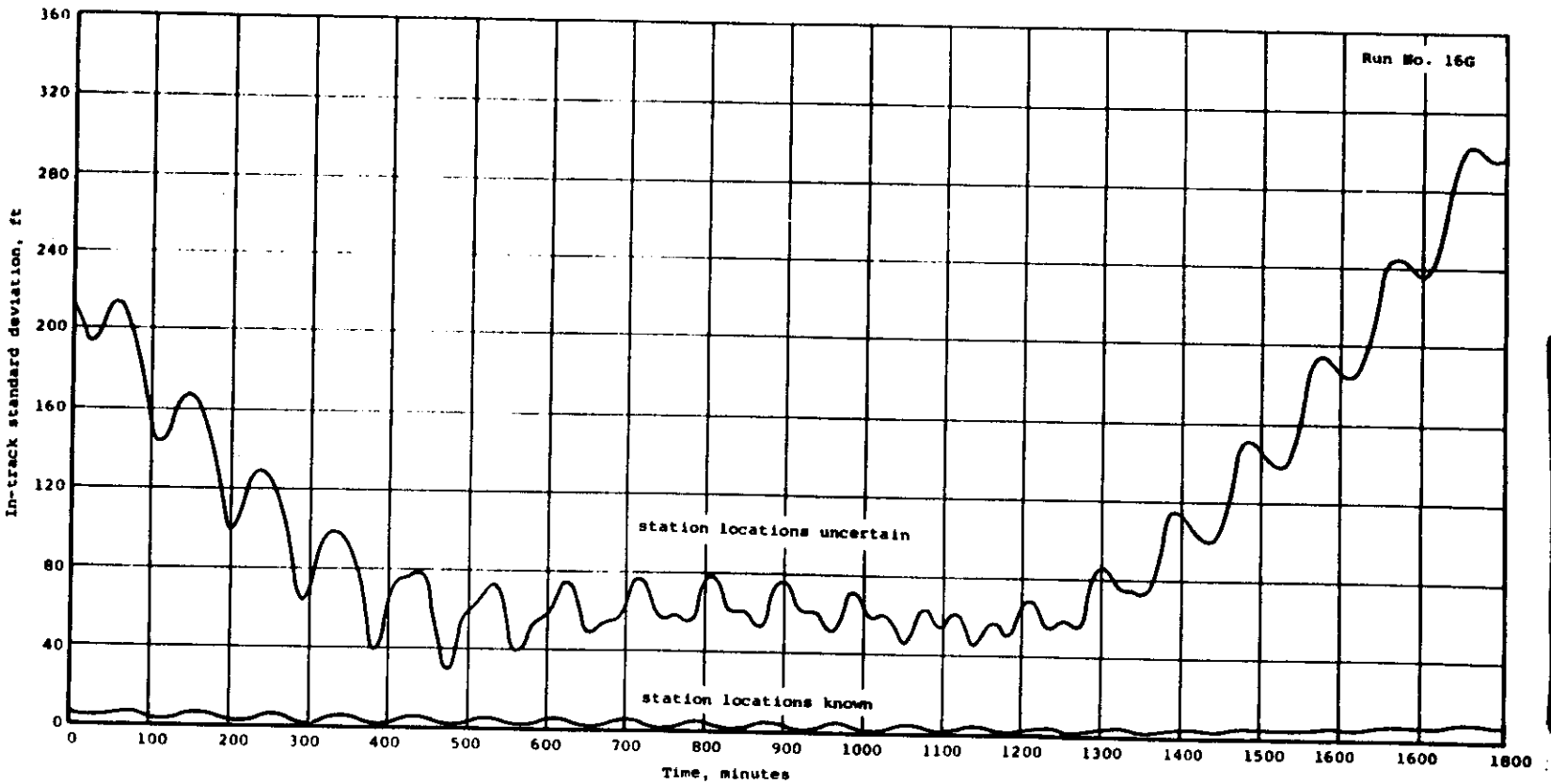

Plot of standard deviation of radial component of orbit position error versus time for a 1-day fit to SGLS network radar observations, showing effect of 100-foot horizontal error in station locations. (This plot, shown here for reader convenience, is presented as Figure 4-6 in Section 4.8.1.)

For the purposes of this feasibility study, however, the assumption has been made that it is possible to separate photogrammetric orbital position measurements from the orbital analysis itself. The photogrammetric orbital observations over regions of strong geodetic control are treated as if they were derived from an auxiliary sensor providing independent orbital position information (see Section 4.2.4). This assumption was justified, a posteriori, by finding that the orbit determination was little affected by the photogrammetric data.

Thus, feasibility of determining certain landmarks on the ground to within the accuracies required must be discussed considering the photogrammetric analyses and data analyses covered elsewhere in these reports. However, one aspect of these analyses was done using the error analysis capability of the TRACE program. This involved the calculation of the covariance matrices for station locations (for example, datum locations and the location of auxiliary sensor stations) for simulated observational data using as input uncertainties in the observational data, physical model parameters and biases on the data. The results of these computer runs are discussed in Section 4.8 and 4.9.

4.2.2.2.5 Input Data Requirements

The amounts, types, distributions, and accuracies of observational data necessary to provide sufficient input to make feasible the above objectives was determined in conjunction with investigating the accomplishment of those objectives. The results of these calculations are discussed in Sections 4.8 and 4.9.

4.2.2.2.6 Physical Models and Computational Techniques

As previously discussed, the adequacy of available or projected physical models can only be determined from actual observational data taken for orbiting satellites. A review of these models is given in Section 4.3. A discussion of the various available computational techniques for orbital analysis and of their relative advantages is provided in Section 4.4.

4.2.2.2.7 Recommended Auxiliary Sensors and Other Requirements

The recommendations of additional sensors, instrumentation, and model and/or computational techniques development are partially contingent upon the investigations mentioned above and follow directly from them. For example, it appears from the investigation of uncertainties in air-drag models and in vehicle-originating forces that it will be highly desirable to incorporate at least an in-track accelerometer aboard the satellite. These recommendations are presented in Section 4.11.

4.2.2.2.8 Orbit Planning

The approach to the recommendation of a set of orbit flight plans must be to parametrically investigate the factors affecting the mission objectives as these factors are influenced by orbital parameters, including launch and recovery requirements, and to produce a set of weighted recommendations based upon the possible conflicting results of these investigations. Section 4.10 contains an elaboration of these considerations as well as several detailed orbit plans.

4.2.3 Description of the TRACE Programs

TRACE is an IBM 7090 computer program developed by Aerospace Corporation for use in satellite orbit determination and tracking system analysis and design. This program was

generously made available to Itek/Vidya for the current project, and the bulk of the calculations reported below were done with TRACE. A brief description of the TRACE program is presented here. This material has been excerpted from references 2 and 3 (see Section 4.2.5), to which the reader is referred for a thorough treatment of the details.

The applications of TRACE include the following:

1. Simple trajectory and ground trace generation.
2. The calculation of visibility times and simulated observation data.
3. The determination of trajectory and model parameters from observations.
4. An accuracy analysis of a satellite tracking and orbit determination system.

Basic to all applications of TRACE is the satellite trajectory. The trajectory is defined by a set of initial conditions together with the differential equations of motion whose coefficients and parameter values reflect the earth's gravitational and atmospheric forces and those of other bodies affecting the satellite's motion. The trajectory is calculated by numerically integrating the differential equations of motion.

The generation of observation data for a given trajectory is basic to the orbit fitting function of the program. TRACE can handle a wide variety of types of observational data including conventional radar, photo-optical, and interferometer and Doppler tracking data, photogrammetric data of the resection type (by referring observations to an earth-centered X, Y, Z system) and relative intersection or so-called "Q" data, altimeter data, and others. In addition, TRACE can calculate satellite visibility times, given the location and characteristics of the observing station.

TRACE estimates, in the least-squares sense, the trajectory that best fits a set of observations. The trajectory of a space vehicle depends upon the initial conditions of the motion and the differential equation parameters which appear in the equations of motion. From a trajectory one may compute at the observation times the expected values of the observations. These expected values depend also on the locations of the observing stations and biases in the observations. The problem of orbit determination is to solve for the set of parameters that minimizes the differences between the computed and measured observations. TRACE is able to solve for such quantities as the ballistic coefficient (a differential equation parameter) of the vehicle, the location of an observing station, the presence of bias in data from a particular station, in addition to the usual set of initial condition parameters.

The method employed for orbit determination in TRACE is the iterative process of differential orbit improvement. A first guess must be provided for each of the parameters being solved for. A trajectory is generated based on this first guess, and the "computed observations" are calculated along with their partial derivatives with respect to the parameters. The normal matrix of partial derivatives is accumulated, and "residuals" are formed by taking the difference between measured and computed observations. The residuals are multiplied by a weighting factor, and the sum of the squares of weighted residuals is accumulated for all of the observations. A correction to the first guess of the set of parameters is computed by inverting the normal matrix, and when this correction has been applied the whole process is repeated. The root mean square of the weighted residuals provides the measure of convergence of the process.

The accuracy analysis aspects of the TRACE program are based on the fact that under certain conditions the inverse of the weighted normal matrix is the variance-covariance matrix of the solution parameters. These conditions are that the observational model is correct, that the

observational errors are independently distributed with mean zero and variance σ^2, and that the weighting factor used is σ^{-1}. With the assumption that these conditions apply, the solution process provides an estimate of the uncertainties in the solution parameters. Insofar as these parameters are differential equation or station or observation parameters, their variances and covariances satisfactorily describe their uncertainties. However, the uncertainties in the motion of the vehicle are not adequately described by the variances and covariances of the inital conditions and other parameters of the trajectory. TRACE has the capability of reporting trajectory uncertainties in several coordinate systems, probably the most useful of which is the orbit plane coordinate system (in-track, cross-track, and radial position and velocity).

A further sophistication arises from the assumption that the value of some of the parameters used in the calculations, but not being estimated by the differential correction process, are also uncertain, thereby inducing uncertainties in the differentially corrected parameters and in the trajectory. (This is a very common situation; most tracking programs do not solve for basic constants and station locations, but their current values must be somewhat uncertain.) Such parameters are referred to as "Q-parameters" in distinction to "P-parameters," which are those being solved for in the differential correction. TRACE will simultaneously report P-parameter and trajectory uncertainties with and without the Q-parameter effects.

4.2.4 Observational Data Sensors and Networks

In the computations that were performed in studying the feasibility of the proposed system, several types of observational data were considered. This section describes the networks of observation sites, lists the assumptions with regard to accuracy and distribution of the data, and discusses the generation of fictitious observational data for simulation purposes.

The SGLS radar network was used. This network is an improved and expanded version of the present Satellite Control Facility (SCF) network, and it is planned that this will be the operational radar tracking and control network at the time that the proposed system will be operating. Locations of SGLS stations assumed in the simulation calculations are given in Table 4-1.

For these stations, the observational data are range, azimuth, elevation and range rate. Standard deviations of the data are 60 feet in range, 0.05 degrees for both angles, and 0.1 feet per second for range rate. For the simulation, observational data were generated, using the data generation option of TRACE, every 30 seconds during the interval that the vehicle was at least 10 degrees above the horizon at each station.

The Navy's TRANSIT network was also used in the simulation. A network of sixteen stations was assumed, with sites as listed in Table 4-2. TRANSIT observations are Doppler frequency shift measurements. The standard deviation of these data, in terms of range rate, was assumed to be 0.5 feet per second. Using TRACE, data were generated for these stations at a rate of one observation per minute, with the restriction of 10 degrees minimum elevation. The areas of tracking coverage from this TRANSIT network are indicated by the shaded areas of the world map in Figure 4-1, for a circular polar orbit of 156.7-millimeter altitude.

The observations from an on-board radar altimeter were also considered. It was assumed that the main use of the altimeter would be over open water areas. Therefore, the data generated to simulate altimeter measurements were restricted to these areas. This restriction was approximately satisfied in using the TRACE program by approximating the outline of the large water areas of the world with a series of circular areas, as shown by the lightly shaded areas in the map of Figure 4-2 (the circles, originally developed on a globe, appear slightly distorted due

Table 4-1 [redacted]

Site	Latitude, degrees	Longitude, degrees
[redacted]	[redacted]	[redacted]

Table 4-2 — TRANSIT Network Sites

Site	Latitude, degrees	Longitude, degrees
Maryland	39.2	287.1
New Mexico	32.3	253.2
London	51.5	359.9
Sao Paulo	-23.6	313.4
Hawaii	19.5	204.5
Manilla	14.0	123.2
Australia	-34.9	138.5
Japan	40.7	141.3
Kodiak	61.3	210.2
Samoa	-14.3	189.3
Thule	76.5	291.4
South Africa	-25.8	28.2
Seychelle Islands	-5.0	55.0
McMurdo	-77.8	166.7
Ascension Islands	-8.0	345.6
Cocos Islands	-12.0	96.8

to the map projection). The simulated data were then generated in TRACE by using suitable minimum elevation angles for fictitious stations located at the centers of the circular areas, the elevation angle depending on the radius of the circle and the altitude of the satellite. The data rate for the altimeter measurements was taken as one observation every 2 minutes. A standard deviation of 50 feet was used.

A comment should be made about the discrepancy in the data rates that have been assumed for the simulation and the actual data rates possible with the sensors listed. The actual rates are much greater than those assumed. The assumed figures have been chosen to keep a balance between the relative weighting assigned to the different data types due to the quantity of observations. The assumed values also reflect the editing and data compaction procedures necessary to control the quality of the data and eliminate large noise effects. For orbit determination in the proposed system, the quality, distribution, and type of data are more signficant considerations than the quantity of data which is presently available from the sensors discussed above. The high redundancy of 2 data type tends to obscure the effectiveness of the data type in fitting an orbit due to the high correlation of errors of observations spaced closely in time. Hence, the assumed data rates were taken to be much smaller than the actual rates at which the sensors are capable of making observations.

Data from the primary sensor of the system was also simulated. Photogrammetric data of the resection type were handled by the TRACE program in the form of position coordinates in an earth-fixed Cartesian coordinate system. Two restrictions were imposed on the generation of photogrammetric data: (1) that observations be made only over land areas where geodetic control was already well established (excluding the Russian and Chinese domains, see Volume 3), and (2) that the area over which a photogrammetric observation was to be made must be illuminated with a sun elevation angle greater than 19 degrees. The first restriction was imposed in a manner similar to that used in restricting altimeter data to open water areas. The regions of good geodetic control were approximated by circular areas, as shown by the darkly shaded areas in Figure 4-2. Fictitious observation stations were associated with the centers of each circular area, and photogrammetric data (values of x, y, z) were generated whenever the satellite was within the "field of view" of this station. The field of view, or more specifically, the minimum elevation angle, for each station was computed from the radius of the circular area and the satellite altitude. The second restriction, solar illumination, was imposed by hand selection of the data cards generated by the TRACE program. A data rate of four observations per minute was chosen on the basis of the nominal orbit altitude of 160 nautical miles and triple overlap of the elongated format. A standard deviation of 30 feet in each direction was assumed, as a working hypothesis. Concurrent analyses, as discussed in Volume 3, have since showed that the assumption of 30-foot standard deviations was conservative but not unrealistic.

The amount and distribution of tracking coverage obtained with the three foregoing data types is indicated in Figure 4-3 for a polar circular orbit of 156.7 nautical mile altitude. In this figure, the number of observations in a 10-minute interval are plotted as a function of time for each data type for a typical day of orbiting. This figure indicates the way in which the photogrammetric, altimeter, and TRANSIT networks complement each other.

Several other tracking networks were originally considered but were not used in this analysis for various reasons. For example, the Army SECOR system promises to be a very useful network; however, there is some question as to the number and availablity of SECOR installations for this program. Similarly, various optical (e.g., Baker-Nunn) and radar tracking facilities will either not be available or will yield sparse, poorly distributed or inaccurate data which will probably be of doubtful value compared with the tracking networks included in this study.

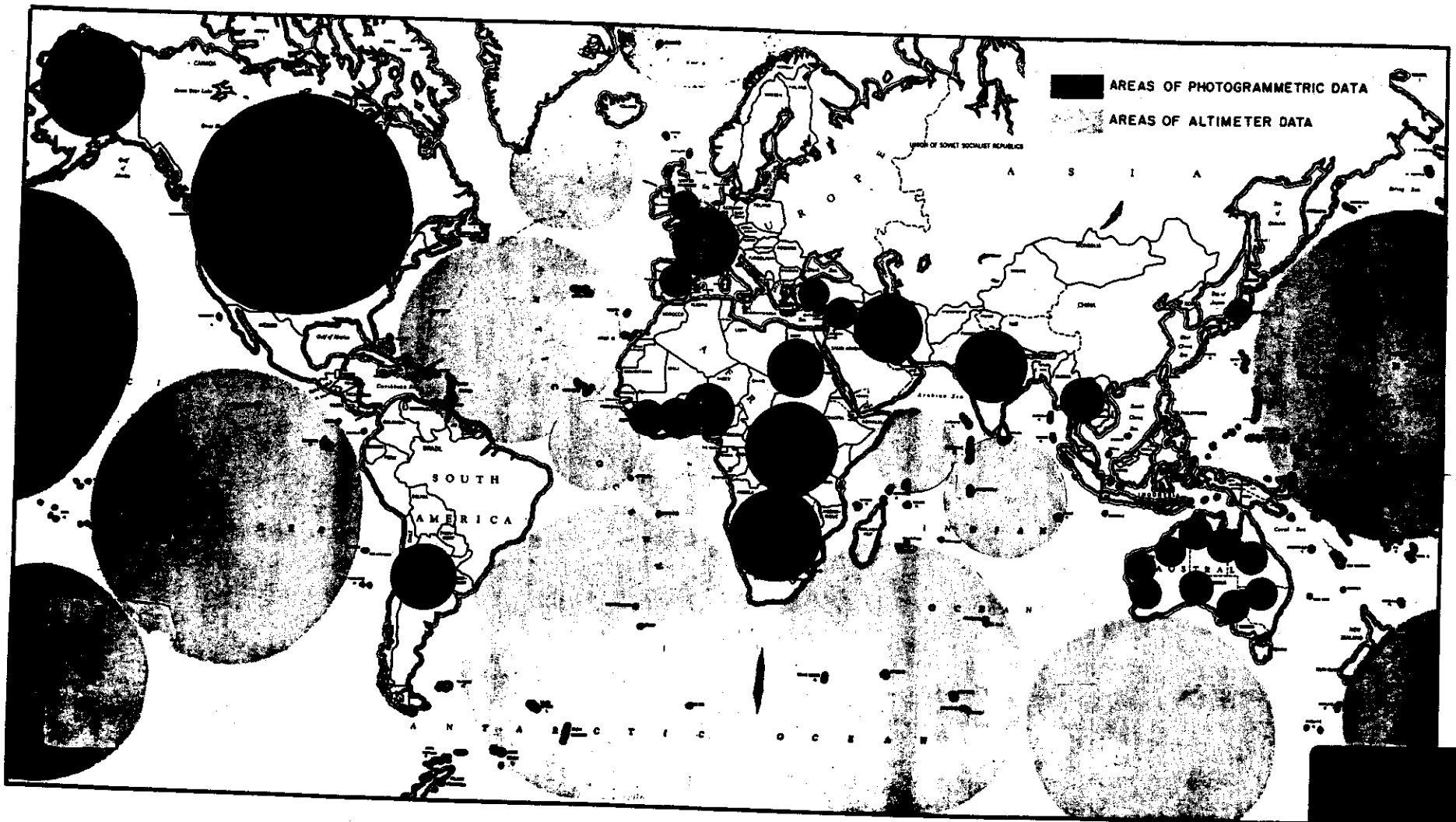

Fig. 4-2 — World map showing approximate areas where photogrammetric and altimeter observations were used for orbit determination calculations

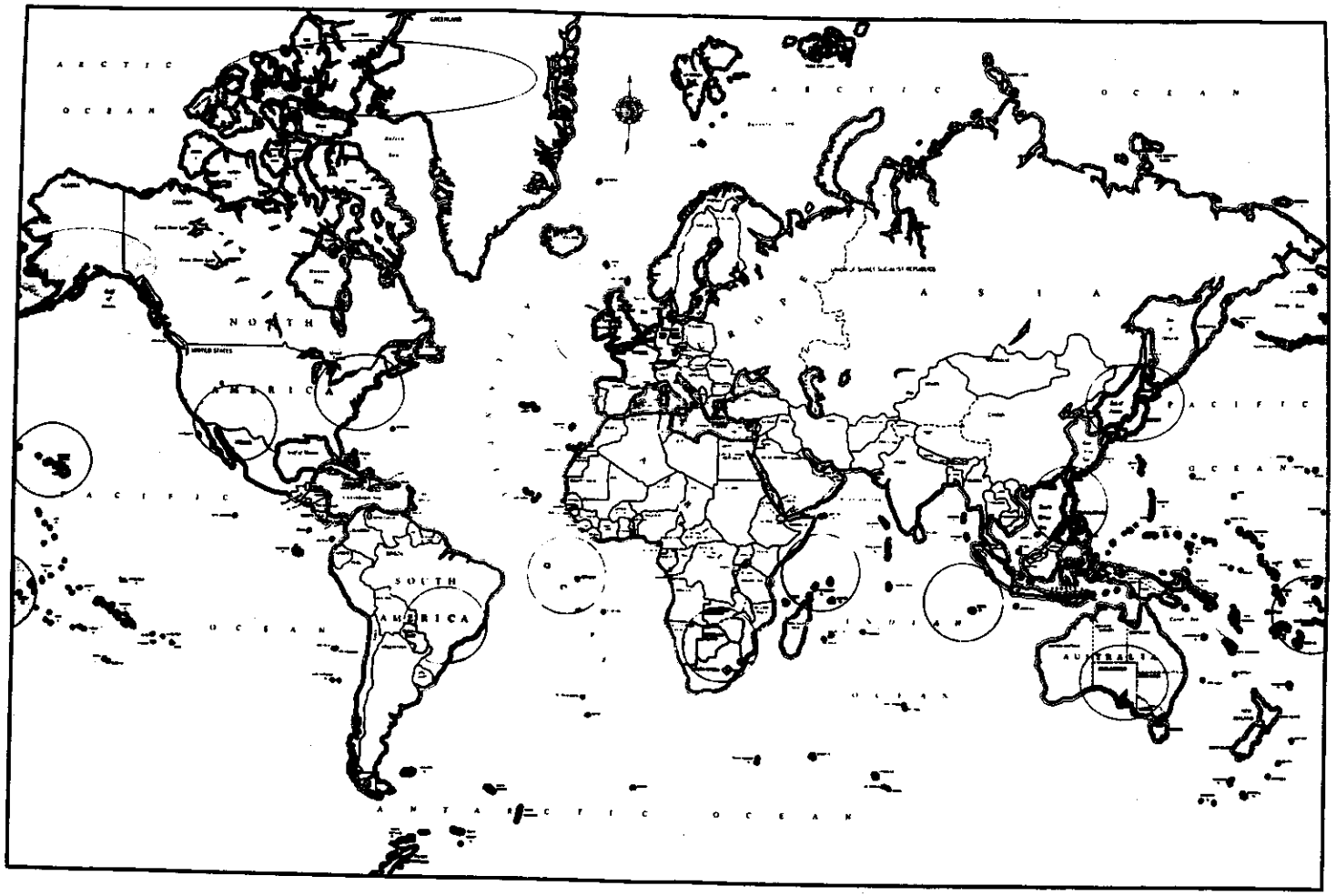

Fig. 4-1 — World map showing coverage from TRANSIT tracking stations for 10 degrees minimum elevation, 156.7-nautical mile circular orbit (McMurdo Sound station not shown)

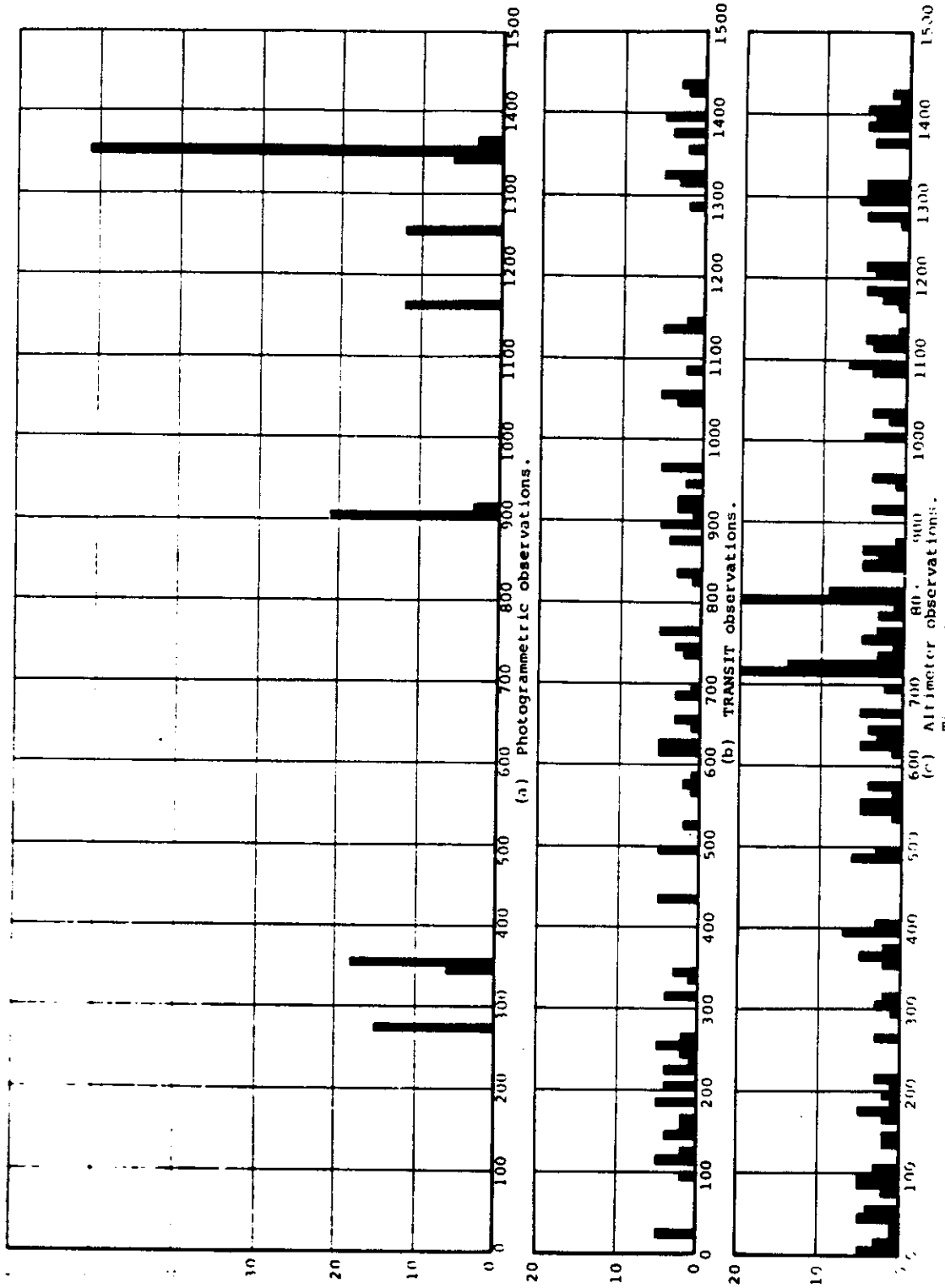

Fig. 4-3 — Bar charts showing number of observations as a function of time for the three data types considered (156.7-nautical mile circular orbit)

The results obtained by the PAGEOS program will undoubtedly be of great utility in helping to establish at least preliminary estimates of station locations, landmark locations, and datum locations. It is doubtful that the observational network for the PAGEOS program will be operational for this program, and this tracking network was therefore not considered.

4.2.5 References for Section 4.2

1. Guier, W. H., Newton, R. R., and Weiffenbach, G. C., Analysis of the Observational Contributions to the Errors of the Navy Satellite Doppler Geodetic System, Report No. TG-653, Applied Physics Laboratory, Johns Hopkins University, Silver Spring, Maryland, Jan. 1965.
2. Mercer, R. J., et al., TRACE Aerospace Orbit Determination Program, Report No. [redacted] Aerospace Corporation, Nov. 1964.
3. Mercer, R. J., et al., TRACE Aerospace Orbit Determination Program, Version D (Rough Draft), Aerospace Corporation, Apr. 1965.

4.3 FORCE MODELS

4.3.1 Gravitational Models

4.3.1.1 Introduction

Inhomogeneities in the earth's gravitational field and uncertainties in the perturbing forces acting on a satellite are the major obstacles to precise orbital predictions. There are essentially two facets to the problem; (1) the accurate determination of the perturbation forces of the gravitational field, (2) and the development of techniques for including the necessary refinements in an orbital prediction program.

There have been several basic approaches to describing the gravitational field of the earth. The two most prominent descriptions involve expanding the gravitational potential in orthogonal polynomials (usually spherical harmonics) with fitted coefficients or utilizing a distribution of mass points each of whose coordinates and magnitudes is adjustable. The magnitudes of the coefficients involved are determined by some fitting process (usually a least-square technique) to (1) data obtained from surface measurements of the gravitational field on the earth (gravimetry) or (2) by fitting a predicted orbit to observations of artificial satellites.

It is the purpose here to describe these approaches and to point out some of the problems encountered both in the measurements and in the application of the results.

4.3.1.2 Gravimetry

The problems associated with the specification of the field by local surface measurements are easily understood in terms of the sampling theorem. This theorem serves to illustrate (1) the source of errors from aliasing (falsely attributing high frequency effects to low frequency components), (2) the error introduced by insufficient data, and (3) the data processing problems introduced by random sampling. It is therefore useful to investigate the sampling theorem before discussing the results based upon gravimetric measurements.

The three situations to be considered are (1) the sampling rate is more than sufficient to specify the function sampled, (2) the sampling rate is exactly sufficient, and (3) the sampling rate is insufficient. The discussion here will be confined to the sampling of a one-dimensional function, since all of the conclusions are easily extended so that they are applicable to measurements taken over a closed two-dimensional surface.

Suppose that a function f(x) with Fourier transform $F(\omega)$ is to be determined by a finite number of samples. Let ω_c be the highest frequency present in $F(\omega)$, that is, $F(\omega) = 0$ if $|\omega| > \omega_c$. The sampling theorem can be derived as follows. Pick some arbitrary frequency ω_o and construct

from $F(\omega)$ and ω_o a periodic function $G(\omega)$ by merely reflecting $F(\omega)$ around $\pm\omega_o$, $\pm 3\omega_o$, $\pm 5\omega_o$ (as shown in Diagram A below). Since $G(\omega)$ is periodic, its inverse transform is a line spectrum with lines occurring at $x_n = n\pi/\omega_o$,

$$G(\omega) = \sum_{n=0}^{\infty} a_n \cos\left\{\left(\frac{n\pi}{\omega_o}\right)\omega - \alpha_n\right\}$$

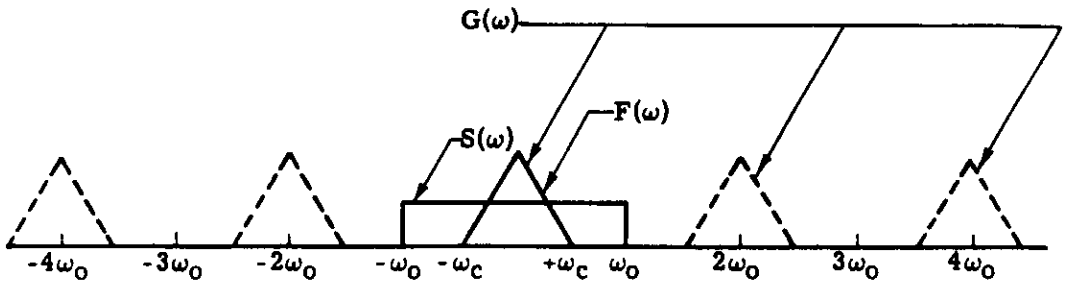

Diagram A

Refer to Diagram B—$F(\omega)$, the transform of the function being sampled, is obtained from $G(\omega)$ by multiplying $G(\omega)$ by a square pulse $S(\omega)$ (see Diagram A) whose amplitude is 1 for $|\omega| S\omega_o$ and 0 for $|\omega| > \omega_o$. The inverse transform of $S(\omega)$ is given by

$$s(x) = \frac{1}{\pi}\,\frac{\sin \omega_o x}{x}$$

Since $F(\omega)$ is given by the product $S(\omega)\ G(\omega)$,

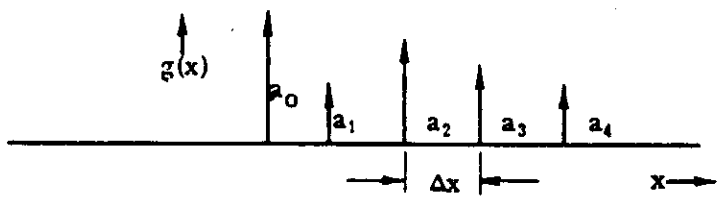

Diagram B — Inverse Transform of $G(\omega)$

its inverse transform can be found by convolving the transforms of S and G:

$$f(x) = \int_{-\infty}^{\infty} G(\xi)S(x - \xi)d\xi$$

This integral simply spreads each line of the function g(x) into the function s(x) as shown in Diagram C. Hence, f(x) is expressed as a sum of functions of the form sin $\omega_o x/x$, each one

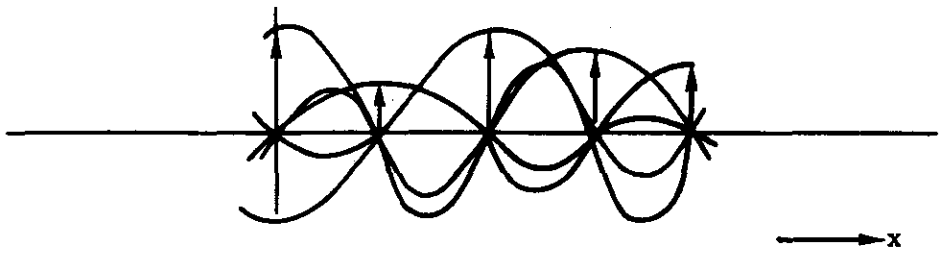

Diagram C

having an amplitude proportional to a line of g(x) and centered at the location of that line. The thing to note about the above diagram is that at each value $x_n = n\pi/\omega_o$, the contributions to f(x) from all samples other than the one located at x_n are zero. Hence, all the samples are independent. This is not true for samples taken at points other than x_n. In general, the value of f(x) at these points is dependent on all other samples.

This discussion shows that sampling an unknown function at equally spaced intervals of size $\Delta x = \pi/\omega_o$, completely determines the function at all values of x. This is true as long as $\omega_o \geq \omega_c$. If $\omega_o > \omega_c$, there has been excessive sampling. If $\omega_o = \omega_c$, the sampling is exactly sufficient. It will be shown below that if $\omega_o < \omega_c$, the sampling is insufficient so that there is insufficient data to determine f(x).

It should be pointed out that maintaining a constant distance between samples is not necessary; it is simply a way of maintaining independence of the samples. This serves to eliminate the computational hazards which arise when f(x) is to be reconstructed from interdependent samples. Theoretically, f(x) can be reconstructed from any set of samples as long as they are sufficient in number to meet the minimum requirements of the theorem. Furthermore, it is possible to contrive other sampling methods in which the samples are not equally spaced but are still independent. In all such methods however, the spacing must be according to a prescribed rule. It is, in general, impossible to obtain a sufficient number of independent samples by random sampling.

The last case to be considered is that of insufficient sampling $\omega_o < \omega_c$. In this situation, a problem arises in the construction of the function $G(\omega)$. Instead of appearing as shown in Diagram A, it appears as shown in Diagram D. Because of the overlapping and subsequent multiplication by $S(\omega)$, the function reconstructed from the samples is the inverse transform of $H(\omega)$ shown in Diagram E instead of f(x), the inverse transform of $F(\omega)$. It can be seen from the figure that the effect of insufficient sampling is to fold the high frequency region. Consequently,

the effects of frequencies too high to be detected by the sampling process are incorrectly attributed to lower frequency effects, an effect which is known as aliasing.

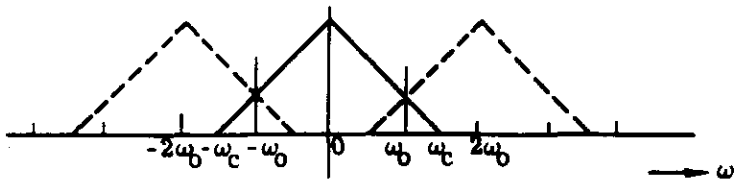

Diagram D

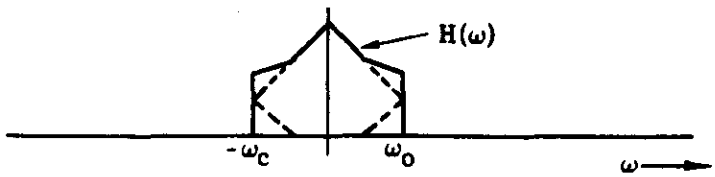

Diagram E

The present state of gravimetry[1*] is such that there are a number of localized areas throughout the globe where extensive measurements have been made. These areas, however, are separated by vast areas where no measurements have been made. One of the problems associated with the improvement of this poor coverage situation is the development of techniques to make accurate measurements over ocean areas.

Various attempts[2, 3, 4] have been made to produce a gravity model from this limited data. Owing to the effects of local masses, the high frequency variations in the field at the surface are quite large. Hence, in using measurements of constant spacing, the "foldover" described above results in an aliasing problem. Subsequent use of these measurements to determine the coefficients in a truncated harmonic expansion of the potential according to some "best fit" criterion results in a good description of the field in the local area as long as this description is not applied beyond the refinement of the original grid. A serious problem arises, however, when the expansion so determined is extrapolated to orbital altitudes. This is easily seen by noting that the nth harmonic in the expansion is attenuated by the factor $(R/r)^{n+1}$ where R is the earth radius and r is the geocentric distance to the vehicle. Since the folded over frequencies result in lumping the higher harmonic terms into the lower coefficients, they are insufficiently attenuated during the extrapolation process. As a result of this, all terms of order greater than 20 which have a sizeable effect at the earth's surface introduce a considerable error. This effect is to be contrasted with a truncated harmonic series derived from measurements of vehicle positions where the high frequencies are properly attenuated before the foldover occurs. Thus, it can be seen that while local measurements may lead to an expansion which provides a good local description, the degree to which the coefficients lack physical significance limits the validity of the description when extrapolated to other regions.

---

*References are listed in Section 4.3.5.

To produce coefficients with greater physical significance, it has been suggested that the aliasing problem be circumvented by randomizing the locations at which field measurements are made.[5] In this situation, the high frequencies would tend to become uncorrelated and therefore average out. Accompanying this procedure are the unavoidable computational hazards associated with interdependent samples. This approach also requires a large sample set.

Surface measurements are further complicated by irregularities in the terrain. In order to handle these data, the measurements are often extrapolated from the point where they were taken to the geoid or some other reference point. This referencing process adds both to the error and to the magnitude of the computational problem.

Summarizing, gravity models based upon terrestrial measurements suffer from poor coverage and errors introduced by large high frequency variations, referencing techniques and data-handling techniques. Additional error is introduced when the field so determined is extrapolated to orbital altitudes. The net result is that the use of such models is at present deemed unacceptable for application to the orbit prediction process when compared to the use of other models where parameters are determined from observations of orbiting vehicles.

4.3.1.3 Observations of Orbiting Vehicles

The determination of the coefficients in the spherical (or oblate spheroidal or ellipsoidal) harmonic gravity potential expansion from satellite observations presents a number of difficulties. First, an orbiting vehicle is subject to forces other than that due to the earth's gravity. Among these are air drag, radiation pressure, electromagnetic forces, micrometeoritic impact forces and lunar-solar gravity forces. Measurement of the gravity coefficients requires that the effects of these forces be considered. Secondly, there is an observational coverage problem owing to the distribution of land and water over the globe, with further restrictions imposed by the diplomatic considerations involved in locating observational stations. Thirdly, the large volume of tracking data sometimes produces a reduction problem so that some preprocessing of the data is necessary.

Among the extragravitational forces, air drag is the one producing the largest effect. The nonconservative nature of the air drag forces, however, enables the separation of drag effects from gravitational effects. The use of "model atmospheres" in conjunction with the measured orbital parameters has resulted in an apparently satisfactory solution to this problem at higher altitudes. At lower altitudes, it has been found that these models must be refined or expanded.

A number of methods have been proposed and are now being developed to solve the coverage problem. They are primarily concerned with the use of data collected by the vehicle itself. Such data alleviates the problems which arise from complete dependence on ground station tracking data.

The preprocessing of data usually involves the reduction of all the observational data collected by a given station during one pass to a single or a few weighted observations. There are a number of techniques by which this data can be reduced, all of which are fairly reliable in a theoretical sense. This is in contrast to the preprocessing associated with referencing in the case of surface measurements where each measurement must be extrapolated to a point on the reference surface according to some conjectural scheme.

Finally, the foldover problem, and hence any aliasing problem are greatly reduced as mentioned in connection with the discussion of the sampling theorem. It should be noted in

connection with this that even if the series is truncated so that aliasing lessens the physical significance of the coefficients, the result is an effective model which is a fair description of the field at the altitude where the measurements were made.

As it was pointed out before, if there is any aliasing, the extrapolation of the field from one altitude to a higher one introduces an error because of insufficient attenuation of the higher harmonics. Since this error would not be introduced if the measurements were made at the higher altitude, there is good reason to avoid such extrapolation whenever possible.

The situation might be summarized as follows. With present day capabilities, the field description is limited by amount of data which can reasonably be processed and by the geographical distribution of available data. Since the extrapolation of such a limited description to higher altitudes is unavoidably accompanied by the introduction of additional error, there is a theoretical advantage in the determination of the field from orbital rather than terrestrial measurements. Second, the "state-of-the-art" of orbital measurements is such that it is much more feasible to obtain estimates for the desired quantities from these measurements rather than from surface measurements, and furthermore, that the quantities so obtained are the more reliable for orbital prediction applications.

In both of the methods described thus far, the result is a set of coefficients in the harmonic expansion for the gravity potential. The computations involved in applying the results to the prediction problem are identical for both methods; the coefficients are simply incorporated into the program so that the earth's field is described by the truncated harmonic series.

4.3.1.4 Determination of Mass Point System

This method deviates from the previous two in that there is no attempt to measure the coefficients in some series for the potential. Instead, it is assumed that in the region outside of the earth, a simulated field closely resembling that of the earth can be produced by a number of properly located point masses. Orbital measurements are then used to determine the magnitude and positions of these masses. The use of a model so far removed from physical reality is justified by the fact that it can be shown that any physically realizable field can be approximated to any degree of accuracy in this manner if the number of masses is sufficiently large. The purpose of using such a model is to investigate the possibility of increasing the accuracy of the description of the earth's gravitational field without a considerable increase in the computational requirements for orbit prediction.

One question which arises in connection with this method is the rate at which the field so produced converges to the earth's field as the number of mass points is increased. Unfortunately, a theoretical answer to this question requires a detailed knowledge of the earth's interior. Since such knowledge is not presently available, recourse must be had to more pragmatic tests. One such method might be to expand the field of several point masses in a harmonic series and then to adjust the masses and positions so that the lower order terms agree with the best known values. After the adjustment, the higher order coefficients can be compared with best known values. Another method, and one which is presently being carried out, is to incorporate this model into a prediction program.[6] Real data can then be used to compare the residuals obtained on the basis of this model with those obtained from the harmonic expansion model.

Preliminary tests using ficticious data have been carried out. The mass sizes and positions were determined so that the zero and first moments of the earth were not altered. (These constraints make the total mass and the position of the center of mass invariant.) The results of this simulation study favorably demonstrated the capability of this model.

The application of this model to orbit prediction is accomplished by direct calculation of the potential from the point masses. Providing that the number of mass points necessary for adequate description of the field is not excessive, the computation time might be considerably reduced. While this approach offers an optimistic outlook, it requires, at the present time, more extensive development and evaluation to determine its value in an orbital prediction program.

4.3.2 Description of Perturbation Forces

The motion of a satellite is described basically as the motion of a small body in the inverse square gravitational field of a large spherical body. All other forces acting on the satellite are called perturbation forces. They include the inhomogeneities of the earth's gravitational field which arise from nonsphericity, the gravitational fields of the sun and moon, air drag forces, radiation pressure, electromagnetic forces, vehicle originating forces, and forces due to micrometeoritic impact.

The oblateness of the earth produces perturbation accelerations of the order of 5×10^{-4} g. The accelerations caused by the remaining spherical harmonics are of the order of 10^{-6} g and smaller. The effects of these field inhomogeneities are accounted for by the inclusion of a gravitational model in the orbit prediction program. The fields of the sun and moon producing accelerations of the order of 10^{-7} g are accounted for by direct computation; the positions of the sun and moon with respect to the vehicle are calculated and the appropriate acceleration is determined.

The air drag forces are computed from the air density which in turn is determined either from a model atmosphere or by direct measurement. The estimated accelerations due to drag forces vary from about 5×10^{-6} g at an altitude of 100 miles to about 10^{-8} g at 300 miles for a ballistic coefficient of about 100 pounds per square foot. The present day model atmospheres and their capabilities for prediction program applications are discussed in Section 4.3.3.

The theory of radiation pressure is well established so that knowledge of the vehicle's geometry and reflectivity properties make the inclusion of this effect a straightforward procedure. The accelerations produced are of the order of 3×10^{-9} g, although uncertainties in the details of the reflection process for an actual surface introduce uncertainties of about a factor of two.

The natures of the electromagnetic interaction phenomena which take place are not very well understood. While conjectures have been made about a number of possible phenomena, which of these actually takes place is still an open question. It is believed however, that these effects contribute negligibly to the perturbations since they have exhibited no discernible effect on the motions of previous satellites.

The effects due to vehicle-originated forces are often either lumped together with air drag forces into adjustable parameters in the air drag model, or, if known, are treated explicitly as discontinuous terms as, for example, in the case of attitude control jets.

4.3.3 Model Atmospheres

4.3.3.1 Introduction

The largest nongravitational perturbing forces affecting the motions of low-altitude satellites are those due to air drag. Since these forces depend directly on air density, a detailed knowledge of the density and its fluctuations is necessary if such forces are to be included in an orbit prediction program.

The theories directed at a detailed description of the atmosphere are due to many investigators, prominent among whom are Nicolet, Jacchia, Paetzold, and Harris and Priester. Generally, these theories agree that the density fluctuations are the result of atmospheric heating of one form or another. Agreement between theory and measurement is obtained by adjusting theorectical parameters so that they correspond with the averages computed from measurements made on artificial satellites. Such averaging procedures are necessitated by the fact that there still exist density fluctuations which are beyond the scope of these theories. As a consequence of this situation, these models have exhibited a certain adequacy when used to predict orbital quantities which depend upon the average atmospheric density along the orbital path; quantities predicted from these models which depend upon the instantaneous density, however, are subject to fluctuations.

A brief description of these theories is given here. Some results of their application are discussed and it is demonstrated that these models require additional refinements before they can be used appropriately to make accurate short term predictions of the positions of orbiting vehicles.

4.3.3.2 Description of the Models

The basis for the present day model atmospheres was provided in 1960 by Nicolet's discovery that the atmospheric densities deduced from satellite drag observations could be explained by assuming that the upper atmosphere is in a state of diffusive equilibrium and that the temperature assymptotically approaches a constant value with increasing altitude.

It should be pointed out that these assumptions have a physical basis and hence, should not be considered as a mathematical contrivance whose only justification is a pragmatic one. The first assumption is in accordance with the observed stability of the solar bulge, which indicates a state of statistical equilibrium in which the heat introduced by the absorption of solar radiation is balanced by reradiation and dissipation to lower altitudes. Hence, a state of diffusive equilibrium is produced in which a temperature gradient can be maintained. The second assumption follows from a consideration of the mechanisms by which temperature (and hence, density) fluctuations are brought about. The predominant factors producing atmospheric heating are the absorption of extreme ultraviolet radiation from the sun, the interaction of high energy solar particles with the atmosphere, and the earth's magnetic field and hydromagnetic effects. Most of the heating takes place in regions of greater air density (between 100 and 200 kilometers). Since temperature perturbations are produced in this region of the atmosphere and since the temperature profile is determined by the diffusion of particles out from this region, it would be expected that the temperature gradient diminish as distance from the perturbed region is increased. Hence, the asymptotic temperature assumption.

The construction of an atmospheric model requires in addition to a theory, a set of boundary conditions. Since there is very little known about the atmosphere between 100 and 150 kilometers, the specification of such a set of boundary conditions is a difficult task. Based upon physical conjectures and some empiricism, Nicolet assumed a set of fixed boundary conditions at 120 kilometers and a constant pressure layer at 150 kilometers. He then constructed his 1961 model by using his diffusion theory to determine the densities of all atmospheric constituents. These densities were, in turn, used to compute average molecular weight density profiles for a number of different assymptotic temperatures.

Nicolet's theory has two inherent weaknesses. The first is the assumption of the steady-state condition, which is valid only if the response time of the atmosphere to solar heating is considerably shorter than 24 hours. This objection is partially offset by the fact that the solar bulge is

nearly symmetrical and lags 12^h local time by only two hours. The second is the invariance of the boundary condition, an assumption which may or may not have a basis in fact.

The subsequent work of Jacchia has consisted mainly of the application of Nicolet's theory. By using Nicolet's model, he was able to find a correlation between the exospheric (i.e., h > 350 kilometers) temperature and the daily value of the 10.7-centimeter solar flux.[7] By using satellite data, a number of empirically derived functions were specified which relate the exospheric temperature to geomagnetic effects, diurnal variations, solar wind and "27 day" (solar rotation period) oscillations.[8] By using Nicolet's revised model and satellite data, Jacchia has demonstrated a close correlation between the predicted and measured exospheric temperatures.[9] Also of interest is the dependence of the atmospheric heating during a magnetic storm as a function of latitude.[9] This relationship is based solely on satellite observations and is not included within the scope of the theory. The measurements have shown that the theoretical heating from magnetic activity, used by Jacchia, is good at low and moderate latitudes, but that this heating increases by a factor of about 4 in the polar regions. It is believed that the heating is the result of the absorption of hydromagnetic wave energy although high energy particles may also contribute to this effect.

In 1964, it was found that the temperature profiles of both Nicolet and Harris and Priester could be approximated by a single empirical relation. Abandoning Nicolet's theory, Jacchia produced a set of temperature profiles by using this approximation, and integrating the diffusion equation assuming a set of boundary conditions at 120 kilometers.[10] The dependence of the exospheric temperature on solar and geomagnetic activity was retained.

The correlations between Nicolet's theory and the geomagnetic indices, satellite drag measurements and solar activity presented in Jacchia's work have served to demonstrate the validity of Nicolet's assumptions and to establish his theory as a sound foundation for future work.

In 1962, Harris and Priester developed a theory which dispenses with the steady-state assumption.[11] The theory is based on the assumption of diffusion equilibrium and is derived from the simultaneous solution of the heat conduction and barometric equations. Combining this theory with the invariant boundary conditions of Nicolet at 120 kilometers, it was found that extreme ultraviolet heating produced a diurnal variation which required an unrealistically high heating efficiency and which exhibited maxima and minima at 17^h and 6^h local time instead of the observed 14^h and 4^h (Reference 12). It was concluded that the diurnal effect could not be explained on the basis of extreme ultraviolet heating alone. This situation was remedied by the introduction of an additional heat source having a diurnal variation with a maximum at 9^h. While this source was introduced to bring the theory into agreement with observations, there is some evidence that it has physical significance in that there is some correlation between this source and independent measurements of solar corpuscular radiation. Its physical significance however, is still a matter of debate so that conclusions about this second source must be deferred until further information is available.

By varying the fluxes of both of these sources proportionally to the long term averages of the 10.7-centimeter solar flux, models of the upper atmosphere have been produced which exhibit in the altitude range, 180 to 600 kilometers, a diurnal density variation which is in good agreement with the densities taken from the observational model of the Bonn University Observatory. The nighttime temperatures are in good agreement with Jacchia's observational model.

The principal objections to the Harris-Priester model are the negligence of horizontal air motions and heat conduction, the restriction to the treatment of equatorial atmospheres at equinox and, as in the models of Nicolet and Jacchia, the assumption of a fixed boundary condition.

However, the Harris-Priester model has served to broaden the scope of theoretical investigations into the nature of the upper atmosphere.

In 1965, Small and Poe reported the results of a comparison between an extended Harris-Priester model and densities derived from the observation of satellite drag forces in the lower thermosphere.[13] The results indicated that the Harris-Priester densities between 120 and 200 kilometers are in error. In order to use the model however, it was necessary to extend it so that it could be applied at all latitudes on all days of the year. The extension which was used was somewhat unsatisfactory on theoretical grounds. While the discrepancies between the Harris-Priester densities and those determined from satellite observations were attributed to the unrealistic boundary conditions, it is difficult to determine how much of the discrepancy was introduced by the extension of the model. It was suggested that the boundary conditions of the original model be corrected and new profiles generated and that the boundary be moved downwards where the temperature is less strongly influenced by solar and geomagnetic activity.

Using the Harris-Priester model, Jacobs has found a strong correlation between the theoretical heating factor (a parameter of the model) and the 3-hour index of geomagnetic activity, K_p (Reference 14). No apparent nonlinearity was observed for variations in K_p as high as $7\frac{1}{3}$. This is in contrast with Jacchia's theory in which a linear correlation was obtained only during magnetically quiet periods.

4.3.3.3 Applications to Orbit Prediction

While Nicolet's theory of 1960 has resulted in notable advances of our knowledge of the upper atmosphere, the present day theories are still incapable of producing models which can account for short period (several hours or less) fluctuations in atmospheric density. This is evidenced by the fact that all successful applications of these models are presented in the form of correlations, and graphs using smoothed or averaged quantities.

As a result, these theories find their application in the prediction of long range secular effects. The accurate prediction of the position of a low-altitude satellite however, requires a detailed knowledge of the instantaneous density along its path of motion. The solution of this problem is therefore still outside the realm of applicability of these models.

It is possible of course that future refinements might alter this situation, but it can also be conjectured that the upper atmosphere never attains a state of equilibrium, in which case the only reasonable description of at least part of these fluctuations is a stochastic one. Thus, with the present knowledge, it is not even clear whether or not it is possible to construct a model which is adequate for application to the prediction problem. The solution of this problem at the present time therefore requires a more direct measurement of satellite drag forces.

4.3.4 Vehicle Originating Forces

A number of sources of perturbing forces exist within the satellite which affect the vehicle motion and thus the accuracy with which the gravitational effects may be determined. These perturbing effects are discussed in this section. In order to assign magnitudes to these effects to assess their relative importance, a typical vehicle configuration is assumed. Its mass is 175 slugs. The attitude control system is assumed to have characteristics typical of the Agena; i.e., cold gas reaction jets located at the rear of the vehicle. The source of perturbing forces considered are the attitude control system, outgassing, cold gas valve leakage, and special vehicle maneuvers using the attitude control.

4.3.4.1 Attitude Control System Forces

For purposes of illustrating the types, magnitudes, and uncertainties of forces produced by a cold gas reaction attitude control system, operation of a typical Agena system will be considered, since this is the most likely vehicle for this program. The Agena has six nozzles located at the aft end of the vehicle and oriented as shown in the diagram below.

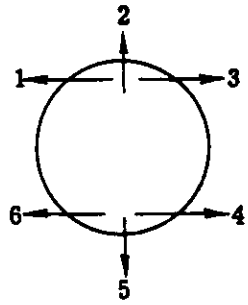

The thrust vectors from these nozzles lie in a plane normal to the longitudinal axis of the vehicle. Nominally, there is no force component along the vehicle axis. The pitch axis uses numbers 2 or 5. The control for the yaw and roll axis is coupled. If only yawing occurs, numbers 1 and 6 or 3 and 4 are used. If only a roll error occurs, couples are used (i.e., 1 and 4). If both yaw and roll errors occur simultaneously, only one nozzle is used to counteract both errors. Two levels of thrust are used and are obtained by varying the chamber pressure to the nozzles. In the ascent mode, each nozzle produces 10 pounds of thrust, whereas in the orbital mode, 0.5 pound is produced. The higher thrust level on ascent is used to correct for large perturbations during orbit injection, such as dumping of the residual fuel.

In the orbital mode, the amount of corrective impulse is varied by changing the pulse width and pulse repetition rate of the thrust pulse. A typical "quiet" operation in orbit produces a pulse width of 0.020 second and a repetition rate of perhaps one pulse every 1 to 2 minutes. The control system has a deadband in all three axes. In a typical operation in which the vehicle is nearly symmetrical in the yaw plane, the control in yaw and roll is in a limit cycle operation across the deadband. The side forces then tend to average out to zero over a long period of time. In the pitch plane, the vehicle tends to operate at one side of the deadband under the action of external perturbing torques. One pitch nozzle then fires more often than the other, and the vertical forces do not tend to average to zero.

Each time a nozzle fires, the 0.5-pound thrust acting on the vehicle induces a nominal acceleration of the center of mass of about 10^{-4} g. This acceleration can vary the order of 10 to 15 percent due to variations in nozzle pressure, dynamics of the gas valve operation, and other factors. This acceleration will occur in either the vertical or cross-track direction.

The components of the attitude control forces along the in-track direction are of greatest interest, since these have the greatest effect on the changes in orbital position of the vehicle. In-track components can arise in two ways. First, the cold gas nozzles may be so aligned or so configured that the thrust vector of the gas leaving the nozzle may have a component in the direction of the vehicle longitudinal axis. A reasonable upper bound on this effect would be a thrust equal to one percent of the total nozzle thrust. This thrust level would produce an in-track

acceleration of about 10^{-6} g. This value is greater than the acceleration due to aerodynamic drag by about an order of magnitude. However, since the nozzle thrust component typically acts for only 20 milliseconds and the nozzle has a very low duty cycle, an average in-track acceleration would be perhaps three orders of magnitude down, or about 10^{-9} g. The second source of an in-track control thrust component is an attitude error of the vehicle. If the nozzle thrust lies in a plane normal to the vehicle longitudinal axis, but the vehicle is at an angle of attack or sideslip, a component of thrust will appear along the direction of motion. A reasonable value for the maximum angle of attack would be about 20 minutes of arc. Thus, this effect produces one-third the effect just indicated for misalignment, and the duty cycle considerations are the same.

Consideration should be given to recording gas valve firings for the present program. If the duration and frequency of gas valve firings are recorded, the impulse produced by the nozzles can probably be computed to within about 20 percent. A check on these computations can be obtained from the gyro output, which should show the vehicle attitude when the valve is fired and an increase in angular rate as the valve is fired. Such data should tend to indicate the significance of in-track components of the attitude control nozzle forces.

4.3.4.2 Outgassing

Outgassing is essentially a momentum efflux of fluid from the vehicle, which causes a reaction force and an acceleration on the vehicle. Generally, the rate of outgassing is poorly known. Thus, it is of interest to determine all the potential sources of outgassing and compute for each an approximate upper limit of its magnitude. If any of the potential sources is found to be capable of producing appreciable perturbing accelerations, consideration can then be given to modifications which would hold the effects to an acceptable level. The various sources and their orders of magnitude are discussed below.

The first source of momentum efflux is the fuel dump maneuver that is performed after injection. Typically, a fuel and oxidizer weight of the order of 200 pounds might be left in the tanks. For safety purposes, this is vented with a pressurized gas system. This represents a large perturbing force, of the order of 10 to 100 pounds, which lasts for perhaps 20 seconds. After the main dump, outgassing due to residual fuel in the tank and fuel splashed on the vehicle occurs at a steadily decreasing rate for many orbits. Typically, the perturbation accelerations due to the fuel outgassing drop off to about 10^{-9} g after about 10 orbits. A second source of perturbation effects during this period is the attitude control. Because the perturbing effects are large, larger cold gas nozzle thrust levels are used in the ascent mode than are used in the orbital mode. In the ascent mode, each nozzle produces 10 pounds of thrust when it fires, which causes an acceleration of 10^{-3} g on the vehicle. Since the nozzles fire in response to outgassing perturbations, whose magnitude and direction is not well known, the pulse width and repetition rate of the cold gas nozzles is not predictable. As a result of these effects, an allowance of perhaps 10 orbits is made for stabilization of the orbit and vehicle attitude, and no payload operation is performed during this period. Since these perturbation effects decay to a negligible level during this orbit adjust period, their influence on the data collection portion of mission is unimportant. A second potential source of perturbing effects is venting of the batteries used for energy on the vehicle. For relatively short missions, conventional batteries are used, because they are simple, proven, and reliable. No outgassing occurs because the batteries do not require venting. For longer missions, or for missions requiring considerable energy, fuel cells become competitive in weight.

The fuel cell generates water or water vapor as the product of the combination of hydrogen and oxygen. The fuel cells operate at relatively high temperatures for improved efficiency. If the water vapor is discharged overboard, it can cause a considerable perturbation to the vehicle. An order of magnitude calculation was made assuming 12 pounds of water were generated at a uniform rate during the 15-day mission. This water weight was obtained using representative numbers for fuel cell characteristics and mission energy demand. A specific impulse of 143 seconds, corresponding to a 600°F vapor temperature was used for the water vapor. Using these numbers and assuming all the vapor is vented overboard in one direction, an average perturbation acceleration level of 10^{-3} g was obtained. This, of course, is considerably higher than any other perturbing acceleration on the vehicle and is unacceptable from the standpoint of the uncertainties induced in orbital position. Two possibilities exist for eliminating this effect as a source of perturbation forces. The water vapor can be continuously vented overboard in a duct having essentially a flat plate over its end with a small gap around the periphery, such as shown below.

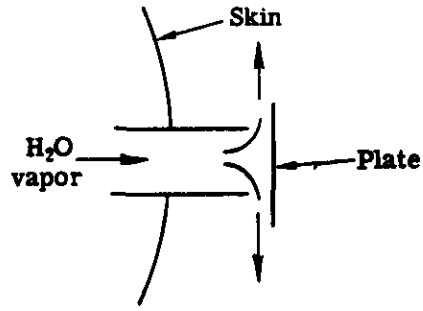

The vapor emerges in all directions around the plate, and its perturbing effect tends to be cancelled. The performance of these outlets has proven to be unreliable, however, and net forces in one direction of the order of 20 percent of the total available thrust are liable to occur due to flow irregularities in the duct. The second, and more satisfactory, method is to provide a container to collect the water vapor, condense it, and store it for the duration of the mission. This method results in a heavier system but a much more reliable way of disposing of the potential perturbating effects of the water vapor. It appears that fuel cells will not be required for the present program. However, if fuel cells are required, the latter momentum dispersion effect is recommended.

A third source of perturbations due to outgassing is the water vapor present in the film. Film is generally packaged or handled in an atmosphere of about 50 percent relative humidity and 70°F prior to placement in a camera system. As a result, film of the type being considered for this program (an estar base film like SO 102 or SO 130) typically contains from 0.8 to 1.6 percent water.[14] If the film is in rolls, as it is in the supply cannister, the water is very slow to evaporate, and the associated time constants for reaching equilibrium are the order of 100 or more hours. However, once the film emerges from the cannister as a strip, equilibrium is obtained in a matter of a few minutes. Thus, it is possible for essentially all of the water in the film to evaporate as the film passes from the supply to the takeup spools. An order of magnitude calculation was made based on a total film weight of 425 pounds and a total water content of 2 percent. A specific

impulse of 100 seconds was used for the water vapor, which corresponds to expansion of the water vapor into a vacuum from an initial temperature of 500°R. If the water vapor is outgassed from the vehicle in one direction at a uniform rate over the 15-day mission, a perturbation acceleration of about 10^{-7} g is obtained. This is of the same order as the in-track air drag perturbation, and is thus significant. It is probable that most of the momentum associated with this outgassing efflux will be primarily in a plane normal to the vehicle axis. This is desirable, since perturbing effects in this plane are less important than those in the in-track direction from the standpoint of uncertainties in vehicle orbital position prediction. However, care should be taken to attempt to dissipate the water vapor as uniformly as possible around the vehicle circumferences so as to minimize the perturbation effects associated with this phenomena. This can be done by design of the openings through which the water vapor can escape from the vehicle.

The last outgassing phenomena to be considered is that due to the vehicle surface itself. This is mentioned only for the sake of completeness, because the effects are extremely small. For instance, the data from Reference 15 for aluminum outgassing rates can be used in an order of magnitude calculation with a specific impulse of 70 seconds to compute the perturbation acceleration caused by one square foot of surface. This calculation indicates a value of about 10^{-14} g. Since this momentum efflux occurs over the surface of a cylinder, essentially, the effects on opposite sides of the cylinder tend to cancel, and the effect is completely negligible.

4.3.4.3 Cold Gas Valve Leakage

In the hard vacuum of an orbital environment, it is essentially impossible to provide gas control valves for a cold gas attitude control system which do not leak. Such leakage as does exist provides a source of perturbing forces whose magnitudes and time variation are unknown. Thus, it is of interest to examine this effect to determine if it can be significant.

Reference 16 indicates typical gas leakage rates for a cold gas attitude control valve after a few cycles of operation in the range of 10^{-3} to 10^{-5} standard cubic centimeter per second. Experience on the Mariner satellite indicates leakage rates of about 2 standard cubic centimeters per hour, which correspond to the upper end of the range just cited. The valves used on the Agena are believed to have somewhat higher leakage rates. If a leakage rate of 10^{-2} standard cubic centimeters per second is assumed and a specific impulse of 50 seconds (which is that of the freon/nitrogen mixture used for control) is used, a perturbation acceleration of 10^{-9} g is obtained. The accelerations of this magnitude arising from the control valves would act basically in the vertical and cross-track directions, since the nozzles are so oriented. This is the same order of magnitude as other perturbing forces, such as solar pressure, acting in this direction. In addition, if most or all of the valves leak, some compensations will occur, since the nozzles occur in pairs pointed in opposite directions. Since uncertainties in perturbing effects in these two axes are not as important as those in the in-track direction, these perturbing effects are of an acceptably low level.

4.3.4.4 Special Vehicle Maneuvers

During the mission, two special maneuvers are required which demand greater rate of application of impulse from the attitude control nozzles than is required by the normal attitude stabilization. These are the maneuver(s) for camera calibration and the pitch maneuver(s) required for recovery capsule ejection. Since there is no strong reason why the forward recovery capsule must be recovered before the end of the mission (for the case of a double capsule recovery), both capsules can be recovered at the end of the mission. The perturbing torques associated

with the pitch maneuver to eject the capsules are then unimportant from the standpoint of the primary orbit determination problem of the mission, although there would, of course, be a need to know the orbit accurately enough to predict the re-entry trajectory of the second recovery capsule, if there is an appreciable delay between the first and second capsule ejections.

There is also some latitude on the timing and frequency of the calibration maneuver. If the maneuvers are carried out at the beginning and end of the mission, the perturbation effects will be unimportant throughout the data collection portion of the mission. If it should prove necessary to calibrate during the mission, sufficient time will have to be allowed for the perturbations to die out. Thus, both of these special maneuvers should cause little effect on the mission requirement imposing limitations on the uncertainty with which the vehicle position must be known.

4.3.5 References for Section 4.3

1. Kaula, M., Determination of the Earth's Gravitational Field, Rev. of Geophys., 1:507-551 (1963).
2. Kaula, M., Statistical and Harmonic Analysis of Gravity, Geophys. Res., 64:2401-2421 (1959).
3. Jeffreys, H., The Analysis of Gravity, Smithsonian Inst. Astrophys. Obs. Spec. Rept., 79 (1961) 12 pp.
4. Uotila, U. A.: Harmonic Analysis of World-Wide Gravity Material, Publ. Isos. Inst. Intern. Assoc. Geod., Helsinki, 39:18 (1962).
5. Shapiro, H. S. and Silverman, R. A., Alias-Free Sampling of Random Noise. J. Soc. Ind. Appl. Math., 8:225-248 (1960).
6. Walters, L. G., Arsenault, J. L., and Mahon, G. H., Earth Model Program Development, Division of Philco Corporation, Aeronutronic, Interim Technical Report Covering Period 15 September 1965 through 30 November 1965, Publication No. U-3360, (30 Nov. 1965).
7. Jacchia, L. G., Nature, 192:1147, (1961).
8. Jacchia, L. G., Variations in the Earth's Upper Atmosphere as Revealed by Satellite Drag, Smithsonian Astrophysical Observatory, (31 Dec. 1962).
9. Jacchia, L. G., The Temperature Above the Thermopause, Smithsonian Astrophysical Observatory, Spec. Rept. 150 (22 April 1964).
10. Jacchia, L. G., Static Diffusion Models of the Upper Atmosphere with Empirical Temperature Profiles, Smithsonian Astrophysical Observatory, Spec. Rept. 170 (30 Dec. 1964).
11. Harris, J. and Priester, W., J. Atmospheric Sci. 19:286-301, (1962) and NASA Technical Note No. D 1443 (1962).
12. Harris, I. and Priester, W., "Heating of the Upper Atmosphere", Space Research III, Proceedings of the Third International Space Science Symposium, Washington, D.C., 2-8 May 1962, John Wiley and Sons, Inc., New York, 1963.
13. Small, H. W., and Poe, R. F., Air Density in the Lower Thermosphere, AIAA Paper No. 65-506 (July 1965).
14. Manual of Physical Properties of Kodak Ainal and Special Sensitized Materials, Section 4, Moisture Properties, Eastman Kodak Company (Jan. 1961).
15. Schrank, M. P., Benner, F. C., and Das, K. K., Theoretical and Experimental Study to Determine Outgassing Characteristics of Various Materials, AEDC TDR-64-53 (Mar. 1964).
16. Lange, B., The Control and Use of Drag-Free Satellites, Stanford.

4.4 ORBITAL COMPUTATION TECHNIQUES

The perturbation methods applied to orbit determination are generally divided into two classes: (1) methods of general perturbations, and (2) methods of special perturbations. The first class includes those methods in which the orbit is determined by the analytical integration of a series expansion for the perturbative accelerations. General perturbations are most applicable in the computation of orbits extending over many periods. The second class includes those methods in which the orbit is determined by the numerical integration of the perturbative accelerations. All perturbation methods are directed at the determination of small departures from some intermediary orbit which approximates the true motion.

In addition to those discussed below, there are a number of other theories and techniques which have been used. Most of them are extensions or refinements of those discussed, while others differ in their choice of coordinate systems, variables, or form of perturbative function. With the exception of purely empirical orbits, however, those mentioned here represent a basic cross-section of the work which has been accomplished thus far.

A rather comprehensive review of these techniques and a list of references is contained in Reference 1.* For additional discussion see References 2, 3, and 4.

In practice, the problem is further complicated by uncertainties in measurements, station locations, geodynamic parameters, etc. Consequently, the integration of the equations of motion is generally carried out in conjunction with some scheme for adjusting these parameters. The criterion most extensively used for such adjustments is the "minimum variance" criterion. According to this scheme, each variable which has an uncertainty is divided by its standard deviation, and the resulting variables are adjusted in such a way that the sum of the squared differences between the measured and computed quantities is minimized.

4.4.1 General Perturbations

The problem of the analytical determination of orbits has been the object of a number of extensive analyses. Three factors contribute to the differences among these analyses: (1) the parameters used to describe the motion, (2) the coordinate system in which the motion is described, and (3) the intermediary orbit from which small perturbations are calculated. The description of the problem in terms of Keplerian elements results in a simple description of the orbit if only the first-order perturbations are retained. The algebra associated with the second- and higher-order perturbations becomes so unwieldy that this approach is not feasible for a more detailed study of the problem. In addition to this drawback, the theory does not apply for (nearly) circular orbits, because the angle of perigee loses its definition, nor does it apply for (nearly) equatorial orbits, because the right ascension loses its definition.

*References are listed in Section 4.4.6.

Secular and long period effects which arise from some of the terms in the spherical harmonic expansion of the earth's potential require the computation of second-order perturbations if accuracy is to be maintained. The Delaunay variables are often used in this application to avoid the complicated expressions which arise from the use of the Keplerian elements.

Satellite theory has been developed in terms of elliptical coordinates by Vinti. The solution to Vinti's equation, including all terms up to second order, has been accomplished by Izsak. This theory does not exhibit any formal singularities so that it applies for all eccentricities and inclinations.

The theories of Brouwer, Sterne, and Garfinkel use intermediary orbits which are the solutions to the equations of motion for potentials which include the Newtonian term and the "oblateness" term. In those theories in which only the Newtonian term is retained, the "oblateness" term represents the largest perturbative force. It is about three orders of magnitude larger than the next highest perturbation. The inclusion of this term in the potential, rather than treating it as a perturbative term, results in an intermediary orbit which is considerably closer to the true orbit than the Keplerian. As a result it can be expected that the perturbations from this orbit converge rather quickly to the true orbit so that first- and second-order perturbations should be adequate for an accurate solution. The theories differ in the form of the "oblateness" term.

The theories of Musen, King-Hele, and Brenner and Latta (a refinement of King-Hele's) determine the orbit by considering perturbations about some slowly moving Keplerian orbit. Musen's theory depends upon a strongly defined perigee and hence is not applicable to low eccentricity orbits. The theories of King-Hele and Brenner and Latta are carried only as far as first-order perturbation and, consequently, will produce precise results only for low eccentricity orbits.

The general perturbation theories afford considerable physical insight into the problem of satellite motions: they determine which parameters are pertinent; they determine the effects of these parameters so that they can be measured indirectly by the observation of satellite motions; they predict the magnitudes of short period, long period, and resonance effects for any given orbit. They are therefore invaluable to the problem of orbit planning. However, owing to the complexity of the expressions involved in these theories, it is very difficult to fit observed data to the analytical orbits. For this reason the problem of orbit determination is most often approahced by carrying out a numerical integration of the equations of motion.

4.4.2 Special Perturbations

The most widely applied special method is the numerical integration of the equations of motion in inertial cartesian coordinates. This is known as Cowell's method. Strictly speaking, this is not a perturbation method, since it is used to determine the orbit itself rather than small departures from some known orbit. While this is the most straightforward numerical method, it suffers in that it generally requires both double precision and very short intervals of integration. These objections however, are being offset by the advent of larger and faster computers. This technique is most useful when the perturbative forces are too large to validate the use of small perturbation techniques.

When the perturbations are sufficiently small, the orbit can be determined by computing departures from a Keplerian orbit. In cartesian coordinates, this technique is called Encke's method. Its advantages are that the intervals of integration can be greatly increased, and that it does not require double precision programming.

Orbit rectification is necessary in the application of either of these two techniques in order to offset the problem of error accumulation. The rectification is accomplished by measurement of the true position and velocity. These quantities are then used as inital conditions for the determination of subsequent positions and velocities. In the present application, the rectification is carried out in conjunction with the "minimum-least-squares" adjustment which replaces the measured positions and velocities by best estimates of these quantities. This refinement minimizes the effects of measurement errors.

Another method which is sometimes used is the variation of parameters method. This method is characterized by a continuous rectification of the reference orbit. This is accomplished by choosing a set of parameters which are unvarying when used to describe the unperturbed orbit. The perturbative forces then cause the parameters to vary. By formulating the equations of motion in terms of these parameters, this variation is continuously accounted for. The advantages of this technique are increased accuracy and decreased computation time. The disadvantages are the complexity of the formulae and the fact that different parameters must be used for different types of orbits.

4.4.3 Perturbed Empirical Orbits

Another approach which has been used to determine orbital elements is the empirical one. The variation of the orbital elements with time is expressed as a Fourier expansion with supplementary terms added. The coefficients in these series are adjusted by comparison with observed variations from observations.

4.4.4 Minimum Variance Techniques

There are a number of reasons for adjusting the parameters according to a minimum variance criterion. Among them are: (1) this technique has a sound theoretical foundation, (2) it is the most easily implemented from among those techniques which are founded in theory, and (3) if the measured values of the parameters in question are normally distributed around the true value, then this technique determines the most probable value of the parameters in question.

In the application of this technique a normal matrix consisting in part of partial derivatives of the orbital variables with respect to the parameters must be constructed and evaluated. These partials can be found in one of several ways. They can, for example, be determined directly from analytical expressions, or the equations of motion can be used to determine the differential equations for the partials in which case these differential equations must be numerically integrated along with the equations of motion. The actual method used should be determined on the basis of the relative complexity and accuracy of the various choices. Since there will be a large number of partials involved in this application, the possibility of computing some of them analytically and the rest by numerical integration should be considered.

4.4.5 Conclusions and Recommendations

With the extreme density of observations in both time and space which will be available, assuming that all of the proposed tracking systems will be utilized as well as the photogrammetric observations over land and altimetry over water, a numerical integration technique may not be the most desireable approach. If a combined analytical and empirical solution were employed to impose the best estimates available for all perturbation parameters, if corrections to these parameters were solved for, and if all uncompensated perturbations by empirical polynomial

terms were absorbed, then such ill-defined forces as upper atmospheric winds will not be as likely to distort the solution. Numerical integration techniques are advantageous for short arc fitting, and are useful in providing numerical checks on other orbital calculational techniques. For very long arcs, numerical integration techniques may require excessive computational time and accuracy. It is however, difficult to choose among the various orbital calculational approaches available, because modern computer capabilities are tending to equalize their relative advantages and disadvantages. The time seems to be quickly approaching when the various schemes can be used with equal confidence.

For the reasons mentioned in Section 4.4.3, it is highly recommended that in choosing a parameter adjustment scheme, a minimum variance technique be used. Because of the number of parameters and the amount of data to be handled, the covariance matrix associated with this technique will contain a large number of elements. Since this matrix must be continually evaluated and inverted, it is to be expected that the parameter adjustment phase of the program will consume much more computer time than the orbit calculations.

4.4.6 References for Section 4.6

1. Kaula, W. M., "Celestial Geodesy, Advances in Geophysics," Academic Press, New York, 1962, pp. 191-293.
2. Baker, R. M. and Makemson, M. W., "An Introduction to Astrodynamics," Academic Press, New York, 1960, pp. 169-205.
3. Mueller, I. I., "Introduction to Satellite Geodesy," Frederick Ungar, New York, 1964, pp. 135-234.
4. Battin, R. H., "Astronautical Guidance," McGraw-Hill Book Company Inc., New York, 1964, pp. 186-219.

4.5 FORCE MEASUREMENT BY ACCELEROMETERS

In the GOPSS program, it is desirable to directly measure nongravitational, or perturbing, forces acting on the vehicle in order to obtain the greatest accuracy in the theoretical models describing the earth's gravitational field and air drag that are deduced from all the data. Accelerometers are well suited to measurement of these forces, and the feasibility of their use has been investigated.

The perturbing forces induce accelerations on the vehicle that range from 10^{-4} g down to values less than 10^{-10} g. From the standpoint of limiting the maximum uncertainty in prediction ahead of position in orbit, it is desirable to measure forces of 10^{-8} g with reasonable accuracy. Thus, a dynamic range of 10^{5} covering an approximate acceleration range of about 10^{-5} g to 10^{-10} g is indicated. From an examination of the state of the art of low g accelerometers, it was found that the Bell miniature electrostatically supported accelerometer (MESA) appears capable of meeting the required performance and has been developed to the point that its use in this program appears entirely feasible, either as a single-axis or a three-axis system.

The major problems associated with the use of accelerometers in a low g orbital application are calibration and the extraneous output induced by the accelerometer location within the vehicle. The MESA is designed such that a continuous variation in range can be obtained by changing the suspension and rebalance voltage. Thus, considerable calibration can be done on the ground down to the minimum obtainable acceleration (about 10^{-5} g) and the results scaled with voltage to the orbital operating range. The one factor which cannot be obtained in a ground calibration is the null bias, principally caused by the mass attraction of the vehicle. In-flight calibration of the null bias appears feasible using vehicle tracking data to determine the decay of the orbit due to drag, which can also be computed using the proper components of accelerometer output.

The problems associated with accelerometer location arise from the inability to locate the accelerometers at the vehicle center of mass and mass attraction (which move during the flight). Any vehicle angular motion causes the accelerometers to sense accelerations which are added to the desired translational accelerations. Since the accelerometer data are to be analyzed after the flight when all of the other flight data will be available, sufficient data on vehicle operation and motion can be recorded to determine these extraneous outputs.

In view of these considerations, the use of a three-axis MESA system located in the Agena forward rack is recommended. Of the three axes, the in-track accelerometer is the most important, since the air-drag effect is significant. It is considered highly desirable, however, to have the other two axes instrumented also, at least on the first two or three flights, because of the many unknowns associated with the problem. The calibration and data analysis necessary to obtain useful accelerometer data appear feasible. A detailed study should be made in Phase II to determine specific data requirements, data analysis techniques, and sources of errors and uncertainties in reduction and interpretation of the data for a realistic accelerometer installation.

An accelerometer measures the force necessary to constrain a proof mass within the case of the accelerometer. In free fall there is no constraint force required and hence no accelerometer output other than biases and intrinsic offsets in the instrument. In a graviational field, an accelerometer measures the force preventing the proof mass from being in free fall; hence an accelerometer can be said to measure gravity in this sense. In an orbital environment, the normal 1 g cannot be measured directly because the vehicle is very nearly in free fall. Thus, an accelerometer is ideally suited to measuring the perturbation accelerations that disturb the satellite from a purely gravitational orbit. Since it is highly desirable to directly measure the effects of these perturbing forces on the vehicle, rather than to obtain them by deduction from tracking data, the use of accelerometers needs to be seriously considered. An additional opportunity that the accelerometer offers is a means of directly obtaining air drag, from which data the validity of the various air drag models can be determined. The characteristics of both the accelerometers and the forces they are required to measure are discussed below as they pertain to the system of interest.

4.5.1 Accelerometer Performance Requirements

The magnitudes of the accelerations induced by the perturbing forces acting on the vehicle, and the accuracy to which these forces need to be measured, determine to a considerable extent the performance required of the accelerometers. The characteristics of these forces are discussed elsewhere, and typical magnitudes are given for the in-track, vertical, and cross-track directions. These may be used to establish approximate values for the operating level and dynamic range of the accelerometers for the three axes.

The vehicle is subject to many cross-track and vertical perturbing accelerations. There are a number of sources of accelerations of the order of 10^{-9} g, such as solar radiation pressure, for instance. There is a potentially larger acceleration due to outgassing of water vapor from the film. The magnitude depends on a number of factors but may be as large as 10^{-7} g. Finally, there are effects due to the attitude-control cold gas jets. These jets generally operate singly and produce 0.5 pounds of thrust for a time duration which is typically 20 milliseconds for a quiet orbital condition. This force acting on a mass of about 175 slugs produces an acceleration of 10^{-4} g, which occurs both in the vertical and cross-track directions.

Along the in-track direction, the air drag is the major perturbing force and is about two orders of magnitude greater than any of the other perturbing forces for an altitude of the order of 150 nautical miles. At this altitude a nominal value of the air-drag-induced acceleration is about 10^{-7} g. This effect is highly dependent on altitude and, for instance, can change two orders of magnitude in going from 100 to 200 nautical miles. Furthermore, there are both spatial and temporal variations in density at a given altitude due to solar activity and other factors. Finally, there are the uncertainties in the data and data reduction used to determine the density model. In view of these circumstances, a reasonable upper level of air drag acceleration is probably between 10^{-5} and 10^{-6} g for the in-track axis. The other major effects which must be considered are in-track components of the attitude control forces. These may occur due to misalignment of the thrust axis of the nozzles or to an angle of attack or sideslip of the vehicle. This effect is about two orders of magnitude lower than the vertical or in-track accelerations caused by the gas jets, or about 10^{-6} g. Thus peak accelerations to be measured in-track would be between 10^{-5} and 10^{-6} g.

Other discussions in Section 4.8 and 4.9 indicate that unknown perturbation accelerations of the order of 10^{-8} g in-track introduce appreciable uncertainties in the determination of position in orbit of the order of the total allowable error budget. Thus accelerations of this magnitude need to be measured. To do so with any accuracy, the threshold of the accelerometers should be no larger than 10^{-9} g and preferably lower. It thus appears that the accelerometers should have a dynamic range of about 10^5 and should have an operating range of about 10^{-9} to 10^{-4} g, or perhaps 10^{-10} to 10^{-5} g.

4.5.2 State of the Art of Low-g Accelerometer Development

There are a number of instruments which have been modified from 1-g designs which appear capable of approaching the range required for orbital application. These are listed in Table 4-3, which is taken from the results of a recent survey performed by Stanford University*. This table lists the pertinent performance parameters of eight such accelerometers, together with comments on reliability, availability, cost, weight, volume, and power requirements. Of these accelerometers, however, only two have been designed expressly for orbital work. These are the Bell MESA and the Bosch Arma Vibrating Spring accelerometers.

The Bell MESA (Miniature Electrostatically Supported Accelerometer) is a single-axis electrostatically suspended and electrostatically pulse rebalanced accelerometer. The proof mass is a flanged cylinder which is supported by eight cross-axis electrodes which have a very low cross-coupling effect with the sensitive axis. This the the predominant factor affecting the minimum measurable acceleration, and with the Bell design, the minimum is reportedly as low as 10^{-12} g. The proof mass is restored to center by the electrostatic forces derived from a voltage pulse triggered by a capacitive pickoff. Thus, the output is a digital pulse rate proportional to the input acceleration. The support and rebalance forces can be scaled by changing the supply voltage to the electrodes. Thus, a high voltage can be used for launch or operation in a 1-g environment, and the voltage can be reduced in orbit to permit measurement of very small accelerations. The scaling is continuous. This device has both the dynamic range and the sensitivity required in the present application.

A number of MESA units have been fabricated. The MESA is supposed to be flight proven by the end of 1965, apparently on a classified flight. The results, if any, of this flight are not known. Several units are to be delivered to NASA Lewis, and this design has been selected for the Advanced Technology Satellite. Inquiries to Bell Aerosystems have indicated that the use of this device in the present program is practical from hardware and delivery standpoints.

The Bosch Arma vibrating string accelerometer is a single-axis device consisting basically of a proof mass supported fore and aft along the sensitive axis by "strings" which are very thin beryllium copper tapes under tension in a magnetic field. The proof mass is supported laterally by a number of strings which provide very high compliance to motion of the proof mass along the sensitive axis but high resistance to motion normal to the sensitive axis.

The fore and aft strings are excited and vibrate at frequencies which are slightly different under zero acceleration. When the proof mass is accelerated, the tension increases in one string and decreases in the other. The changes in tension change the frequency of vibrations; these are measured and converted into an acceleration. The operating range of this device is determined by

* References are listed in Section 4.5.5.

the mass of the proof mass. A dual range device has been built in which, for low g operation, a second and much larger mass is clamped onto the smaller initial mass when in orbit. This device posses the required dynamic range for the present requirement, but does not have as low an operating range as the MESA, although it may be adequate.

The vibrating string accelerometer has been developed and two units have been delivered to the Air Force. It has not been determined whether these units have been or are to be flight tested in the near future. Inquiries to Bosch Arma have indicated that the device is not sufficiently far along in the development stage to warrent serious consideration for this program.

The environmental requirements of both the MESA and the vibrating string units are modest, if the ultimate in performance is not required. Both can operate in a vacuum and require only a nominal temperature environment, provided the temperature gradients within the instruments are small. However, if the full 10^5 dynamic range is to be obtained, a thermal environment with a temperature control of ±1 degree is required.

Both units have been developed and delivered to date as single-axis instruments. However, there is no fundamental reason why a three-axis device cannot be built, and this may, in fact, now be under development. At the least, however, three single-axis units could be used, if so desired, at some penalty in weight, size, and power requirement over an integrated three-axis design.

4.5.3 Installation and Operational Considerations

The concern in this section is with the influence of the vehicle and its operation in orbit on accelerometer output. Three areas are discussed: installation considerations, methods of calibration, and data analysis.

4.5.3.1 Installation Considerations

The first consideration has to do with the environment and equipment requirements imposed on the vehicle by the accelerometers. As has been indicated previously, the accelerometers do not require any pressurization to operate satisfactorily. However, a controlled thermal environment will be required to achieve the desired level of performance. Since the accelerometers will probably be located in the forward rack area of the Agena, there will be a greater temperature variation than can be tolerated for the ultimate in accelerometer performance, which is on the order of ± 1 °F. The most reasonable solution is a container surrounding the accelerometers which has an active thermal control system, much as the Agena attitude control gyros have. The container would be supplied by the accelerometer manufacturer, based on compartment temperature excursions determined by the system thermal design. Approximate power requirements for thermal control are shown in Table 4-3; power requirements for a three-axis MESA would perhaps be an average of 5 watts continuously. This number can change considerably based on the detailed thermal design, and would have to be more accurately determined during the Phase II design program. The accelerometers are not sensitive to external magnetic fields and need not be shielded. The weight and volume requirements are noted in Table 4-3 and are not excessive. The outputs of the accelerometers are basically pulses, each pulse corresponding to a velocity increment of the vehicle. The number of pulses needs to be recorded and can be put on magnetic tape.

The second consideration involves the orientation of the accelerometers. It would be most desirable to align the sensitive axes of the accelerometers with (and normal to) the velocity vector. Thus, direct in-track measurements would be obtained. However, this is impractical,

[redacted]

Table 4-3 — Accelerometers for Orbital Use

Type	Operating Range(s), Dynamic Range	Dynamic Range	Performance	Lab Tests	Simulation of Orbital Calibration (e.g., flotation with liquid or gas)	Power	Weight	Volume	Reliability	Cost	Availability	Comments
ESA – 3 axis analog force rebalance.	May go as low as 10^{-9} to 10^{-10} g	10^5 analog (10^6 being developed)	Design goals all errors 2×10^{-5} of preload (maximum support capacity)		Gas flotation with modification of gap dimension	6 watts	5 pound ESG, 10 pound electronics for ESG (ESA would require less)	65 in.^{3} (ESG)	Many hours of field experience as ESG; 40,000 hour MTBF for entire ESG	[redacted] (estimated)	+9 months	Present ESA is the support system for the ESG. A pulse rebalance system is being developed.
ESA – 1 axis with electrical support for the other axes. Pulse rebalance (5 hr maximum).	10^{-2} to 10^{-4} g 10^{-1} to 10^{05} g; others may be chosen	10^5	1. 0.5ug/cross axis g ^{2}F; 0.01 to 0.04 percent scale factor/$^\circ$F 2. Negligible magnetic sensitivity 3. Cross coupling 10^{-4} to 10^{-5} g/cross axis g is principal limitation	3 to 5×10^{-7} g on quiet pad, Lotts load, 0.2 arc second optical reading resolution 10^{-7} g	Flotation not practical; calibrated on 1 g range and scaled	3.5 watts (3 axis + 6 watts) +3 to 5 watts for temperature control if needed	4 pounds including electronics (3-axis, 10 pounds) 3 pound design in process	100 in.^{3} (3 axis)	To be flight tested in 1965. Will stand 100 g launch environment.	[redacted]	8 months delivery 1 units delivered 1965	Selected for advanced technology satellite now in definition phase
Vibrating string, 1 axis, frequency difference output. PM preload 1 hz.	1 to 10^5 g 10^{-4} to 10^{-9} g	10^5	1. Third order nonlinearity 30ug/g^2 (can be calibrated) 2. Bias drift improves with age 10ug/day initial, 0.4ug/day after a year for 30 g design 3. 40 $^\circ$F – log, 10^{-1} of full scale for +0.5 $^\circ$F for 30 g design	Dual proof mass (ratio 10^5) permits lab calibration by conventional techniques. Obtained 10^{-7} g resolution using dividing head and optical measurement. Feels 10^{-9} g possible on quiet pad (disturbances are all long term)	Flotation not applicable; uses dual proof mass for calibration	1 watt including electronics +10 watt temperature control if needed	18 pounds (5 pounds for future units)	+300 in.^{3} (3 axis) (200 in.^{3} for future units)	30 g conventional vibrating string with extensive field data; 300,000 hour MTBF	[redacted]	2 built in 1964	John Hopkins APL interested for drag measurements
Force rebalance, 1 axis pendulum. Flexure support pulse or analog.	10^{-2} to 10^{-6} g (goal)	10^5 (goal)	Design goals, accuracy 10^{-6}, low temperature sensitivity	JPL unit used as level indicator in range of 10^{-7} g	Gas or liquid flotation possible	10 to 100 milliwatts	50 to 100 grams	< 100 cc (10 in.^{3})			2 years	In preliminary stages
Torque rebalance, 1 axis, floated.	As low as 10^{-7} or 10^{-8} g				Not applicable	Heater 30 watts (total)	17 pounds (gyro)	+300 in.^{3}	Gyro; field proven; 2-year life			Example of modification of 1-axis gyros
Force rebalance, 1-axis pendulum. Flexure support, pulse or analog.	10 to 10^5 g (studies to 10^{-10} g)	10^7 (in use, errors limit to 10^5)	(PM12, PM01) 1. 2×10^{-7} of full scale/ F 2. 10^{-5} g/day drift without shock and vibration disturbance	2 units (back to back) on pier 5×10^{-6} g limited by test equipment	Patent held for a case rotation orbital calibration technique	1 to 2 watts, including electronics; heater as low as 2 watts	0.25 pound instrument +0.25 pound electronics + packaging	5 in.^{3} including electronics	PM01: 100,000 hour MTBF PM12: [redacted] for 10 months	[redacted]	4 to 6 months	PM12 has five times the predictability of PM01. With development could get another factor of 5 or 10.
Quartz resonator, 1 axis, PM output $\Delta f = 1$ percent f.	10^{-1} to 10^{-7} g	10^5	1. Repeatability 10^{-5} 2. Calibratable nonlinearities 10^{-4} 3. Performance limited to 10^{-4} by frequency drift in crystals (new design to improve)		Flotation not applicable	1 to 2 watts (maximum)	+5 pounds				6 to 18 months	100× increase in existing proof mass to be developed, if funded.
Floated, 1 axis pendulum, analog force rebalance.	10 to 10^{-6} g	10^5	1. Require temperature control 2. 10^{-5} to 10^{-6} g/day drift on selected units (some may be as poor as 10^{-4} g/day)		Flotation not applicable	5 watts (10 watts maximum) ?	7 ounces + electronics	2.5 in.^{3} + electronics	Have built 10,000 units		3 months	

and an alignment with vehicle axes would be used. The possibility then arises of cross-coupling effects. An angle of attack or slideslip would cause a component of a relatively large air-drag acceleration to appear in the cross-track or vertical accelerometer outputs, which might mask other, smaller perturbations along these axes. The importance of this effect depends on the excursions permitted by the vehicle attitude control system. For typical variations in pitch and yaw of 20 minutes of arc, the cross-coupling effect would be proportional to sine (20 minutes) or 6×10^{-3}. Thus, the maximum air-drag component appearing in the cross-track and vertical accelerometer outputs would be the order of 10^{-9} g. This would be a variable error whose magnitude could be obtained by continuously recording vehicle attitude. In any case, attitude information would be necessary to convert the vehicle axis readings into a velocity-vector-oriented axis system.

A fixed error due to accelerometer orientation would arise from misalignment of the accelerometer sensitive axes with vehicle axes. Both the relations between the accelerometer axis and the mounting flange and the flange-to-vehicle axis must be controlled very accurately. The former can be controlled to within one minute of arc by proper manufacturing procedures. The latter can also be controlled accurately (the gyro alignment problem is similar), but considerable care must be taken in alignment upon installation of the accelerometers into the vehicle. One possibility is optical alignment using an accurately aligned reflecting surface on the accelerometer assembly and a theodolite. This or other techniques must be considered during the detail design phase, and uncertainties in alignment should be considered in the data analysis study.

The third consideration has to do with the location of the accelerometer with respect to the vehicle center of gravity. The vehicle undergoes angular velocities and accelerations induced by perturbation forces, the attitude control system and, in the pitch plane, the orbital rate. In addition, there may be angular motion due to programmed motions, such as the camera calibration maneuver or the payload ejection maneuver. During these angular motions about the center of gravity (center of rotation), any point in the vehicle not at the center of rotation will sustain a centripetal acceleration aligned along a radius vector from the center of rotation to the point. Thus, an accelerometer mounted away from the center of rotation will put out a signal due just to the vehicle rotation, in addition to any signals due to the acceleration of the vehicle center of mass itself and the resulting solid body translation. The magnitude of this effect can be estimated by using typical angular rates together with a distance from the accelerometer to the center of rotation. The center of mass will be on, or very near, the longitudinal axis of the Agena, very likely in the propellant tank. A reasonable assumption for the location of the accelerometers would be on the forward rack of the Agena on the vehicle centerline, which would place them perhaps 5 feet forward of the center of mass. The orbital rate is approximately 2π radians per 90 minutes and the vehicle rotates in the pitch plane. The centripetal acceleration due to this angular velocity at a distance of 5 feet is about 2×10^{-7} g. This acceleration would appear in the in-track accelerometer ouput and is of the same order as the air-drag effect. This is, however, a predictable error that can be accounted for in the data analysis process. The normal maximum angular motions induced by the pitch attitude control are on the order of 10^{-4} radians per second. This angular velocity is an order of magnitude smaller than the orbital rate and thus produces a centripetal acceleration signal two orders of magnitude smaller, or about 2×10^{-9} g. A similar yawing angular velocity caused by the attitude control jets would produce the same signal on the same (in-track) accelerometer. These effects occur randomly in time and can only be eliminated from the accelerometer data by having vehicle attitude rate data available. However, they are two orders of magnitude lower than the air-drag effect and may be unimportant.

Steady angular velocities in pitch, roll, and yaw will not produce signals in the vertical and cross-track accelerometers if they are on the vehicle centerline. However, angular accelerations in pitch and yaw will. If we take the pitch attitude control thrust to be 0.5 pound acting 25 feet from the center of mass, this will produce an angular acceleration in pitch ($\dot{q}$) of about 4×10^{-4} rad/sec^2. The vertical acceleration at the accelerometer location 5 feet from center of mass will be about 10^{-4} g. A similar effect will be obtained in the cross-track accelerometer due to a yawing angular acceleration. These effects will last for the duration of the attitude control jet pulse, which is on the order of 20 milliseconds in a typical orbital mode. Again, the effects are random in time and can only be eliminated from the data by separate angular acceleration rate data. In this case, however, the signals due to vehicle rotation completely dominate any signals due to solid body translation caused by perturbing forces. Thus, it is most important that good vehicle rate data be obtained and properly employed in the data analysis.

Another factor which becomes important in this program is the accuracy with which the location of the launch center of gravity of the vehicle is known and the distance it moves during the flight. The launch center of gravity is determined during the vehicle manufacture and assembly by a combination of weight measurement and computation, and is known reasonably well (probably less than 1-inch uncertainty). For a nominal axial distance from the vehicle center of gravity to accelerometer location of 5 feet, an uncertainty along the vehicle centerline in the launch center of gravity of 1 inch represents about two percent uncertainty in the corrections that are applied during the data analysis to the in-track accelerometer data to remove vehicle motion effects from the data. For instance, the orbital rate correction uncertainty is about 3×10^{-9} g. If the accelerometers are mounted on the vehicle longitudinal axis, upon which the center of gravity is assumed to be, but the center of gravity is off the axis by, say, 1 inch, a number of additional effects due to angular velocity and acceleration are introduced into the accelerometer outputs. For instance, roll effects will then be present, and a pitch acceleration ($\dot{q}$) component will appear in the in-track accelerometer output. These effects will be quite small, however, and should be negligible.

The above considerations for uncertainty in launch center-of-gravity location apply equally to the location uncertainty due to center of gravity movement during flight. The two main causes of center of gravity movement are the film motion, which produces basically a longitudinal forward movement of about 9 inches, and the gas ejected overboard by the attitude control, which also produces basically a forward longitudinal movement of about 7 inches. In the post-flight data analysis, information on film usage rate and control gas usage will be available. The latter can be obtained from the gas valve firing data and the gas valve characteristics.. The film usage rate information will be very accurate (for center of gravity shift calculation purposes); the gas usage data will be less accurate because any bias errors in estimated valve performance will integrated as the center of gravity shift throughout the flight is computed. The uncertainties in the accelerometer data due to the center-of-gravity location uncertainty (both at launch and during flight) will be of the same magnitude as the null output and are not considered to be sufficiently large to affect the usefulness of the data. However, these effects need to be considered in the planning of the data analysis in Phase II in order to determine the magnitudes of the effects, their uncertainties, and the resultant effect on orbit position error determination.

The fourth consideration involves the influence of the location of the accelerometers within the vehicle on the mass attraction between the proof mass and the vehicle. Between any two masses, there exists an attractive force lying along the line connecting their centers of mass whose magnitude is given by the expression M_1M_2G/R^2, where M_1 and M_2 are the two masses,

G is the universal gravitational constant and R is the distance separating the two masses. Such an attraction exists between all elements of mass of the vehicle and the accelerometer proof mass. If the accelerometer is placed at the vehicle center of mass attraction, these attractive forces cancel when integrated over the entire vehicle.

As was indicated above, it is unlikely that the accelerometers will be located at the center of mass. (The centers of mass and mass attraction are not necessarily coincident, although they will be close). Consequently, an order of magnitude calculation was made to determine the size of the mass attraction effect for the in-track accelerometer. It was assumed to be located one foot aft of the interface between the Agena and the DCM. The vehicle mass was represented as four point masses located along the vehicle centerline: the Agena, the DCM, the film, and the recovery section. The film was considered separately so the effect of its movement forward during flight could be assessed. With the film in the supply cannister, the acceleration of the proof mass due to mass attraction was about 3×10^{-9} g, which is about two orders less than the air-drag effect. After the film was transported forward into the recovery sections, the mass attraction acceleration was about 10^{-9}g. This effect appears as a bias in the accelerometer output, and, with the film motion and attitude control gas usage, the bias will change with time during the mission. With an accelerometer set for a range of 10^{-4} to 10^{-9} g, the mass attraction biases computed above are of the same order as the null output of the accelerometer. For measurements of air drag of 10^{-7} g, the bias is 1 to 3 percent of the drag acceleration, which is relatively small. The uncertainty in mass attraction bias is even smaller. Thus, it appears that mass attraction bias will not be significant problem, at least at an altitude of 150 nautical miles.

The vertical and cross-track accelerometers will also sustain the same type of bias. However, since these two accelerometers have their sensitive axes at right angles (essentially) to the general motion of the film, these biases should change considerably less than that of the in-track accelerometer as the film is transported forward (or as gas is used). It should also be indicated that a detailed study (similar to a weights and balance study) can be made of the entire vehicle configuration to determine reasonably accurately the magnitude of the self-attraction bias. While it is desirable to check the in-track accelerometer bias by in-flight calibration, it is not as important to do so for the other two axes.

4.5.3.2 Calibration

The performance parameters of a low-g (10^{-4} to 10^{-10}) accelerometer such as the Bell MESA, that are of interest are the null output, stability, bias, and the scale factor linearity and stability. Of these, information on null output and stability, and scale factor linearity and stability can be derived from tests on the ground in a 1-g environment. However, there is no method of obtaining null bias in a 1-g environment, and recourse must be had to its measurement or calibration in flight. The following discussion is divided into considerations of methods of calibration prior to launch and methods available in flight.

The feature of the MESA design that permits its use in measuring very low acceleration levels is its capability to have the cross axis suspension force level reduced as the measurement level is reduced, since suspension cross-coupling effects determine the minimum measurable acceleration. This feature permits considerable calibration to be done in a 1-g environment, with subsequent scaling to a low g-range. The basic method used consists of mounting the accelerometer on a precision dividing head located in an extremely quiet environment. As the head is rotated, the acceleration along the sensitive axis can be changed from "zero" to 1 g.

The minimum practical acceleration that can be obtained in this manner is about 10^{-5} g, which corresponds to an angular attitude of the sensitive axis of 2 seconds of arc from the horizontal. A given angle can be resolved with optical reading to about 0.2 second of arc, which corresponds to a resolution of 10^{-7} g. Using this technique, scale factor linearity, repeatibility, and stability can be determined for a range down to perhaps 10^{-5} g. Since the null output varies with the cross axis suspension level, the variation of null output with suspension level can be obtained by changing the suspension excitation voltage and measuring the output pulse-rate variation. The known scale factor can then be used to obtain the null output for a given acceleration range (or excitation voltage). Temperature sensitivity of scale factor and null output can also be obtained with the dividing head. Since the suspension and rebalance forces scale in a known manner with excitation voltage, the results obtained for a 1 to 10^{-5} g range can be scaled to, say, a 10^{-4} to 10^{-9} range to obtain the anticipated performance in orbit.

While much calibration information can be obtained prior to launch, it is highly desirable to obtain calibration data in orbit as well. Of greatest importance is knowledge of the null bias, particularly as affected by the vehicle installation, since this information cannot be obtained in a 1-g environment. Of importance also is information on scale factor, since the launch and orbital environments may cause changes in performance over that determined prior to launch. The factors contributing to variations in accelerometer performance could include temperature variations, power supply variations, vibration, shock, and vehicle mass attraction effects.

For null bias, a method is available whereby the fixed or slowly changing bias of the in-track accelerometer can be determined from flight data. Considerable data will be available on the velocity and position of the vehicle during many orbits. These would include clock time, photography, ground tracking, and altimeter data. From this information, the decay of the orbit and the energy lost in a given time, say one or two orbital periods, will be known to a high accuracy. This energy is lost because of nongravitational forces present in the in-track direction. The in-track accelerometer output, together with the vehicle mass, will give the variations of in-track drag with time over the same period. The product of vehicle velocity and the drag given by the accelerometer is the rate of decrease of energy; this rate integrated over the given time will also give the total energy lost. These two values of decrease of energy will, in general, be different because of the errors and bias of the accelerometer. If these are assumed constant over the period of integration, their magnitude can be determined. This correction can then be applied to the instantaneous accelerometer readings to get true accelerations due to perturbing forces in the in-track direction. It should be noted that since the accelerometer data will not be available during the flight, this calibration work will occur during the post-flight data analysis, and the time intervals for integration can be selected on the basis of expected time constants of the bias and the quality and quantity of vehicle position and velocity data. The time increment over which the computation is made will also depend upon the altitude, or size of the drag. A low altitude, or high drag, will give a relatively large change in orbital period per revolution, which can be accurately determined. The higher the altitude, the smaller the change in period per revolution and the greater the number of revolutions required for a given accuracy. Another factor that must be considered is the short term cyclic changes in period due to gravitational inhomogenieties which are superimposed on the secular period change due to drag. These two effects can be of the same order of magnitude. However, again, since all of the flight data are available during the data analysis, these two effects can be distinguished and the secular change obtained.

Cross-coupling effects between accelerometer axes will have to be taken into account using this calibration technique, and may, in fact, form a basis for using this technique for calibration of the cross-track and vertical accelerometers. Since the in-track drag must be

used with the energy decay computation, the in-track accelerometer output must be corrected throughout the integration interval for any deviations of the longitudinal axis from the in-track direction (angles of attack and sideslip). This can be done using recorded vehicle attitude control system information. In addition, the possibility exists that the vehicle can be flown successively at moderately small angles of attack and sideslip in order to obtain an in-track drag component along the vertical and cross-track accelerometer axes. For instance, an angle of attack of 20 degrees will provide a component along the vertical accelerometer axis of 1/3 of the in-track drag which, in turn, will be on the order of twice the zero angle drag.* Since such vehicle altitudes would have to be maintained for at least an orbit with the attendant higher drag and more extensive control gas valve operation, it would be desirable to accomplish this calibration once near the end of the flight. Since the biases in these two accelerometers will be much less affected by film motion and gas usage than that of the in-track accelerometer, one calibration per flight probably would be sufficient.

A second method for obtaining the mass attraction bias is suggested in Reference 3. If two accelerometers are located along a given vehicle axis at different distances from the center of mass attraction with their sensitive axes accurately aligned with the vehicle axis, the mass attraction bias will be different for each accelerometer. For instance, in the example cited in the previous section, the mass attraction acceleration for the in-track accelerometer 1 foot aft of the Agena-DCM interface (all film in the recovery section) is about 10^{-9} g. An in-track accelerometer located 2 feet further forward would have a mass attraction of 4.4×10^{-9} g, based on the same approximate calculational model. The differences in output of these two accelerometers for a given in-track drag would contain this bias difference, as well as bias differences in the suspension and cross coupling of the accelerometers, differences due to scale factor, and centripetal accelerations due to vehicle angular motion. Depending on the accuracy to which the vehicle center of gravity is known, the uncertainty due to the vehicle angular motion correction could be as high as 3×10^{-9} g, as indicated previously. In addition, the null output due to suspension cross coupling will be on the order of 10^{-9} g if the accelerometer is scaled to the 10^{-4} to 10^{-9} g range. Furthermore, an additional accelerometer for each axis is required, with attendant weight, space, and power demands. Thus, this method of deducing mass attraction bias does not appear attractive at this time. However, the detailed system study may change this conclusion if, for example, only one axis is instrumented, or if the accelerometer range is enlarged or changed, or if the center of gravity uncertainty is very small, or if it proves desirable to have two coaxial instruments of different, but overlapping, ranges.

A method of obtaining an inflight determination of scale factor is suggested in Reference 3. The method consists of moving a known mass a known distance, where both the initial and final mass positions are accurately known with respect to the accelerometer location. Since the mass attraction of the known mass is accurately known, this method amounts to imposing a known acceleration change on the accelerometer at a known time and measuring its output. The uncertainties in the other inputs, such as vehicle motion effects, are not significant, provided the test mass is moved rapidly compared to the time constants of the other inputs. The feasibility of this method depends to a great extent on the range to which the accelerometer is scaled, because it is difficult to impose acceleration changes greater than 5×10^{-9} g with a practical mass size (say 20 to 30 pounds) and initial separation distance. Thus, the calibration acceleration input is of a sufficiently small size that the accuracy in output is very low. This method is better adapted to a case where the accelerometer is scaled to 10^{-10} g minimum reading, or lower.

---

* The analysis of Reference 2 for a vehicle having the fineness ratio of the order of 7 to 9 was used to obtain the variation of drag coefficient with angle of attack.

A variation of this method would use the vehicle as the test mass and move the accelerometer away from the center of mass attraction. Since the vehicle mass attraction is on the order of 10^{-9} g, the same accuracy problem exists as before. There is an additional loss in accuracy due to the position uncertainty of the center of mass attraction. Again, the method is better adapted to a lower g range.

An additional method for determining accelerometer bias for all three axes is suggested by the procedure to be followed after a flight in fitting the various data to an analytical orbital model. In this procedure, data will be input to a computer in the form of the reading plus an unknown bias. The computer forms the best fit of all the readings to a basic model which then gives the values of the various constants in the model and values of the biases. Although the specific details have not been worked out, it should be possible to treat the accelerometer data for all three axes in the same fashion. Some preconditioning of the data will probably be required to remove vehicle motion effects and perhaps other known biases. This technique will produce information on accelerometer biases which can be compared with other sources of bias computation to evaluate the accelerometer data and data analysis techniques.

In summary, calibration of the accelerometers prior to launch will give results for scale factor linearity, stability, and temperature sensitivity, null stability, and an indication of null output. These results can be scaled with suspension voltage to values appropriate to the orbital g range. The major anticipated vehicle influence, mass attraction bias, can be computed reasonably accurately and is anticipated to be on the order of the null output, that is, 10^{-9} g. In-flight calibration of fixed or slowly varying biases appears feasible for the in-track accelerometer and possibly for the other two axes also. In-flight calibration for scale factor for any axis does not appear promising at this time, based on a 10^{-4} to 10^{-9} g range, but may be feasible if the range is lowered to 10^{-10} g. The data fitting process performed during the postflight data analysis can serve as an additional check on the estimation of accelerometer bias for all three axes.

4.5.3.3 Data Analysis

In this program, there is no requirement for real time processing and analysis of most of the flight data. The significant data reduction, analysis, and interpretation will be done after the flight when all the data are available. Specifically, in the reduction and analysis of accelerometer data, other information on vehicle motion and position, radar altitude, attitude control system operation, and ground tracking data will be available to aid in interpretation. Some of the considerations involved in using these data are described below.

The accelerometer data contains, in addition to vehicle translation accelerations due to perturbing forces, output ("or noise") from the following sources: vehicle angular motion about a center of mass whose location changes with time; null bias due to vehicle mass attraction (also time varying); uncertainties in null output and scale factor due to possible changes in accelerometer characteristics from prelaunch calibration to flight environment; and cross-coupling effects between accelerometer axes due to angles of attack, sideslip, and bank. The calibration problems are considered in the previous section. Knowledge of the other inputs depends on obtaining data which will yield the motion of the vehicle center of mass, center of mass attraction, vehicle attitude, and attitude rates.

As has been indicated, the vehicle center of mass will be known to probably within 1-inch uncertainty for the flight condition at orbit injection after all of the fuel has been dumped. The factors that will cause travel of the center of mass are motion of the film forward as it is exposed,

and usage of gas by the attitude control. Since information will be available on the operation of the camera, the effect of film motion on center of mass travel can be computed as a function of flight time with only a small uncertainty. Control gas usage rate must be obtained more indirectly.

The Agena cold-gas attitude control system has been used for a number of years, and a considerable amount of information is available on its operation. The principle of operation is shown in the following sketch.

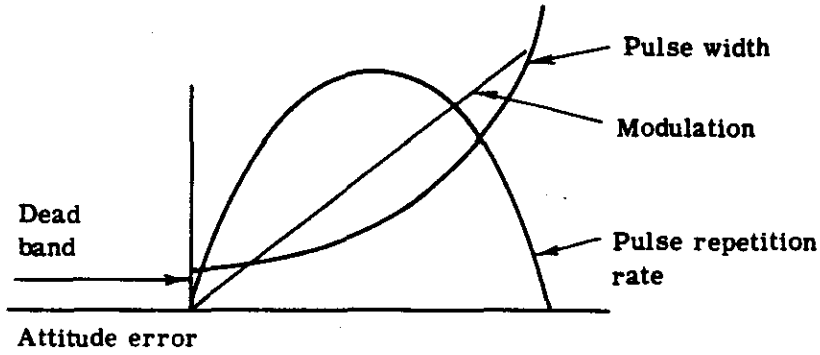

Both attitude and attitude rate are used to determine an error. When the error exceeds the dead band width, one or two gas valves open to emit a pulse of gas. The pulse width increases as the magnitude of error increases, as shown. The pulse repetition rate also depends on the magnitude of the error, as shown. The product of these two determines the modulation factor, or overall characteristic of the system. Large errors are characterized by infrequent long pulses such that the valve is open most of the time. Under normal quiet orbital operation, the error does not greatly exceed the dead band value. The pulse width curve is relatively flat, so that the pulse width can be assumed constant at about 20 milliseconds. The repetition rate will then vary to supply sufficient torque to keep the vehicle oscillating about the dead band or against one end of the dead band, depending on the perturbing forces. A typical repetition rate is on the order of one pulse per minute. Although Itek does not have the specific data, it is very probable that the valve flow characteristics are very well known, both typical performance and statistical variations from the mean. Consequently, with a known pulse width, the gas usage rate can be determined by recording when each valve fires. Such data have been obtained in the past on Agena flights. The pulse repetition rate will indicate whether or not the control system is operating on the flat end of the pulse width curve. If the flow characteristics for the specific valves installed are not available, typical characteristics may be used, and an error analysis can be made using the statistical performance data. For the case where the specific valve performance has not been measured and is different from the assumed mean performances, a consistent error in gas usage will be computed. However, the error should be small and can probably be neglected in computing center of mass travel.

The center of mass attraction must be determined analytically. Its travel during the flight is also dependent upon film usage and control gas usage. The computation of travel can be made using the same methods of mass-motion determination as described above.

The vehicle attitude and attitude rate can be determined by recording appropriate information from the attitude control system. The Agena system uses gyros for short-term attitude information. These are corrected periodically by the horizon sensors, since the gyros will drift with time. In addition, the pitch gyro is continuously torqued at a rate equal to the orbital rate. There is considerably more noise in the horizon sensor output than in the gyro output. Consequently, the method of getting the best data out of the system consists of measuring attitude using the gyro output for relatively short-time periods and checking this with the horizon sensor data. The attitude data are differentiated to give angular velocity and acceleration information. Smoothing of the data during the differentiation and back-integration process is used to improve the quality of the data. A check on the data can be obtained by correlating measured acceleration with operation of the gas valves. Since the roll and yaw axes are coupled in the control system, care must be taken to properly interpret the roll and yaw attitude data.

Using these techniques and data, the magnitudes of the major nontranslational effects can be obtained and removed from the accelerometer data in order to obtain the desired translational effects due to perturbation forces on the vehicle. The accuracy with which this can be done is difficult to assess but is probably reasonably high. During the Phase II work, a detailed study should be made of this entire area of accelerometer data handling to determine methods, accuracies, and uncertainties in obtaining the desired data.

4.5.4 Evaluation of the Utility of Accelerometers

It is highly desirable to have aboard the vehicle instruments to measure directly the perturbing forces acting on the vehicle. By their basic nature accelerometers are ideal devices for obtaining such forces. A state-of-the-art survey has shown that an accelerometer possessing the proper sensitivity and dynamic range has been developed and proven to the point where its use in this program is considered feasible. Its demands on vehicle power and data storage do not seem unreasonable. The question remaining is whether or not the accelerometer data, with their known and unknown errors, biases, and extraneous input, are sufficiently valuable to warrant the design and development effort associated with installation, operation, and readout of the accelerometers in the vehicle and the subsequent data reduction program.

The major problems with undesirable content in the accelerometer output stem from the location within the vehicle of the accelerometers. It has been indicated that bias due to vehicle self-attraction and signals due to vehicle rotation, as opposed to translation, are functions of the distance from the accelerometers to the center-of-mass attraction and center of mass, respectively. These two locations are not identical but are probably very close. As this distance decreases, the undesirable content of the accelerometer output decreases. Until a detailed study of the installation problem is made, the sizes of these effects will not be known. The nature of the effects and methods for their computation and/or calibration have been discussed. From the discussion, it appears feasible to use accelerometers and operate on their output to obtain reasonably accurate and valuable information. In view of the desirability of having accelerometer data, it is strongly recommended that accelerometers be used and that a detailed study be made to consider the sizes of the undesirable effects for a practical installation and ways in which the uncertainty in their magnitudes can be reduced by ground and in-flight calibration and test techniques and processing methods in the data reduction program.

It has been noted that the uncertainties in the in-track components of perturbing forces cause much greater uncertainties in position prediction than those in the vertical and cross-track forces. Thus, accelerometer data for the in-track axis is more desirable than data for the other two axes.

It is felt that because of the many unknowns associated with this problem, a three-axis accelerometer system should be installed in the first two or three flights, providing the power, readout, and installation requirements are not unreasonably great. However, examination of the vertical and cross-track data may show that no significant advantages result from obtaining these data. If so, these two accelerometers can be removed in subsequent flights. It is better to follow this procedure than to discover that significant effects were occurring in these two axes which were not measured because instrumentation was not provided.

4.5.5 References for Section 4.5

1. Final Engineering Report of Advanced Research in Guidance, Control, and Instrumentation, Stanford University Report, Contract AF33(615)-1411 (January, 1966).
2. Sentman, L. H., Free Molecule Flow Theory and Its Application to the Determination of Aerodynamic Forces, Lockheed Missiles and Space Company, AD 265409 (1961).
3. Evaluation of the Performance Characteristics of the Miniature Electrostatic Accelerometer (MESA) in a Manned Orbiting Vehicle, Bell Aerosystems Report No. 6500-953001 (July 1965).

4.6 THE ZERO-DRAG SATELLITE

The zero-drag satellite is desirable from the standpoint of enabling an orbit controlled essentially only by gravitational effects. Under these circumstances, the vehicle position and velocity tracking data can be considered to reflect only the gravitational effects and may be used to directly fit a gravitational model. The uncertainties associated with the prediction of future orbital positions are considerably reduced. In addition, considerations of the force required to balance the in-track component of the perturbing forces can be used to produce an air drag and an air density model.

There are a number of practical difficulties of implementing a zero-drag concept. Foremost among these are the necessity for locating the proof mass at the centers of mass and mass attraction of the vehicle, incorporating a low level, in-track thrust system in the vehicle, and combining the zero drag and attitude control systems, at least in the case of a three-axis system. The technology required to achieve a zero-drag satellite is relatively new and undeveloped, although the small amount of work done to date indicates that a system nulled to forces per unit mass of the order of 10^{-9} g is mechanically feasible.

In view of these considerations, a major redesign of any existing orbital vehicle would be required to incorporate a zero-drag capability, even in only one axis (in-track). The schedule of the present program precludes success in obtaining reliable flight hardware for a three-axis, zero-drag system. It is considered worthwhile, however, to initiate a study to determine the feasibility of a one-axis in-track system, with the possibility that later flights in this program might incorporate such hardward. Such a study is recommended, particularly since in-track forces are much more effective in influencing satellite orbital positions than forces directed in the cross track or altitude directions.

Consider an orbital vehicle containing a completely enclosed cavity within which is a spherical proof mass. The vehicle is equipped with a translation control system that causes the vehicle to pursue the proof mass such that the two never touch. Since the cavity shields the proof mass from such effects as air drag and solar pressure, the orgit of the proof mass, and thus of the vehicle, is determined almost entirely only by gravitational forces. If this arrangement can be achieved in a practical system, the effect of the major perturbing forces is automatically eliminated from the orbit, and the vehicle's position will be determined only by the earth's geopotential and solar-lunar gravitational effects. This greatly reduces the uncertainties in the computation and the prediction of future orbital positions. An alternate, but equivalent (in principle) method is to measure accelerations and use the accelerometer output as an error signal to drive a feedback control system to produce the necessary forces to counteract disturbances. The considerations involved in the use of such a system for the present application are discussed in this section.

4.6.1 Design Requirements of the Zero-Drag Satellite

There are a number of limitations and/or design features that the drag-free principle imposes on the orbiting vehicle. The first of these involves the thrust capability of the vehicle. The Agena vehicle normally has a cold gas reaction attitude control system comprised of nozzles located at the aft end of the vehicle and oriented in a plane normal to the vehicle centerline. In addition, there is a restartable engine used for orbit adjustment which provides a thrust along the vehicle axis. However, none of these control systems provide the low level, continuous force in the in-track direction that is required for drag compensation. At an altitude of 150 nautical miles, the air drag is approximately 10^{-3} pounds. Thus, an in-track thrust system would have to be incorporated in the Agena to provide this level of thrust. With a typical freon-nitrogen gas mixture having a specific impulse of 50 seconds, approximately 35 pounds of gas would be consumed during a 15-day mission. Thus, the thrust system for drag compensation would be similar in weight and size to the present attitude control system.

In the vertical and cross-track directions, the present attitude control system provides a 0.5 pound thrust pulse whose pulse length and repetition rate vary according to the attitude error signal. The perturbation forces in these directions arising from all causes except the attitude control are at least two orders below the in-track air drag. Thus, extremely small forces (on the average) would be required to obtain a zero-g orbit in these two directions. These forces could be obtained from pulsing small thrusters. Since there would be two demands made on the thrusters acting in the vertical and cross-track directions, the attitude control and zero-g control functions would have to be combined to achieve both results simultaneously. Very likely, the attitude control mode would have to be changed to a pure couple from the present unbalanced force method, and an unbalanced force mode used to obtain zero-g. The locations of the thrusters would have to be changed since it is not possible at present to obtain a pure couple in either yaw or pitch. Thus, a new study would have to be made of the entire attitude-zero-g control problem, and the implementation of the results of the study would involve, at a minimum, relocation of the control thrusters and, very likely, considerably more modification to the present system.

The second design feature that the zero-drag principle imposes on the vehicle is the limitation on proof mass location within the vehicle. The two effects which arise are the accelerations that the proof mass senses due to vehicle angular motion if the proof mass is not located at the center of mass, and the mass attraction that can bias the proof mass if it is not located at the point of zero mass attraction of the vehicle. These two points are not necessarily coincident. In order to obtain an orbit which, for all practical purposes, is purely gravitational, the perturbing accelerations should be kept below about 10^{-9} g. The magnitudes of the vehicle rotation and mass attraction effects were given in connection with the discussion of accelerometers. It was noted that accelerations of about 10^{-7} g are induced by the orbital angular rate if the proof mass is five feet from the center of mass. Rotation effects will produce control actions which will add to, rather than nullify, the perturbing accelerations on the vehicle. The approximate calculations noted in the accelerometer discussion for mass attraction indicate effects of the order of 10^{-9} g. These represent a bias on the proof mass which will produce a continuous control action attempting to compensate for what the proof mass thinks is a perturbing force. Both of these effects are larger than the desired limit on acceleration unbalance.

For the case in which the proof mass is carried aboard as an accelerometer to measure forces, some biases and spurious signals can be tolerated because the output of the accelerometer is used in the post flight data reduction process, in which much other data are available to aid in the interpretation of the accelerometer output. For the zero-drag satellite case, however, the

purpose of having the proof mass aboard is to eliminate directly the uncertainties due to perturbing forces, and no opportunity is available for compensating or calibrating in flight for spurious effects. One must design the system initially to have uncertainties or errors less than an arbitrary level set by overall accuracy and system performance considerations. These considerations apply equally to the unsupported proof mass configuration, (the case where the vehicle pursues the proof mass) and the supported proof mass (accelerometer) which is used to sense an acceleration that becomes an error signal in a control system. However, there are, in general, bias and stiction effects in an accelerometer which have no counterpart in the unsupported proof mass, and these make the accelerometer approach less desirable than the unsupported proof mass for a zero-drag application.

There are a number of other considerations of a more detailed nature which have a bearing on the design and performance of the zero-drag satellite. These are covered very well in Reference 1* and will not be discussed here. The primary considerations are the two discussed above.

4.6.2 Single Axis Zero-Drag System

Since the photographic system requires attitude control of the vehicle, an interesting possibility is an in-track-only zero-drag system. The uncertainties in the in-track components of the perturbing forces have a much greater leverage on the predicted orbital position uncertainties than do uncertainties in the vertical and cross-track forces. Since the vehicle will be oriented towards the local vertical to within perhaps 20 to 30 minutes of arc, a thrust system to overcome air drag and any other perturbing forces along the in-track axis would have only a small interaction with the attitude control (for near-circular orbits). Thus, the interconnection between the zero-drag control and attitude control necessary for a three-axis zero-drag system could be eliminated. The same problems with location of the proof mass in relation to the centers of mass and mass attractions remain, however, and one would basically have to design the vehicle around the proof mass. Nevertheless, the elimination of control for zero acceleration in two axes makes the single-axis system more attractive than the three-axis system.

4.6.3 State of the Art of Zero-Drag Technology

There have been several applications of the zero-drag principle. The most familiar is flying an aircraft on a zero-g trajectory. A pilot may suspend an object in the cockpit, watch the object, and control the airplane so that it follows the same free-fall path of the object. In this way, his aircraft is using control forces to counterbalance the lift, drag and other disturbances that would prevent it from following a purely gravitational path. One can utilize the object as a model of a zero-g trajectory because an aircraft can shield it from nearly all disturbances except the gravity forces acting on it. The principle can also be applied to guidance system in re-entry vehicles to reduce the amount of dispersion caused by random aerodynamic forces during re-entry. At the high speeds of re-entry, the propulsion requirements become excessive, however, and it is not a practical system. On the other hand, the principle is practical for a short-range ballistic missile, and units have been built and are in operation.

Other than these sub-orbital applications, there are at least two programs involved in developing a zero-g satellite utilizing an unsupported proof mass as the sensor. The Lockheed

* References are contained in Section 4.6.5.

Missle and Space Company is developing a single axis control in which an unsupported proof mass is constrained in the directions normal to the velocity vector. A high degree of accuracy is not required for this program and is not being sought. The program may reach flight state within a year or two.

At Stanford University, an extensive development program to achieve a full three axis zero-drag control has been underway for approximately a year. There are two principal applications of interest: (1) aeronomy experiments in which the drag forces will be determined by measuring the control forces necessary to cancel them; (2) an unsupported gyroscope of performance many orders of magnitude better than can be achieved in the presence of support forces. An extensive analysis that was begun in 1962 has been published by Lange (Reference 1).

Professor Lange has shown that the drag and disturbing effects can be reduced to the order of 10^{-9} g in a zero-drag satellite which is properly designed. The principal limitations are (1) the mass attraction of the satellite itself on the proof mass, and (2), the disturbing force of the electric fields on the proof mass if electrostatic relative position measuring techniques are used.

Laboratory development work underway at Stanford has been principally concerned with two areas: (1) establishing that an electrostatic pickoff can be used with sufficiently low excitation such that the disturbing forces are not the limitation in zero-drag satellite performance, and (2), developing a control system which will minimize both the use of control propellant in the presence of external disturbances and noise inherent in the sensing and control system.

Suitable electrostatic pickoff and proof mass combinations permit a wide range of design parameters. The most significant factor is that the disturbance level of a given responsivity-to-noise ratio of the sensor is proportional to d/D^5 where d is sensor spacing and D is the ball diameter. Great design flexibility is permitted through the use of the fifth power of the ball diameter, and further, it has been shown in the laboratory that acceptable noise levels can be achieved with excitation levels of a few volts on a capacitive pickoff using a 0.12-inch gap and a 2-inch diameter ball. The disturbance that would be created by a sensor of this type for a ball displacement of one-third of its gap is less than 10^{-9} g. For this reason, most of the development work presently being pursued at Stanford University is involved in optimizing the control system mechanization.

Detailed evaluations have been performed through hardware simulation and analysis of bang-bang controllers, pulse-width pulse-frequency thrust modulation, and derived rate control. The latter two systems show considerably less noise sensitivity. For large excursions, a derived rate system does not display as effective damping characteristics as a rate circuit used in conjunction with a pulse-width pulse-frequency modulator. However, this consideration may be of little importance for application to a drag-free satellite. Either system appears adequate for the job and the final decision on which method will be utilized for flight hardware will be determined by power and reliability considerations of the detailed design.

For a drag-free satellite with a body-fixed sensor at its mass center, no attitude control is required. By sensing the vehicle displacement with respect to the proof mass in the same body coordinates that the thrust system is mounted, it is not necessary to perform any coordinate transformations nor to know the orientation of the vehicle with respect to the disturbing force. The only problem arises from the vehicle angular velocity when the proof mass is offset from the center of the vehicle. The rotation causes each pickoff plate gap to oscillate with respect to the proof mass as it rotates. The information which is derived from differentiating the relative position signal is not the significant rate that is needed for damping purposes. The velocity that

is important is the relative motion of the mass centers of the satellite and the proof mass. When the oscillation rate due to rotation becomes high compared with the desired velocity information, a correction using knowledge of the vehicle angular velocity must be made.

Complete mechanizations of a capacitive proof mass sensor, several control systems, and rate information correction using a rate gyro, have been simulated on a zero-g satellite simulator developed in the Stanford laboratories. This simulator is composed of an air-cushioned vehicle which floats over a granite table on a very thin film of air supplied from a tank on the vehicle. This permits the vehicle to move over the surface with extremely low friction levels corresponding to an equivalent disturbance of 10^{-7} g. The table can be accurately tipped within a range of 1/2 degree using manually operated differential screws. Once the desired orientation is established, it is maintained with a precision of 0.1 arc-seconds for short periods of time and with a stability of 0.2 to 0.5 arc-seconds for periods up to 12 hours. The gravity due to table tilt is used to simulate the orbital disturbances on a vehicle. Accurate simulations in the laboratory have been achieved in real time to disturbance levels corresponding to 275 km in altitude.

Based on the research at Stanford University, there appears to be no fundamental reason why a zero-drag satellite, using an unsupported proof mass, cannot be designed to achieve a performance of 10^{-9} g equivalent orbital disturbance if the unsupported proof mass can have first priority in location in the satellite and suitable attention is paid to proper mass distribution of the vehicle.

4.6.4 Evaluation of the Zero-Drag Concept for the Program

The above discussion of the zero-drag concept has noted its desirability from the standpoint of directly producing an orbit controlled essentially by gravitational effects only. Under these circumstances, the vehicle position and velocity tracking data can be considered to reflect only the gravitational effects and may be used to directly fit a gravitational model. The uncertainties associated with the prediction ahead in orbit are considerably reduced. In addition, considerations of the force required to balance the in-track component of the perturbing forces should yield a relatively accurate air drag and air density model.

The practical difficulties of implementing a zero-drag concept have been discussed. Primary considerations among these are the necessity for locating the proof mass at the centers of mass and mass attraction of the vehicle, incorporating a low level, in-track thrust system in the vehicle, and combining the zero-drag and attitude control systems, at least in the case of a three-axis system. The technology required to achieve a zero-drag satellite is relatively new and undeveloped, although the work done to date indicated that a 10^{-9} g system is mechanically feasible.

In view of these considerations, a major redesign of any existing orbital vehicle would be required to incorporate a zero-drag capability, even in only one axis (in-track). The schedule of of the present program precludes success in obtaining reliable flight hardware for a three-axis zero-drag system. It is considered worthwhile, however, to initiate a study to determine the feasibility of a one-axis system, with the possibility that later flights in this program might incorporate such hardware. Such a study is recommended.

4.6.5 Reference for Section 4.6

1. Lange, B., The Control and Use of Drag-Free Satellites, Stanford Report SUDAER NO. 194 (June, 1964).

4.7 PASSIVE ATTITUDE CONTROL

The feasibility of passive attitude control using aerodynamic, gravity gradient, and solar pressure torques as the controlling means has been examined. These effects require basically no power source or control hardware in the vehicle. The interest is prompted by the desire to reduce the uncertainties in the forces required in the Agena cold gas system to maintain the attitude necessary for the earth oriented photographic system.

Since all of these passive attitude control torques exist at the altitudes of interest, an attitude control system based on any one effect must operate in the presence of the other effects. Aerodynamics and gravity effects decrease with altitude, but at different rates. Consequently, an altitude regime exists for each method, in which the desired control torque is able to overcome all other naturally-occurring torques and, in principle, maintain the vehicle attitude within acceptable limits. These altitude ranges rule out the use of solar pressure for the present program, since altitudes in excess of about 1000 miles are necessary to achieve the low level of the other disturbing torques capable of being overcome by solar pressure torque. An altitude of 150 nautical miles falls between the commonly accepted ranges for aerodynamic and gravity systems, and thus is in a region where torques due to both effects tend to have roughly equal effects on satellite attitude.

The major problem areas in aerodynamic and gravity gradient stabilizations are lack of experience and success, and the dynamics of attitude motion. Since no inherent damping exists at these altitudes, large low-frequency motions are likely to occur and artificial damping must be employed. Gravity-stabilized satellites have been flown with damping mechanisms at altitudes of over 400 miles, but no flights with aerodynamic stabilization are known to have occurred.

It is concluded that, with the proven reliability of the Agena vehicle and the time schedule of the present program, the risk in attempting to use passive attitude stabilization is excessive. Considerable study and redesign of the vehicle would be required to incorporate either aerodynamic or gravity stabilization for this intermediate altitude, and the hardware and design criteria required for successful operations are not well enough established to make such an effort worthwhile.

The major attraction of passive altitude control is its simplicity. Simplicity implies lower cost, greater reliability, and sometimes quicker development. It also implies a long-life system, since little or no power is required from the vehicle. For the present application, it also implies a lower uncertainty in the perturbing forces. The forces that are available during orbit for passive altitude control also represent perturbing forces and as such, they cannot be eliminated. The introduction of an active control system, as the Agena has, to overcome these forces merely adds additional forces which have uncertainties associated with their magnitude and direction, and it is these that are eliminated by using the natural forces available in orbit. Thus, the possibilities of using passive altitude control are of interest and are discussed in this section.

4.7.1 Characteristics of Passive Attitude Control Systems

Attitude control systems for space vehicles can be considered as falling into four catagories: (1) momentum storage such as spinning the entire vehicle, (2) momentum exchange systems such as flywheels whose speed can be varied, (3) common momentum ejection systems such as the gas reaction jets on the Agena, and (4) external torques such as those due to gravity gradients, solar pressure, and aerodynamic moments. It is the latter catagory that is of interest here because the torques have a known, or preferred, orientation and offer the opportunity for the elimination of much of the control system hardware, such as attitude sensors, control circuits, and thrustors.

Gravity gradient, solar pressure, and aerodynamic effects, cannot be considered separately. Since all these phenomena exist to some degree at all altitudes, an attitude control based on one of these torques must operate successfully in the presence of the other two (and any other) effects. Two of the three, aerodynamic and gravity torques, are altitude-dependent, and their magnitudes drop off with increasing altitude. Thus, at low altitudes, aerodynamic effects generally predominate. These decrease rapidly, and there is an intermediate altitude region where gravity gradient effects can be made to dominate, since these decrease less rapidly with altitude than the aerodynamic effects. Finally, at great altitudes, solar torques become the major effect. The regions in which each dominate depend to some extent on the vehicle configuration and attitude, but a typical Agena configuration with the long axis vertical might have the characteristics shown in Figure 4-4.

A second important factor is the relation between the desired orientation of the vehicle being stabilized and the preferred orientation of the torques. For a typical orbital vehicle, aerodynamic torque is related to the angle between the vehicle longitudinal axis and the velocity vector. Thus, for a circular or near-circular orbit, aerodynamic torques represent a potential method of obtaining an earth-oriented vehicle. Gravity gradient torques are related to the radius vector between the earth center and the satellite. This method, too, offers potential for an earth oriented vehicle. Solar torques are related to the radius vector from the sun to the vehicle. Thus, some additional control mode must be used to obtain an earth-oriented vehicle, as is required in this program.

A third factor which is common to all three methods has to do with the dynamics of the motion of the vehicle. There is no natural damping of the vehicle motion at altitudes over, say, 100 miles. Figure 4-4 illustrates the gravity gradient case, which requires the axis of minimum moment of inertia to be aligned with the vertical (α = 89 degrees). A similar figure could be prepared for the aerodynamic case (α = 1 degree), wherein the aerodynamic drag would be lower and the aero-gravity cross-over point would occur at a lower altitude. The altitude region between the two crossovers (α = 89 degrees, and α = 1 degree) is one in which both effects are significant. In addition, the restoring torques are very small. Thus, attitude stabilization using passive means is characterized by motions having small angular velocities and very long periods, of the order of many minutes to hours. As a result of these characteristics, the initial orbit injection maneuver is critical. The vehicle must be injected such that the attitude is reasonably close to the desired stable attitude and, more important, there must be very small residual angular velocities. Under these circumstances, the passive attitude control can capture the vehicle and stabilize it at the desired attitude. Another result of these characteristics is that considerable thought and ingenuity has gone into developing damping devices to cut down the amplitude of the motion and obtain more rapid stabilization.

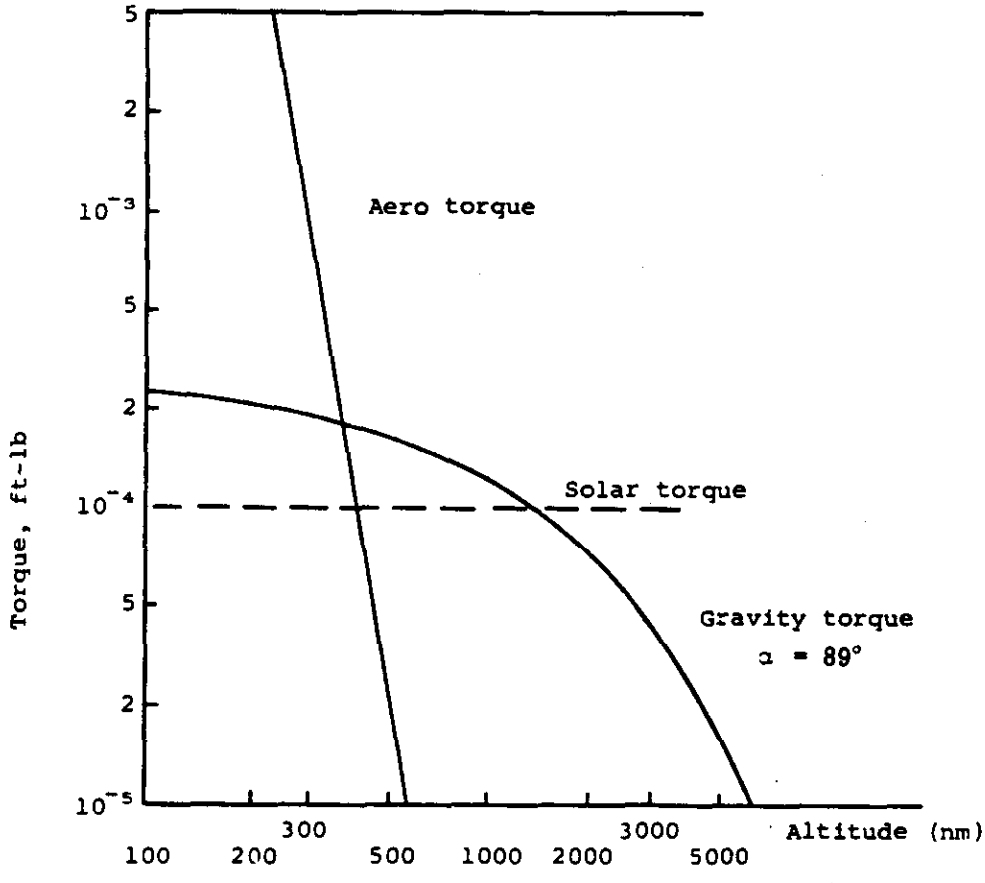

Fig. 4-4 — Torque environment for typical Agena configuration at 90-degree angle of attack

4.7.2 Operation of Passive Attitude Control Systems

The general method of operation of the three types of passive attitude control schemes is discussed in this section. The study of the satellite motions resulting from these torques and their suitability for control, both theoretical and experimental, is quite complex. As a result, this discussion will be limited to those results which would have a bearing on the suitability of the methods for the present program.

Aerodynamic stabiliation requires that the center of pressure lie aft of the center of mass for a range of attitudes around the desired stable orientation. This method lends itself well to an earth-oriented satellite, because the restoring torques depend on the relative attitude of the vehicle with respect to the velocity vector. Thus, the stable attitude in pitch is one providing proper orientation for a camera system. The same considerations apply to the yaw axis, where aerodynamic stabilization is also obtained. However, stabilization in roll is not inherent in the method; a separate control is required for roll attitude control. This would involve probably some other control means, such as momentum transfer, but a more active type of control is necessary in that roll attitude must be sensed.

An aerodynamically-stabilized vehicle will have an equilibrium attitude in pitch (as well as the other axis) such that the aerodynamic torque is just balanced by other disturbing torques, primarily those due to the gravity gradient. For this attitude to be small (the order of 1 degree with respect to the velocity vector) for camera considerations, the altitude range must be such that sufficient air density is available all the time to give a large enough torque at, say, 1 degree angle of attack to equal the other disturbing torques. The upper limit of this altitude range depends on many things, the most important of which are vehicle configuration and spatial and temporal variations in density. This problem is discussed in Reference 1.* For the cylindrical vehicle model used in that study, the cylinder is homogeneous, has a length to diameter ratio of 5, and has centers of pressure and mass both on the longitudinal axis but separated by 2 percent of the length. The upper range of altitude for essentially zero stabilized attitude error in pitch is indicated to be about 120 status miles. While it may be feasibile to successfully operate this type of control at 150 nautical miles from an equilibrium attitude standpoint, considerable care would have to be taken with the aerodynamic shape and distribution of mass to get the proper center of pressure and moments of inertia about the three axis, since the latter determine the gravity-induced torques.

Most attempts at designing and operating a practical, aerodynamically stabilized satellite have been defeated by the dynamics of the attitude motion. Since the air density varies rapidly with altitude, an elliptical orbit has a considerable variation in density along its track. Even "circular" orbits have some variation because of the oblateness of the earth. As the vehicle approaches perigee, the density increases which feeds energy into the vehicle motion and there is no damping to decrease the amplitude of the motion. The motion is thus periodically excited at orbital (eccentricity effect) and twice orbital (oblateness effect) frequencies, and tends to have unacceptably high amplitudes of motion. To date, all attempts (at least those in the open literature) to design an effective damping system for an aerodynamically stabilized vehicle have not been successful. There have been no attempts reported to obtain aerodynamic stabilization for an orbital vehicle, although it is believed that some work of this nature is going on in classified programs.

---

*References are contained in Section 4.7.4.

Gravity gradient attitude stabilization makes use of the gradient in gravity due to a central force field to align the vehicle axis of minimum moment of inertia with the radius vector from the earth's center to the vehicle. This can be best visualized with a dumbbell shaped vehicle. If the two balls are equidistant from the earth, there is no torque. However, if the dumbbell is displaced slightly, the ball nearer the earth has a larger force due to gravity than the other ball has, and the dumbbell will rotate to align the long axis with the vertical. This is the stable attitude. Since the "reference" for this torque is local vertical, this method is also suitable for an earth oriented vehicle. Furthermore, both roll and pitch control (in a velocity vector coordinate system) is obtained directly with the gravity gradient system. Thus no additional attitude control is required for the camera.

The lower limit in altitude for successful use of a gravity gradient system is that altitude at which the aerodynamic torques (and other lesser ones) have decreased to the extent that they can just be balanced by the gravity gradient torque at, say, one degree of angle of attack. Again, referring to the study of Reference 1, this altitude is about 300 statute miles for the cylinder vehicle model used. In this case the longitudinal axis of the cylinder (axis of minimum moment of inertia) is aligned with the vertical, rather than with the horizontal as in the aerodynamically stabilized case. This result is also close to that shown in Figure 4-4 for an Agena vehicle.

Dynamic motion is again a problem because of the lack of natural damping. However, since gravity gradient stabilized vehicles are limited to higher altitudes, the forcing inputs due to air density variations are much lower and the damping problem is somewhat easier. A great deal of work has been done on damping devices, based on such principles as the hysteresis of a spring extension, viscous effects, and eddy currents. Reference 2 has an excellent review of this work. In addition, Reference 2 also has a good discussion on a number of theoretical studies on the instabilities which can occur in gravity stabilized vehicles.

There have been gravity gradient stabilized systems used successfully in satellites. These include the TRAAC (1963 22A) and the TRANSIT Satellites. Due to the small size of these satellites, the instrumentation was minimal and only qualitative altitude behavior was verified. The altitudes of these satellites were the order of 400 to 700 miles.

With regard to the influence of the configuration on the successful application of either aerodynamic or gravity gradient stabilization, it is obvious that much can be done, in principle, to minimize the unwanted of these two effects. For aerodynamic stabilization, one would want all three axes to have similar moments of inertia. For gravity stabilization, one would want the center of aerodynamic pressure and center of mass to be identical for all attitudes. The freedom to achieve these goals would widen the altitude limitation of each method of control. There are, of course, many other limitations on vehicle shape and mass distribution besides those of the attitude control. In a practical vehicle, for a program such as this, these limitations tend to be controlling and would put the 150-nautical mile operating altitude in the gray region between the accepted altitude ranges for these two types of passive stabilization.

Solar radiation attitude stabilization is based on having the center of pressure for solar radiation away from the mass center. If solar radiation pressure is the predominate disturbing torque, the vehicle axis containing the center of pressure and mass will align itself with the radius vector from the sun to the satellite. The torques obtainable from solar pressure are very small, and the system is thus limited to very high altitudes where other disturbing torques are small. This may be seen in Figure 4-4, which indicates a crossover between solar and gravity torques at about 1500 nautical miles. Furthermore, the method does not lend itself to an earth-oriented vehicle because the sun line is continually changing relative to the vertical. For these reasons, a more extensive discussion of solar radiation stabilization is not warranted.

4.7.3 Evaluation of Passive Attitude Control for the Program

The preceeding discussion has outlined the advantages and disadvantages of three passive attitude control methods which use naturally-occurring perturbing torques. From this discussion, the following observations can be made. First, solar radiation pressure is unsuitable because of the altitude limits and earth orientation requirement. Second, gravity gradient stabilization is not practical at 150 nautical miles because of this low an altitude, extensive redesign of the Agena would be required to reduce the aerodynamic torques to a level which the gravity torques could overcome. In addition, there are numerous studies which would have to be performed on attitude capture, cross-coupling effects, and motion instabilities as affected by orbital eccentrities in order to arrive at a suitable vehicle design having the required attitude stabilization accuracy. Third, aerodynamic attitude stabilization presents too great a risk in reliability, considering the time schedule of this program and the proven capability of the present Agena vehicle. The primary problems in this method are the attitude dynamics, the lack of a developed and flight-proven damping system, and the auxiliary control required in the roll axis.

The perturbing effects which provide a potential source of attitude control represent disturbances which the present cold gas reaction control must overcome. To this extent, examination of these effects is necessary to attempt to define the uncertainties in both these effects and the gas reaction control forces used to overcome these effects. It is recommended, however, that no consideration be given to using these passive control effects as a source of direct attitude control.

4.7.4 References for Section 4.7

1. DeBra, D. B., "The Effect of Aerodynamic Forces on Satellite Attitude," Vol. 3, Advances in Aeronautical Sciences, Plenum Press, 1958.
2. DeBra, D. B., Principles and Developments in Passive Attitude Control, American Astronautical Society Report 65-135, (Dec. 1965).

4.8 COMPUTATIONAL RESULTS

A number of calculations were made while studying the feasibility of the proposed system. A presentation of the results of these computations is made in this section. The organization of this section is, for the most part, in historical sequence. The purpose is to document rather than interpret the computational results. The discussion and evaluation of these results is contained in Section 4.9.

4.8.1 Auxiliary Tests of Computational Program

As already noted in the description of Section 4.2.3, the bulk of the calculations were performed using the TRACE program which was made available to Itek through the cooperation of Aerospace Corporation. The early utilization of the program was for purposes of familiarization with its many features and options. To gain confidence in proper use of the program, some auxiliary test runs were made. Scaling of variances, numerical roundoff, and gravity model truncation effects were investigated.

The effect of scaling variances was tested in both the tracking and error analysis modes of the program. This was done using simulated data for the SGLS Network, a polar circular orbit of approximately 140-nautical mile altitude, and one day's observations. Two runs were compared in each case, using nominal values for standard deviations of the observations in one case, and ten times nominal in the second case. In the tracking mode, it was found that the elements of the variance-covariance matrix were 100 times larger in the second case than in the first as expected. In the error analysis mode, the uncertainties in the position and velocity components in the orbit plane coordinate system were found to differ by the expected factor of ten.

The effect of numerical roundoff was tested using simulated data for two days of photogrammetric observations along for a polar, circular orbit of 140 nautical mile altitude. An orbit fit solving for the six initial conditions plus a drag parameter was made to the simulated data (perfect data, no noise) starting with an initial guess deviating from the nominal initial conditions by approximately 2500 feet. The iteration procedure converged, it was found, to within 1 part in 2^{36} of the nominal inital condition. Differencing the ephemerides for the iterated solution and the nominal initial conditions provided a measure of the effect of limited numerical accuracy. A plot of the along-track component of this difference is presented in Figure 4-5, showing an accumulated error of approximately 130 feet over the 2-day interval.

Also shown in Figure 4-5 is the result of the test of the effect of gravity model truncation. This run was set up with the same orbit and observations as the numerical roundoff case. The simulated data, which were generated with a standard gravity model with zonal hormonics up to J_9 and tesseral harmonics up to J_{66}, were then used to solve for the six initial conditions plus $C_D A/W$, again starting with the same off-nominal initial guess as above. This seven-parameter

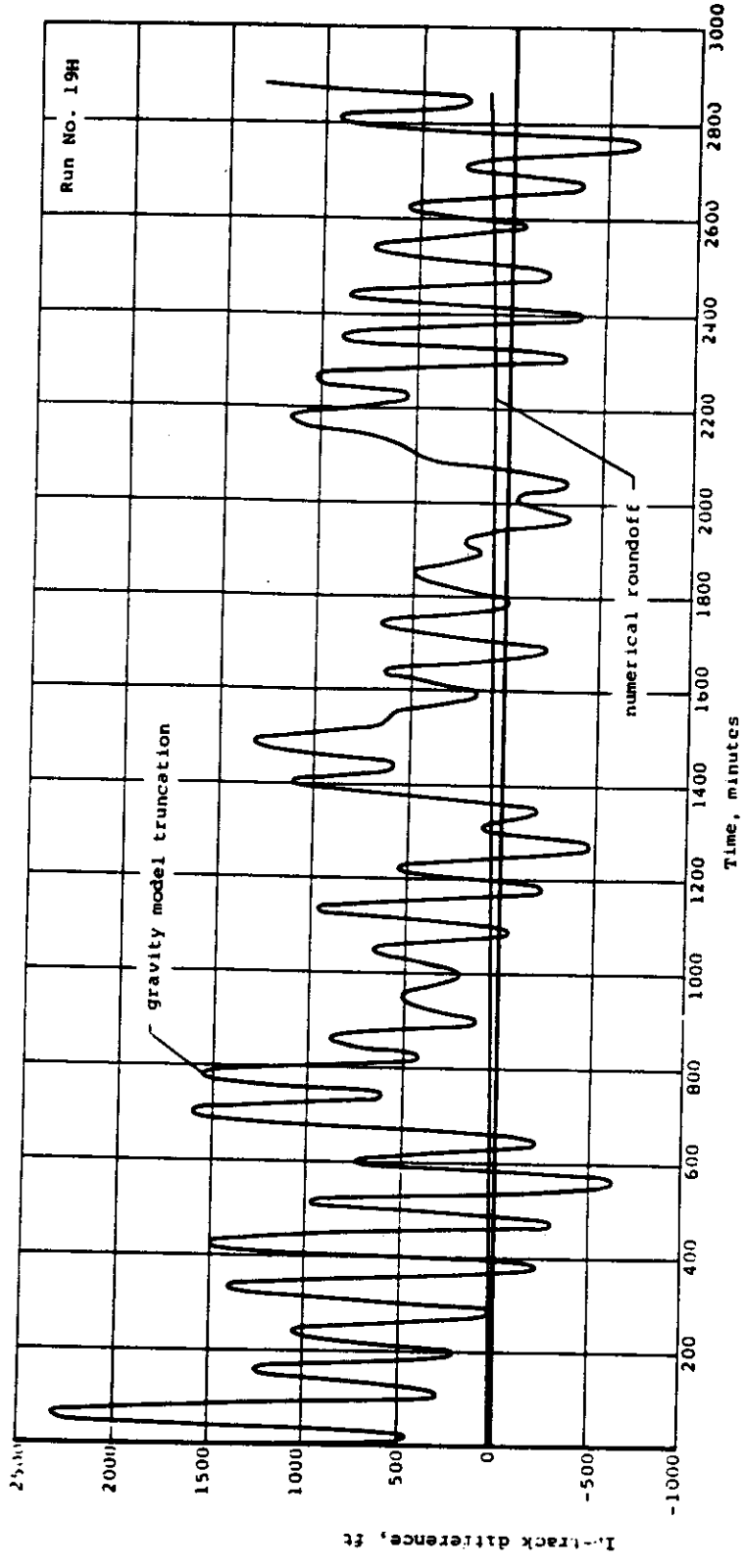

Fig. 4-5 — Plot of in-track ephemeris difference versus time showing effects of numerical roundoff and gravity model truncation in orbit determination using 2-days' observations of photogrammetric data

fit was made, however, using a truncated gravity model including the original zonals only up to J_5 and the tesserals through $J_{4,4}$. The fitting procedure was continued for four iterations, at which point no significant improvement could be made in the residuals. Differences were computed between the ephemerides of the nominal case and of the iterated solution. The in-track component of that set of differences is plotted in the Figure 4-5, showing deviations as large as 2000 feet.

An additional test run was made in order to become familiar with the use of P and Q parameters in the error analysis mode of the program. The SGLS net was used for one day's observations of the 140 nautical mile polar circular orbit already mentioned. Seven P parameters were used: the six initial conditions and C_DA/W. Fourteen Q parameters were used: the latitudes and longitudes of each of the SGLS tracking stations. Variances of the Q parameters were chosen to simulate 100-foot uncertainties in each horizontal direction. The results of this run are presented in Figure 4-6 where the in-track position uncertainties are plotted as functions of time for the cases of both zero and 100-foot uncertainties in the Q parameters.

4.8.2 Uncertainties in Orbital Position Due to Lack of Precision in Observations

A series of calculations was performed to investiage the effect of observation uncertainties and data distribution on the precision with which position in orbit could be determined. The effect of combinations of different data types was also studied. These calculations are reported here. A summary of results for four selected times for this series is presented in Table 4-4. Certain typical results are also presented graphically.

For this series of calculations, a circular polar orbit of 156.7-nautical mile altitude was chosen. In all cases, the orbit fit was for one day's observation. For this period, the following quantities of observational data were generated for the three data types considered: 294 photogrammetric observations (98 x-, 98 y-, and 98 z-), 167 from TRANSIT, and 321 altitude measurements. The plane of the orbit was chosen so that it included the sun, which was taken to be at its southernmost point (winter solstice). In the orbit fit, the normal matrix was accumulated for the six initial conditions (in spherical coordinates) plus the drag parameter, C_DA/W. Station locations and gravity-model parameters were considered known, and no biases of the data were considered. The Lockheed-Jacchia atmosphere model, Reference 1*, was used. The standard gravity model of TRACE D, from unpublished data by Guier for tesseral coefficients up to sixth order and degree and zonal up through J_9, was used. The nominal initial conditions for this series, and for a large number of the calculations reported later, are as follows:

Epoch: 21 December 1968, 12 hrs. UT
Right ascension, α = 270.12 degrees
Declination, δ = 0.0001 degree
Flight-path angle, β = 90 degrees
Azimuth, A = 180 degrees
Radius, R = 21,872,397 feet
Velocity, V = 25,368.922 feet per second
W/C_DA = 120 pounds/feet^2

* References are contained in Section 4.8.16.

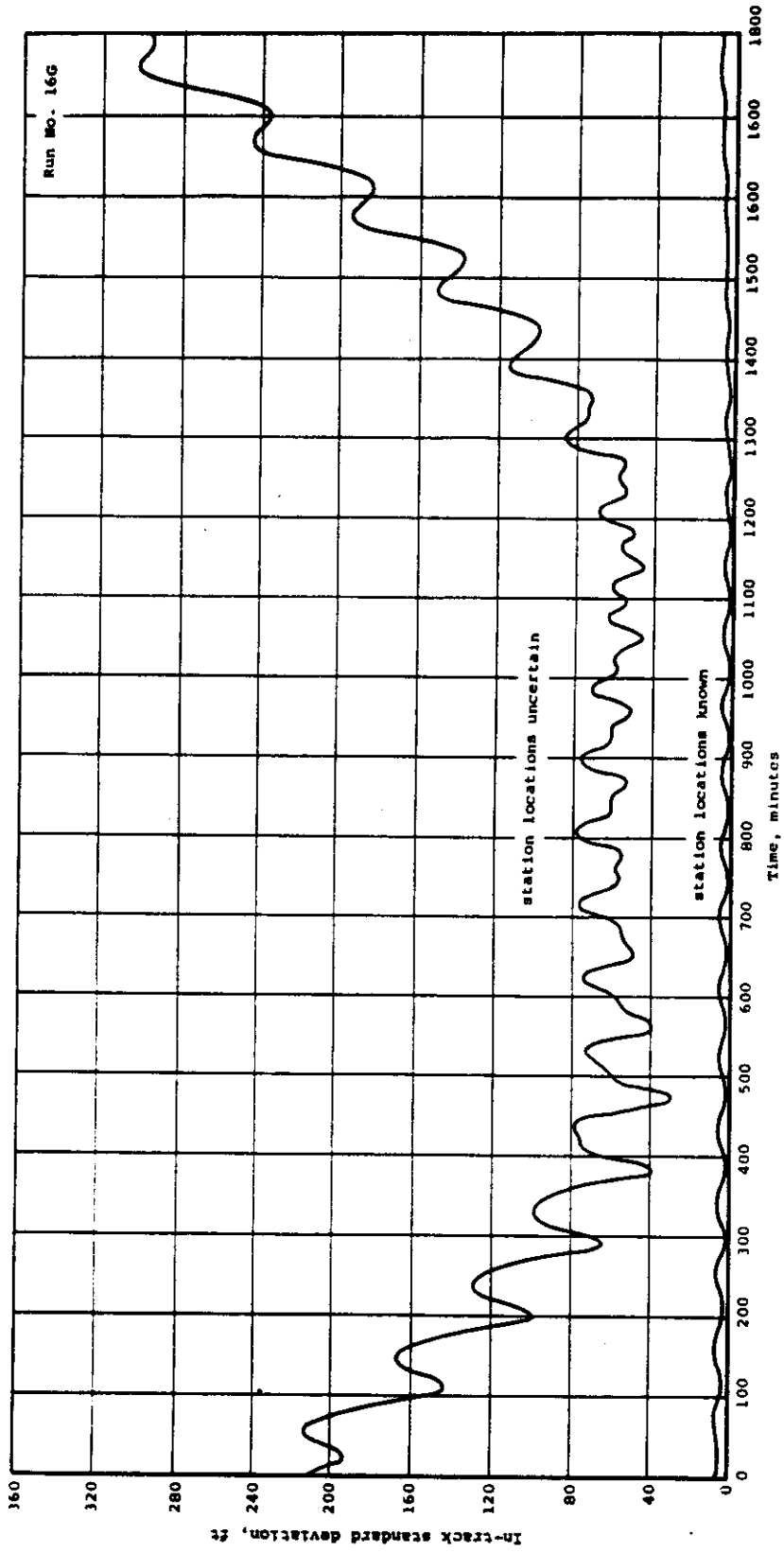

Fig. 4-6 — Plot of standard deviation of in-track component or orbit position error versus time for a 1-day fit to SGLS network radar observations, showing effect of 100-foot horizontal error in station locations

Table 4-4 — Selected Computed Results for 10 Cases Showing Effects of Observation Errors on Orbit Position Errors

Case	Time, minutes	Orbit-Plane Error Components, feet: Radial Minimum	Radial Maximum	In-Track Minimum	In-Track Maximum	Cross-Track Minimum	Cross-Track Maximum	Comments
1	0	2.5	6.6	16.0	27.0	3.4	7.0	Full set photogrammetric observations
	720	2.5	6.7	8.6	26.0	3.4	6.9	
	1440	2.6	6.7	5.3	26.0	3.4	6.9	
	1800	2.6	6.7	12.0	30.0	3.5	6.7	
2	0	7.8	21.0	44.0	85.0	10.0	21.0	10 percent photogrammetric observations
	720	8.1	21.0	25.0	82.0	10.0	21.0	
	1440	7.8	21.0	15.0	83.0	9.9	21.0	
	1800	7.7	21.0	38.0	89.0	10.0	21.0	
3	0	4.6	18.0	40.0	72.0	6.0	22.0	Northern half photogrammetric observations only
	720	4.6	18.0	24.0	83.0	4.6	22.0	
	1440	5.0	18.0	9.7	76.0	5.7	22.0	
	1800	5.4	18.0	33.0	69.0	5.1	22.0	
4	0	4.7	26.0	19.0	110.0	9.0	20.0	Southern half photogrammetric observations only
	720	5.8	26.0	9.4	100.0	5.1	21.0	
	1440	4.8	26.0	7.1	100.0	4.2	21.0	
	1800	4.1	26.0	12.0	100.0	7.5	21.0	
5	0	3.5	9.4	18.0	38.0	4.8	9.9	50 percent photogrammetric observations
	720	3.6	9.5	12.0	37.0	4.8	9.8	
	1440	3.8	9.5	7.4	37.0	5.4	9.8	
	1800	3.7	9.5	17.0	40.0	4.8	9.7	
6	0	2.5	4.3	23.0	26.0	4.9	9.9	50 percent photogrammetric observations plus full altimeter
	720	2.4	4.3	12.0	20.0	4.9	9.6	
	1440	2.5	3.6	7.3	18.0	5.4	9.8	
	1800	2.6	4.4	17.0	22.0	4.8	9.7	
7	0	3.2	7.2	23.0	32.0	4.9	9.9	50 percent photogrammetric observations plus 10 percent altimeter
	720	3.2	7.2	12.0	29.0	5.2	9.6	
	1440	3.3	7.2	7.4	29.0	4.8	9.8	
	1800	3.3	7.2	18.0	32.0	4.8	9.7	
8	0	2.2	2.4	9.6	12.0	4.7	8.7	50 percent photogrammetric observations plus full TRANSIT
	720	2.2	2.4	7.5	9.6	4.7	8.6	
	1440	2.2	2.4	5.6	9.3	5.2	8.6	
	1800	2.2	2.4	9.7	14.0	4.7	8.5	
9	0	3.3	3.4	13.0	16.0	18.0	23.0	TRANSIT only
	720	3.3	3.4	10.0	12.0	18.0	22.0	
	1440	3.2	3.4	11.0	14.0	19.0	22.0	
	1800	3.3	3.5	20.0	24.0	18.0	22.0	
10	0	1.9	2.1	9.3	12.0	4.7	8.7	50 percent photogrammetric observations plus TRANSIT plus full altimeter
	720	1.9	2.1	7.3	9.1	4.7	8.6	
	1440	1.9	2.1	5.5	8.4	4.7	8.6	
	1800	1.9	2.1	9.6	13.0	4.7	8.5	

The first case considered was with photogrammetric data alone. Using all the data available and considering the 19 degrees sun elevation restriction for illumination requirements, the results of Figure 4-7 were found. The three parts of this figure show plots on in-track, cross-track, and radial components of the uncertainty in orbit position, measured by the standard deviation as functions of time. As will be noted, the results for times greater than 1440 minutes (one day) are for a period where no observational data was obtained. The results for this same case are reported in Table 4-4 for four selected times: start (t = 0), middle (t = 720), end (t = 1440), and end plus six hours (t = 1800). As the standard deviation is an oscillatory function, maximum and minimum values in the neighborhood of the specified times are given.

The second case was run to find the effect of reducing the quantity of observational data. All conditions were identical with the first case, except that only every tenth observation was used. The selected results are reported in Table 4-4, showing an increase in uncertainty by a factor very close to the square root of ten, as is to be expected.

The next two cases were run to determine the effect of poor distribution of the data. All conditions were identical to the first case except that in the third case, observations south of the equator were not used, and in the fourth case, observations north of the equator were not used. The tabulated results show the importance of data distribution. The number of observations in both of these cases is nearly the same, and therefore nearly equal to one-half of the number of observations of the first case. (Although there is more land area in the northern hemisphere, the illumination considerations favored the southern hemisphere due to the southern position of the sun taken in these cases.) Yet the maximum uncertainties in these cases differ by a factor much greater than the square root of two from the results of the first case. For the fourth case, with observations only in the southern hemisphere, the maximum uncertainties are larger than in the case where only 10 percent of the observations were used (case 2). Plots of in-track uncertainty for the cases of northern observations only and southern observations only are presented in Figures 4-8 and 4-9, respectively. Plots for the radial and cross-track components are not presented, as these components bore the same relationship to the in-track component as in the first case. Thus, the figure showing the in-track component conveys most of the information about the results. The same condition applies to the following cases, so that only plots of in-track components are presented for comparisons.

The fifth case was taken as a realistically nominal case for photogrammetric data, considering the effect of clouds. Two assumptions were made with regard to the effect of cloud cover. Between 60 degrees south latitude and 60 degrees north latitude, half of the photogrammetric observations will not be useful because of obscuration of visible details beyond these latitudes, only one-fourth of the observations will be useful. To simulate this state of affairs, conditions were taken identical to the first case, except that every other observation was not used in the middle latitude region, and only every fourth observation was retained in the regions of latitude beyond 60 degrees. (For this set of cases, no resection type photogrammetric observations were obtained in the high latitudes. Due to the illumination constraint and distribution of areas of geodetic control.) Thus, only 49 observation times were used, yielding 147 data points. The results listed in Table 4-4 show an almost exact factor of $\sqrt{2}$ over those of the first case, as expected. The in-track component of orbit position uncertainty is plotted versus time in Figure 4-10 for comparisons with later results.

The remaining cases investigated in this series of calculations were concerned with the effect of adding other data types to the photogrammetric observations. In case 6, the effect of adding altimeter data was studied. The conditions were the same as case 5 above (photogrammetric

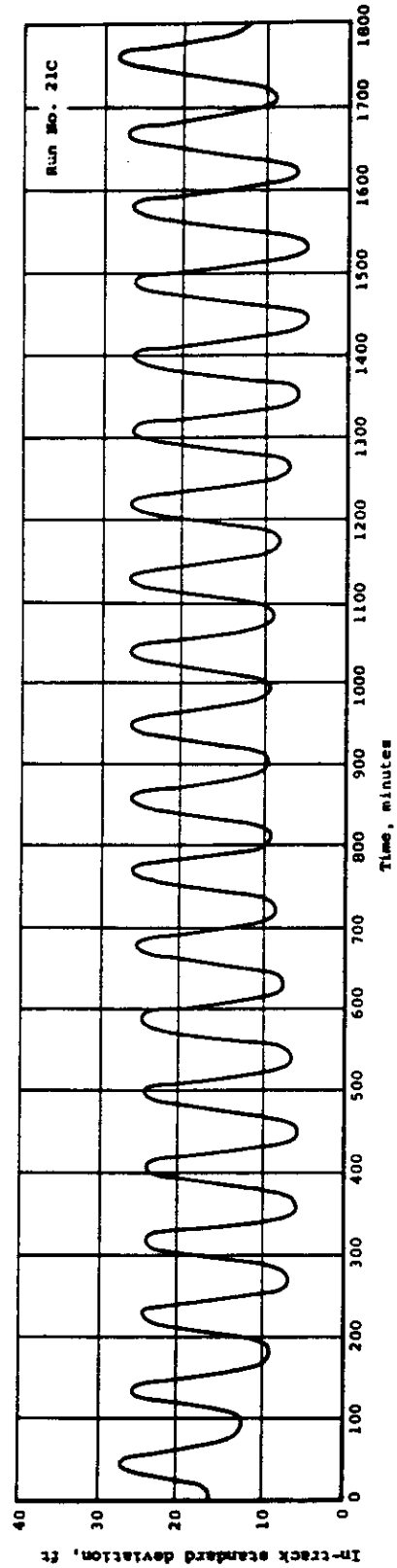

Fig. 4-7(a) — Plot of standard deviation of in-track component of orbit position error versus time for case 1, full set of photogrammetric observations

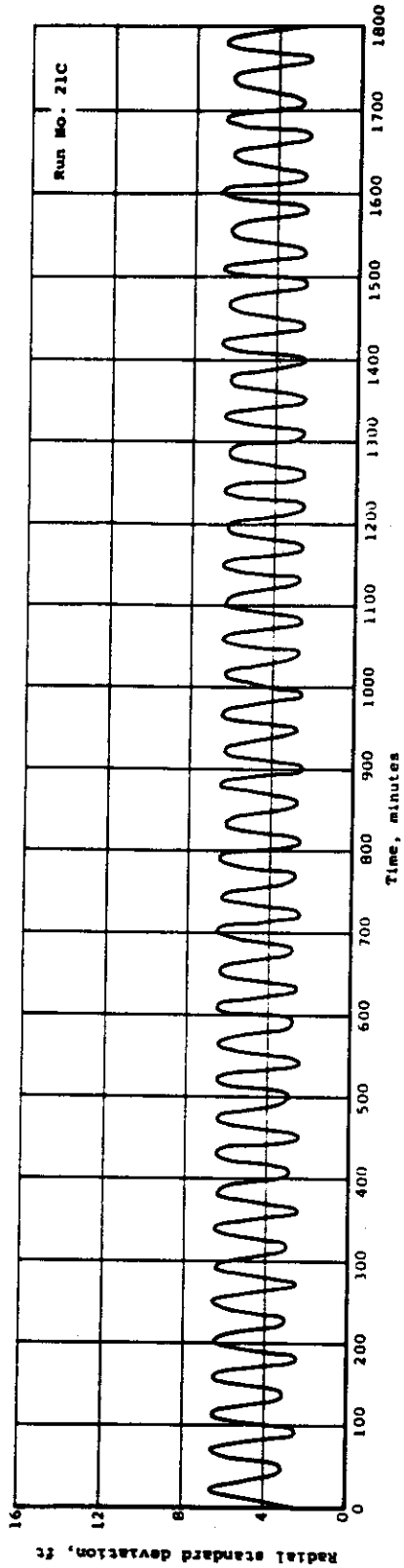

Fig. 4-7(b) — Plot of standard deviation of radial component of orbit position error versus time for case 1, full set of photogrammetric observations

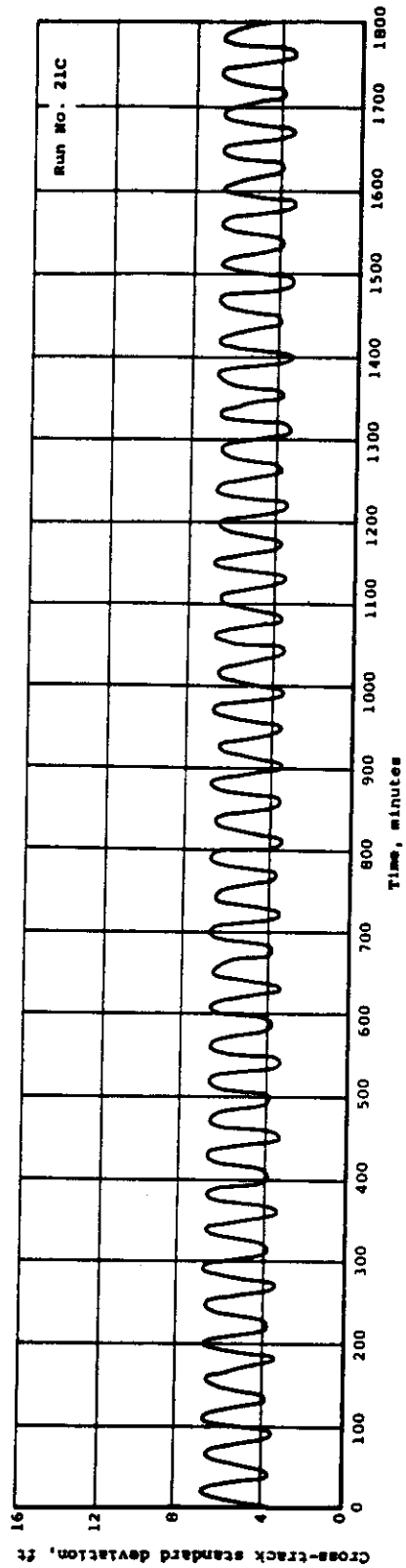

Fig. 4-7(c) — Plot of standard deviation of cross-track component of orbit position error versus time for case 1, full set of photogrammetric observations

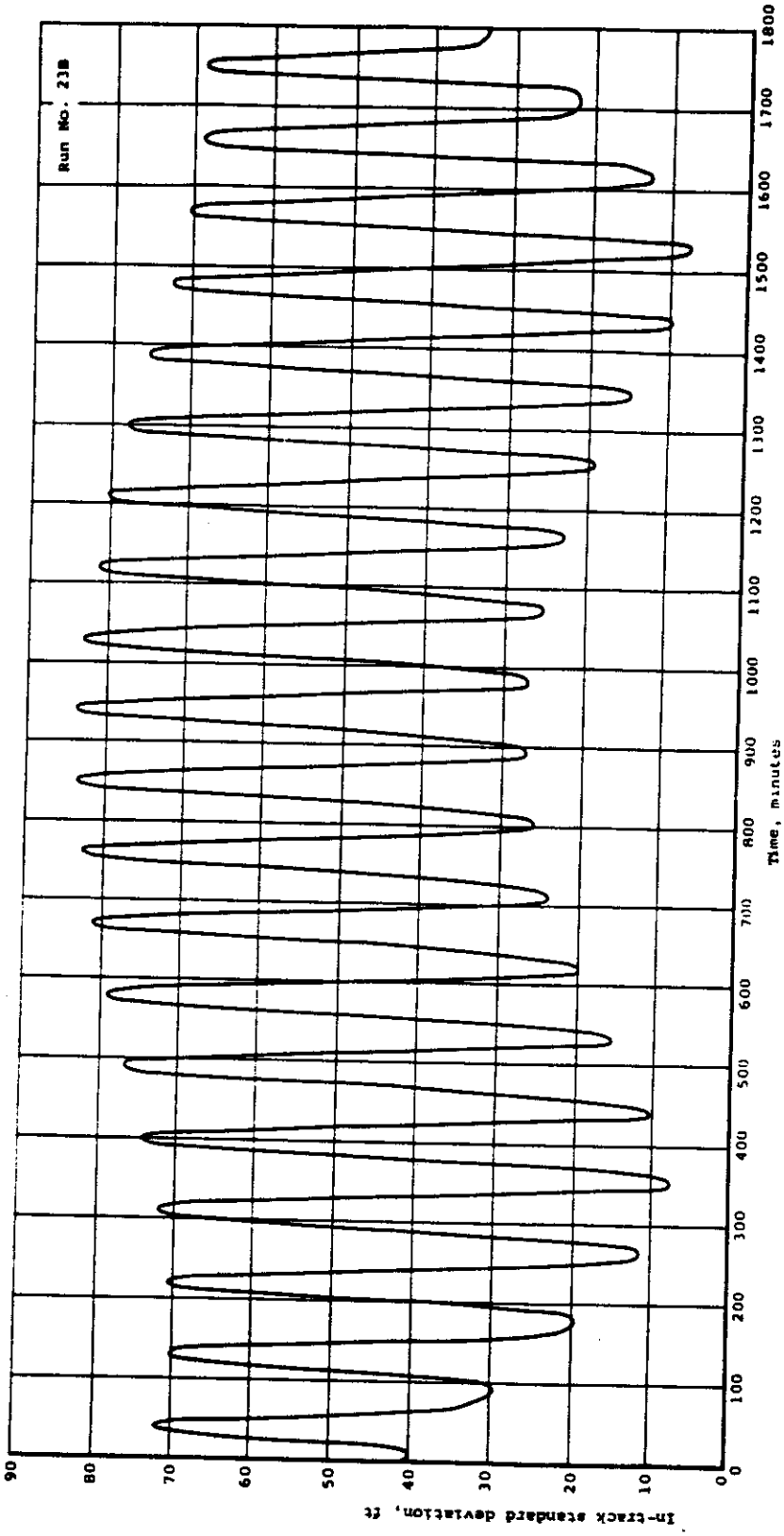

Fig. 4-8 — Plot of standard deviation of in-track component of orbit position error versus time for case 3, northern half of photogrammetric observations

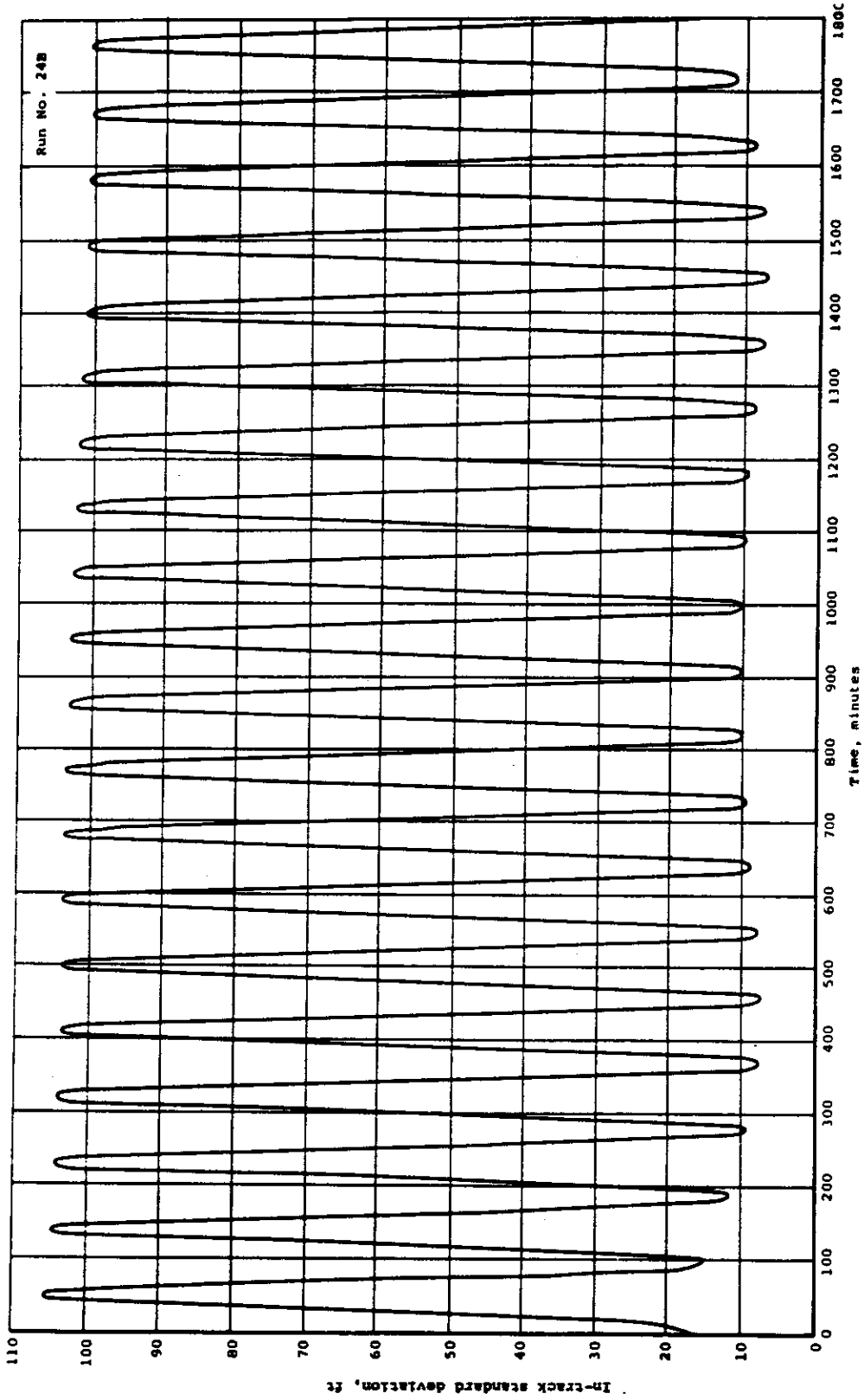

Fig. 4-9 — Plot of standard deviation of in-track component of orbit position error versus time for case 4, southern half of photogrammetric observations

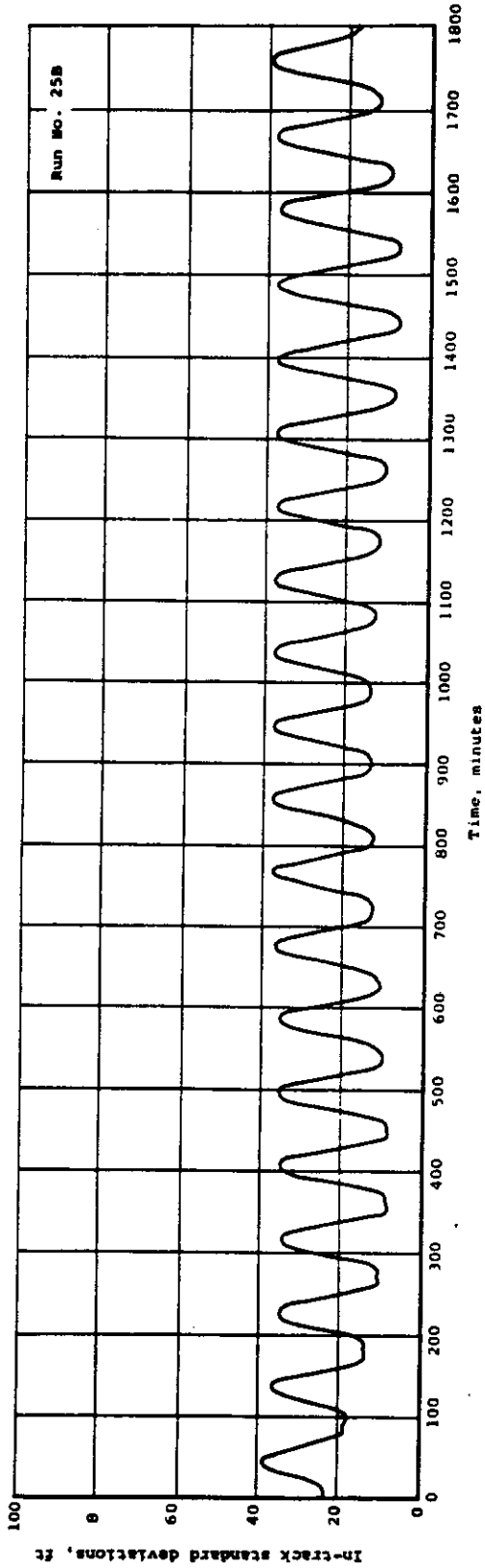

Fig. 4-10 — Plot of standard deviation of in-track component of orbit position error versus time for case 5, using 50 percent of photogrammetric observations

data, with cloud cover effects) except that altimeter data were included over open water areas, as discussed in Section 4.2.4. The results for this case, combining the 321 altitude measurements with the 147 photogrammetric observations are shown in Table 4-4.

The seventh case was an extension of the sixth case to study the effect of varying the amount of altimeter data used. Conditions were identical to case 6 except that only 10 percent of the available altimeter data were used (every tenth observation, 32 total). Selected results are also tabulated for this case.

In the eighth case, the effect of adding TRANSIT data to the photogrammetric observations were studied. The conditions for this run were the same as for case 5, except that 167 TRANSIT observations for the sixteen station network described in Section 4.2.4 were included with the 147 photogrammetric observations. The results for this case are also tabulated.

The effect of TRANSIT data alone was also studied. Conditions for case 9, were the same as in case 8 except that the photogrammetric data were left out. The results for this case are tabulated for comparison.

The tenth and last case of this series combined the photogrammetric data with both altimeter (full set, not 10 percent) and the TRANSIT observations. The effect of these combined types of data is indicated by the results listed for the last case in Table 4-4. A plot of the in-track component of orbit position uncertainty as a function of time is presented in Figure 4-11 for this case.

4.8.3 Uncertainties in Orbital Position Due to Lack of Precision in Observations and Uncertainties in Station Locations and Reference Datums

The next series of calculations was made to study the effects of station location errors and unkown datum shifts on the orbital position uncertainties already calculated. These runs were similar to the ten cases presented in the preceding section, except for the ninth (case number 19 here). The inital conditions, atmosphere, and gravity models were the same. The results of these ten cases are listed in Table 4-5 for comparison with the results already presented in Table 4-4. In addition, plots of in-track uncertainty versus time are presented for some of the cases, as noted below.

Direct simulation of station location uncertainties as "Q" parameters in the error analysis mode of the TRACE program was not possible because of the large number of parameters involved. In order to overcome this limitation, an indirect approach was used to get a conservative estimate of this effect. For the photogrammetric data, the simulated error in datum position was added directly to the error of the observation. Thus, for each set of x-, y-, z- observations referenced to a particular datum, the variance-covariance matrix was developed. This was done by a supplementary computer program. The elements of this matrix were composed of two parts. The first was the variance of the basic observation (in this case, 900 square feet). The second part was the contribution due to the uncertainty of that datum position. The error assigned to datum positions had a standard deviation of 50 feet in the two horizontal directions and 30 feet vertically. No correlation among errors in the three directions was assumed. The variance-covariance matrix was built up by adding the variances due to the two effects, as though they acted as independent random effects.

Using the option in TRACE where by the variance-covariance matrix of each observation may be used instead of assigning a standard error to all observations of a given type, each x-, y-, or z- observation was input along with the variance-covariance matrix associated with the datum to which the observation was referenced.

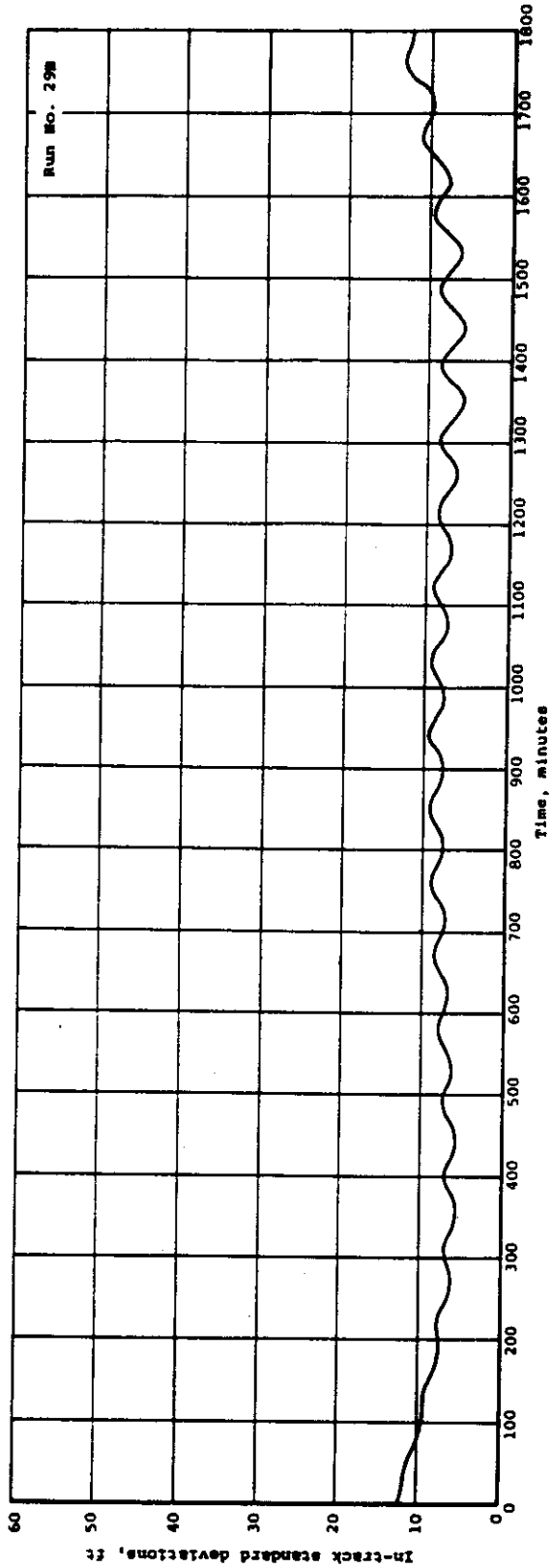

Fig. 4-11 — Plot of standard deviation of in-track component of orbit position error versus time for case 10, using combined set of 50 percent photogrammetric, TRANSIT and all altimeter observations

Table 4-5 — Selected Computed Results for 10 Cases Showing Effects of Observation and Station Location Errors on Orbit Position Errors

Case	Time, minutes	Orbit-Plane Error Components, feet: Radial Minimum	Radial Maximum	In-Track Minimum	In-Track Maximum	Cross-Track Minimum	Cross-Track Maximum	Comments
11	0	4.1	9.5	31.0	43.0	6.6	14.0	Full set photogrammetric observations
	720	4.1	9.7	16.0	39.0	6.6	13.0	
	1440	4.2	9.7	10.0	38.0	6.5	13.0	
	1800	4.2	9.7	24.0	43.0	6.5	13.0	
12	0	13.0	30.0	84.0	140.0	19.0	41.0	10 percent photogrammetric observations
	720	13.0	31.0	47.0	130.0	20.0	41.0	
	1440	12.0	31.0	29.0	120.0	19.0	41.0	
	1800	12.0	31.0	72.0	140.0	20.0	40.0	
13	0	6.8	27.0	75.0	110.0	11.0	45.0	Northern half photogrammetric observations only
	720	6.7	27.0	45.0	130.0	8.8	43.0	
	1440	9.0	26.0	19.0	110.0	11.0	42.0	
	1800	7.8	27.0	62.0	100.0	9.8	42.0	
14	0	6.7	37.0	37.0	150.0	19.0	38.0	Southern half photogrammetric observations only
	720	8.8	37.0	18.0	150.0	9.4	40.0	
	1440	6.9	37.0	13.0	140.0	8.1	41.0	
	1800	6.4	37.0	22.0	140.0	15.0	41.0	
15	0	5.8	14.0	26.0	62.0	9.3	19.0	50 percent photogrammetric observations
	720	5.8	14.0	23.0	56.0	9.3	19.0	
	1440	5.9	14.0	14.0	54.0	9.2	19.0	
	1800	5.9	14.0	25.0	60.0	9.2	19.0	
16	0	3.1	4.7	43.0	46.0	9.4	19.0	50 percent photogrammetric observations plus full altimeter
	720	2.9	4.6	22.0	29.0	9.3	19.0	
	1440	3.0	4.6	14.0	23.0	9.3	19.0	
	1800	3.2	4.7	32.0	34.0	9.2	19.0	
17	0	4.7	8.6	44.0	51.0	9.4	19.0	50 percent photogrammetric observations plus 10 percent altimeter
	720	4.6	8.6	23.0	40.0	9.3	19.0	
	1440	4.7	8.6	14.0	35.0	9.3	19.0	
	1800	4.8	8.7	34.0	44.0	9.2	19.0	
18	0	5.4	5.8	30.0	31.0	9.2	18.0	50 percent photogrammetric observations plus full TRANSIT
	720	4.9	5.8	18.0	25.0	9.2	18.0	
	1440	4.8	5.7	12.0	24.0	9.2	18.0	
	1800	4.9	5.8	28.0	33.0	9.1	18.0	
19	0	2.7	2.9	13.0	14.0	8.6	13.0	Same as 18 but no station error in TRANSIT
	720	2.6	2.8	9.1	11.0	8.5	13.0	
	1440	2.6	2.8	8.5	11.0	8.5	13.0	
	1800	2.7	2.9	17.0	17.0	8.5	13.0	
20	0	2.9	3.8	30.0	30.0	9.3	18.0	50 percent photogrammetric observations plus TRANSIT plus full altimeter
	720	2.8	3.7	17.0	21.0	9.2	18.0	
	1440	2.8	3.7	12.0	18.0	9.1	18.0	
	1800	2.9	3.8	24.0	28.0	9.1	18.0	

The size of the datum position uncertainty used was obtained from a consideration of the results anticipated from the PAGEOS program. This program will establish a worldwide network of high precision geodetic control from satellite observations. Using this established network the uncertainties in the relative positions of the traditional geodetic datums are expected to be reduced to 50 feet for horizontal errors, and 30 feet vertically.

To simulate station location errors for the TRANSIT data, it was necessary to interpret the position uncertainty of the observing site as an uncertainty in the range rate of change. This was done by considering the following equation for a Doppler type observation

$$\Delta f = f_0 \frac{V \cos \theta}{c}$$

where f_0 = frequency transmitted
Δf = frequency deviation
$f_0 + \Delta f$ = frequency received
V = velocity of vehicle
C = velocity of light
θ = angle between velocity vector and line from vehicle to observer

Taking the differential of the above equation:

$$d(\Delta f) = \frac{V}{C} \cos \theta \, df_0 + f_0 \cos \theta \, d\left(\frac{V}{C}\right) + f_0 \frac{V}{C} \sin \theta \, d\theta$$

The first term represents the effect of a small change of the transmitted frequency; the second term, a small change in velocity of the vehicle or of signal propagation (as caused by refraction, for example); the third, the direction of the vehicle relative to the observer. This last term can be used to simulate an uncertainty in the location of the observation station. Consider the following sketch:

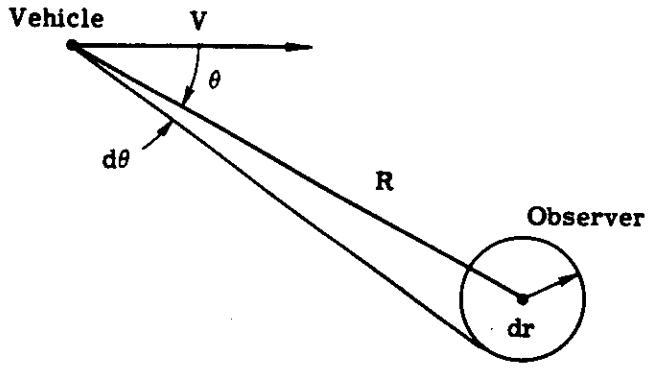

If the radius of uncertainty of the location of the observer is dr, this causes an uncertainty in the angle θ given, for the worst case, by the following:

$$d\theta = \frac{dr}{R}$$

where R is the range to the satellite. As a conservative estimate, the minimum range, which is the altitude of the vehicle, is used. For an uncertainty of 50 feet, an altitude of 160 nautical miles:

$$d\theta = \frac{50}{(160)(6080)} \text{ radians}$$

Substituting this value above and converting from frequency deviation to range rate by

$$\dot{R} = \frac{C}{f_0} \Delta f$$

gives the following value of range rate uncertainty

$$d\dot{R} = V \sin\theta \, d\theta = 25{,}000 \, (1) \frac{50}{(160)(6080)} \approx 1.3 \text{ foot per second}$$

A value of 1.5 foot per second was used in the computer runs to simulate the effect of TRANSIT station location errors along with the nominal observational error of 0.5 foot per second.

Thus, the effect of station location uncertainties for the TRANSIT sites and errors in the position of reference datums used in the photogrammetric observations was simulated by increasing the uncertainty associated with both the photogrammetric observations and the TRANSIT data. The altimeter data is not subject to a similar source of error.

The first five of the ten cases investigated in this set were again considered with the photogrammetric data alone. The results tabulated in Table 4-5 are nearly a factor of two larger than those for corresponding cases in Table 4-4. This is as expected since the effective standard deviation due to the use of the variance-coveriance matrix is just about double the standard deviation due to observational errors (slightly less than $\sqrt{50^2 + 30^2} = 58.3$ as compared to 30). Figure 4-12 presents the in-track component of the results for case number 11, which used all of the photogrammetric data. Figure 4-13 is a similar plot for the case number 15, using only half of the data to simulate effects of cloud cover.

The results for the case number 16, which combines altimeter data with the photogrammetric data, are presented in Table 4-5. The in-track component of orbit position uncertainty is shown in Figure 4-14. The seventeenth case, which used only 10 percent of the altimeter data of the case 16, gave the results shown in the table.

For case number 18, using photogrammetric and TRANSIT data only, the results shown in Table 4-5 indicate the effect of station location and datum errors when compared with the results of case number 8, and shown in Table 4-4. The plot of in-track error versus time is presented in Figure 4-15.

In the nineteenth case a change was made over the conditions of case nine in the preceding section. It would not have been worthwhile computing the station location error effect for this case, since the answer could be predicted to be ecactly three times as large as in the previous

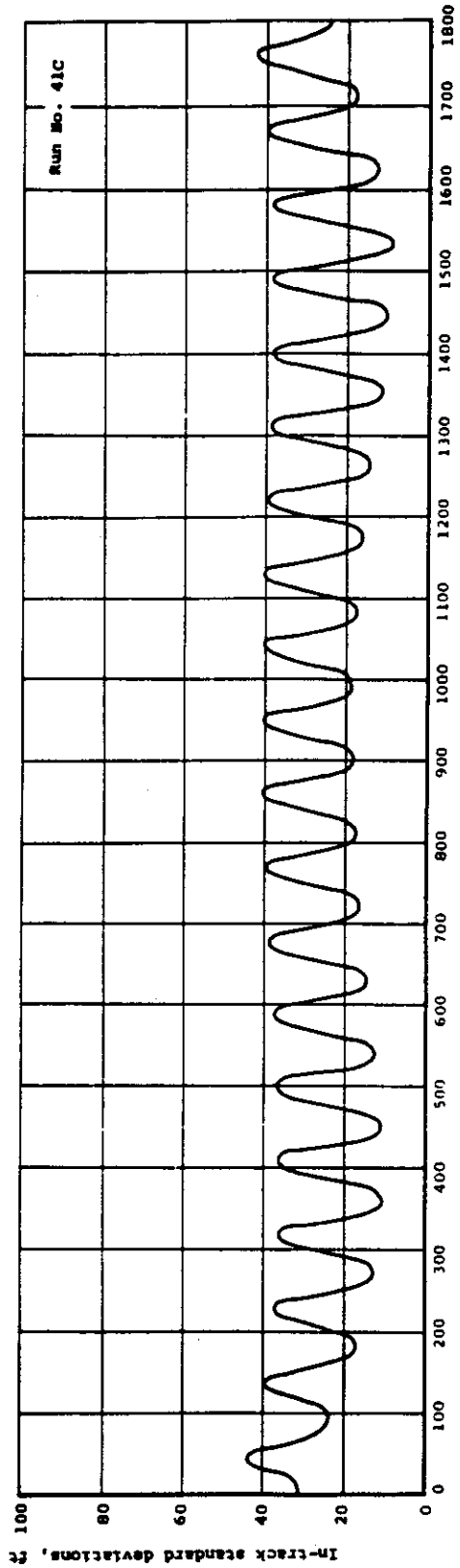

Fig. 4-12 — Plot of standard deviation of in-track component of orbit position error versus time for case 11, using full set of photogrammetric data and simulating datum position uncertainties

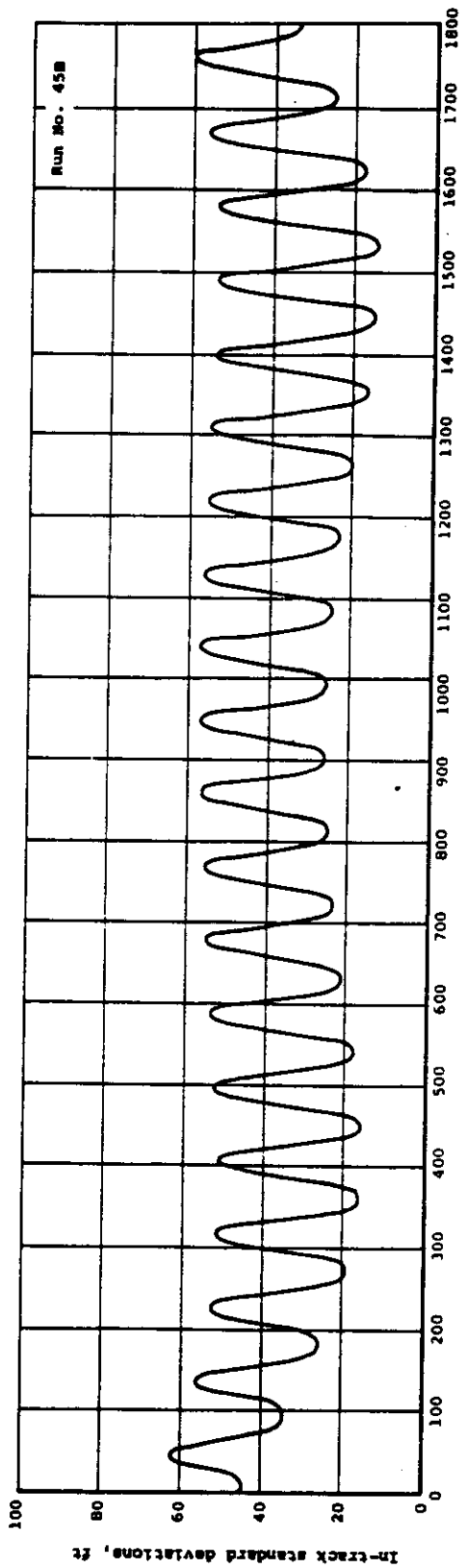

Fig. 4-13 — Plot of standard deviation of in-track component of orbit position error versus time for case 15, using 50 percent of photogrammetric observations and simulating datum position uncertainties

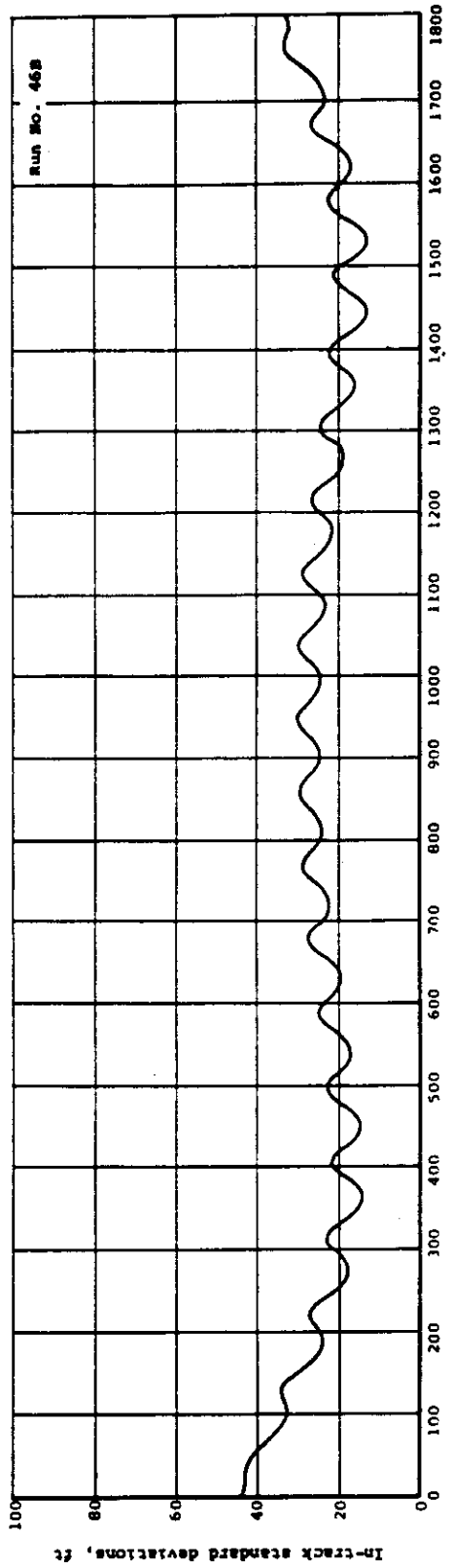

Fig. 4-14 — Plot of standard deviation of in-track component of orbit position error versus time for case 16, using 50 percent photogrammetric plus all altimeter observations and simulating datum position uncertainties

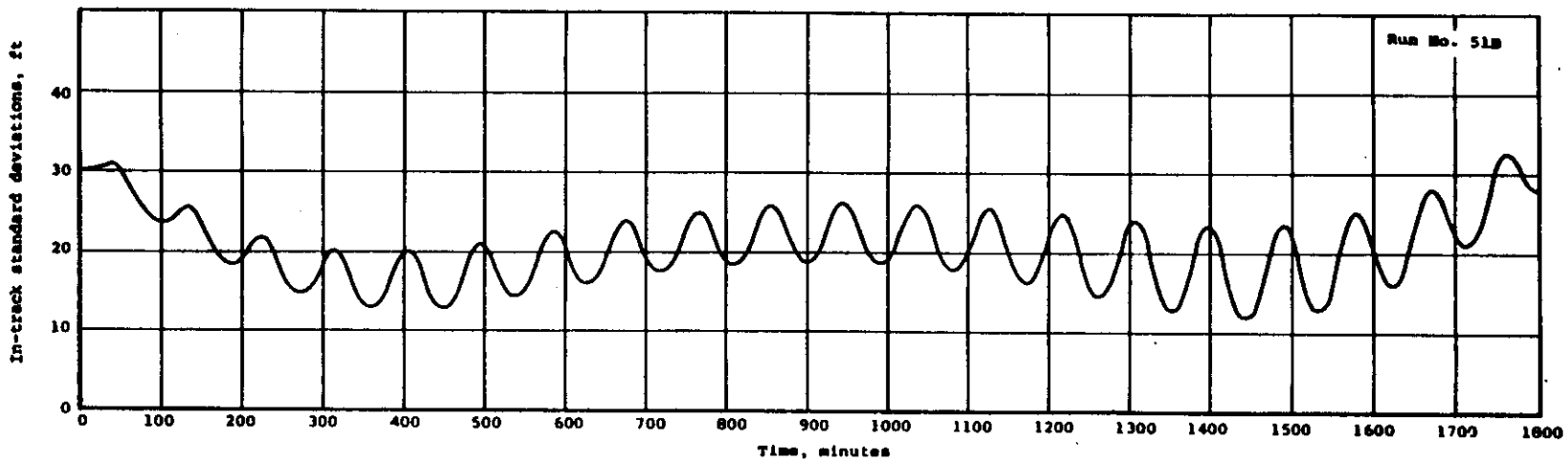

Fig. 4-15 — Plot of standard deviation of in-track component of orbit position error versus time for case 18, using 50 percent photogrammetric and all TRANSIT observations and simulating datum position and station location errors

series of runs because the effect of TRANSIT station location error was simulated by using observations with three times the nominal standard deviations. Instead, in case 19, only the datum errors were simulated and the TRANSIT station locations were considered error-free. Selected results for this case are shown in the table.

The last case of this series, number 20, using all the observations, photogrammetric, TRANSIT and altimeter is reported in Table 4-5. Figure 4-16 presents graphically the in-track component of orbit position error as a function of time. A comparison of this figure with Figure 4-11 shows the effect of station location and datum errors when using the three data types together.

4.8.4 Uncertainties in Orbital Position Due to Drag Uncertainties

The effect of a one percent uncertainty in the drag parameter, C_DA/W, was studied using the Q-parameter option of the error analysis mode. The orbit and observations were the same as for case 20, the combination of all three data types with the effects of station location and datum position errors. For these conditions, and error analysis run was made using the six initial conditions as P-parameters and the ballistic coefficient as a Q-parameter. The results of that case are presented in Figure 4-17, showing the in-track component of orbit position uncertainty with and without the one percent drag uncertainty. This case was numbered 21 in the sequence of calculations.

4.8.5 Uncertainties in Orbital Position Due to Uncertainties in Selected Gravity Model Parameters

An effort was made to use the error analysis mode of TRACE using certain coefficients of the gravity potential expansion as Q-parameters. However, the results appeared erroneous. Upon investigation, it was suggested by Aerospace personnel familiar with the details of TRACE that, because of the way in which the normal matrix is manipulated in the error analysis mode, severe effects due to numerical round-off occur in the case when gravity coefficients are used as Q-parameters. Therefore, this aspect of the computations was considered no further except as discussed in Section 4.8.10.

4.8.6 Uncertainty in the Determination of Selected Gravity Model Parameters Due to Observational Errors

Three cases were tested to determine the effect of observation errors on the uncertainty of solving for selected gravity model parameters. Two parameters were considered, $J_{2,2}$ and $J_{4,2}$. Using the observations of case number 20 (i.e., photogrammetric, TRANSIT, and altimeter data for a one-day polar, circular orbit, with simulated station location and datum errors) and solving for the six initial conditions and one gravity parameter in the first two cases, and both gravity parameters together in the third case, the following results were obtained:

Case	Gravity Parameter, $J_{n,m}$	Standard Deviation, σ_J/J
22	$J_{2,2}$	0.00254
23	$J_{4,2}$	0.01092
24	$J_{2,2}$	0.00256
	$J_{4,2}$	0.01087

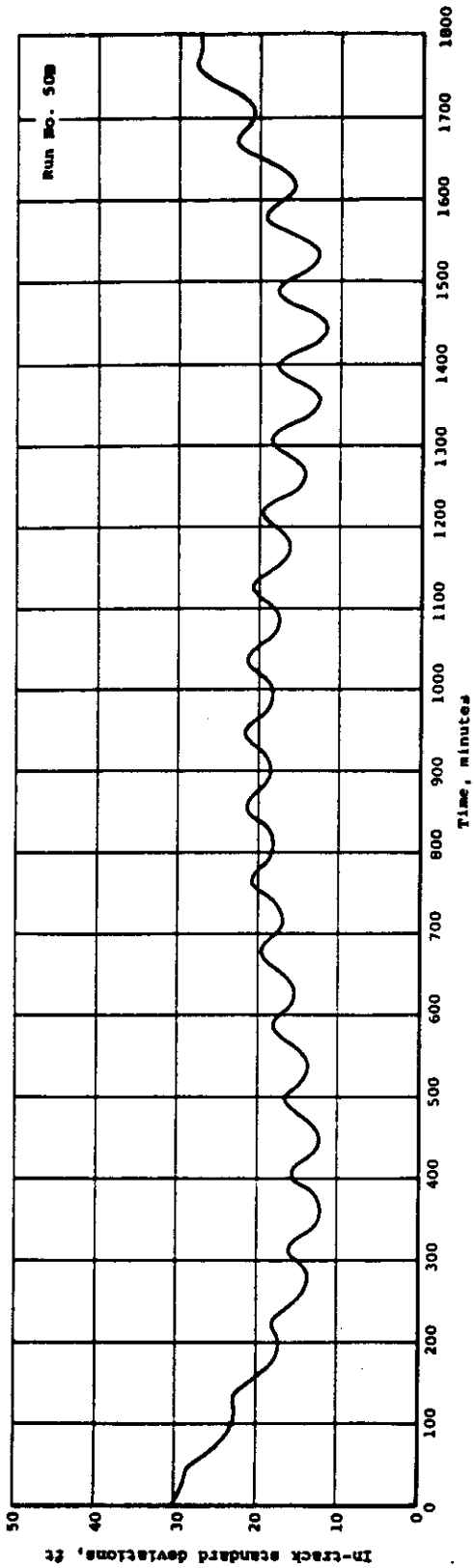

Fig. 4-16 — Plot of standard deviation of in-track component of orbit position error versus time for case 20, using 50 percent photogrammetric, all TRANSIT and all altimeter observations, and simulating datum position and station location errors

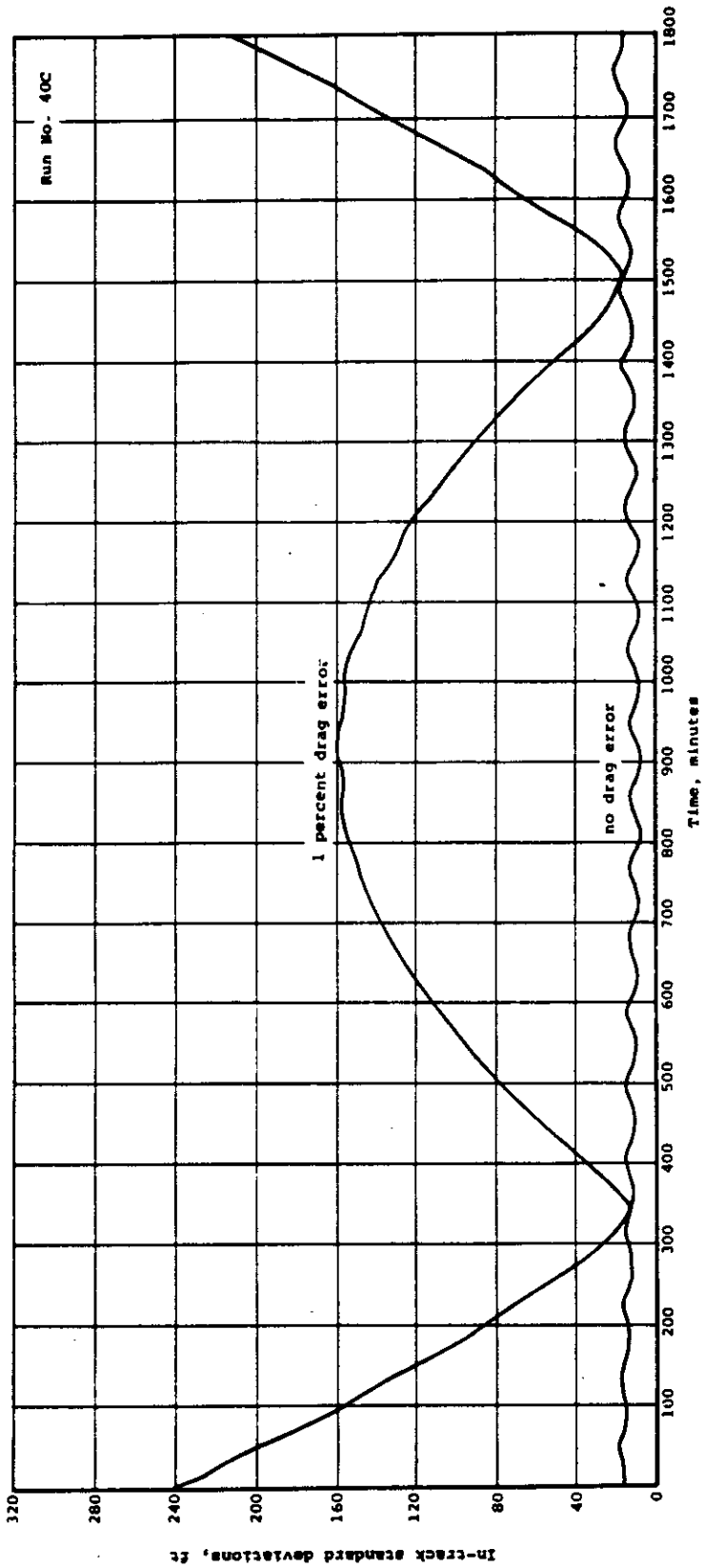

Fig. 4-17 — Plot of standard deviation of in-track component of orbit position error versus time for case 21, showing effect of a 1 percent uncertainty in ballistic coefficient

4.8.7 Uncertainties in Datum Positions Due to Observation Errors

A set of runs was made in an effort to determine how sensitive the proposed system would be for detecting shifts in the various geodetic control datums. It was necessary to use the photogrammetric data network, in this set but since the x-, y-, z- observation in TRACE does not depend on station location (it is referred to an earth-centered system) another approach had to be taken. This was done with the aid of a supplemetary computer program that used the x-, y-, and z-observation data to generate an equivalent set of radar observation data (range, aximuth, and elevation). That is, a fictitious radar station was assigned a location within an area of geodetic control (for example, the North American Datum), for each datum considered. For each x-, y-, and z-observation, the location of the vehicle was defined, and knowing the location of the fictitous radar station, the vector from the station to the vehicle was computed and resolved into range, azimuth, and elevation components. The stadnard deviations of the range, aximuth, and elevation were computed for each observation so that the error distribution of the orbital position remained spherical. That is, for equal standard deviations in the x-, y-, and z- directions ($\sigma_X = \sigma_Y = \sigma_Z = \sigma$), the standard deviations of the equivalent radar observations were computed from:

$$\sigma_R = \sigma$$

$$\sigma_E = \frac{\sigma}{R}$$

$$\sigma_A = \frac{\sigma}{R \cos E}$$

The equivalence of the two sets of observations (x-, y-, z-and equilvalent R, A, E) was verified by comparing the corresponding normal matrices for the two sets. These checked to two significant figures.

Using the photogrammetric data network, equivalent radar observations were generated for the polar, circular orbit of 156.7 nautical miles altitude for one day under the same conditions as in preceding computations. Five goedetic control datums were considered, in the following geographic areas: North America, South America (Argentina), Africa, Asia and Australia. (Insufficient observations of the European area were obtained, as this area was straddled by adjacent revolutions for the set of conditions chosen for this one-day case.) Three cases were tested. First, case 25 solved for the six initial conditions, drag, and four of the five station locations (latitude, longitude, and altitude) that represented datum positions. Second, case 26 solved for five of the six initial conditions (holding right ascension fixed), drag, and all five station locations (datum positions). Last, case 27 solved only for the five station locations, considering the orbit completely known without error. The results of this set of calculations are presented in Table 4-6, showing the computed standard deviations in latitude, longitude, and altitude of the five datums considered for the three cases.

An extension of this set of calculations was made, using the Q-parameter option of the error analysis mode of TRACE to determine the effect of datum position uncertainties on orbital position errors. This was done in order to check some of the assumptions used in cases 11 through 20 discussed in Section 4.8.3 where datum position uncertainties were simulated by adding observational uncertainties. The results are listed in Table 4-7 for the first two cases above with and without Q-parameter effects. Case 28 is the error analysis run for the normal matrix of case 25, and case 29 corresponds similarly to case 26. The in-track component of orbital

Table 4-6 — Errors in Computed Datum Position Due to Photogrammetric Observation Errors for Three Cases

		Datum Errors, feet		
	Component	Case 25	Case 26	Case 27
North America	Latitude	–	30	25
	Longitude	–	31	11
	Altitude	–	15	10
South America	Latitude	35	36	27
	Longitude	26	21	12
	Altitude	15	17	11
Australia	Latitude	79	95	28
	Longitude	22	9	8
	Altitude	13	13	10
Asia	Latitude	66	70	28
	Longitude	19	15	13
	Altitude	11	16	11
Africa	Latitude	54	61	32
	Longitude	18	6	5
	Altitude	13	15	9

Table 4-7 — Selected Computed Results for 4 Cases Showing Effects of Observation and Datum Location Errors on Orbit Position Errors (see Section 4.8.7)

		Orbit-Plane Error Components, feet						
	Time,	Radial		In-Track		Cross-Track		
Case	minutes	Minimum	Maximum	Minimum	Maximum	Minimum	Maximum	Comments
28(P)	0	2.5	6.6	16.0	27.0	3.4	7.0	No errors in datums
	720	2.5	6.7	8.6	25.0	3.4	6.9	
	1440	2.7	6.7	5.3	26.0	3.4	6.9	
	1800	2.6	6.7	12.0	28.0	3.4	6.9	
28(Q)	0	12.0	21.0	93.0	106.0	21.0	27.0	50 by 50 by 30 feet
	720	11.5	21.0	53.0	97.0	21.0	28.0	datum error
	1440	11.5	21.0	36.0	87.0	22.0	27.0	(4 datums)
	1800	12.0	21.0	100.0	117.0	22.0	26.0	
29(P)	0	2.5	6.6	16.0	27.0	3.4	7.0	No errors in datums
	720	2.5	6.7	8.6	25.0	3.4	6.9	
	1440	2.7	6.7	5.3	26.0	3.4	6.9	
	1800	2.6	6.7	12.0	28.0	3.4	6.9	
29(Q)	0	14.0	26.0	98.0	127.0	20.0	26.0	50 by 50 by 30 feet
	720	13.5	26.0	54.0	114.0	21.0	27.0	datum error
	1440	14.0	25.0	36.0	106.0	21.0	27.0	(5 datums)
	1800	15.0	26.0	102.0	134.0	21.0	26.0	

position uncertainty for case 28 is plotted in Figure 4-18. This should be compared with Figure 4-7(a) (for datum positions known) and Figure 4-12 (for datum positions uncertain). (See discussion Section 4.9.)

4.8.8 Orbit Determination With Real Data Flight 1169

A set of real data was obtained from [redacted] for use in this study. Identified as Flight 1169, the data consisted of compacted radar observations (three points per pass) from the Satellite Control Facility tracking network for an orbit similar to the one used for the simulated data studies of the preceding sections. The elements were approximately as follows:

Perigee height = 167 nautical miles
Eccentricity = 0.002 (apogee height = 182 nautical miles)
Inclination = 82 degrees

The data were furnished for an interval of approximately two and one-half days. The estimated data errors, used in weighting the observations, are given by the following standard deviations: 100 feet for range, and 0.2 degree in both azimuth and elevation.

A nine parameter orbit fit was determined in three iterations, solving for the six initial conditions (the time of the ascending node was used instead of solving for the declination at a specified time), ballistic coefficient, and range bias parameters for two of the five tracking stations. The residuals obtained are summarized in the following tabulation in terms of RMS values of the range residuals for each tracking station.

Station	Number of Observations	RMS range Residual, feet
[redacted]	27	408
	36	508
	21	676
	18	590
	72	360

The normal matrix obtained in the orbit fitting was later used in the error analysis mode to compare observed residuals with uncertainties predicted by a statistical analysis. The weightings associated with the observations in forming the normal matrix were chosen as follows: range, 100 feet; azimuth and elevation, 0.2 degree each. The angles were arbitrarily given less than normal weighting to emphasize the stronger range data. The results of the error analysis computation are:

Component	Standard Deviation, feet maximum	minimum
Radial	20	9.5
In-track	78	18
Cross track	24	15

A large difference is noted between the RMS range residuals and the errors in orbit position predicted by a statistical analysis of the normal matrix. Although the range residual cannot be directly compared with the in-track, radial, or across-track component of orbit position uncertainty because its direction is not necessarily parallel with any of them, the vector sum of the

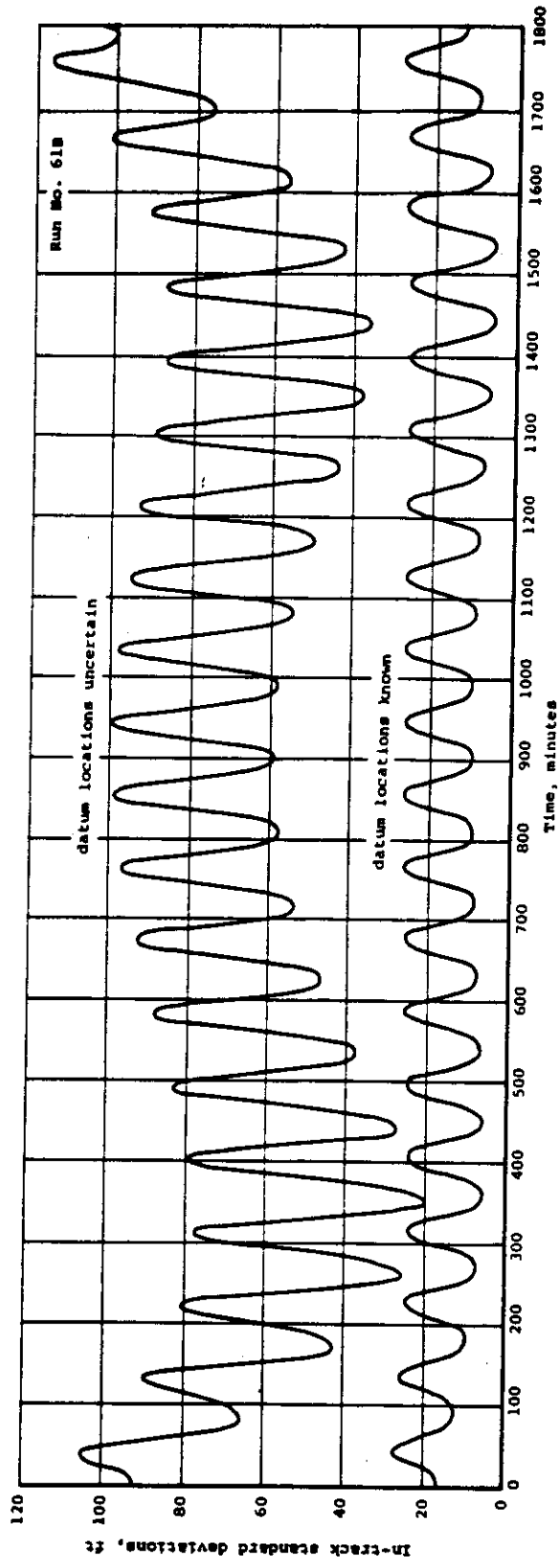

Fig. 4-18 — Plot of standard deviation of in-track component of orbit position error versus time for case 28, showing effect of errors in station locations for set of radar observations equivalent to photogrammetric observations

components should be somewhat comparable. The discrepancy between the sector sum and the observed range residuals is treated in the discussion of Section 4.9.

4.8.9 Solving for the Complete Gravity Model

Three cases were investigated in which an effort was made to solve for all of the tesseral harmonic coefficients of the gravity model. The orbit used for all the calculations of this series was the same polar, circular orbit of 156.7-nautical mile altitude of the earlier sections. In the first of these cases, case number 30, simulated observations from the five stations of the present SCF network for one day were used. The results for this first case appeared anomalous. This was attributed to the poor distribution of data for this form of the problem, and further work with this case was not undertaken.

In the second case of this series, case number 31, the full set of combined observations of case 10, including the photogrammetric, TRANSIT, and altimeter observations was used. The number of unkowns for this problem was 45, consisting of the six initial conditions, $C_D A/W$, 19 gravity model coefficients (from $J_{2,2}$ through $J_{6,6}$) and the corresponding 19 phase angles or longitudes ($\lambda_{2,2}$ through $\lambda_{6,6}$). For the initial guess, the gravity coefficients were made in error by a factor of approximately two in most instances, and the longitudes were altered from 10 to 20 degrees. The first guess for the initial conditions corresponded to an error in position of approximately 2500 feet, and the drag parameter was changed by 10 percent.

For the first interation, the RMS of all the weighted residuals was very large (3.5×10^3), indicating that the inital estimates were far from the best solution. The x-, y-, and z-residuals were of the order of 10^5 feet.

Two more interations solving for the same 45 parameters brought the weighted RMS residual figure to 7.8, and few x-, y-, or z-residuals exceeded 1000 feet. It was noticed in these first three iterations that little if any change occurred in the gravity model parameters. All of the correction was being accounted for by the six initial conditions and drag. Therefore, the next four iterations were taken holding the gravity model parameters fixed and solving only for the initial conditions and drag. The last iteration of this sequence was bad (i.e., the weighted RMS of residuals increased over that of the previous iteration), so the values of the solution in the sixth iteration were used to continue the study. The weighted RMS for this solution was 5.6.

The calculation was continued with the next (seventh) iteration, in which all 45 parameters were solved for. The solution for this case was bad. The corrections to the gravity model parameters were still quite small, with the notable exception of one angle, in which the change tried to exceed the bounds of 20 degrees which had been imposed on the solution. In addition, certain anomalies were observed in the correlation matrix for this solution. This calculation was abandoned at this point.

It was thought that the difficulty encountered in the second case could be overcome by using observations from orbits of differing inclination. The third case was carried out to check that conclusion. In case number 32, the observation data of case 31 was combined with simulated TRANSIT observations from two other circular orbits. For an inclination of 120 degrees, an altitude of 190 nautical miles was chosen as the second orbit. The third orbit was taken with inclination equal to 145 degrees and altitude equal to 177 nautical miles. As in the preceding case, the solution was started with off-nominal conditions, solving for the full parameter set in the first interation (59 parameters consisting of the 45 of case 31 plus 14 more from the six initial conditions and drag for the other two satellites). The weighted RMS of the first iteration

was 212. Two additional iterations were then performed, holding the gravity model parameters fixed and solving only for the 21 initial condition and drag parameters. This brought the weighted RMS to 4.8, and predicted very little improvement in the next iteration. Therefore, the calculation was continued from this point with the full parameter set (59 unknowns). The solution again was bad in that insignificant changes occurred in all of the parameters except isolated angles (dominantly $\lambda_{6,2}$, $\lambda_{3,1}$, $\lambda_{6,1}$, $\lambda_{5,2}$ and appreciable changes in $\lambda_{4,2}$, $\lambda_{3,2}$ and $\lambda_{3,3}$). The anomalies noted in the correlation matrix of the previous case were much less in evidence in this case.

Due to the long time required to make one iteration of orbit fitting with 59 unkowns, further calculations were not attempted for this case. It was concluded that determination of large numbers of gravity model parameters simultaneously could not be handled adequately by the program version of TRACE available to Itek, since this problem requires special numerical and analytical treatment.

4.8.10 Calculation of Orbit Position Differences for Two Gravity Models

The effect of fitting an orbit, data for which had been generated using one gravity model, to a different gravity model was considered in the calculations of case number 33. For the same polar, circular orbit of 156.7-nautical mile altitude, observation data were generated in TRACE using a gravity model different from the standard TRACE gravity model (unpublished Guier sixth degree model). Parameter values for this model, including terms from $J_{2,1}$ through $J_{7,6}$, were obtained from Reference 2 and private communication with Doctor R. J. Anderle. Data were generated for the three types considered: photogrammetric, altimeter, and TRANSIT. Using these combined observations, three iterations of orbit fitting, solving for six initial conditions plus drag, were performed to minimize residuals using the standard TRACE gravity model. The ephemeris of the original orbit with the different gravity model was then differenced with the ephemeris of the orbit fitted to the standard TRACE gravity model, and the components of that orbit position difference are plotted against time in Figure 4-19. A summary of the maximum and minimum values attained by these differences in case 33 is summarized in the following tabulation.

Component	Orbit position differences, feet	
	maximum	minimum
In-track	4136	2621
Radial	727	1027
Cross-track	1106	1090

The effect of high order resonance terms in the gravity model was also investigated with simulated data. In case number 34, the combined observations (generated with the standard TRACE gravity model) of the same 156.7-nautical mile polar circular orbit over a one-day period were fitted to a gravity model in which those high-order terms near the resonance condition were added to the standard TRACE gravity model. The terms used and their values are listed here:

n	m	$J_{n,m}$	$\lambda_{n,m}$, degrees
17	16	0.261×10^{-24}	14
17	17	0.247×10^{-25}	14.5
32	32	0.1095×10^{-50}	6.8

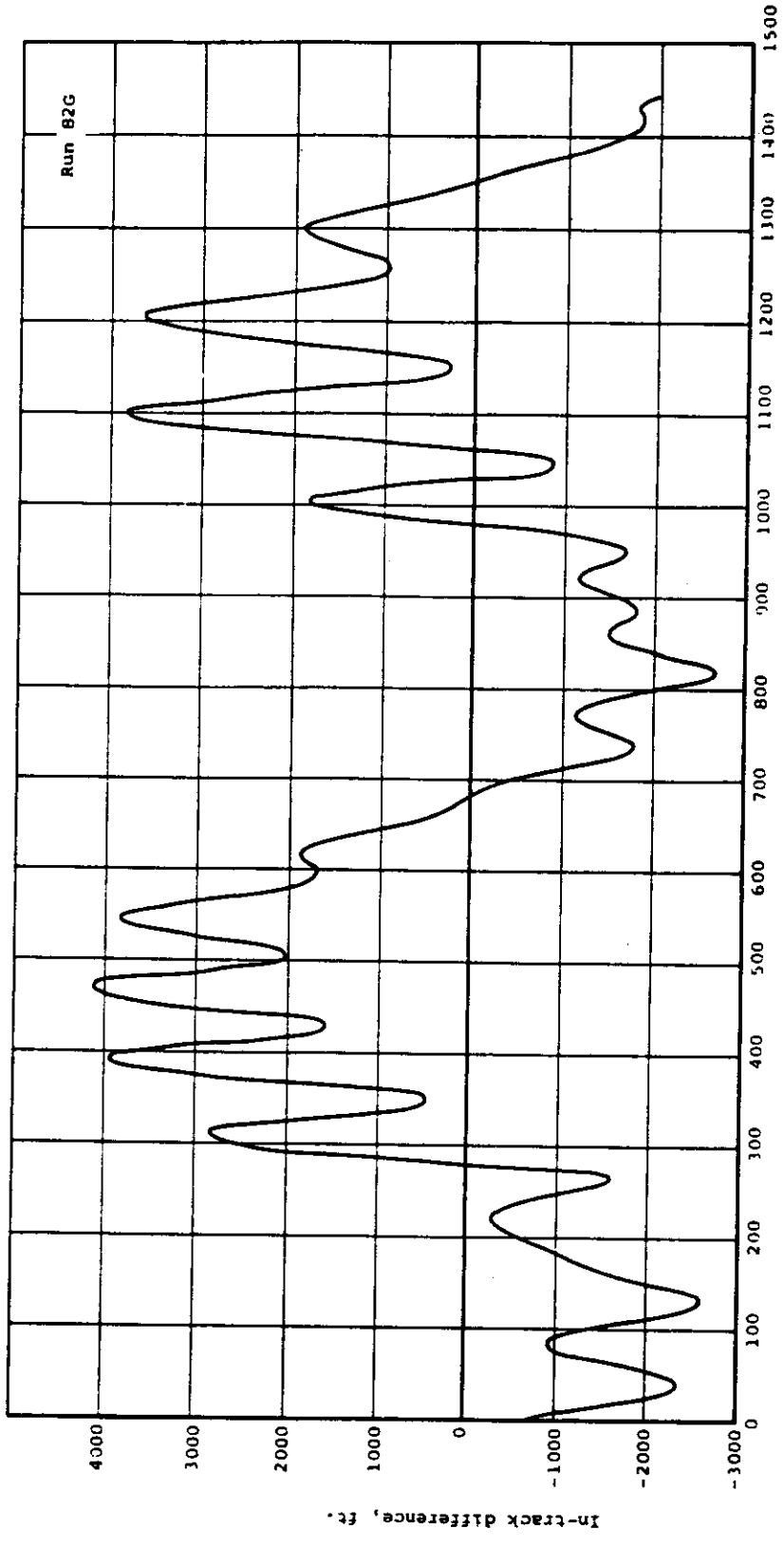

Fig. 4-19(a) — In-track component of ephemeris differences showing effect of fitting observations from a (7,6) gravity model orbit to the standard TRACE gravity model (6,6), case 33

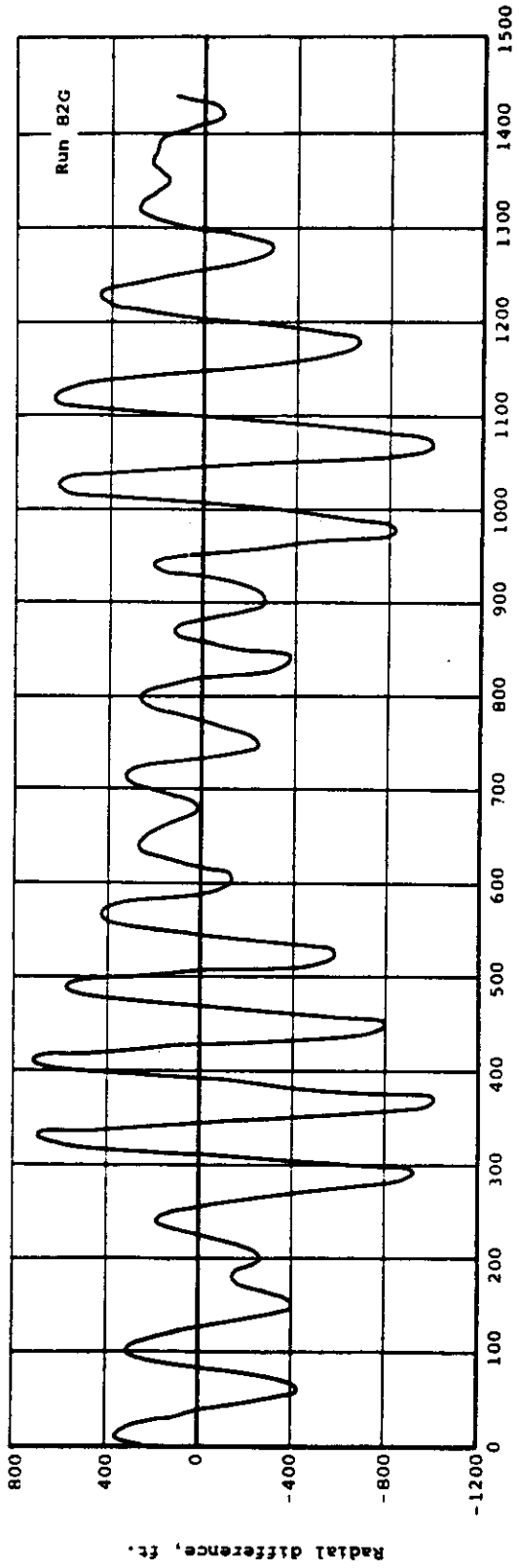

Fig. 4-19 (b) — Radial component of ephemeris differences showing effect of fitting observations from a (7,6) gravity model orbit to the standard TRACE gravity model (6,6), case 33

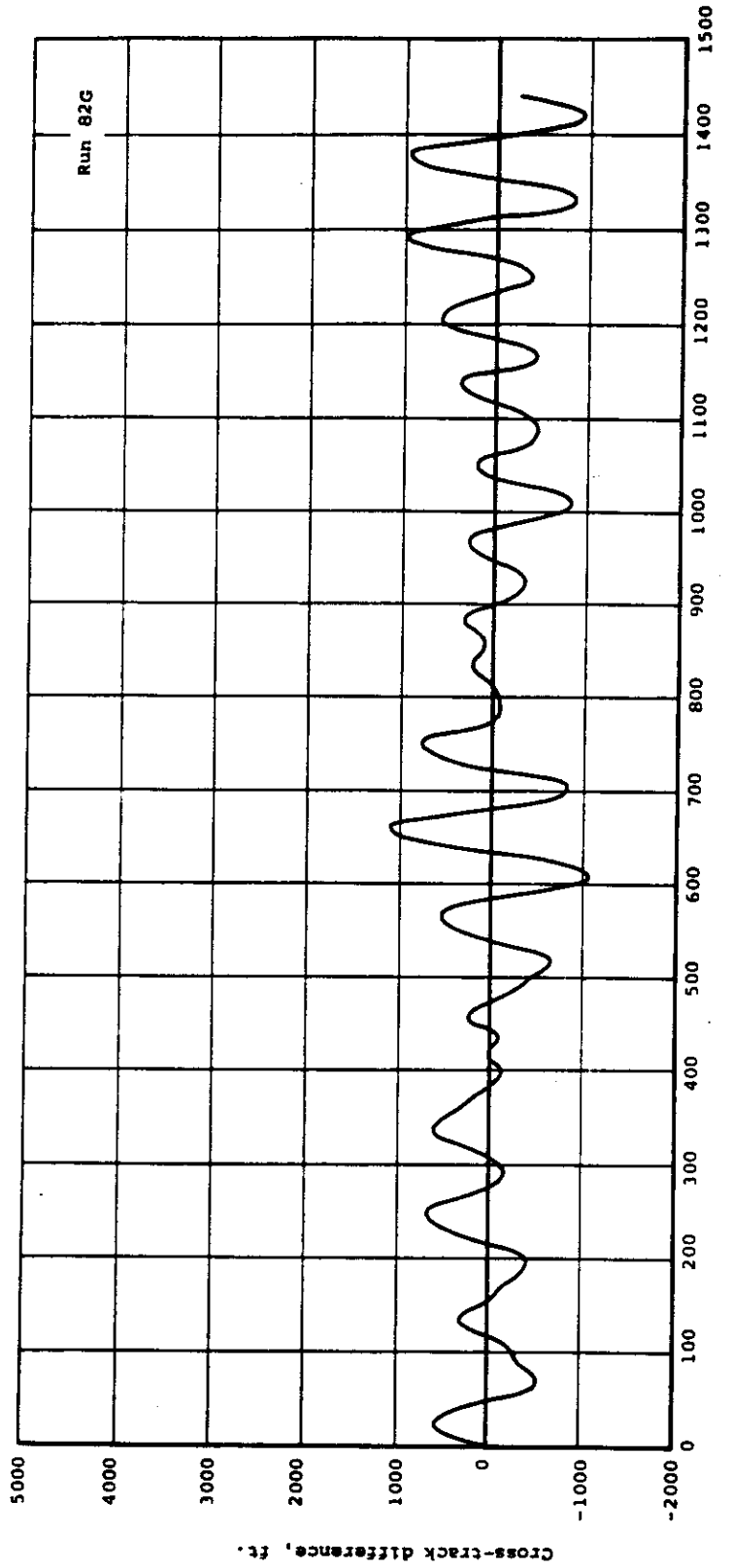

Fig. 4-19(c) — Cross-track component of ephemeris differences showing effect of fitting observations from a (7,6) gravity model orbit to the standard TRACE gravity model (6,6), case 33

Differences in the position between the original orbit and the fitted orbit were taken. The along-track component of this ephemeris difference is presented in Figure 4-20. Maximum and minimum values are listed below for case 34.

Component	Orbit position differences, feet maximum	minimum
In-track	350	-57
Radial	32	-29
Cross-track	178	-176

The results of the ephemeris differencing for two models differing by high degree resonance terms are seen to be much smaller for a one day period of orbiting than for the ephemeris differencing for two models differing primarily in the number of lower degree terms. For comparison purposes, since ephemeris differences over an entire mission is of primary importance, it may be more meaningful to compare RMS differences over the entire mission. It is estimated that such RMS ephemeris differences would be one-half to one-third times as large as peak differences quoted in this section.

4.8.11 Calculation of Orbital Position For Different Atmosphere Density Models

To study the effect of errors in the atmospheric density model, the calculations of case number 35 were performed. In this case, observations which were generated with the Lockheed-Jacchia Atmosphere Model, Reference 1, were fitted to an orbit using the ARDC 1959 Standard Atmosphere. For this case and for all the calculations to be described in following sections, the ballistic coefficient was changed from that of the preceding runs. This change, $W/C_DA = 75$ pounds/foot^2, reflects better information obtained during the course of this investigation.

In this case, then, the simulated observations were regenerated for the 156.7-nautical mile altitude circular polar orbit, using the standard TRACE Gravity Model and the Lockheed-Jacchia Atmosphere Model. These observations were then used in a seven parameter fit (six initial conditions plus C_DA/W) with the ARDC 1959 Atmosphere Model. After a start with an off-nominal initial guess, three iterations of the fitting process brought convergence of the solution. This fitted solution was then compared to the nominal solution, with the Lockheed-Jacchia Atmosphere Model, using the ephemeris differencing mode of the TRACE program. The in-track and radial components of the differences are plotted against time in Figure 4-21(a) and (b). Cross-track differences are not reported because they were quite small (± 2 feet) as was expected for an effect caused by vehicle drag.

4.8.12 Calculation of Orbital Position Differences for An Error In Drag

Continuing the study of effects of drag, a calculation was made to determine orbit position differences for a 1 percent error in the drag parameter. This was labeled case 36. The simulated observations generated for the calculation reported in the preceding section were now used in a six parameter fit (initial conditions only), using a value for W/C_DA of 74.25 pounds/foot^2, a 1 percent decrease. Again, the off-nominal initial estimate required three iterations to converge. The ephemeris for this converged solution was differenced with the ephemeris for the nominal solution (with which the observations were generated). The in-track and radial components of this difference are presented in Figure 4-22(a) and (b) as functions of time. Again, cross-track differences are not reported because of their insensitivity to this effect (± 1 foot).

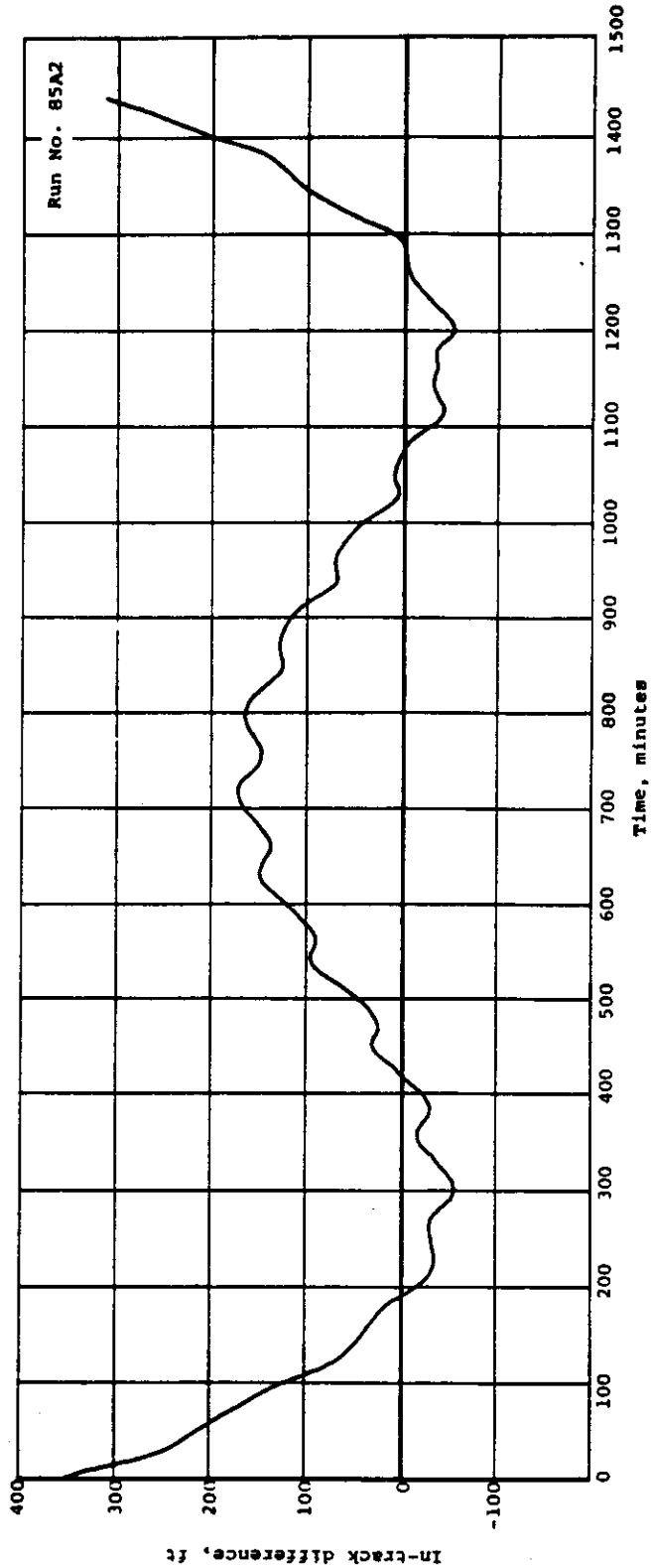

Fig. 4-20 — In-track component of ephemeris differences showing effect of including three high-order gravity model terms near the resonance point, case 34

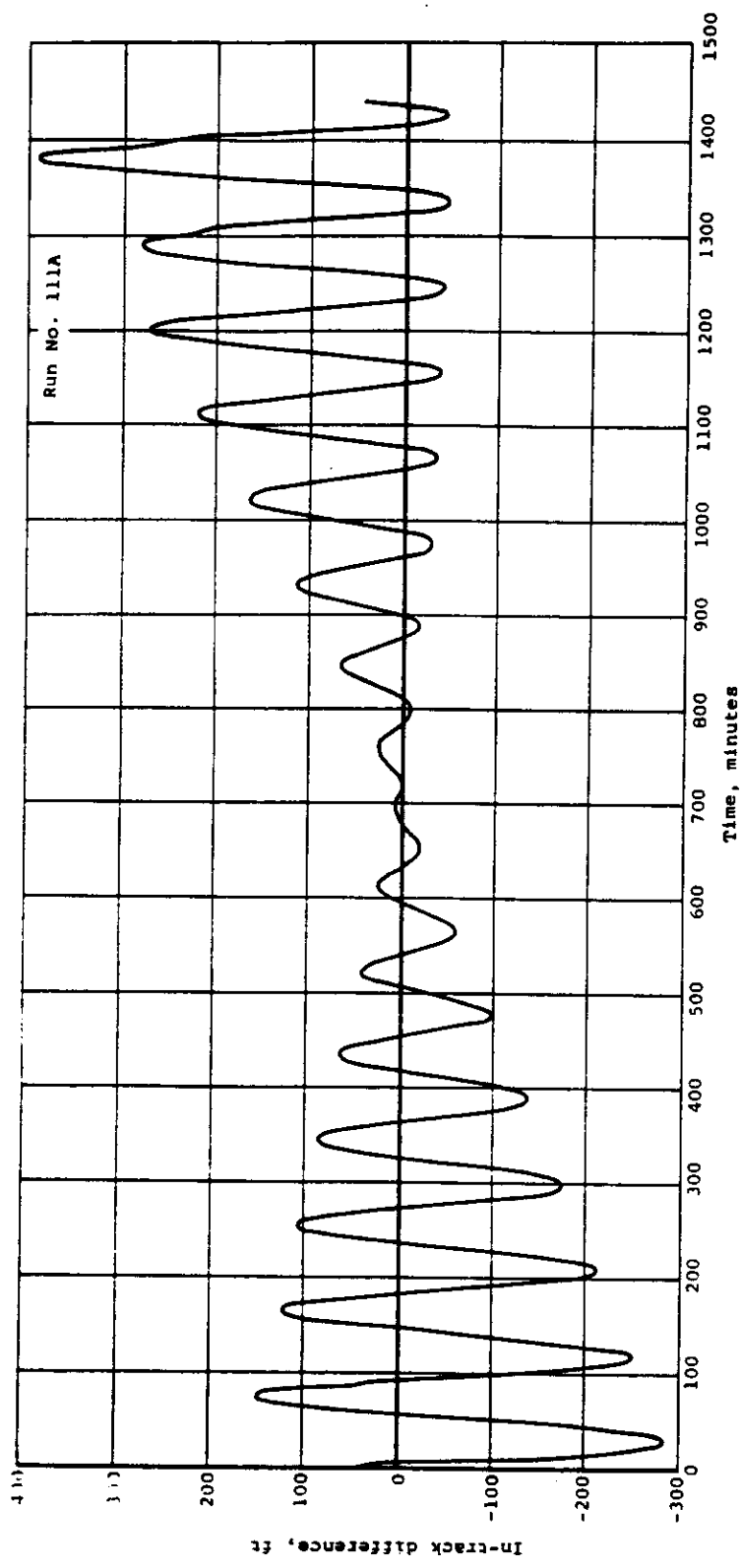

Fig. 4-21(a) — In-track component of ephemeris differences for two different atmosphere density models for 156.7-nautical mile altitude orbit, case 35

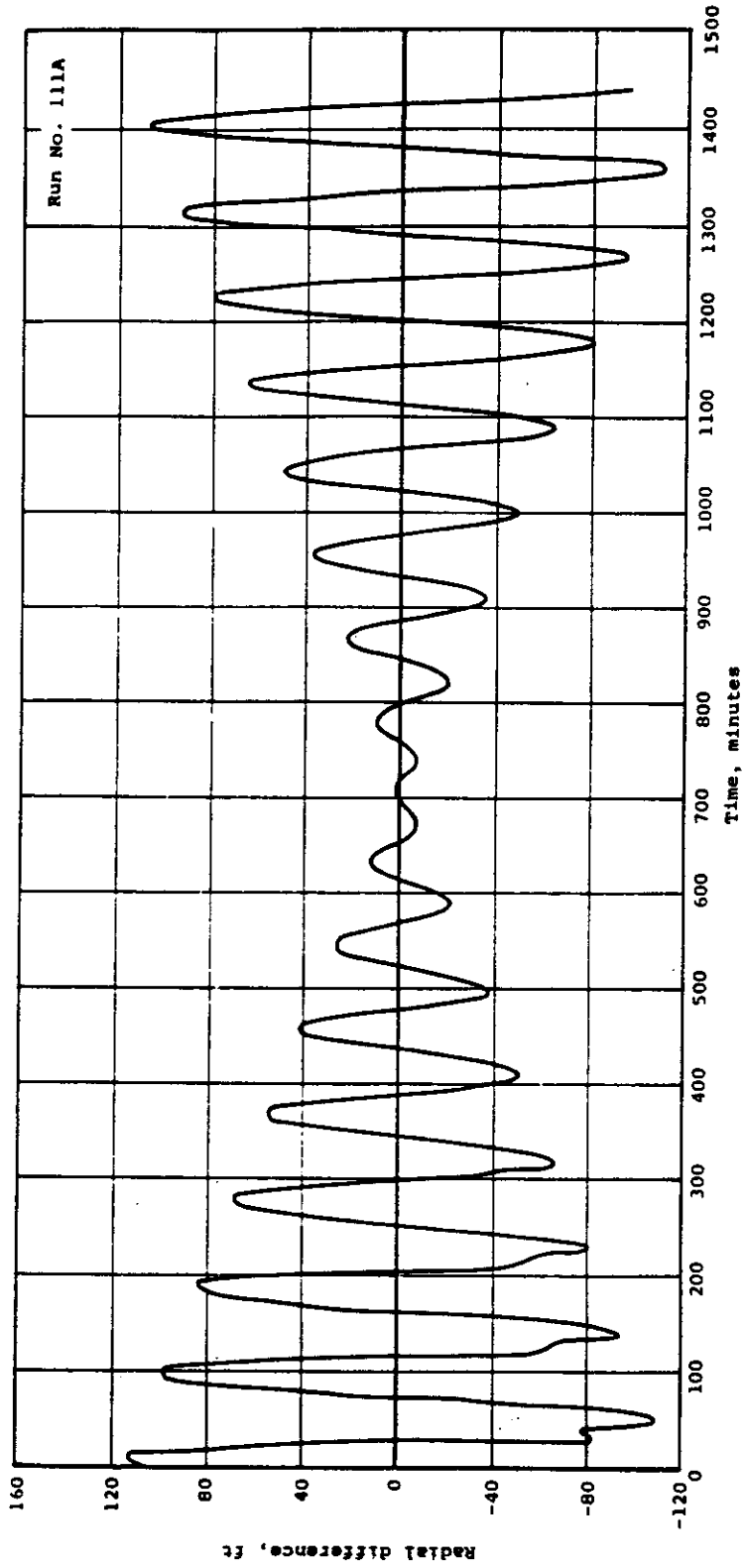

Fig. 4-21(b) — Radial component of ephemeris differences for two different atmosphere density models for 156.7-nautical mile altitude orbit, case 35

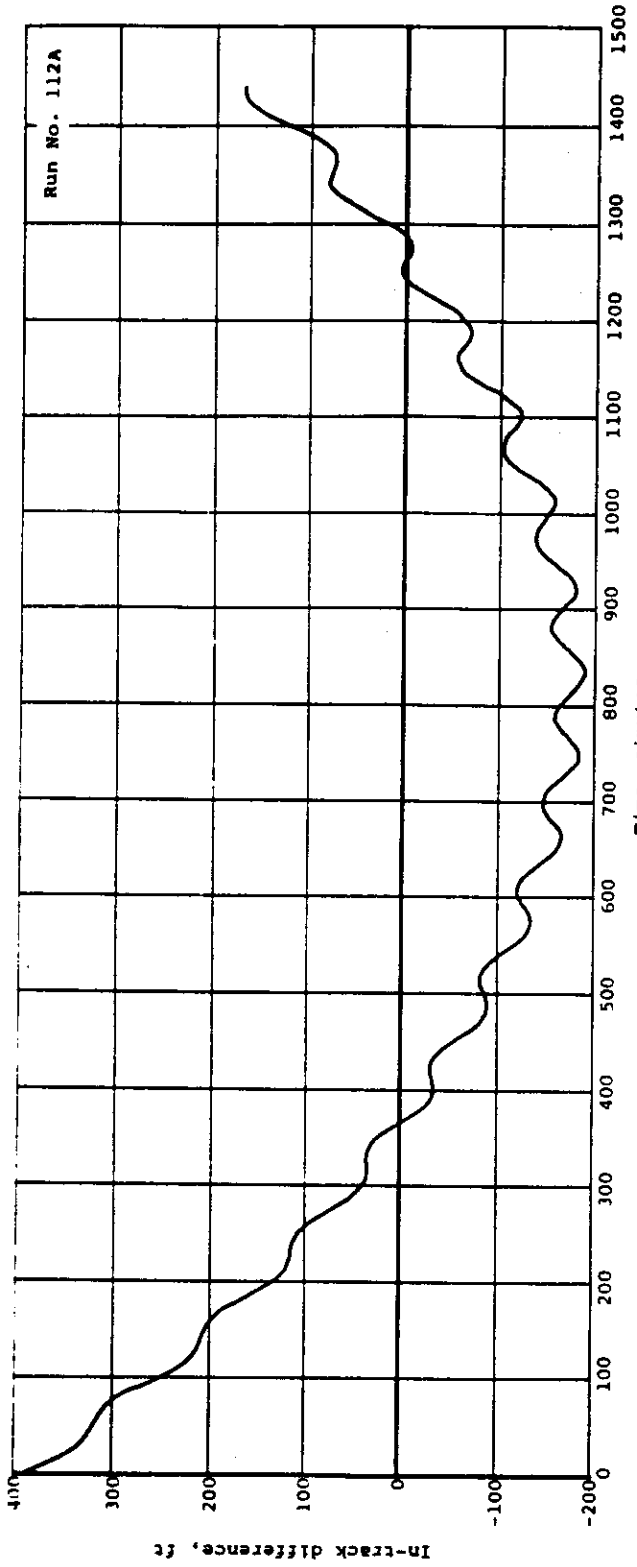

Fig. 4-22(a) — In-track component of ephemeric differences showing the effect of a 1 percent drag error for 156.7-nautical mile altitude orbit, case 36

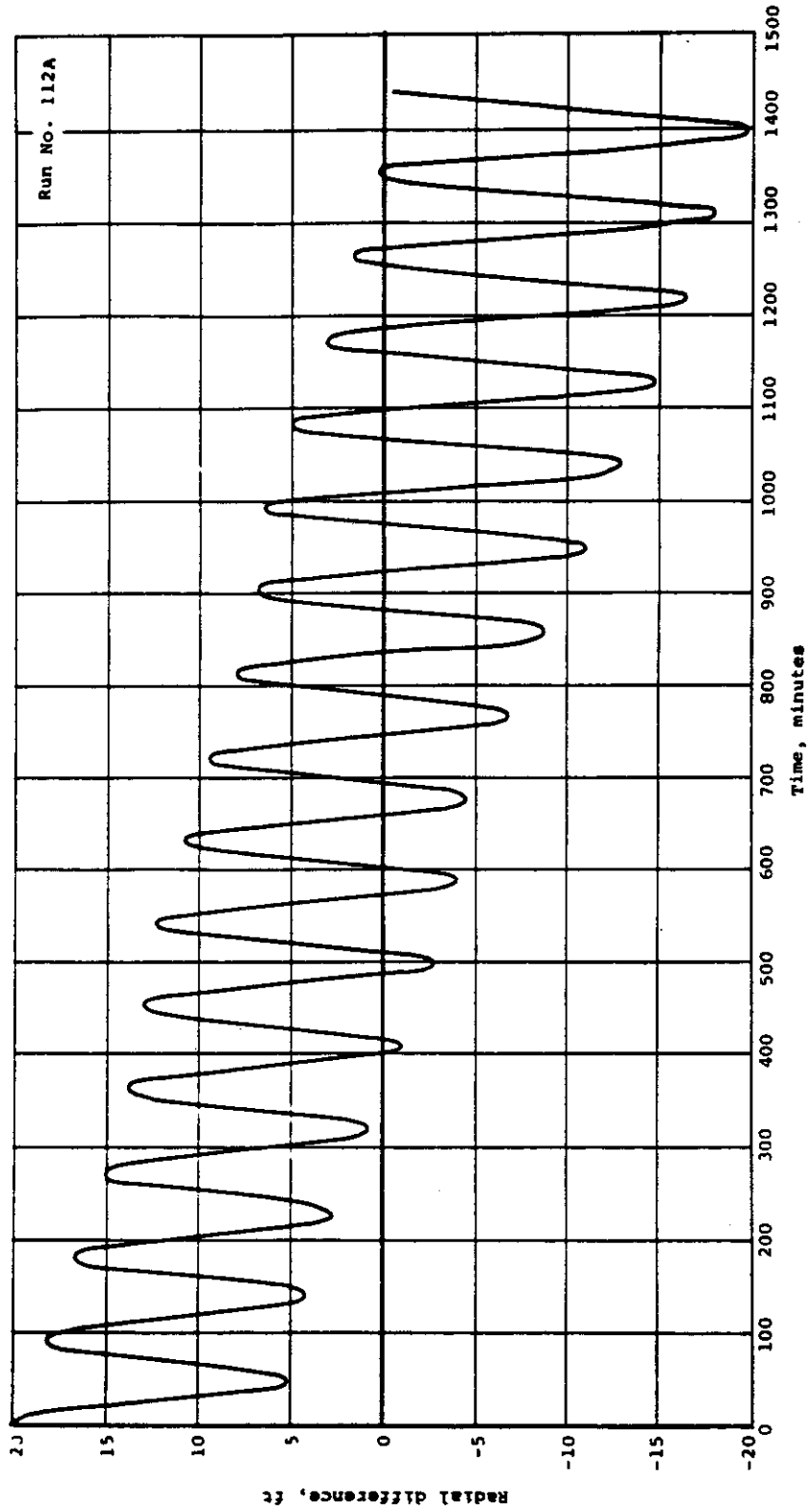

Fig. 4-22(b) — Radial component of ephemeris differences showing the effect of a 1 percent drag error for 156.7-nautical mile altitude orbit, case 36

4.8.13 Calculation of Orbital Position Differences for Errors In Station Locations

A set of calculations was made to determine the effect of errors in station locations and datum positions on orbit position using the ephemeris differencing option of TRACE. The same circular polar orbit of 156.7-nautical mile altitude was used in this case. Station location errors were introduced by reassigning the latitude, longitude, and altitude of the TRANSIT stations, moving them ± 50 feet north, ± 50 feet east, and ± 50 feet in altitude. The algebraic sign of the change in location was arbitrarily chosen in such a way as to simulate a random pattern.

The datum position errors were introduced by assigning biases to the x-, y-, and z-observations. This was done in a supplementary computer program by finding the components in the x-, y-, and z-system of a change in position of a point central to each of the datum considered. The magnitude of the position change was again taken as ± 50 feet north, ± 50 feet east, and ± 30 feet in altitude, the signs being mixed in a random pattern. Thus, all x-, y-, and z-observations which occurred in the area of one datum were assigned the same x-, y-, and z-biases, simulating directly the effect of errors in that datum position of 50 feet in the two horizontal directions and 30 feet vertically.

As the altimeter data is unaffected by station location errors, its use in these calculations was unchanged from its use in past calculations.

In case 37, observations of the three types (TRANSIT, altimeter, and photogrammetric or x, y, and z) for one day were used, along with the erroneous station locations and imposed biases, to determine a best fit solving only for the six initial conditions and drag. This best fit was then differenced with the orbit of the nominal initial conditions and drag. This ephemeris difference is presented in Figure 4-23, showing the in-track, radial, and cross-track components of orbit position differences due to errors in station locations and datum positions.

4.8.14 Calculation of Orbit Position Differences Due to Biases in the Observational Data

A number of calculations were made to determine the effects of biases in the observational data on the determination of orbital position. Using the combined observations for one day of the 156.7-nautical mile altitude polar circular orbit again, the following cases were investigated:

1. Case 38, using 100-foot bias in altimeter measurements
2. Case 39, using 1.0- foot/second bias in range rate measurements
3. Case 40, using 60-foot bias in the x-, y-, and z-measurements
4. Case 41, combining the biases in all three observation types

The size of these biases was obtained by arbitrarily doubling the standard deviation for each observation type.

The bias for the altimeter was taken always in the same direction. The directional sense of the range rate biases was alternated among the several TRANSIT stations arbitrarily to simulate a random distribution. Likewise, the sense of the bias in x-, y-, and z-measurements was alternated for the different datums to simulate a non-uniform effect.

Each of the cases was investigated by fitting an orbit to the biased observations and then taking the ephemeris difference between this and the nominal orbit. In cases 38 (altimeter bias alone) and 40 (x-, y-, z-biases only) the results of the orbit fitting led back to the nominal initial

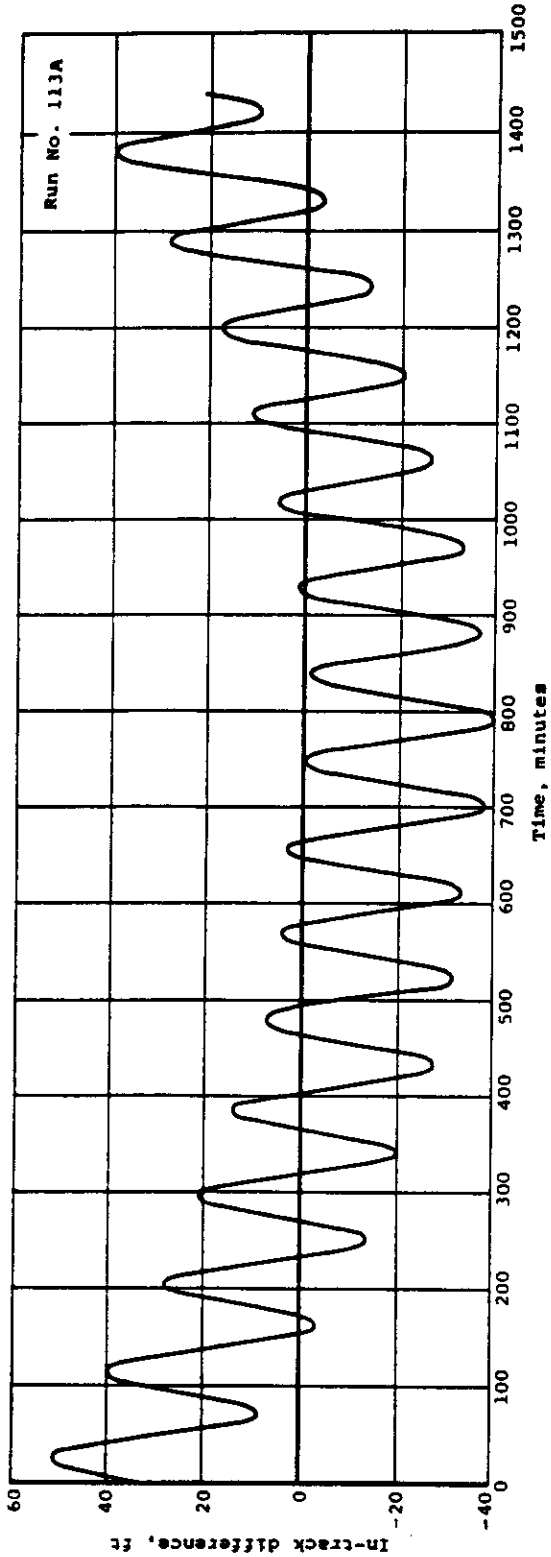

Fig. 4-23(a) — In-track component of ephemeris differences showing effect of station location and datum position errors, case 37

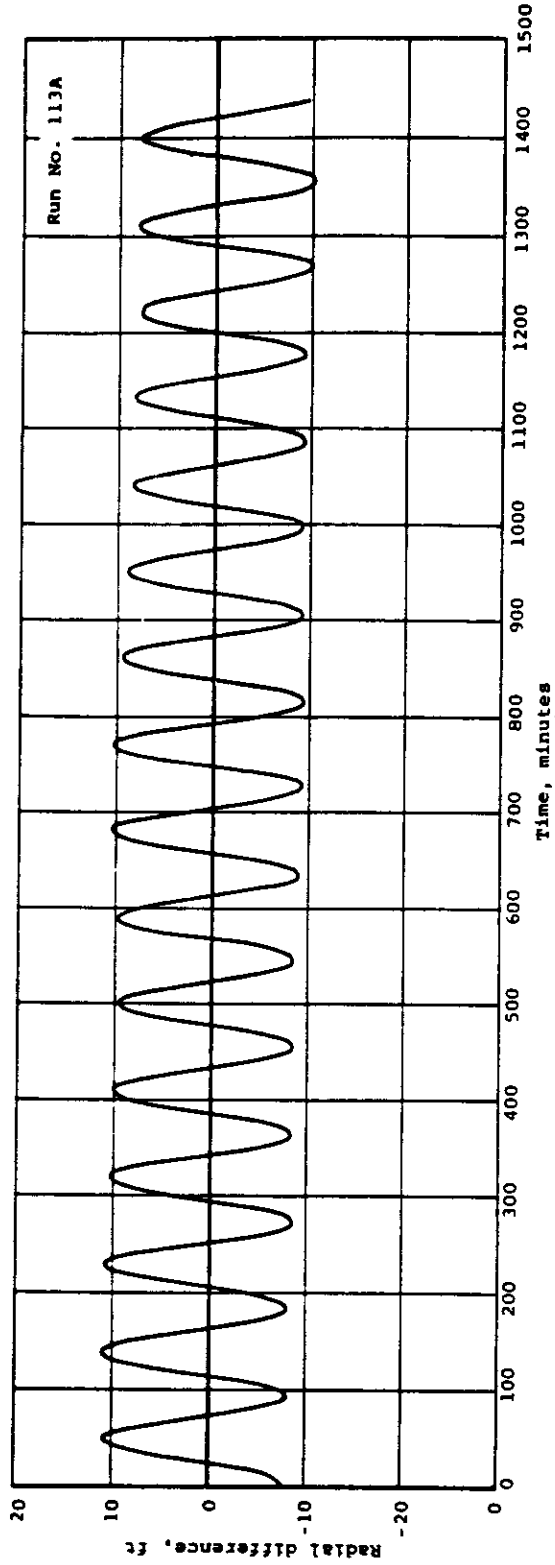

Fig. 4-23(b) — Radial component of ephemeris differences showing effect of station location and datum position errors, case 37

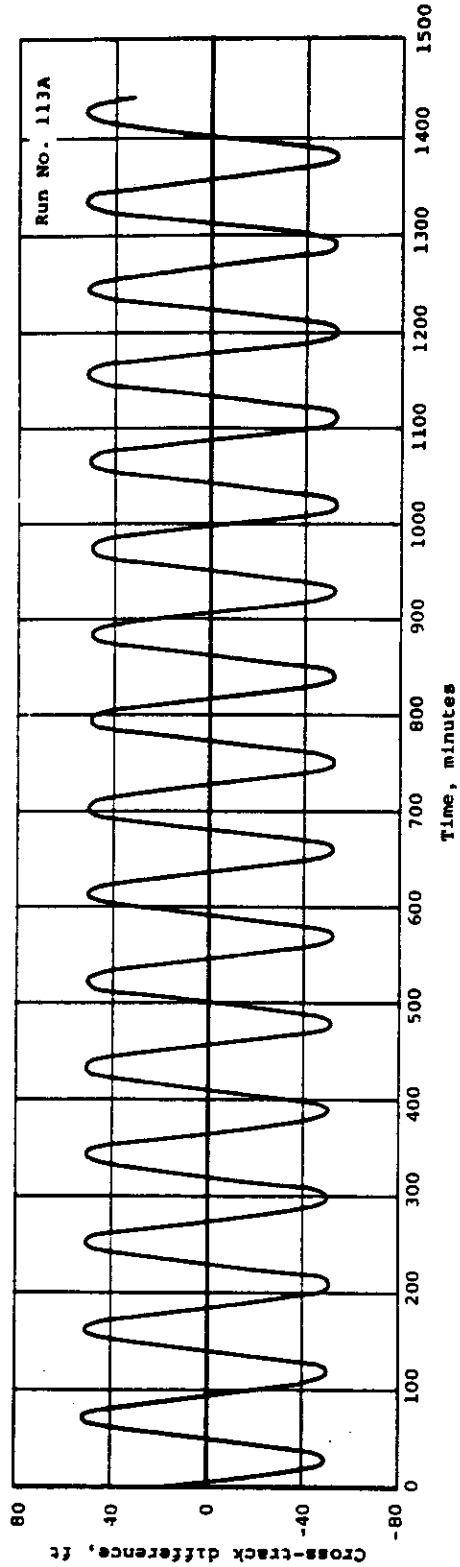

Fig. 4-23(c) — Cross-track component of ephemeris differences showing effect of station location and datum position errors, case 37

conditions (or very nearly so), so that the results of the ephemeris differencing for these cases are as much due to roundoff within the program as to the effect of using the biased observations. No ephemeris differencing results are reported, since no definite effect was observed.

A definite effect was observed in the cases of biased range rate observations. The in-track component of orbit position difference for case 39 (using biases only in range rate) is plotted against time in Figure 4-24. The radial and cross-track components for this case were much smaller (extrema of 16 feet and 4 feet, respectively). Examination of the residuals summarized for each observation station (the input observations were perfect except for the biases introduced in range rate) showed near zero residuals for the unbiased observations, and RMS residuals very nearly equal to the imposed biases for the range rate observations. This indicated that the small adjustment of the initial conditions performed in fitting this case was unable to accommodate the biased observations, and hence the solution that minimized the residuals was very close to the true solution with unbiased observations. The effect of the biases in this instance was merely to increase the weighted RMS residuals, not to alter the solution appreciably.

For case 41, including biases from all three data types, a similar situation applied. The in-track component of orbit position difference is presented in Figure 4-25. Comparison of this with the preceding Figure 4-24 indicates the along-track differences are only slightly larger in the present case. The radial components were similar (with extrema ± 14 feet, compared with 16 feet of before), but the cross-track component was much larger (± 53 feet) than before (± 4 feet). This increase can be attributed to the effect of the altitude and x-, y-, and z-biases.

4.8.15 Calculations for a Polar Circular Orbit of 225-Nautical Mile Altitude

Three sets of calculations were performed to investigate the advantages of extending the orbital altitude beyond the range originally considered for the system. The first two of these cases dealt with the decreased sensitivity of orbit position errors to uncertainties in vehicle drag effects. The last case dealt with the enhanced capabilities of orbit determination due to the increased number of observations.

The simulated observational data were regenerated for the same conditions as listed in Section 4.8.2 except for an altitude of 225 nautical miles at the equator. Thus, the initial conditions were:

Epoch: 21 December 1968, 12 hrs UT
Right ascension, α = 270.12 degrees
Declination, δ = 0.0001 degree
Flight-path angle, β = 90 degrees
Azimuth, A = 180 degrees
Radius, R = 22,293.769 feet
Velocity, V = 25,128.014 feet/second (circular)
W/C_DA = 75 pounds/foot^2

The number of observations obtained during the simulated one-day period are, for each of the data types: 324 altitude measurements, 308 from TRANSIT, and 150 photogrammetric (50 x, 50 y, and 50 z). This last figure reflects the 50 percent reduction, to simulate cloud cover effects, of the 300 photogrammetric observations available. It is noted that the number of altimeter and photogrammetric observations is nearly the same as for the 156.7-nautical mile altitude orbit, as is expected since these occur over the same areas of the world as before. However, the number of TRANSIT observations has increased by nearly a factor of two over

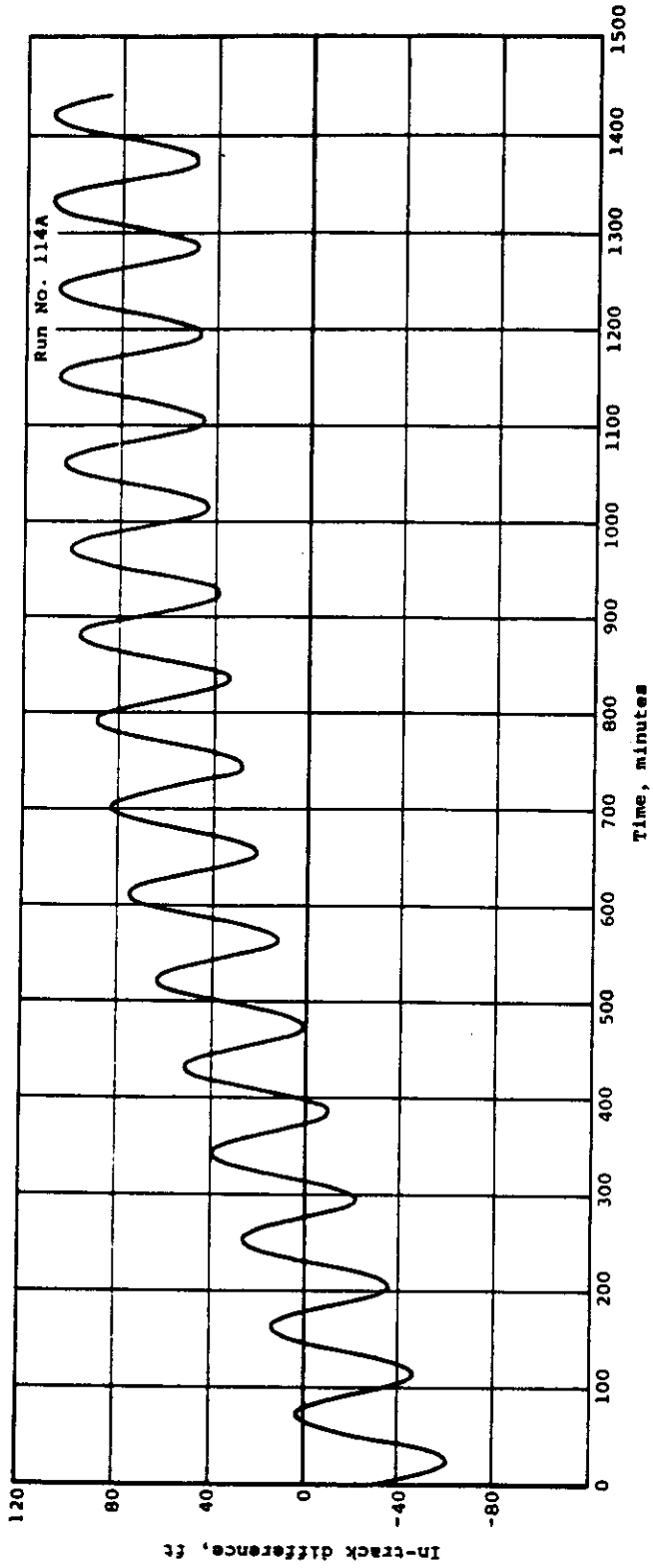

Fig. 4-24 — In-track component of ephemeris differences showing effect of range rate bias on the orbit determination from combined observations, case 39

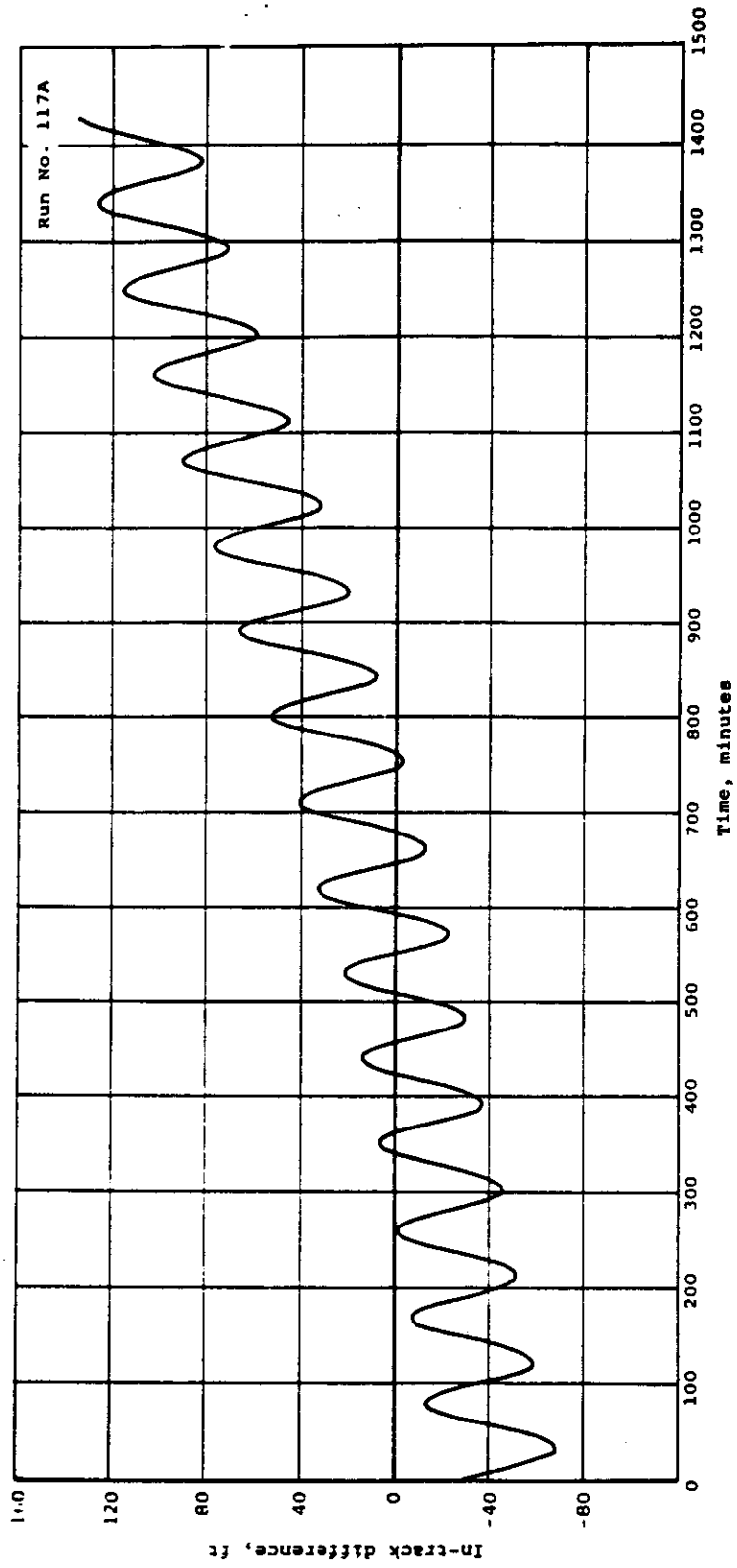

Fig. 4-25 — In-track component of ephemeris differences showing effect of biases in range rate, altitude and X, Y, Z-measurements on the orbit determination from combined observations, case 41

the previous case (167 from Section 4.8.2), because the vehicle can be tracked for longer periods at the higher altitudes due to the extended duration of visibility from each of the tracking sites.

The effect on orbit position of using different atmospheric density models was studied by repeating the calculation of case 35, (presented in Section 4.8.11), for the higher altitude observations. The results for the in-track component for this case, case number 42, are presented in Figure 4-26. Comparison of this plot with the plot for the 156.7-nautical mile altitude case in Figure 4-21(a) indicates a reduction of error by a factor between 4 and 5. A similar reduction in the radial component was also noted, although no plot for the radial component of the current case is presented.

Again, across-track errors were found to be so small that they could be attributed to numerical limitations of the calculation.

The calculation of the effect of a 1 percent error in drag was repeated for the higher altitude orbit. In a manner similar to that in case 36 (discussed in Section 4.8.12), the ephemeris of the nominal case for the 225-nautical mile altitude orbit was differenced with the best six parameter fit to the observations using an imposed error of 1 percent in the ballistic coefficient. This case was labeled case number 43. Results are presented in Figure 4-27, showing the in-track component of orbit position difference for this case. Comparison with the corresponding results for the 156.7-nautical miles case in Figure 4-22(a) shows a reduction factor of 4 to 5 again. The radial component showed similar behavior.

The last case examined for the higher altitude condition was essentially a repetition of the calculations of case 10, discussed in Section 4.8.2. For this last case, case number 44, an orbit determination was made using the combined altimeter, TRANSIT and photogrammetric observations (reduced in number to simulate cloud cover effects) solving for the six initial conditions and drag. The accumulated normal matrix was then used in the error analysis mode of TRACE, updating the covariance matrix in orbit-plane coordinates. This gave the results of Figure 4-28, which shows the in-track component of orbit position uncertainty, measured by the standard deviation, as a function of time. The corresponding results for the lower altitude orbit were presented in Figure 4-11 in Section 4.8.2, case number 10. Comparison of the values listed in Table 4-4 for that case with the values listed below for this case indicates the improvement in orbital determination accuracy achieved at the higher altitude:

	Orbit Plane Error Components, feet					
	Radial		In-track		Cross-track	
Time, minutes	Minimum	Maximum	Minimum	Maximum	Minimum	Maximum
0	1.6	2.0	10.3	11.1	3.3	6.0
720	1.5	1.9	5.6	8.1	2.9	5.7
1440	1.6	1.9	3.1	8.2	2.9	5.8
1800	1.6	1.9	8.6	11.9	3.0	5.6

4.8.16 References for Section 4.8

1. Density of the Atmosphere. Report No. LMSC-A08233, November 1, 1961, Lockheed Aircraft Corporation, Missiles and Space Division, Sunnyvale, California.
2. Anderle, R. J., Geodetic Parameter Sect NWL-5E-6 Based on Doppler Satellite Observations. NWL Report No. 1978, April 1965, U. S. Naval Weapons Laboratory.

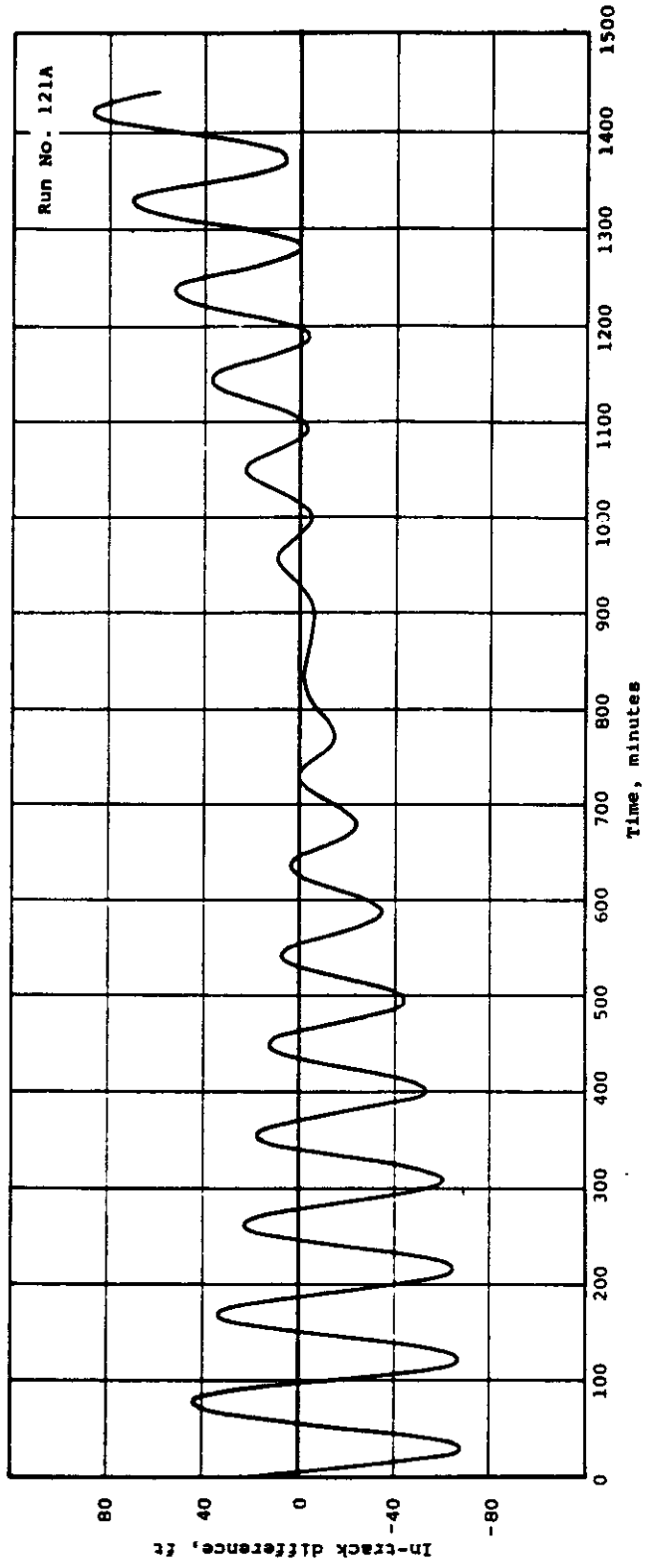

Fig. 4-26 — In-track component of ephemeris differences for two different atmosphere density models for 225-nautical mile altitude orbit, case 42

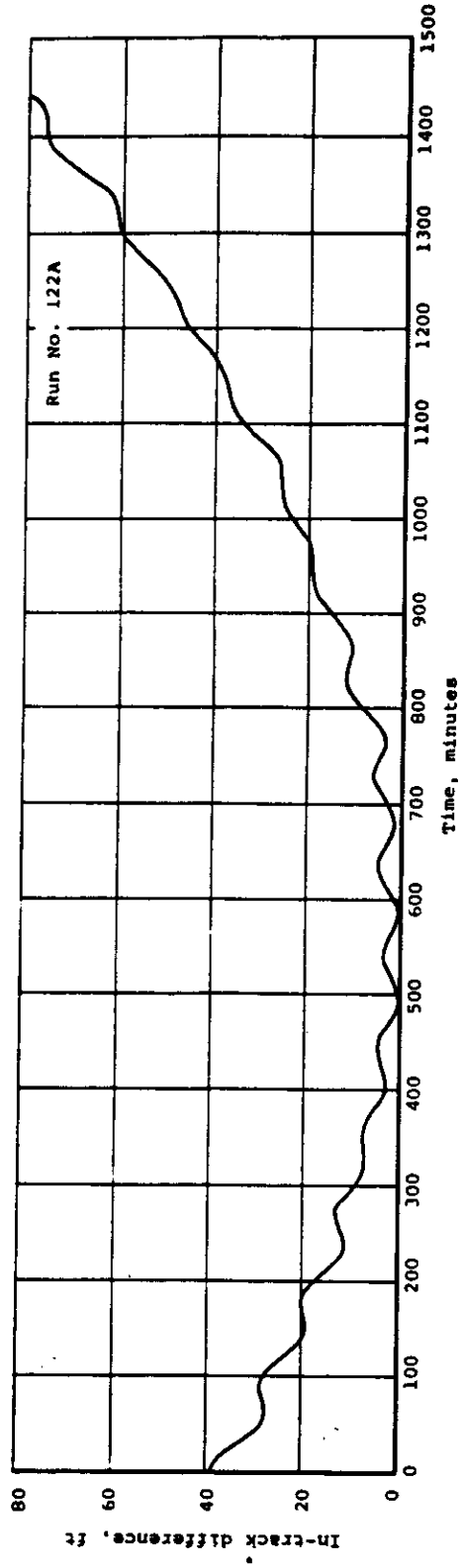

Fig. 4-27 — In-track component of ephemeris differences showing the effect of a 1 percent drag error for 225-nautical mile altitude orbit, case 43

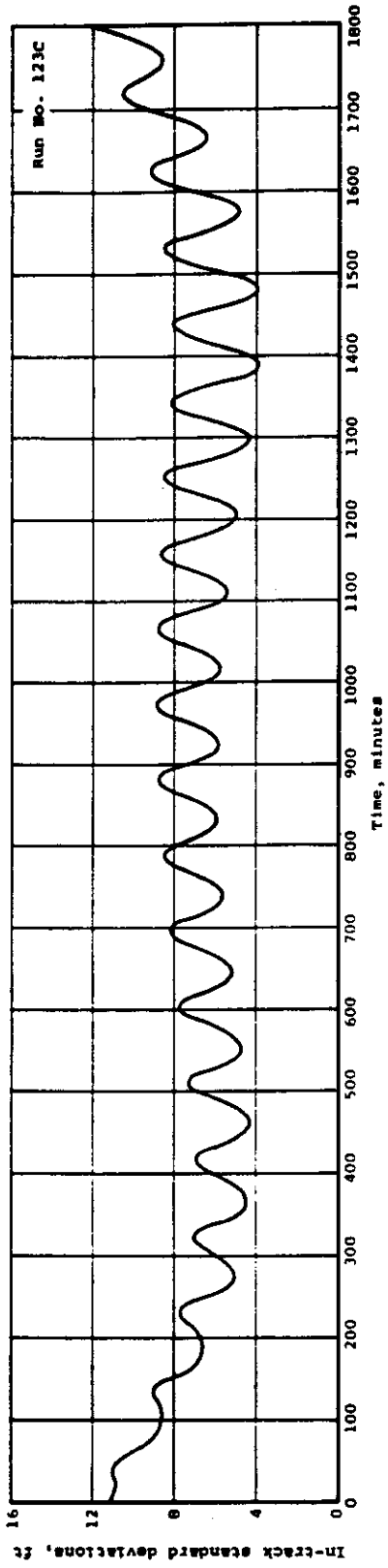

Fig. 4-28 — Plot of standard deviation of in-track component of orbit position error versus time for case 44, using combined set of 50 percent photogrammetric plus full TRANSIT and altimeter observations for 225-nautical mile altitude orbit

4.9 DISCUSSION OF COMPUTATIONAL RESULTS

The considerations performed to implement some of the approaches to the objectives listed in Section 4.2 have been described in Section 4.8. Other calculations for the specialized purposes of orbit planning are described in Section 4.10. The results of the calculations described in Section 4.8 are given in Figures 4-5 through 4-28 and Table 4-4 through 4-7. In analyzing the results of these calculations, the inherent limitation of the procedures used in the calculations and in the posited physical models must be kept in mind, as discussed in Sections 4.2 and 4.3.

4.9.1 Tracking Network Considerations

The relative effectiveness of various tracking networks in accurately defining orbital position can be seen from the results plotted in Figures 4-6 through 4-11 and tabulated in Table 4-4, where orbital position uncertainties are given as functions of time from epoch for observations of a satellite in a circular polar orbit at 156.7-nautical mile altitude. Typical observational uncertainties have been assumed, but the physical models, station locations, biases, etc., are assumed to be fixed and known. Similar results for a circular polar orbit at 225-nautical mile altitude for the observational network of case 10, Table 4-4, are shown in Figure 4-28.

The use of photogrammetric data alone and the effects of varying amounts and distribution of data are shown in Figures 4-7 through 4-10 (cases 1, 3, 4, and 5 of Table 4-4). It is seen that a fairly realistic set of photogrammetric data such as for the case used in Figure 4-10 yields in-track standard deviations of 38 to 40 feet. Poorly distributed data, as seen from Figures 4-8 and 4-9, can double or triple this uncertainty even if the total quantity of data is not appreciably reduced. The effect of adding altitude data from the ocean areas reduces the along-track uncertainty considerably to a range of from 18 to 26 feet (case 6, Table 4-4).

The addition of the TRANSIT network to the above data-taking network reduces the in-track uncertainties even more drastically to a range of 8.4 to 13 feet (case 10, Table 4-4). It is evident that the high accuracy and good distribution of the TRANSIT data are very effective in defining the orbit. This conclusion is further reinforced by considering the SGLS network results shown in Figure 4-6. This radar network utilizes accurately-measured Doppler data as do the TRANSIT stations, and the results (for no station location errors) again show the effectiveness of this type of data.

The TRANSIT data alone are not as effective as the photogrammetric data, however, in defining the cross-track position in orbit. Case 9 in Table 4-4 shows cross-track uncertainties of 22 feet as compared with about 9.7 feet uncertainty in cross-track for the photogrammetric network of case 5 of Table 4-4. The combination of these two observational networks as shown in case 8, Table 4-6, reduces the cross-track uncertainty to within about 8.6 feet. Thus, although the photogrammetric network data contributes little to the in-track accuracy achieved using only TRANSIT network data, it contributes substantially in controlling across-track errors. This appears reasonable since the Doppler signal is not very sensitive to cross-track position.

Radial position uncertainties are well controlled by both the TRANSIT network and the photogrammetric network with the TRANSIT network exhibiting stronger control.

From the foregoing numbers, it appears that, even without TRANSIT data, the on-board sensors of the GOPSS will provide sufficient high quality data to accurately define the orbit. However, the addition of TRANSIT data substantially strengthens this orbit determination, and, as is mentioned in Sections 4.9.3 and 4.9.7, these data are extremely useful in discovering and removing biases in the observational data, and in station location and datum bias determination.

4.9.2 Effects of Station Location Uncertainties

The results of the calculations (described in Sections 4.8.2 and 4.8.3, and particularly in Section 4.8.1) for orbital position uncertainties for various combinations of tracking networks and for a nominally circular polar orbit at about 160-nautical mile altitude are given in Figures 4-6 through 4-16 and in Table 4-5. Figure 4-6 shows the large effect which would be introduced into these uncertainties by uncertainties in the locations of SGLS stations. This effect is further illustrated for other tracking networks by comparison of Figures 4-7, 4-10, and 4-11 (cases 1, 5, and 10 of Table 4-4) with Figures 4-12, 4-13, and 4-16 (cases 11, 15, and 20 of Table 4-5), respectively, in which typical along-track standard deviations due to observational errors alone are contrasted with in-track standard deviations for both observational errors and station location errors. A typical ephemeris differencing example including station location, observational, and datum location uncertainties is shown in Figure 4-23.

It is obvious from these results that typical station location uncertainties can increase orbital position uncertainties by as much or more than a factor of two. This is especially true for the most highly effective tracking networks. On the other hand, this large effect tends to give confidence that it will be possible to better define station locations accurately from tracking data derived from such sources, in the final data analysis. There is an obvious need to include the SGLS and TRANSIT station locations as unknown parameters in the final data adjustment.

The effect of the altimeter data is seen to be minor from a consideration of cases 8, 18, 10, and 20 from Tables 4-4 and 4-5 when TRANSIT data is available. Except for its obvious utility in defining the undulations of the geoid over ocean areas, and applications to constraining photogrammetric data over land areas, the utility of altimeter data in orbit definition will be limited when TRANSIT data are available.

The comments made at the end of Section 4.9.1 concerning the effectiveness of the TRANSIT network in defining in-track and radial orbit position and the utility of the photogrammetric data in reducing cross-track uncertainties are valid here. This can be seen from a comparison of the results of cases 15 and 18 of Table 4-5.

4.9.3 Effects of Biases in Observational Data on Orbit Positioning Uncertainty

The calculations of the effects of biases in observational data on orbital positioning accuracies are described in Section 4.8.14 and results for two cases are plotted in Figures 4-24 and 4-25. These calculations were performed by ephemeris-differencing orbits obtained using observations with and without biases, respectively. A combined observational sensor network of TRANSIT, photogrammetry, and altimeter was used. Biases in altimeter and photogrammetric observations, as described in Section 4.8.14, contributed very little to changes in the calculated orbit, presumably because of the overing effectiveness of the TRANSIT network data. On the other hand, biases in TRANSIT data (range rate) contribute appreciable uncertainties (about -60 to +110 feet) to

the in-track positions (Figure 4-24) as well as smaller uncertainties to the cross-track and radial positions. The increased uncertainties introduced into this case by biases in altimeter and photogrammetry readings (shown for the in-track component in Figure 4-25) are principally manifested by the growth of the cross-track uncertainty to ± 53 feet compared with +4 feet without biases in the previous case. This change can be attributed primarily to the biases in the photogrammetry since the TRANSIT observations do not control the cross-track positions as strongly as radially and in-track. The typical behavior shown in Figures 4-24 and 4-25, which are indicative of curves of residuals in a real case, is sometimes useful in detecting the presence of biases in the observational data.

These results indicate the strong necessity for eliminating biases from the observations by instituting analytical procedures to test for, solve for and eliminate biases in the data and, if possible, from the original sensors. The final data analysis program must also have provision for properly treating biases in the data when solving for geodynamic parameters or landmark locations. Although biases may be determined and removed from multiple long-arc data for a single sensor, the redundant data available from using a multiplicity of sensors, i.e., photographic, TRANSIT, SGLS, and altimeter should prove to be very useful in removing biases from each of the individual sensors and aid materially in landmark location.

4.9.4 Effects of Drag Uncertainties on Orbital Position Determination

The results of calculations investigating the sensitivity of orbit position determination to uncertainties in drag forces are given in Figures 4-17, 4-21, 4-22, 4-26, and 4-27. Both error propagation studies (covariance analyses) and ephemeris differencing (Monte Carlo techniques) were used. A 1 percent variation in the ballistic coefficient (W/C_DA = 120) for the 156.7-nautical mile circular polar orbit, using the nominal observation network described in Section 4.8.4, yielded standard deviations of up to 250 feet in-track (Figure 4-17). The differences in ephemeris arising from attempting to fit an ARDC atmospheric density model to data generated using the Lockheed-Jacchia model and with W/C_DA = 75 for the same altitude exhibit magnitudes of -300 to +400 feet in-track and large radial magnitudes. Cross-track differences are small. Ephemeris differences between cases with a 1 percent difference in ballistic coefficient are shown in Figure 4-22. In this case, differences of -200 to +400 feet are obtained in-track and from +20 to -20 feet in the radial coordinate.

At a higher altitude (225 nautical miles), the results of ephemeris differencing for the two different atmospheric model (ARDC versus Lockheed-Jacchia) are shown in Figure 4-27. A reduction by a factor of 4 to 5 in differences is noted over the corresponding case of the lower altitude (156.7 nautical miles). Similar ephemeris differencing for a 1 percent change in W/C_DA = 75 at 225 nautical miles produced the results shown in Figure 4-27. Again, reduction of a factor of 4 to 5 is noted over the lower altitude case.

Various insights into the effects of incorrect air drag models or parameters can be obtained from examining the typical shapes for curves obtained by differencing of ephemeris. For example, Figure 4-22 and 4-27 show the typical shape of curves for residuals which would be obtained when an incorrect value of the drag parameter is used to attempt to fit observational data. Figures 4-21 and 4-26 show the typical behavior of curves for residuals which would be obtained when an incorrect type of air density model is used to attempt to fit observational data obtained from another model. The shapes of these two types of curves are sufficiently different that a diagnosis as to what has occurred in the analysis may be possible.

The calculations discussed above have indicated the severity of the uncertainties which may arise due to air-drag uncertainties. The importance of the air-drag uncertainties is reduced at the higher altitudes primarily because of the lower air densities and hence lower drag perturbation forces encountered, and also because of the increased coverage of the tracking networks.

The necessity for incorporating considerations of possible solar activity fluctuations and magnetic storms occurring during the periods of observations has been investigated by Bruce (Reference 1*). For one case of a low altitude satellite (i.e., 100 nautical miles and $W/C_DA = 50$ pounds/foot^2) he finds that a sudden severe magnetic storm may change an in-track position prediction by as much as 10 kilometers in 12 hours. On the other hand, such storms are relatively infrequent and for short time periods (of say 12 hours) it is often possible to assume constant solar activity and to use a static atmospheric model by absorbing the magnitude of absolute atmospheric density in the adjustment of the ballistic parameter.

It is thus essential that the calculational programs for the final data reductions are capable of solving for the air-drag parameters and that sufficient flexibility is available to incorporate sophisticated air-drag models in the programs, and that a sufficient number of adjustable parameters be available to at least empirically describe the effects encountered.

In addition, the incorporation of on-board sensors (accelerometers) to measure the magnitude of these forces is highly desirable because of the magnitude of the uncertainties in the physical models and air-drag parameters, and the magnitude of the orbital position differences induced by these uncertainties. The accelerometers would thus aid in establishing accurate orbit positions for the satellite and also in providing data for improving the physical models of the atmosphere.

4.9.5 Effect of Gravity Model Uncertainties Upon Orbit Position

As described in Section 4.8.5, numerical round-off difficulties in the computations limited the extents of the error analysis (covariance analyses) performed to test these effects. However, several ephemeris differencing calculations were performed in order to indicate the magnitude of the effects of gravity model coefficient errors, as described in Sections 4.8.1 and 4.8.10. The results of these calculations are presented in Figures 4-5, 4-19, and 4-20. These figures indicate, respectively, (1) the effects of model truncation from J_{66} to J_{44}, and J_9 to J_5, (2) differences between two different models, that is, the standard TRACE (unpublished Guier sixth degree model) and the NWL-5E-6 (Figure 4-6), and (3) the effects of adding several resonance terms to the standard TRACE model. These calculations were run for fairly low altitude circular polar orbits, that is, 140 nautical miles for the first case and 156.7 nautical miles for the second and third. The effects of model truncation on orbit position are very severe as indicated in Figure 4-5 where in-track differences of up to 2300 feet are noted. At least equally severe are the differences arising from the use of different models, leading to differences of thousands of feet both in-track and across-track, as well as large radial differences (Figure 4-19). Resonance terms introduce much smaller effects over the short times used in the calculations, but are also not negligible as shown in Figure 4-20.

This difference in magnitude of effect over various periods for lower and higher degree terms in the gravitational potential harmonic expansion can be used to separate these terms from each other. Thus, for example, short arcs are less influenced by differences in high degree terms and, to a first approximation, these low degree terms can be obtained from short arcs by ignoring the contribution from higher degree terms.

---

*References are contained in Section 4.9.9.

It is important to point out that the most recent and accurate gravity models which are available today could not be compared in this analysis because of the limitations of the computational program used here. Similarly, proper error analysis could not be performed. As was pointed out in Section 4.2, it is impossible to assess the validity of any given physical model except by comparison with real data. However, it is expected that comparison of ephemeris calculated using the most recent models would yield much smaller differences.

The calculations performed indicate the strong sensitivity of orbital position determination to the magnitude of higher harmonics in the gravity potential. This sensitivity will enable much more accurate evaluation of these coefficients to be made (assuming that correlating terms such as air drag can be independently evaluated), and hence lead to accurate orbital position determinations. These results also indicate the strong necessity for obtaining the best determination of the various gravity model parameters possible and, in particular, at the altitudes used here, the effect of the higher degree harmonics can be very important. It is thus essential that the capability for incorporating gravity models which include terms up to high degree as well as selected resonance terms be provided in the data analysis program.

Kaula (References 2 and 3) has investigated the effects of various terms in the harmonic expansion of the earth's potential on satellite motion. A term in the harmonic expansion is of the form

$$V_{nm} = \frac{GM_e}{r}\left(\frac{a_e}{r}\right)^n P_{nm}(\sin\phi)[C_{nm}\cos m\lambda + S_{nm}\sin m\lambda]$$

for

$$0 \leq m \leq n$$

where G = gravitational constant

M_e = earth's mass

a_e = earth's equatorial radius

r = radial distance

ϕ = latitude

λ = longitude

P_{nm} = associated Legendre polynomial

C_{nm} = constant

S_{nm} = constant

P_{nm} non-zero at the poles only if m is zero and P_{nm} has $n-m$ zeros along a meridian from pole to pole and $2m$ zeros along the equator.

Kaula shows (Reference 2) that if the coordinates above are converted into the coordinates of a Keplerian ellipse (a, e, I, M, ω, Ω) which coincides with the position and velocity of the satellite, the equation for any of the elements may be expressed by

$$\Delta S_{i,nm} = \sum_{p,q,} \frac{f_{inmpq}(a,e,I)}{\dot{A}_{nmpq}} \left[\begin{Bmatrix} C_{nm} \\ \text{or} \\ S_{nm} \end{Bmatrix} \sin A_{nmpq} - \begin{Bmatrix} S_{nm} \\ \text{or} \\ C_{nm} \end{Bmatrix} \cos A_{nmpq} \right]$$

where $\dot{A}_{nmpq} = (n - 2p)\,\dot{\omega} + (n - 2p + q)\,\dot{M} + m\,(\dot{\Omega} - \dot{\theta})$

appears in the denominator, p and q being summation indices and θ is Greenwich Sidereal Time.

The main effect of satellite motion is thus expressed by the term $(n - 2p + q)\,\dot{M}$, and that of the earth's rotation by $m(\dot{\Omega} - \dot{\theta})$, since $\dot{\omega}$ is very small.

From an examination of these terms we arrive at the following three conslusions,

1. Tesseral harmonics of order m cause perturbations of approximately m cycles per day.

2. Resonant effects occur at altitudes such that

$$\frac{\dot{M}}{\dot{\theta}} \approx \frac{m}{k}$$

where $k = n - 2p + q$ is a constant. From Kepler's law we have

$$\dot{M} \approx \left(\frac{GM_e}{a^3} \right)^{1/2}$$

so that the approximate altitudes for a given resonance may be determined. Yionoulis (Reference 4) has determined these altitudes and the so-called "beat period" (beat period in days = 1/revolutions per day - m), as a function of altitude. For low altitude satellites, principle resonances will occur for tesserals with m = 15, 16, 30 and 32.

3. Orbital period terms for which $(n - 2p + q) = 0$ will be superimposed on the longer terms. These terms tend to average out the motion. As mentioned below, the lead terms in the perturbation are those with $q = 0$ or ± 1. Therefore, the important terms for these oscillations will be those for which $p = n/2$ for n even, and $p = n \pm 1/2$ for n odd.

The terms f_{inmpq} in the expression above contain quantities of the form

$$GM_e \frac{a_e{}^n}{a^{n+1}} F_{nmp}(I)\, G_{npq}(e)$$

where the p, q indices are the same as above and a_e is the equatorial radius of the earth. Because of the $1/a^{n+1}$ term, resonant effects will be more important for low altitude satellites than for higher altitude vehicles.

In addition, the function $G_{npq}(e)$ is of order $e^{|q|}$, so that for small eccentricities, the $q = 0$ and $q = 1$ terms will be the most important terms in perturbing the motion. Therefore, the lead terms in the expansion for ΔS_i will involve terms in A_{nmpq} for which $n - 2p + q = n = 2p = 0$, or $n - 2p + q = n - 2p \pm 1 = 0$, or $p = n/2$ for n even, or $p = n \pm 1/2$ for n odd. Thus, harmonics which

differ in degree by an even number will have the same rates for their leading perturbations in a given orbit, and the only way to separate these terms will be to utilize the dependence of the amplitude f_{inmpq} on the inclination I through term F_{npq} (I). Thus, in order to separate out a variety of terms from which j even differences of degree can be constructed requires j + 1 inclinations. For example, it is necessary to use three satellite inclinations to separate the highly correlated V_{62}, V_{42}, and V_{22} in an expansion extending out to n = 6. Similarly, it would be necessary to use three satellite inclinations to separate $V_{15,15}$ from $V_{17,15}$ and $V_{19,15}$.

Some of these effects are illustrated by the results plotted in Figures 4-5, 4-19, and 4-20 for the three cases mentioned above. In Figure 4-5, the principal periods evident appear to be those due to terms with n = 6 or 5 and m = 2, 3, or 4 with periods corresponding to 720, 480, and 360 minutes respectively, and perhaps for m = 1 with a period of 1440 minutes. Other periodic terms are evidently present, but are hidden by the longer term effects as well as the orbital period. The long period secular effects attributable to $J_{6,0}$ through $J_{9,0}$ are not particularly evident for this short calculational period.

In Figure 4-19, the strong effect of an m = 2 term with a 720 minute period is evident as well as other higher order, shorter period terms which are evidently present but hard to distinguish. Again, the period of time of calculation is not sufficient to recognize m = 1 effects or any other long period secular effects.

In Figure 4-20, the effects of the long period beat frequencies which should be present are not easily seen because of the short period of calculations. There is a small indication of the effect of the m = 32, or 45-minute perturbation, but the m = 16 oscillation is obscured by the satellite period.

4.9.6 Determination of Geodynamic Parameters from Observational Data (See Section 4.2.2.2.3)

Atmospheric density models have been discussed in connection with air-drag considerations in Section 4.9.4 and also in Section 4.3.3. Other perturbations are discussed in Section 4.3.2.

Attempts to investigate the sensitivity of the determination of geodynamic parameters to observational errors and station location errors have been discussed in Sections 4.8.6 and 4.8.9. Unfortunately, numerical difficulties (presumably due to round-off in the multiple matrix manipulations) precluded a sensitivity analysis for a complete set of gravity parameters. The results obtained from investigating a few parameters at a time are reported in Section 4.8.6. Typical results obtained indicate that nominal observational and station location errors for the typical tracking network used will allow determination of these selected low-degree gravity coefficients to accuracies of the order of one percent.

4.9.7 Determination of Landmark and Datum Positions (See Section 4.2.2.2.4)

As was mentioned in Section 4.2.2.2.4, the accuracy of landmark location can be discussed only in conjunction with consideration of the photogrammetric analyses. This subject is discussed more fully in Volume 3 of this report.

The accuracy of locating datums was, however, investigated, based upon orbital analyses and considering the photogrammetric data as being derived from an equivalent radar tracking network, each of whose station location accuracies was determined by the datum location accuracy for the

pertinent continent. These calculations are discussed in Section 4.8.7 and results are listed in Table 4-6. The data indicate that, if the orbit were perfectly fixed by auxiliary sensors, for example and if the accuracy of the photogrammetric observations were 30 feet in all three coordinates, then each of the datums could be located to within about 30 feet in latitude and considerably less in longitude and altitude. Using only the photogrammetric observational data network to determine the orbit, and assuming that the physical models are perfectly known, degrades the accuracy by as much as a factor of 3.

The result of this calculation indicates that, if the orbit can be well enough defined, especially by the use of observational data from auxiliary sensors such as the TRANSIT network and accelerometers, and the physical models are adequate, it will be possible to fix landmarks to well within the specified accuracies. It can be noted from, for example, Figures 4-5 and 4-19 where in-track differences for ephemerides for different gravity models are presented, that it will be necessary to consider high frequency effects in the photogrammetric analysis. This is true, for even relatively short orbital arcs, since, over the arc lengths used, differences of a hundred feet or more may result from orbits calculated using models which contain only low degree terms and orbits calculated using higher degree term models.

4.9.8 Calculations Using Real Data from Flight 1169

The calculations performed using the SCF radar network observations for this data are described in Section 4.8.8. Even after station biases were removed for two of the tracking stations (range biases of the order of several hundred feet were found) range residuals of the order of 400 to 700 feet were found. The error propagation analysis for this data, using radar sensor accuracies quoted for the SCF network, showed very much smaller in-track standard deviations, on the order of 80 feet maximum. Although range residuals and in-track standard deviations are not directly comparable, the discrepancy of these numbers by almost an order of magnitude is indicative that something is in error. The suspect quantities are quoted station locations, quoted observational errors, other station biases, and physical model uncertainties. It is also possible that some of the discrepancy is due to numerical roundoff errors in the TRACE program itself. The resolution of these discrepancies can only be obtained from further analysis and, if possible, more data from similar flights.

Analyses of this type utilizing data from only a relatively restricted data-taking network such as the SCF network (i.e., only five stations of modest observation accuracies) indicate the need for geographically-well-distributed high-accuracy data and an adequate data reduction program such as will be available from the GOPSS program. Such data will be necessary in order to remove station location errors, station biases, and to improve knowledge of physical models so that accurate orbital positions and landmark locations may be obtained.

4.9.9. References for Section 4.9

1. Bruce. R. W., in King-Hele, D. G., Mullen, P., and Righini, G. (Ed.) "Space Research," Vol. V, Dynamic Atmospheric Effects Upon Satellite Motion and Satellite Lifetime, North Holland Publishing Company, Amsterdam, 1965.
2. Kaula, W. M., Analysis of Gravitational and Geometric Aspects of Geodetic Utilization of Satellites, NASA TN D-572 (Mar. 1961).
3. Kaula, W. M., The Use of Artificial Satellites for Geodesy, presented 1965 Annual Meeting, American Astronautical Society, San Francisco, publication No. 452, Institute of Geophysics and Planetary Physics, University of California.
4. Yionoulis, S. M., A Study of the Resonance Effects Due to the Earth's Potential Function, Applied Physics Laboratory, The Johns Hopkins University, Report No. TG-708, (July 1965).

Section E

ORBIT PLANNING

4.10 ORBIT PLANNING

4.10.1 Objectives of Orbit Plan

The objectives of the orbit plan are to develop typical orbital specifications and operational instructions for use with the GOPSS to accomplish the aims of the program. Practical considerations concerning the launch phase, the attainment of thermal equilibrium, in-flight calibrations, and the recovery aspects are involved with operational considerations to satisfy the overall mission requirements.

4.10.2 Considerations in Orbit Selection

The orbit plan can be specified only after consideration of many different and often conflicting factors.

4.10.2.1 Photographic Coverage

The orbit or group of orbits should be so planned that the ground swaths swept out by the camera's field of view will cover all land areas of the earth. Each vehicle will have approximately a 10- to 16-day observational lifetime; at least 5 percent sidelap in the ground swaths will be required on adjacent passes.

Although one indicated operating altitude is 120 to 180 nautical miles, it is obvious that the coverage problem would be much simpler if the altitude could be raised to about 240 to 360 nautical miles since the swath width on the ground would essentially be doubled. In addition, the drag effects would be drastically reduced. However, camera ground resolution would also be reduced by approximately half. Most of the following analysis is based on the lower operating altitude.

4.10.2.1.1 Altitude

The mean altitude will be fixed by the requirement for appropriate interlacing of ground swaths, as discussed below. Conversely, the width of the ground swath is set by the vehicle altitude. For the given camera focal length of 300 millimeters and format width of 230 millimeters

$$w = \frac{230h}{300}$$

where w = width of ground swath
h = altitude

4.10.2.1.2 Inclination

Sufficient swath-to-swath sidelap will be most difficult to provide along the equator. Width of the ground swath along this line is given by

$$l = \frac{w}{\sin i}$$

where i = orbital inclination angle

The most critical inclination angle with respect to sidelap at a given altitude is thus 90 degrees with sin i of 1.

Figure 4-29 shows the displacement in longitude between two ground tracks generated 16 orbits apart, as a function of injection altitude (equatorial horizonal injection heading south) and orbital inclination as calculated by the TRACE program. These curves are taken from Figure 4-30. A given displacement will occur with slightly higher orbit altitudes, and slightly wider ground swaths are generated at inclinations greater than 90 degrees. This wider ground swath gives more coverage, and thus permits more leeway in orbit period.

Inclination on at least one flight will have to be in the neighborhood of 90 degrees because of the mission requirement that all land masses, including Antarctica, be observed.

4.10.2.1.3 Effects of Redundancy

The number of times a particular point is within the field of view of the camera depends primarily on orbit inclination and the point's latitude, with greatest redundancy (up to one observation per pass at the poles on a polar orbit) at the highest latitudes attained with the given orbit inclination. Curves showing redundancy of observation (neglecting illumination factors) as a function of latitude and orbit inclination are shown in Figure 4-31, where N represents the average number of times per orbit a point is within the field of view of the camera. (Because of illumination requirements, photography is possibly fewer than half the times a point is within the field of view). These curves are presented for an altitude of 150 miles, and redundancy is directly proportional to altitude.

4.10.2.1.4 Effects on Q-Data Generation

Valuable constraints on the calculated orbit can be obtained using data obtained from intersecting orbits, or orbits with overlapping ground swaths, from each of which the camera can observe the same point on the earth at different times. If possible, the observations should be from orbits where ground tracks are inclined with respect to each other at approximately 90 degrees. The number and latitudes of such points are functions of the orbit inclination, with polar orbits exhibiting only two—at the poles. In nonpolar orbits, one of the observations will be in the ascending portion of the orbit (latitude increasing) and one in the descending portion. If both these points are to be illuminated sufficiently for photography, the maximum latitude of the ground track in the hemisphere containing the point must be attained near midday.

4.10.2.1.5 Interlace

One of the most stringent limitations on orbit parameters is the requirement that the photographic ground tracks interlace to provide complete coverage of all land masses between the

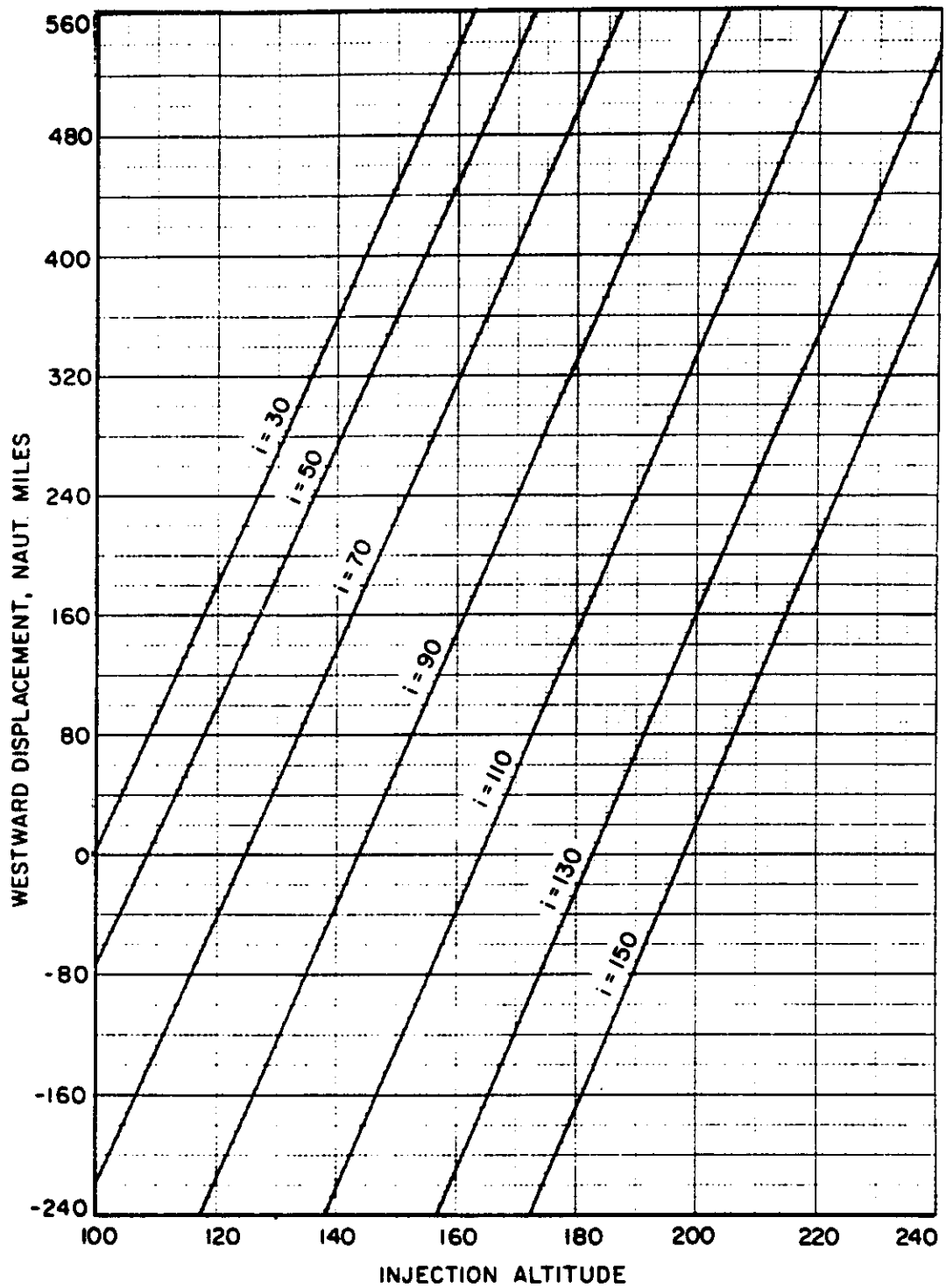

Fig. 4-29 — Displacement of ground track after 16 passes from equatorial injection in southerly direction

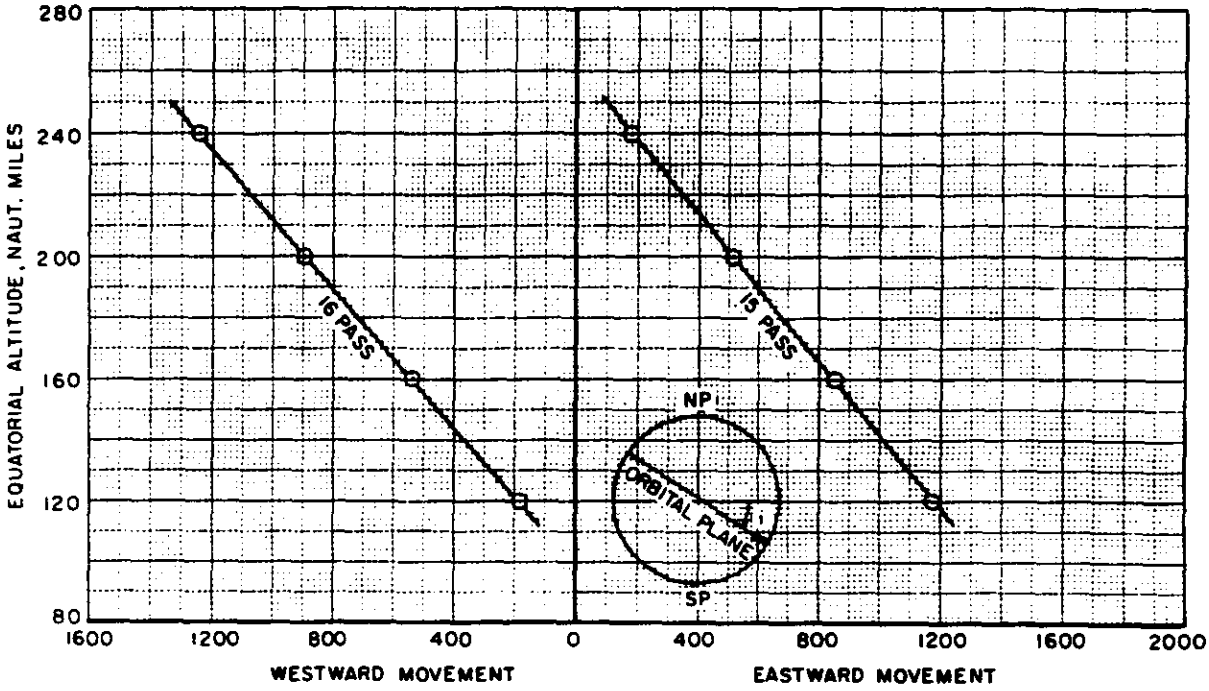

(a) i = 30°

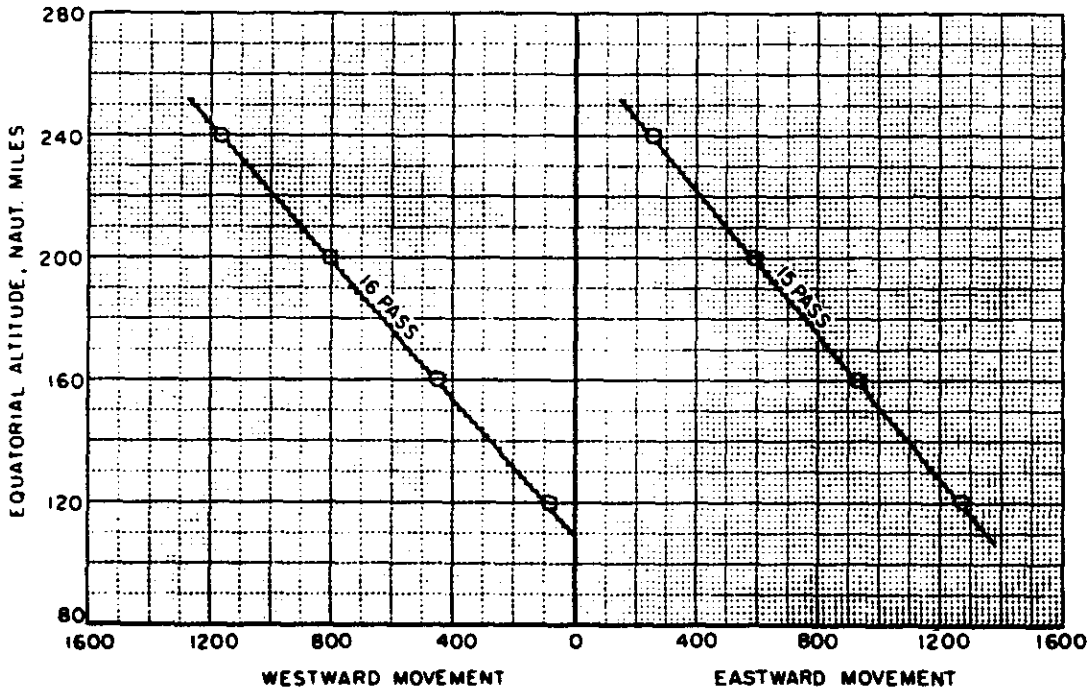

(b) i = 50°

Fig. 4-30 — Daily movement of ground trace of satellite launched horizontally at the equator in southerly direction, $W/C_DA = 75$

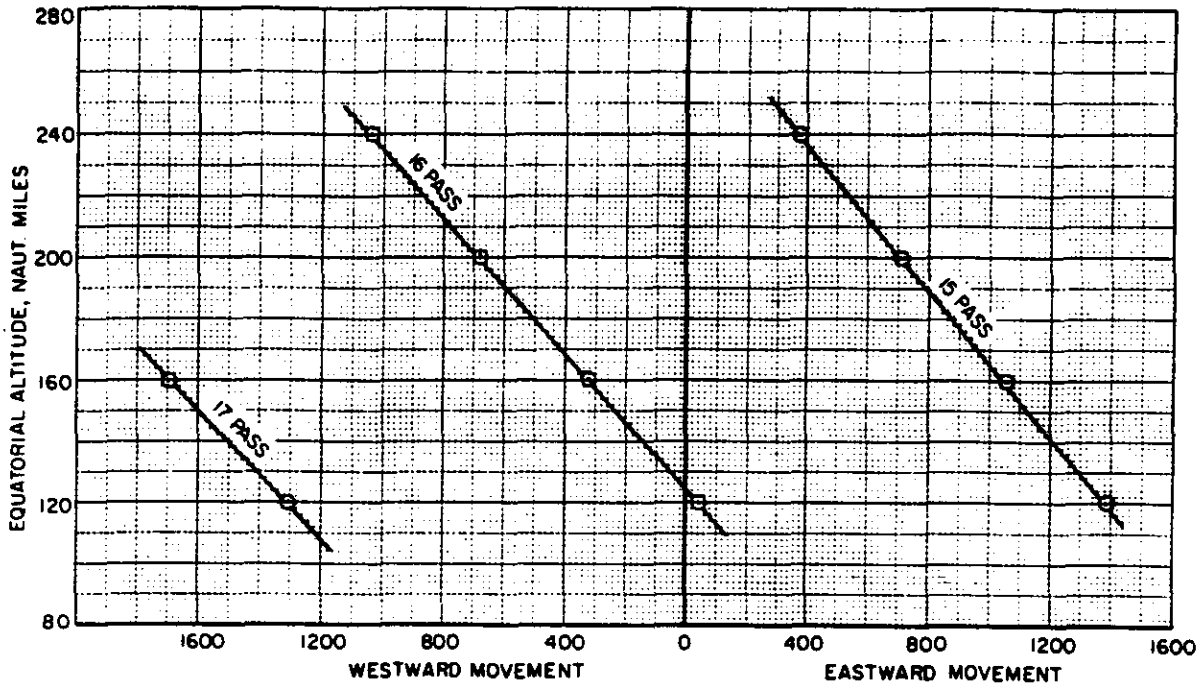

(c) i = 70°

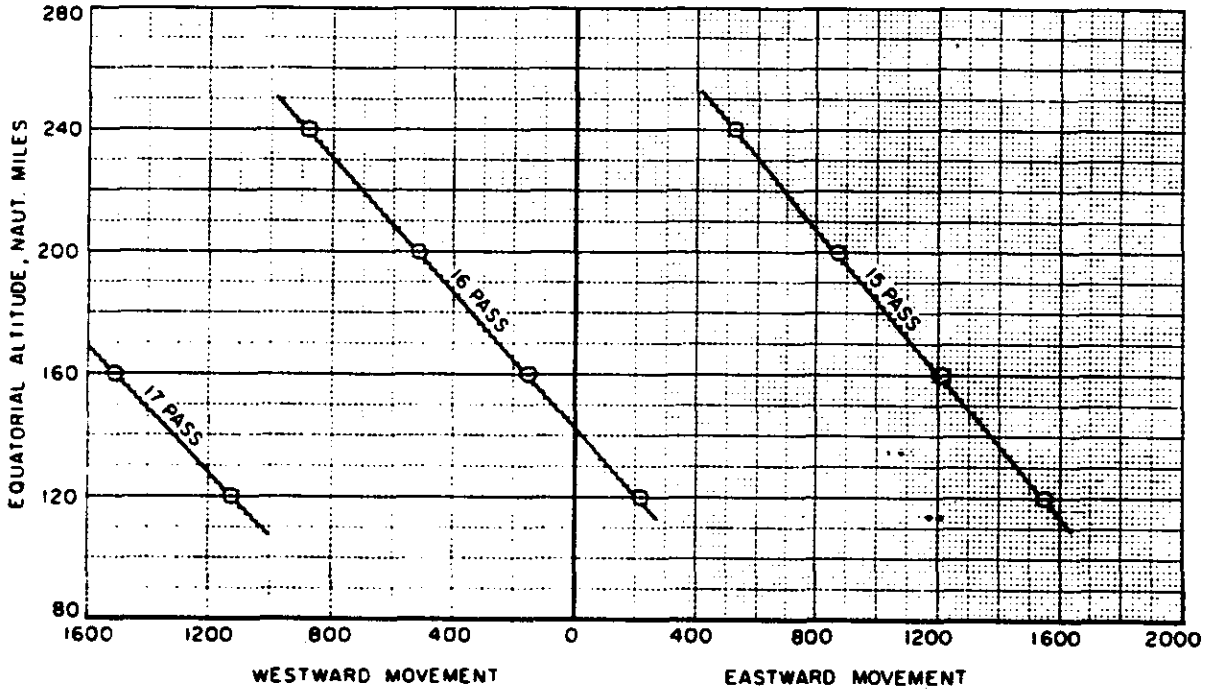

(d) i = 90°

Fig. 4-30 (Cont.) — Daily movement of ground trace of satellite launched horizontally at the equator in southerly direction, $W/C_DA = 75$

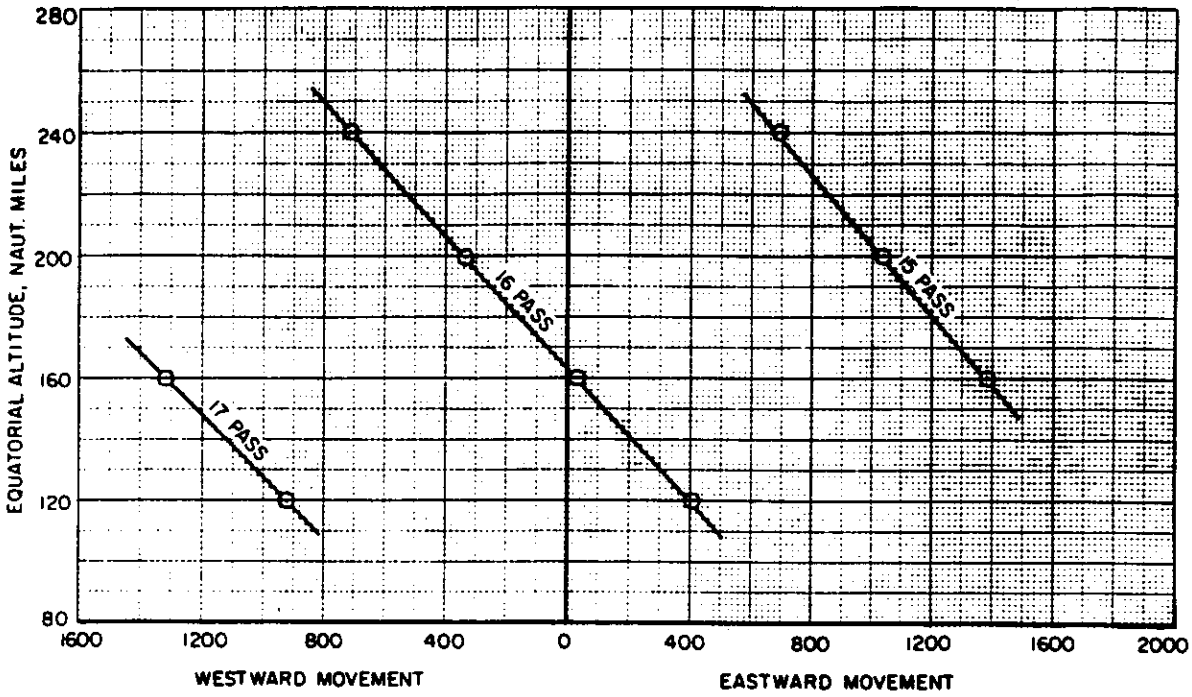

(e) $i = 110°$

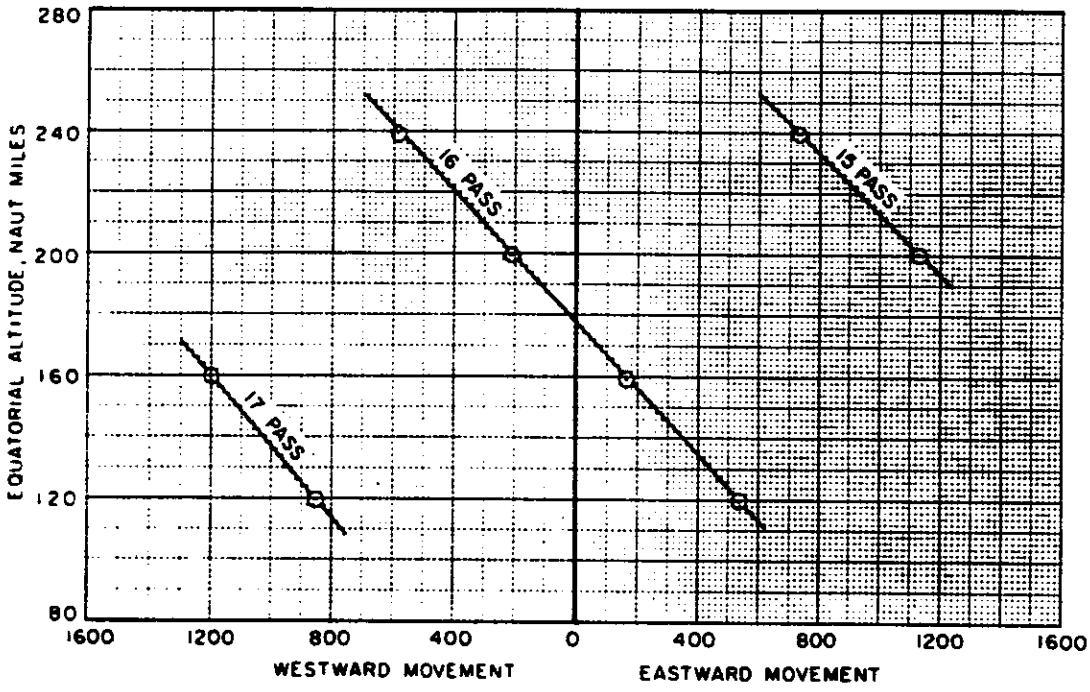

(f) $i = 130°$

Fig. 4-30 (Cont.) — Daily movement of ground trace of satellite launched horizontally at the equator in southerly direction, $W/C_DA = 75$

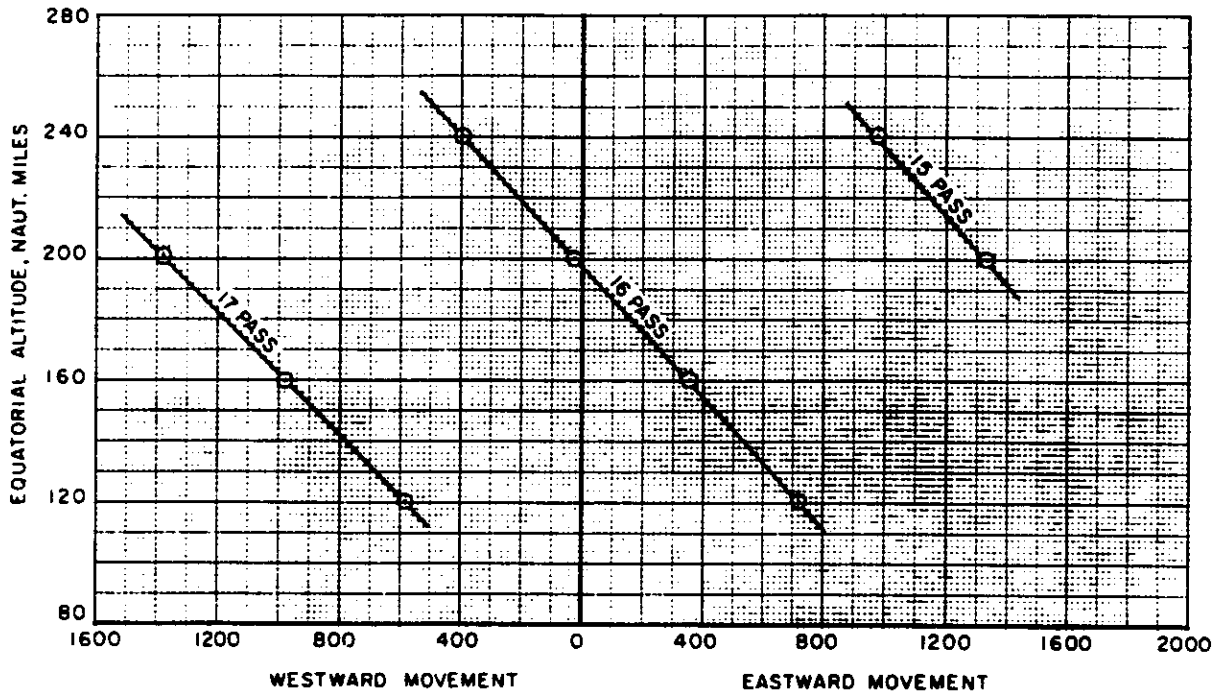

(g) i = 150°

Fig. 4-30 (Cont.) — Daily movement of ground trace of satellite launched horizontally at the equator in southerly direction, $W/C_DA = 75$

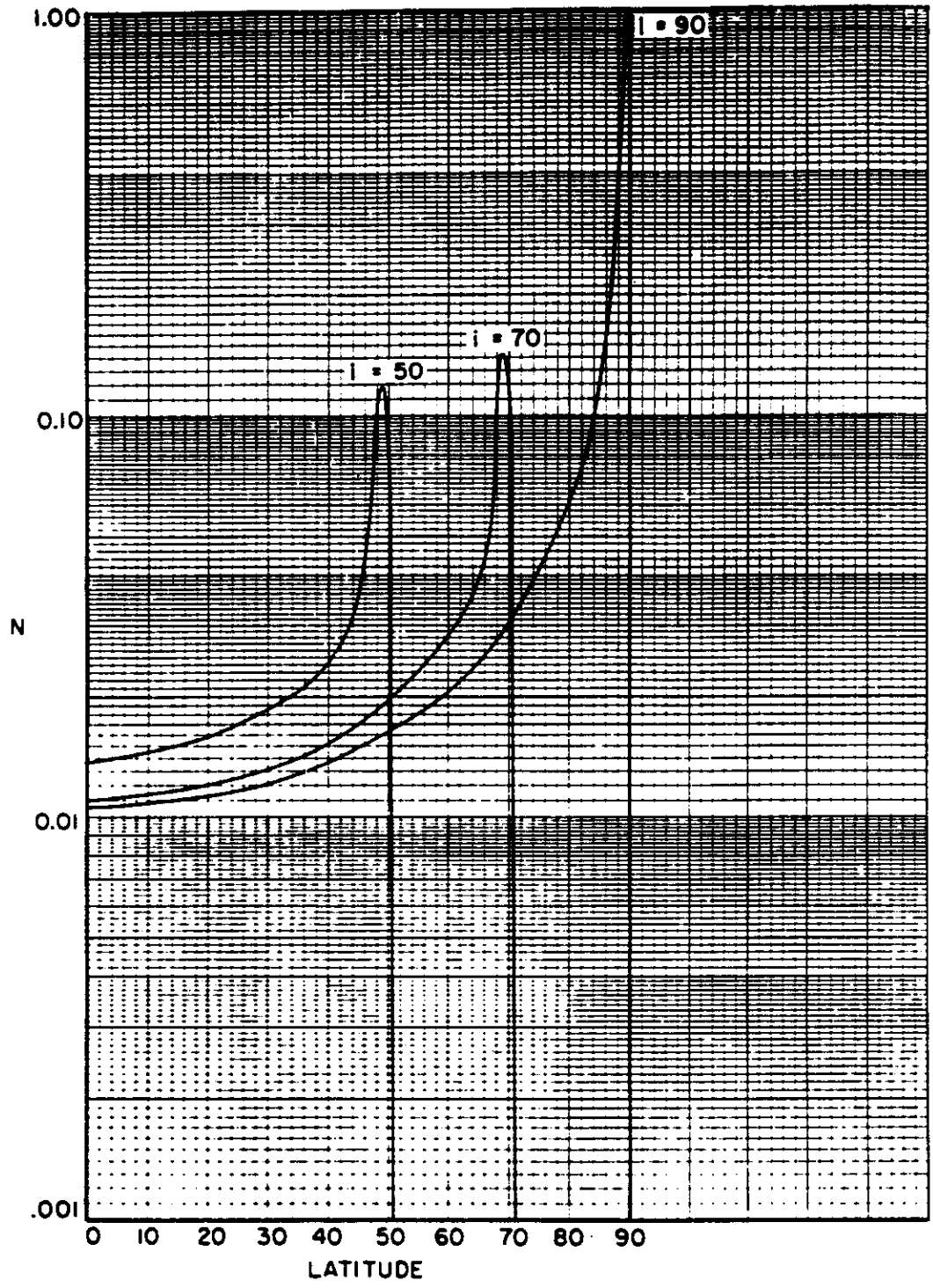

Fig. 4-31 — Coverage as a function of latitude

maximum latitude excursions of the orbit. Several possible interlace patterns can be conceived—with the ground tracks on successive days adjacent, skipping one swath, skipping two swaths, etc. The ground track displacement must be such as to permit later interlace to cover the initially unovserved areas. Most of these possible patterns can be ruled out immediately if it is assumed that photographic altitudes should be below about 180 nautical miles due to camera considerations, while average altitude should be above about 150 nautical miles to minimize drag. Such altitudes are only compatible with ground track displacements of the order of a few degrees between successive days, i.e., orbits in this altitude range are near resonance of order 16 (see Figure 4-29). For orbits with i = 90 degrees, the only permitted orbits are those with daily longitudinal displacements between 60 and 330 nautical miles west. For retrograde orbits of about 110-degrees inclination, only daily displacements of about 150-nautical miles west to 130-nautical miles east give circular orbits in the desired range. In this case, the choice must be limited to adjacent swaths.

It should be noted that westward displacement is desirable because of the fact that major storms move generally west to east. Thus, an orbit with easterly displacement of the ground swath on successive days might continually photograph a particular storm and not the ground. However, orbits with inclinations greater than 110 degrees will not permit sufficient westerly displacement unless the altitude is greater than 180 nautical miles.

There are reasons for preferring adjacent swaths on successive days for all the missions. Consider first an idealized case with no air drag, and postulate an interlace pattern in which 15 days are required for complete photographic coverage, with approximately two swath widths' displacement between successive days and subsequent interlace of the initially unobserved areas. In this case, 7 or 8 days will elapse between the viewing of adjacent swaths. The position of adjacent swaths will depend on the orbital periods, with shorter periods corresponding to smaller westward displacements. The average distance between adjacent ground tracks should be slightly over 90 nautical miles at the equator in order to permit coverage in 15 days of the approximately 22.5 degrees between consecutive orbits postulated in this example. Displacement between ground tracks laid down on successive days is then a little over 181 nautical miles. For a 90-degrees inclination, this corresponds to a circular orbit altitude of approximately 163 nautical miles. Each swath will be about 125 nautical miles wide. Since distances between adjacent ground tracks are 91 miles, an average overlap at the equator between adjacent swaths will be about 34 miles. Of this amount, 5 percent (6 miles) of the swath width is required for minimum overlap, leaving 28-nautical miles leeway for uncertainties in orbit period.

The interlace pattern is such that the ground track on the ninth day will be between the ground tracks of the first and second days, and that laid down on the tenth day will be between the ground tracks of the second and third days. This means that there are 127 orbital periods between adjacent swaths viewed on the first and ninth days and 111 orbital periods between adjacent swaths viewed on the second and ninth days. The maximum allowable error in longitudinal displacement per orbit is then 28/127, or about 0.22 nautical mile. The earth rotates 1/4 nautical mile per second so this corresponds to a maximum permissible deviation of period from the desired value of about 0.9 second. Our information is that the operational uncertainty in orbital period after the orbit adjust maneuver may be of this order of magnitude and that interlace is thus operationally unfeasible at this altitude range.

Considering a second mode of operation, if adjacent swaths are viewed on successive days, the uncertainty in the positions of the ground tracks for a given uncertainty in period is much less. This can be used to reduce orbital lifetime and film requirements for the same coverage.

For instance, for the same nondrag polar orbit with 5-percent minimum overlap, a 0.9 second uncertainty in orbit period will mean the same uncertainty in longitudinal displacement per orbit of 0.22 nautical mile and in this case, only 16 orbits intervene between adjacent swaths (except for the closing orbit treated below). This means that provision need be made for only 16 × 0.22, or 3.5 nautical-mile overlap in addition to the minimum of 5 percent of the swath width. It is clear that the use of adjacent swaths on successive days puts a less stringent requirement on accuracy of orbital period necessary to control overlap than does the use of interlacing swaths. If operation at higher altitudes is allowable within the accuracy of the photogrammetry, then the use of interlace becomes feasible.

What we have just described has been postulated on no change in orbital period with time; i.e., we have neglected drag. For the purpose of calculating overlap for a 24-hour period, this assumption can be supported, but over 15 days, there are significant changes in orbital period which have a great effect on overlap. Let us define overlap before showing the effect of drag. Consider Figure 4-32 in which the satellite has moved west along the equator a distance (d) between nodal crossing (n) and n + 16. The swath width (w) and the overlap (o) are related as follows:

$$o = w - d = h\,\frac{230}{300} - d$$

The quantity (d) is obtained from the longitude difference in satellite position for the $(n)^{th}$ $(n + 16)^{th}$ nodal crossings. Note that we have assumed a near circular orbit so that the altitude has not changed. (The effect of altitude changes due to eccentricity will be discussed subsequently.)

The effects of drag on overlap have been calculated for a slightly retrograde orbit (i = 95 degree), for several altitudes near that for zero overlap. The results are shown in Figure 4-33. The first calculated point shown is for the overlap between the second and eighteenth nodal crossings. The results are shown for two altitudes for 5 days and for one altitude for 15 days. The h_o = 160-nautical mile result shows an initial overlap of about 13 nautical miles increasing to about 44 nautical miles at the end of 15 days. The altitude at the equator only changed by about 2 nautical miles during the 15 days so that the increase in overlap is almost entirely due to changes in d. The initial overlap of 13 miles is close to a 5 percent overlap (8 miles) plus the 3.5-mile allowance for an orbital period uncertainty of 0.9 second previously mentioned. The increased overlap due to drag represents a weight penalty in film. It can be minimized through the use of higher operating altitudes or eccentricity. The foregoing example for h_o = 160 nautical miles will be used in the example orbit plan.

If we desire to use an eccentric orbit, it is necessary to place apogee close to the equator on the sunny side of the orbital plane. We will thus obtain a wider swath width than for a circular orbit. In fact, to obtain the same overlap, it is necessary for the eccentric orbit to have a slightly greater period than the circular orbit. This means it must have a greater semimajor axis than the circular orbit and a slightly higher average operating altitude. For one calculated case, the rate of change of orbital period with time for the eccentric orbit was nearly the same as that for the circular orbit with the same overlap. Accordingly, the original swath width was wider and remained wider for the 15-day period, despite reduction in apogee altitude due to drag. As a result, complete coverage of the equator was obtained in a shorter period than for a circular orbit with the same initial overlap. The best manner of utilizing eccentricity to reduce film weight must take account of the motion of the line of apsides which, over 15 days, can be considerable. A complete analysis of this problem has not been made and is recommended as a subject for further study.

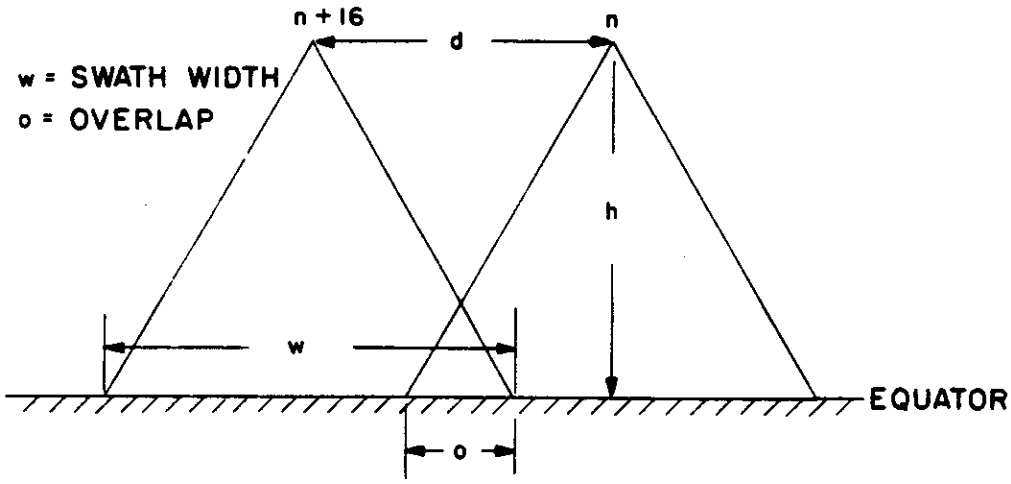

Fig. 4-32 — Swath width and overlap

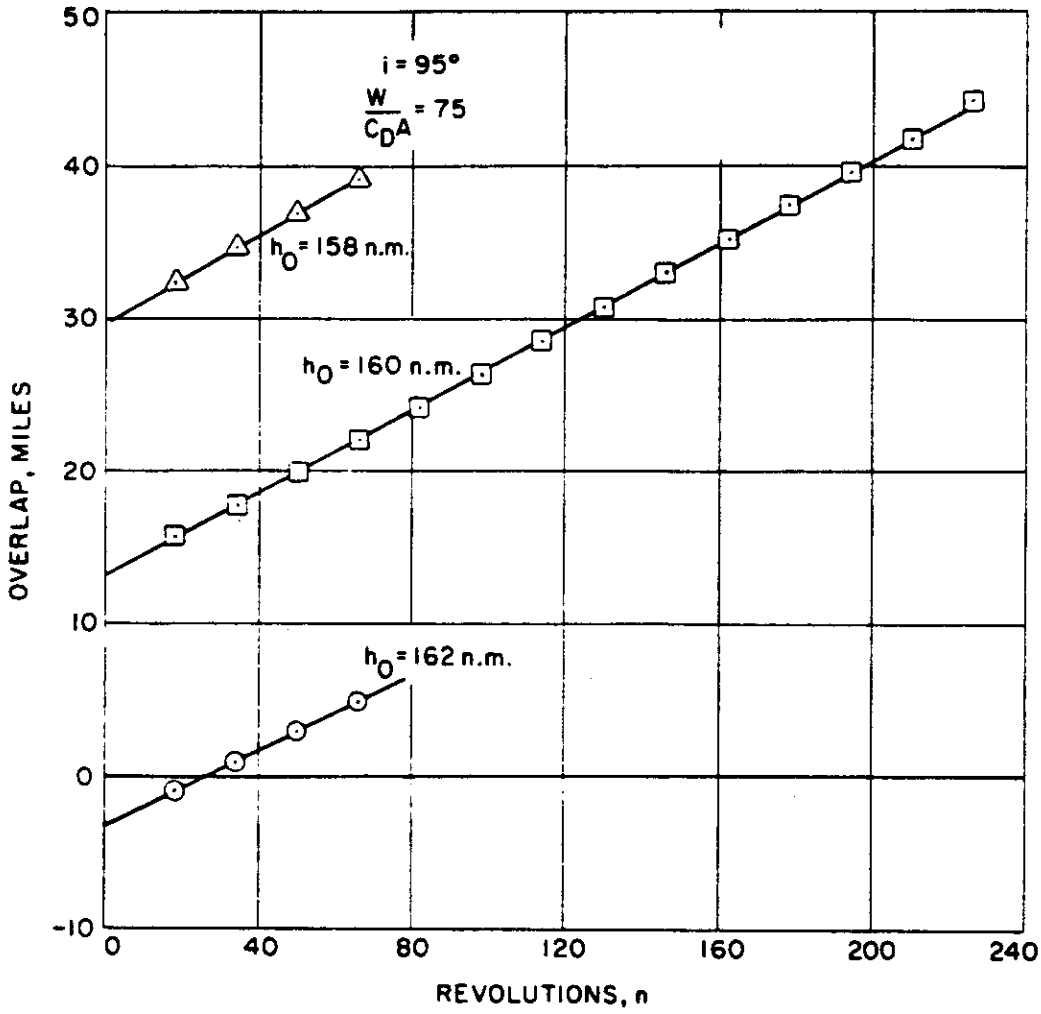

Fig. 4-33 — Effect of drag on overlap for southerly horizontal launch at altitude h for a slightly retrograde orbit

4.10.2.2 Camera Considerations

4.10.2.2.1 Altitude

The camera characteristics enter into the orbit plan since coverage varies directly with satellite altitude, and the time to cover a given area and the film weight vary inversely with altitude. On the other hand, the resolution on the ground decreases as the altitude is increased. In Section 4.10.2.1, it was shown how operation near 150-nautical mile altitude is required to control the overlap at the equator with a swath width of about 115 miles. In this case, about 14 days are required to cover the earth's surface at least once. The next natural operational altitude is near 300 miles for side-by-side overlap one day apart with a swath width of about 230 miles. In this case, complete coverage would be obtained in about 7 days with about one half the weight of film.

If the accuracy with which a ground point can be located is sufficient for the purposes of the system near 300 miles, then operation near 300 miles (m = 15) rather than near 150 miles (m = 16) is desirable from the coverage point of view. In the first place, the density at 300 miles is lower by an order of magnitude than at 150 miles so that air drag fluctuations will be minimized. Also, the change in satellite period during the 7-day period will be so small as compared with that at 150 miles that interlace will be possible where it is not feasible at 150 nautical miles. At 150 miles, the ground traces for succeeding days are adjacent, and there is some correlation for day to day insofar as weather is concerned. This correlation can be minimized by interlacing at 300 nautical miles so that the chances of continually photographing clouds from a particular storm is reduced. These factors all point to a 300-mile operating altitude when advanced cameras are available.

4.10.2.2.2 Camera Duty Cycle

As part of the orbit planning task, it is necessary to determine what part of the total time the camera is taking pictures. Also, the times to turn the camera on and off must be determined. Some calculations have been made to develop computational techniques for obtaining this information. The camera will be operated if the sun angle is large enough to obtain sufficient illumination for photography and if the camera is over land. The sun angle may be obtained from the TRACE program or from a side calculation described in Section 4.10.2.4. Also, it is necessary to go to a map to see if the camera is over a continental land mass. A statistical analysis of this kind with a required sun angle of 19 degrees or greater has been made for an i = 95-degrees noon orbit at summer solstice. The results for 2 days based on sampling every 2 ½ minutes are shown in Table 4-8.

It is seen that the camera duty cycle is about 13 percent. At this rate, the total linear coverage is about 2810 nautical miles per orbit. It is noted that the sun angle is less than 19 degrees about 60.5 percent of the time. This compares reasonably well with the theoretical value of 60.6 percent for a noon orbit as summer solstice. The camera during time of adequate illumination is over land about 32 to 33 percent of the time. This figure is to be compared with about 2 7 of the earth's surface being land. The camera duty cycle calculated here takes no account of cloud cover so that, in the present example, a large amount of film will be expended taking pictures of clouds. Some statistical data on cloud cover are given in Section 4.10.2.4.2.

Calculation of camera duty cycle is now a tedious process since maps must be used to see if the camera is over land or water. It is thus desirable to program some means for determining when the camera is over land or water. Then, the camera on-off cycling could be obtained by automatic computation, and the camera duty cycle for different kinds of orbits could be readily obtained.

Table 4-8 — Camera Duty Cycle, Statistical Analysis

	First Day		Eighth Day	
	Times	Percent	Times	Percent
In dark	350	60.7	348	60.3
Over land	73	12.7	76	13.2
Over sea	153	26.6	152	26.5
	576	100	576	100

To permit automatic computation of the camera duty cycle, a table could be prepared in which, for each latitude, the increments in longitude are tabulated between which land is to be photographed. At any time in the trajectory, the program could then specify whether the camera is over land or sea. This information, taken together with the calculated sun angle, would then specify in the output whether the camera is off or on. An alternate means of determining whether the camera is over land or water is to try to cover the land mass with overlapping circles, and then determine if the satellite is in a cone of view fitted to these circles. This would be an expansion of an existing sighting program.

4.10.2.2.3 Camera Calibration

It is desirable to make measurements at changes in the film plane metric and in the angular orientations of the earth camera and the stellar cameras with respect to one another during flight conditions, since thermal or other effects may introduce uncertainties. The method of calibration would be to maneuver the Agena so that each pair of cameras takes simultaneous pictures of known stellar fields. In this way, the three included angles between the optical axes are determined and distances on the film can be associated with known angles.

The question of when to calibrate the camera must take some cognizance of the possible cause of any optical axis misalignment. About 15 to 20 orbits must take place before thermal equilibrium will be attained with a somewhat lesser number required for outgassing of the Agena.[1*] Accordingly, during the first 15 to 20 orbits, we should probably not try to take quantitative data. It is desirable to obtain a calibration both entering and leaving the light side of the earth since orbital temperature fluctuations may cause changing thermal effects at orbital period. This should be done before taking quantitative data. To minimize the errors in orbital residual calculations, it is recommended that the calibration not be done during the picture-taking portion of the mission. However, it should be done again at the end of the mission in the same way as at the beginning. If there is any appreciable change in image plane metric or in optical axes orientations from dark to light sides of the earth or from the beginning to end of the mission, extensive inflight calibration will be required or redesign will be required to eliminate the changes.

4.10.2.3 Resonance Effects

The gravitational potential of the earth, the so-called geopotential, is expressed in Reference 2 by

$$U = \frac{K}{r}\left\{1 + \sum_{n=2}^{\infty}\sum_{m=0}^{n}\frac{P_n^m(\sin\phi)}{r^{n-1}}\left[C_n^m \cos m(\lambda - \Lambda_G) + S_n^m \sin m(\lambda - \Lambda_G)\right]\right\} \; ; \; n \geq m$$

* References are listed in Section 4.10.9.

where C and S = constants
K = earth's gravitational constant
r = radius to point of potential U
λ = right ascension of satellite of time t
Λ_G = right ascension of Greenwich at time t
$\lambda - \Lambda_G$ = latitude of satellite measured in plane containing earth's axis and r
ϕ = declination of satellite

$$\pi_n^m (\sin \phi) = \frac{(n-m)!}{(n+m)!} (1-x^2)^{m/2} \frac{d^m}{dx^m} P_n (x)$$

x = sin ϕ
m = order
n = degree
$P_n (x)$ = Legendre function of the first kind

For a fixed value of n, there are m sinusoidal waves of perturbation around the equator due to the sine and cosine terms. There are (n-m) zeros in $\pi_n^m (\sin \phi)$ in the longitudinal direction.

The condition for fundamental resonance is that a satellite going around the earth appears directly above points it was over m revolutions before. Let us define the earth's nodal period (τ_n) as the time it takes a point on the earth to make one complete revolution from the line of nodes back to the line of nodes.

$$\tau_n = \frac{2\pi}{\omega_e - \dot{\Lambda}_o}$$

where τ_n = earth nodal period, seconds
ω_e = sidereal rate of earth, $7.29211585 \times 10^{-5}$ rad/sec
$\dot{\Lambda}_o$ = regression rate of ascending node, rad/sec

The value of $\dot{\Lambda}_o$ is due principally to the oblateness of the earth and, for circular orbits, depends on satellite radius and orbit inclination. The regression of the line of nodes per satellite nodal period is (Reference 3 Section 4.10.9).

$$\Delta \Lambda_o = 57.3\ (3\pi)(1.0826)(10^{-3})\left(\frac{a_e}{r}\right)^2 \cos i \text{ degs/rev}$$

where a_e = equatorial radius of earth
r = radius of circular orbit
i = inclination of orbital plane

For resonance, the satellite period must be an integral fraction of the earth nodal period.

$$\tau_s = \frac{\tau_n}{m} = \frac{2\pi m}{\omega_e - \dot{\Lambda}_o}$$

where τ_s = satellite period

Knowing how the satellite period changes with satellite altitude or the inclination of the orbit plane, we can easily determine when resonance occurs.

A systematic series of runs has been made using the TRACE D program to determine the values of Λ_0 and τ_s for satellites launched southward at various altitudes above the equator at zero flight path angle for various inclinations. From these calculations, which include small effects of drag and oblateness of Λ_0 and τ_s, we have determined the altitudes for fundamental resonance for m = 15 and m = 16. The results are illustrated by the set of charts in Figure 4-30. These charts are all for southerly launch. It should be pointed out that these orbits are not perfectly circular because of the pear shape of the earth. If for a polar orbit the equatorial altitude for a southerly equatorial crossing is 160 nautical miles, the altitude is about 3.5 nautical miles less for the northerly equatorial crossing.

In these charts is plotted the distance east or west of its starting point on the equator that the satellite crosses after 16 passes. For polar orbits (i = 90 degrees), it is seen that the sixteenth pass will cross on its starting point if launched at zero flight path angle at an equatorial altitude of about 144 nautical miles. At this condition, we obtain perfect resonance to m = 16. The corresponding m = 15 resonance occurs at about 300 nautical miles. Other resonance points can be read off the charts.

4.10.2.4 Illumination and Cloud Cover

4.10.2.4.1 Illumination Considerations

The intensity of sunlight available for photography is a function of the cosine of the sun angle from the zenith. It is possible to obtain adequate sunlight for photography at solar angles up to 80 degrees or more. For purposes of this analysis, we will assume that the sun must be 19 degrees or more above the horizon for picture taking.

Shadows probably restrict the ability to photograph more than overall illumination. Pictures are easier to interpret with solar zenith angles of about 45 degrees, giving small but helpful shadows. At solar zenith angles near zero, photography loses apparent contrast, and at large zenith angles, the shadows become so long they may cover much of the area of interest, particularly in rugged terrain.

For orbit planning purposes, it is desirable to be able to calculate the angle of the sun as measured from the local satellite zenith on the local horizon. Let ϕ be the angle between the local zenith and the sun. It can then be shown that

$$\cos \phi = \sin \delta \sin \delta_s - \cos \delta \cos \delta_s \cos (\alpha_s - \alpha)$$

where δ - declination of satellite
α = right ascension of satellite
δ_s = declination of sun
α_s = right ascension of sun

(The quantities δ and α are printed out in the TRACE program as a function of Greenwich mean time as well as ϕ.) The values of δ_s and α_s can be obtained from an ephemeris.

One of the requirements of the present system is to obtain general world photographic coverage including the north and south polar regions. It is of interest, therefore, to examine the illumination conditions for the extremes of the north and south poles. At the winter solstice, the north pole is inclined 23.4 degrees away from the sun, and the declination of the sun (δ_S) is -23.4 degrees. The angle ($\alpha_S - \alpha$) is the longitude measured east or west of the meridian for which local time is noon. We can therefore plot curves of constant sun angle as a function of latitude (δ) and longitude ($\alpha_S - \alpha$). Figure 4-34 is such a plot for the winter solstice.

Consider a noon orbit at the winter solstice, i.e., an orbit containing the polar axis and the earth-sun line. For this orbit, local time is always noon or midnight. The figure shows that the noon orbit will have adequate illumination from 47 degrees north latitude to 90-degrees south latitude. In fact, for 3.4 degrees of latitude around the south pole, the sun angle will be 20 degrees or higher for 24 hours a day. This circumstance will generate multiple coverage of points near the south pole with pictures every orbit. Q-data generation is therefore well served by the present orbit.

What is true for the antarctic coverage at the winter solstice is equally true for arctic coverage at the summer solstice. The sun angle exceeds 19 degrees at the poles for a period of about 2 months. Since satellites can be launched at about 2-month intervals, it would be desirable to schedule polar launches for the beginning of these periods, so that a second launch in the same orbit can be made in case of trouble with the first. If the sun angle requirement for illumination can be relaxed to sun angles (90-ϕ) or less than 19 degrees, a greater period of time around the solstices will be available for launch.

4.10.2.4.2 Cloud Cover Considerations

An important limitation on photographic coverage from a satellite is cloud cover. Some knowledge of the distribution of cloudiness over the earth with time of year is required in order to determine the most favorable launch time for viewing specific areas. Figures 4-35 and 4-36 are maps of the distribution of mean cloudiness over the earth during the months of January and July. These are taken from Reference 4. The lines on the figures are lines of constant mean cloudiness, in tenths, of the total area of the sky. If the sky is cloudless, the cloudiness is 0; if it is completely covered, it is 10. The mean cloudiness is found by averaging a large number of observations and, therefore, yields no information concerning the frequency distribution of various levels of cloudiness. For example, a mean cloudiness of 5/10 could result from the sky being completely clear 50 percent of the time and completely covered by clouds the other 50 percent, or from the sky being 50 percent covered by clouds 100 percent of the time.

An examination of the two figures indicate that:

1. Mean cover is greatest near the arctic and antarctic circles, near the equator, and near some mid-latitude continental shore lines.

2. Mean cover is generally greater over the oceans than over the land masses.

3. Mean cover over the land masses is generally less in July than in January, the main exception being in the tropics where the monsoon season occurs around July.

In addition, other data on cloud cover indicate that diurnal maxima can be expected in early afternoon in the tropics, and probably in the morning and evening in temperate latitudes subject to heavy fogs. Yearly minima in temperate latitudes generally occur in summer, but there is a great deal of variability. Storms move primarily from west to east.

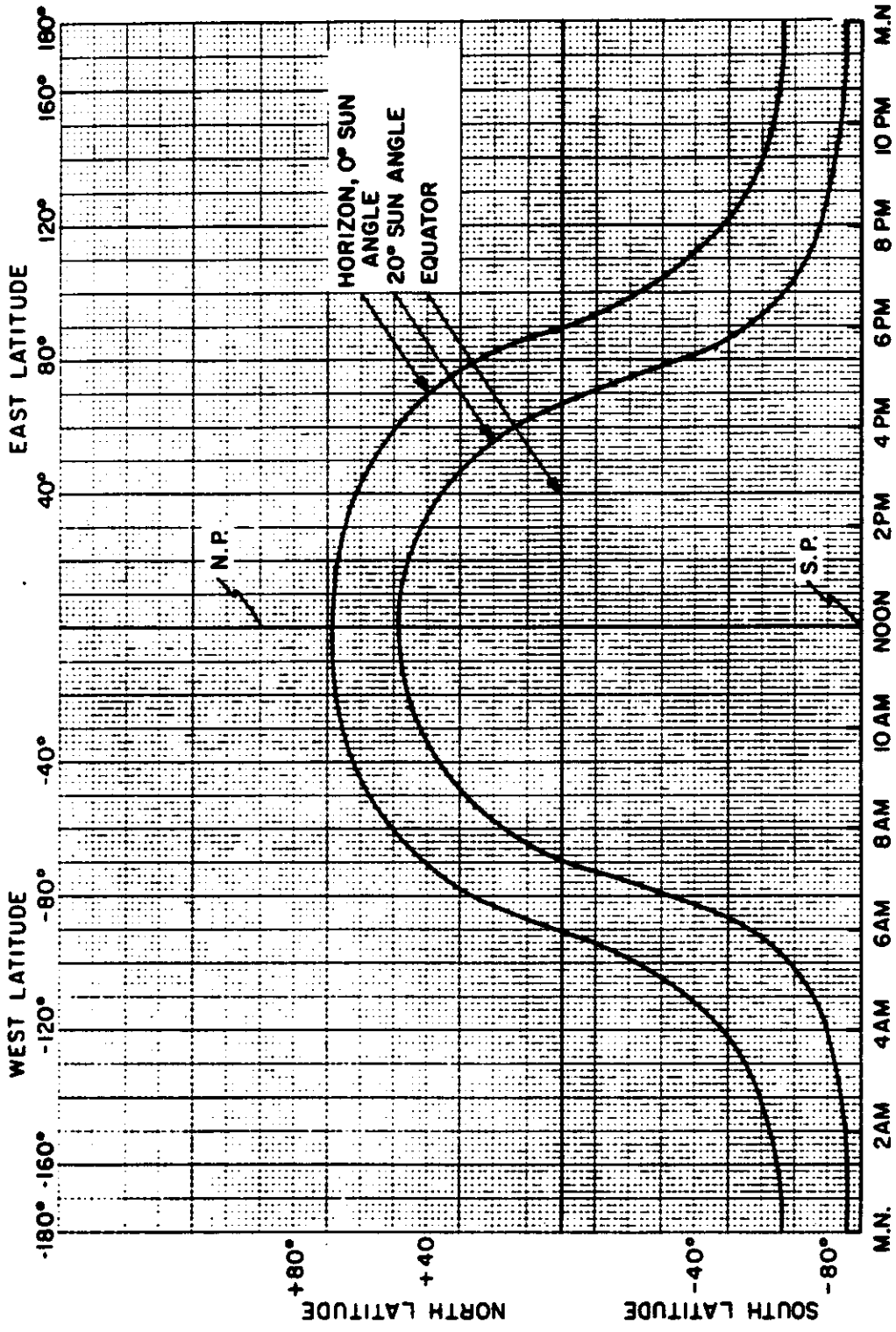

Fig. 4-34 — Area of earth's surface with 20-degree sun angle at the winter solstice

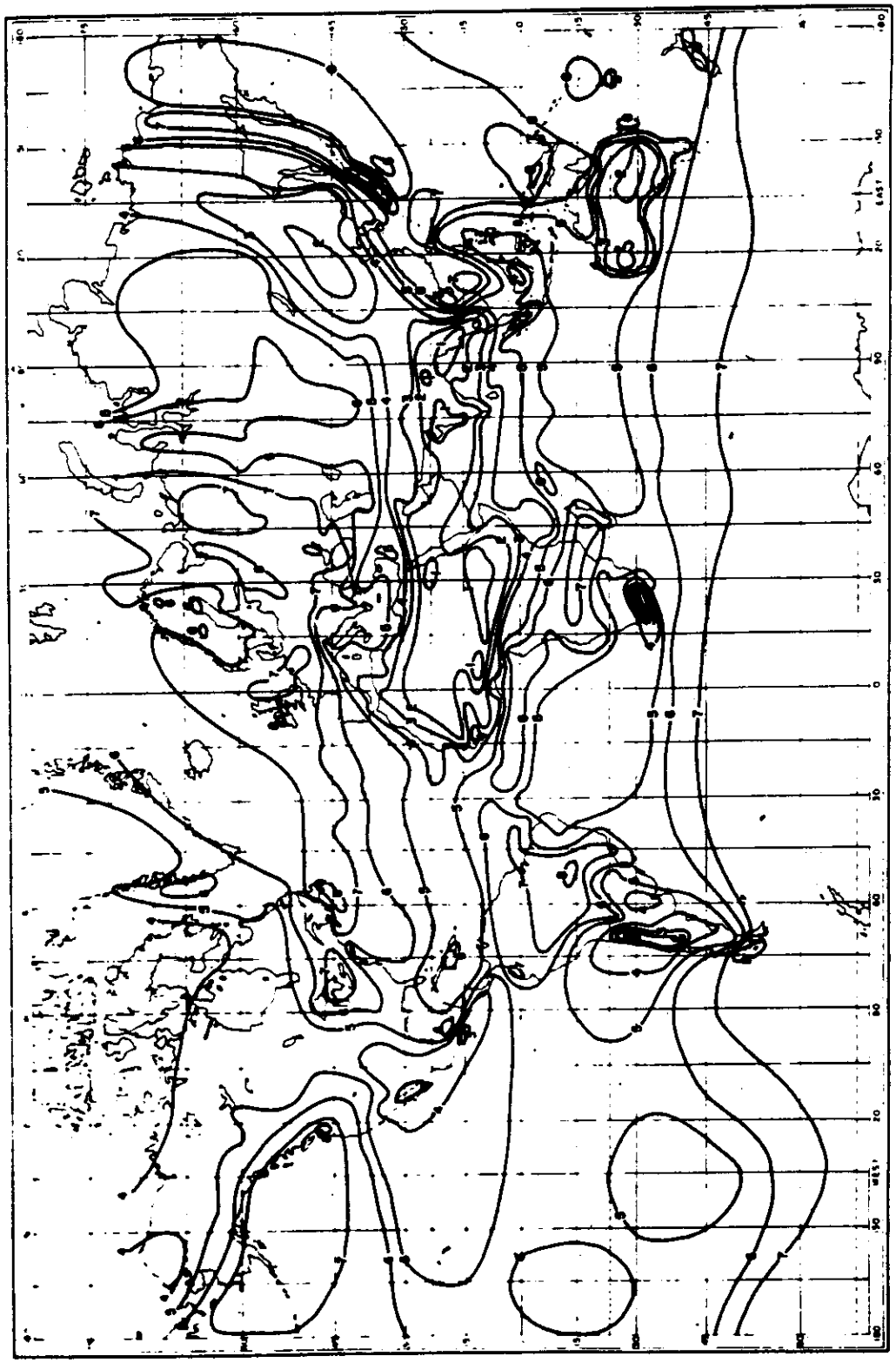

Fig. 4-35 — Mean cloudiness in January

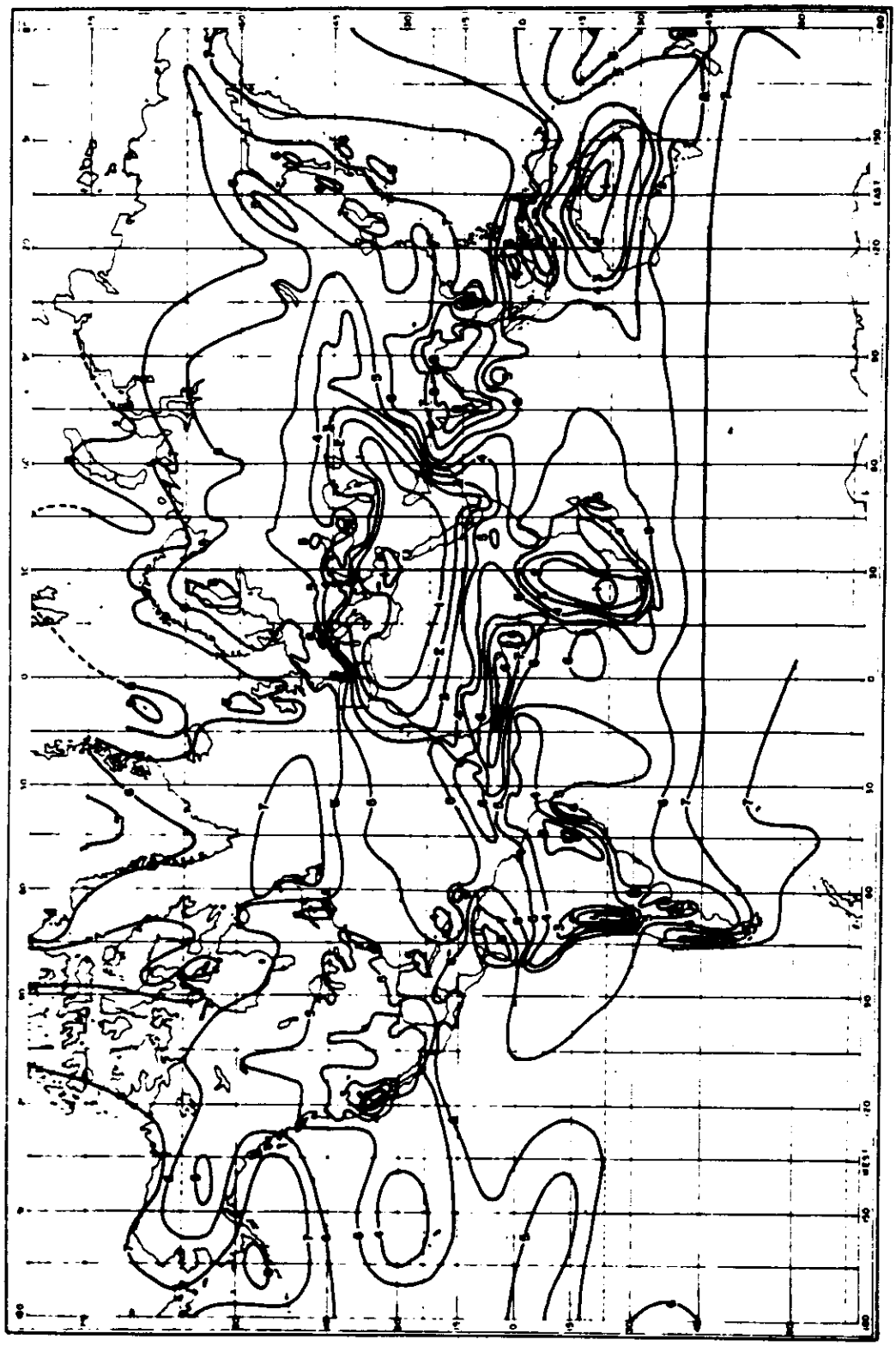

Fig. 4-36 — Mean cloudiness in July

It should be emphasized that there is a great deal of variability within the general behavioral pattern described above and that local areas may exhibit strongly anomalistic behavior.

It is of interest to interpret the cloud data presented in Figures 4-35 and 4-36 in terms of the number of times a given location must be viewed in order to have a given probability of seeing the surface. If it is assumed that cloud conditions on successive viewing days are not correlated (this is probably a good assumption if the mean cloud cover is between 0 and 5/10)

and

P = probability of successful viewing
C = mean cloudiness
N = number of times an area is viewed

then

$$P = 1 - C^N$$

or

$$N = \log (1-P) - \log C$$

Table 4-9 has been prepared for a 90-percent probability of successful viewing. If this table is used in conjunction with Figures 4-35 and 4-36, the mean cloudiness can be interpreted as viewings. For example, a mean cloudiness of 5/10 would require four viewings to have a 90-percent probability of seeing the surface. A mean cloudiness of 2/10 would require two viewings.

Since the present concern is with photographic coverage from a satellite, the number of interest is the number of missions required to have a 90-percent probability of seeing a point. Since, for a particular orbit, there is redundant coverage at certain latitudes (see Section 4.10.2.1.3), the number of missions is not necessarily equal to the maximum number of viewings required. Figures 4-37 and 4-38 have been prepared to show the number of missions required for a specified orbit. Figure 4-37 is for a noon, polar orbit in January, and Figure 4-38 for a noon polar orbit in July. For the January orbit, satisfactory illumination of the earth's surface for photographic purposes is obtained from about 47-degree north latitude to the south pole. In July, the range is from the north pole to 47-degree south latitude. The surface of the earth has been broken into areas 15 degrees in longitude by 5 degrees in latitude. Using Figures 4-35 and 4-36, an estimate of the average mean cloudiness has been made over each of these areas. Table 4-9 has been used to convert this estimate to the number of viewings for a 90-percent probability of seeing; this number has been divided by one over the cosine of the latitude

$$\text{number of missions} = \frac{\text{number of viewings}}{\frac{1}{\cos (\text{latitude})}}$$

since, for a polar orbit with each point on the equator covered once in a mission, the redundancy is one over the cosine of the latitude. Also included on these figures is a histogram showing, for each 15- or 5-degree area, an estimate of the percent of that area which is land.

These figures, together with earlier remarks, indicate that:

1. Redundant coverage of high latitudes is desirable (and inevitable with orbital inclinations near 90 degrees).

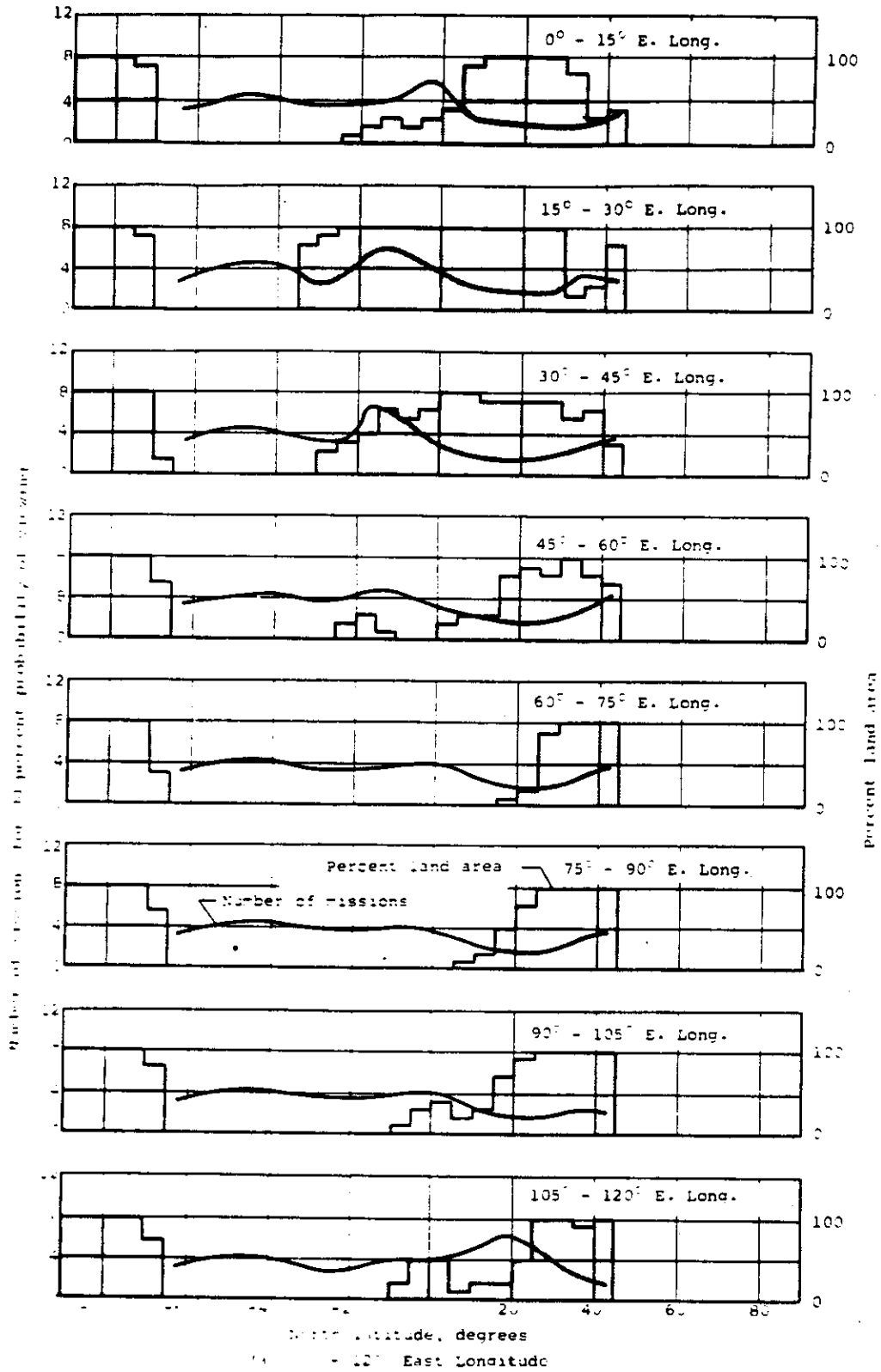

Fig. 4-37 — Variation in number of missions and percent land area for a noon, polar orbit in January

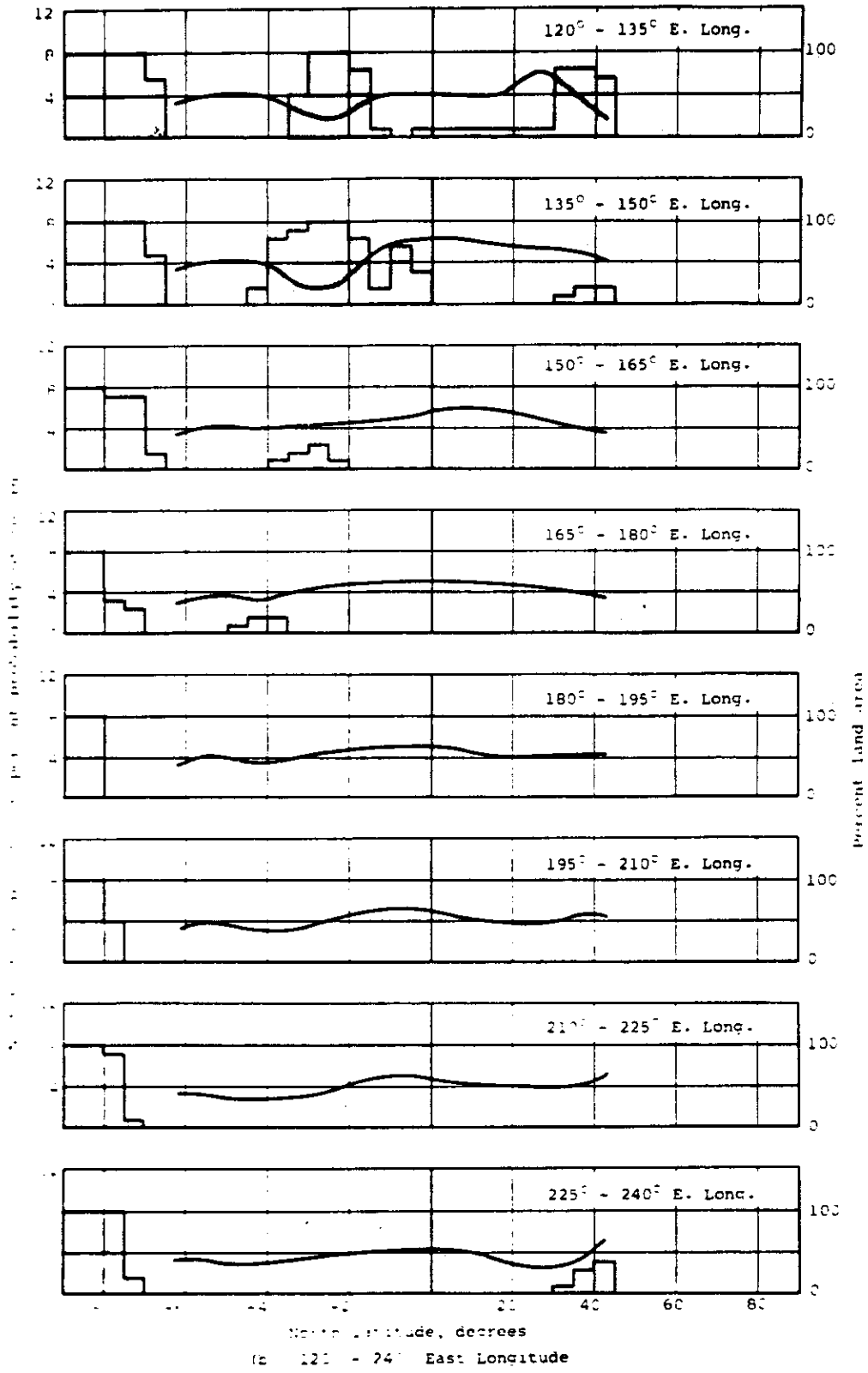

Fig. 4-37 (Cont.) — Variation in number of missions and percent land area for a noon, polar orbit in January

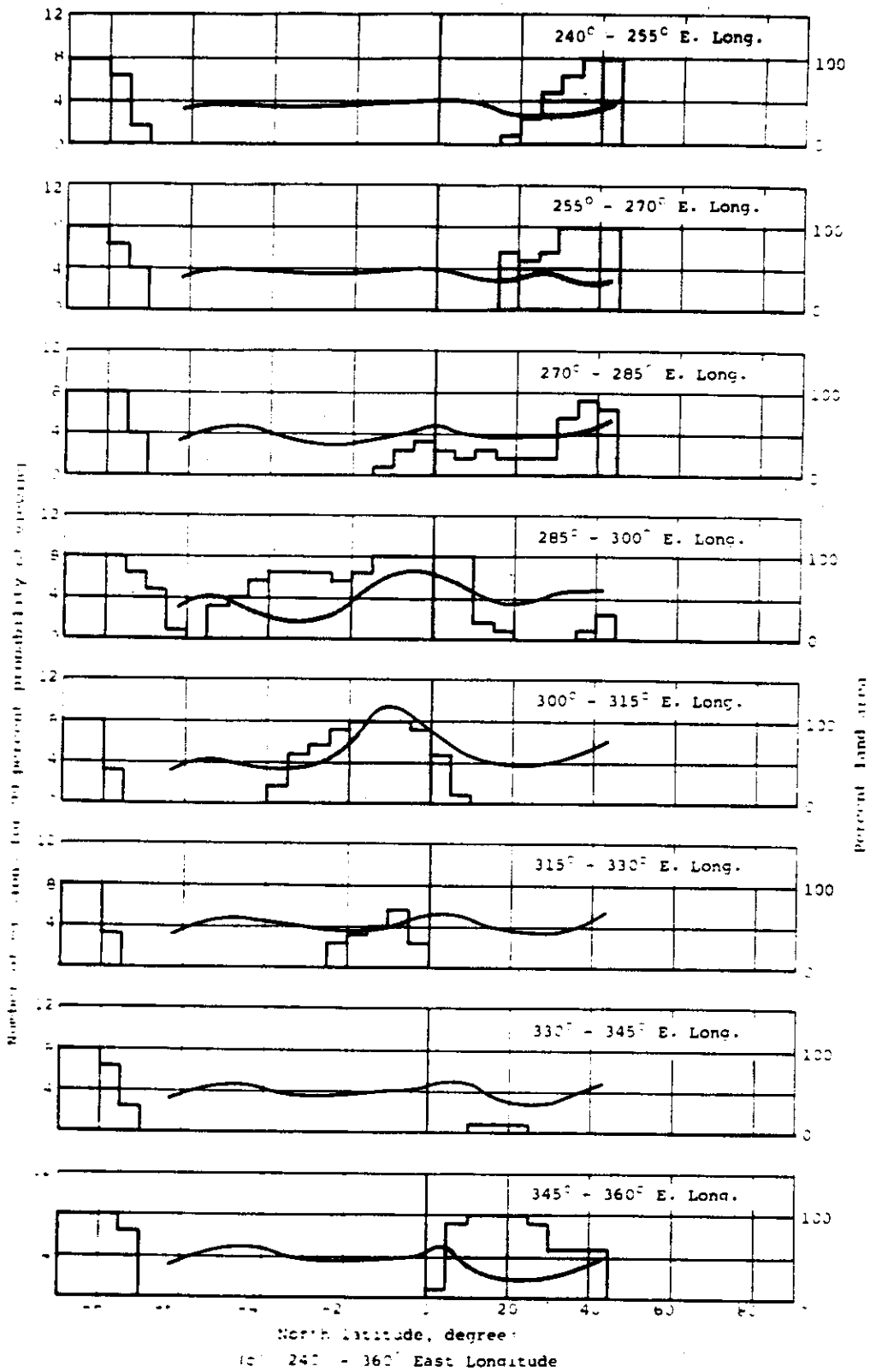

Fig. 4-37 (Cont.) — Variation in number of missions and percent land area for a noon, polar orbit in January

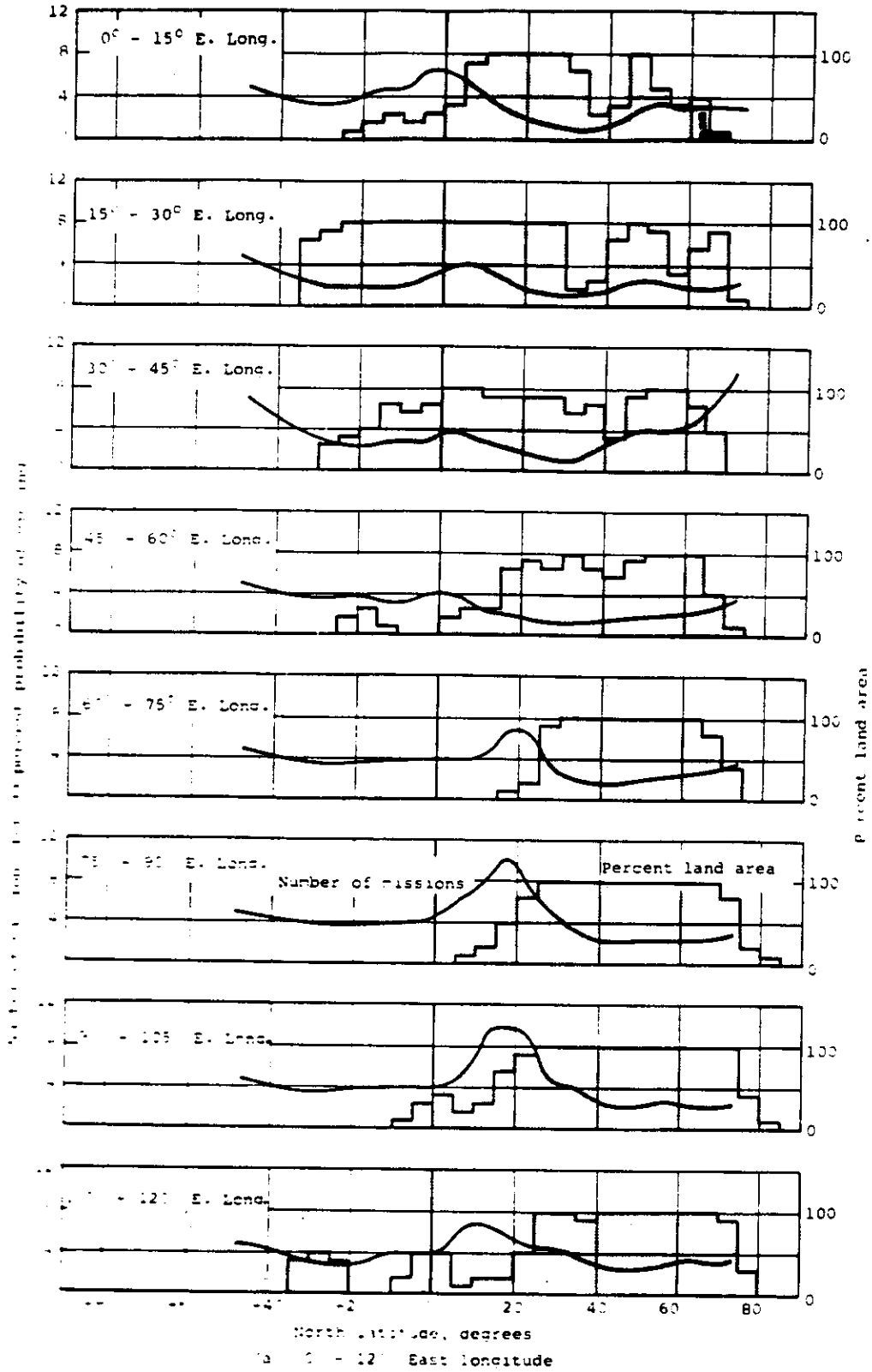

Fig. 4-38 — Variation in number of missions and percent land area for a noon, polar orbit in July

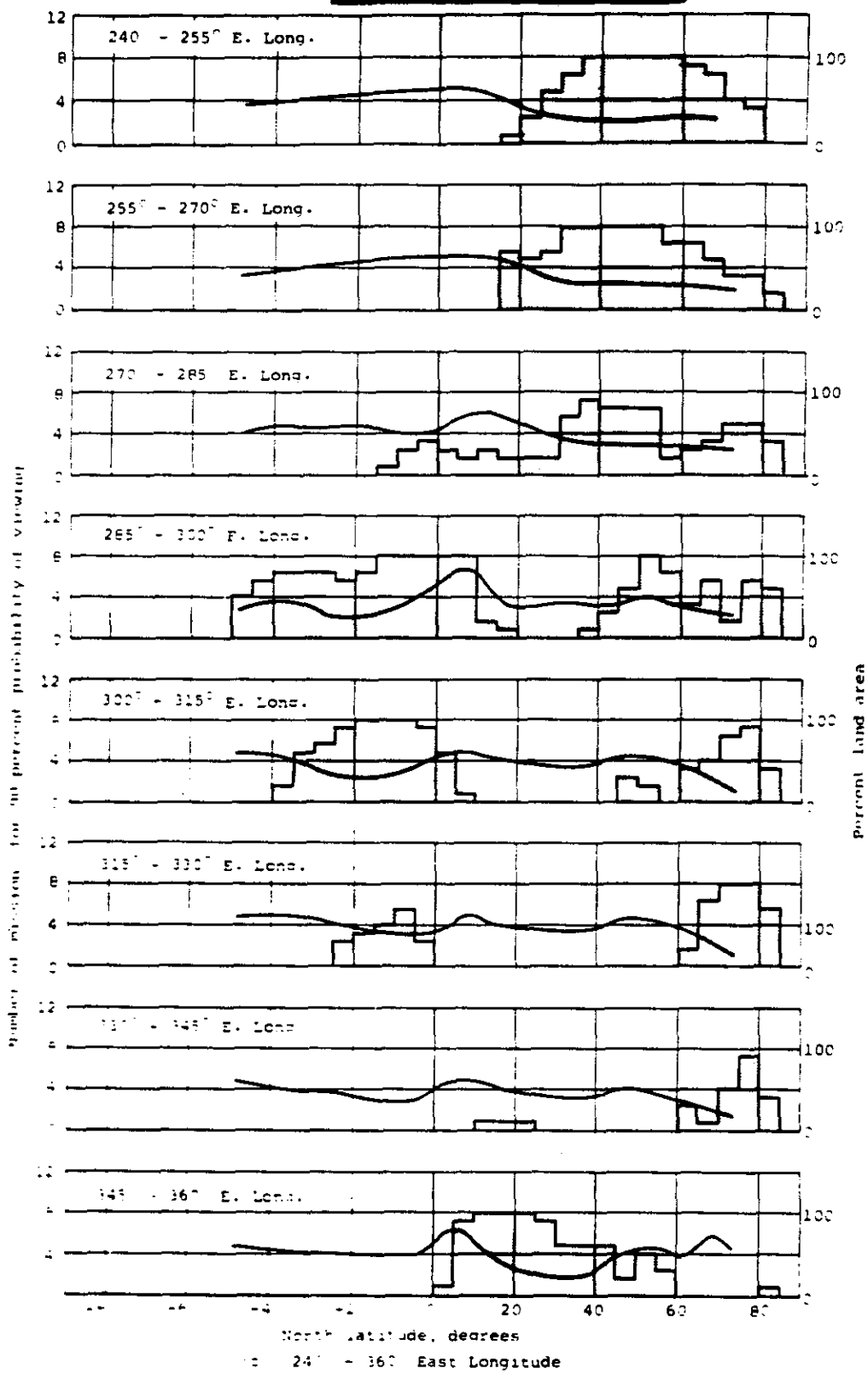

Fig. 4-38 (Cont.) — Variation in number of missions and percent land for a noon, polar orbit in July

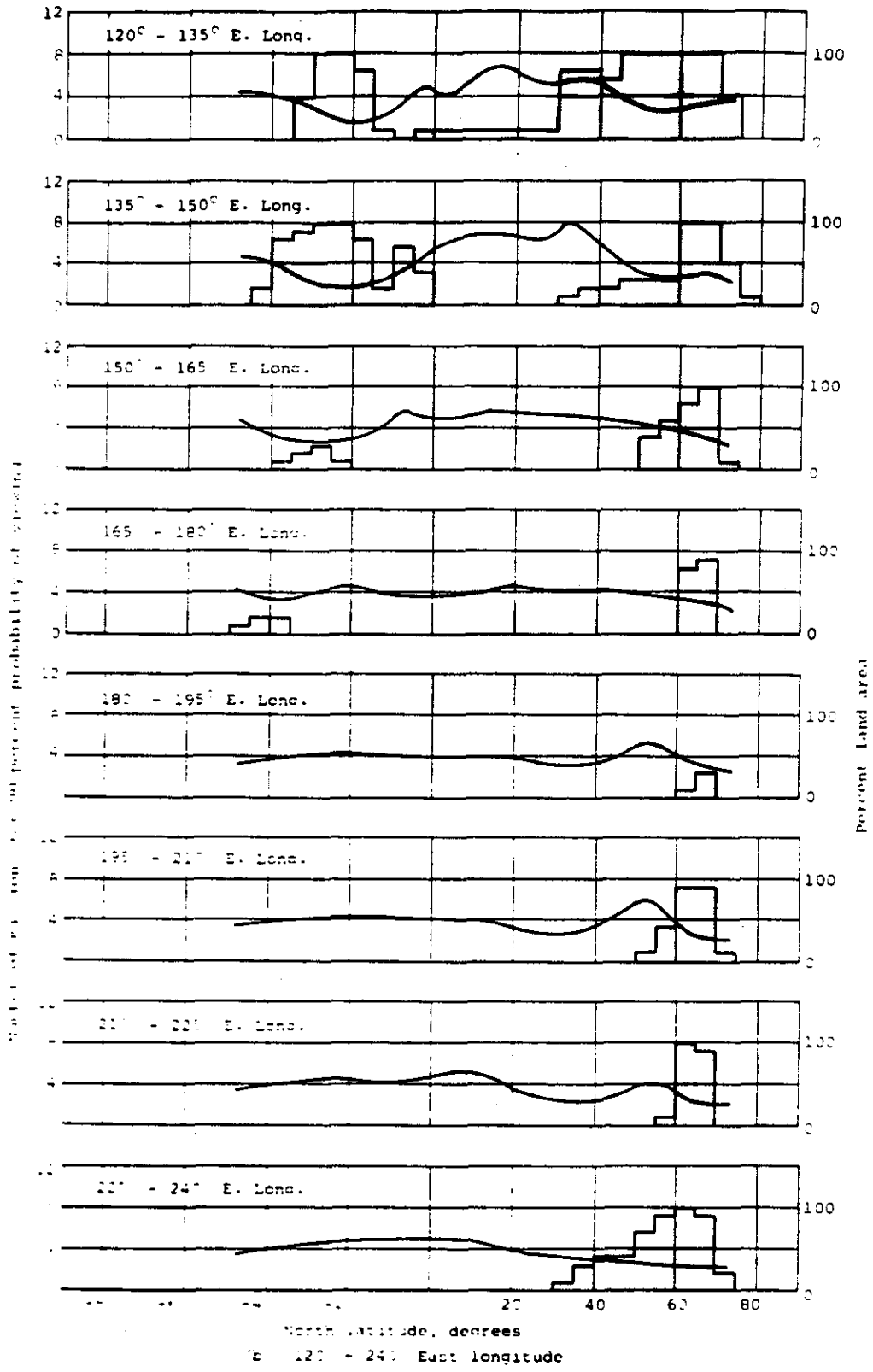

Fig. 4-38 (Cont.) — Variation in number of missions and percent land for a noon, polar orbit in July

Table 4-9 — Number of Viewings Required for a 90-Percent Probability of Successful Viewing

Number of Viewings	Mean Cloudiness, tenths
1	1.0
2	3.2
3	4.6
4	5.6
5	6.3
6	6.8
7	7.2
8	7.5
9	7.7
10	7.9

2. Summer flights are most apt to give good coverage.
3. Westward diurnal motion of the ground swath is desirable to prevent observing clouds from a given storm for several days.
4. Orbits crossing the equator before noon and higher latitudes around noon are most apt to be free of cloud cover.

4.10.2.4.3 Launch and Recovery

Combination of cloud cover and illumination conditions indicates the following:

1. Launch times about 10 a.m. at Vandenberg are probably acceptable for launches near the summer and winter solstices. These orbits should be polar or nearly so, and the morning launch both gives acceptable solar angles at the latitude of the sun and improves the chances for minimum cloud cover in the tropics. If there is any departure from a polar orbit, it should be retrograde near 21 June, and the direct near 21 December to provide better cloud-cover conditions, in the hemisphere of importance.

2. Launch times about noon at Vandenberg with southerly retrograde orbits are probably best for vehicles launched near the equinox. In these orbits, the equator will be crossed in the morning, northern latitudes somewhat later in the day. It is believed that the coverage of northern hemisphere land masses is most important on these orbits. There is relatively little land in the southern hemisphere and it should be covered adequately on the polar orbits. Also, if launched south at noon near the equinoxes, the satellites can be recovered near local noon while moving down into the Pacific from the North Pole. This is the preferred recovery method.

4.10.2.5 Drag Considerations

4.10.2.5.1 Effect on Period, Overlap, and Interlace

As previously mentioned, the effect of drag is to shorten the period and decrease the altitude, making interlace very difficult for any pattern but one which overlaps the ground swaths generated on successive days. Increasing altitude to reduce drag effects could be practical if photogrammetric accuracy permits.

4.10.2.5.2 Uncertainties in Drag

Uncertainties in knowledge of drag force may seriously affect in-track position. Uncertainty in W/C_DA may give initial errors in the orbit elements but these errors are subject to correction as the orbit is observed, since W/C_DA should remain constant with time.

Uncertainty in air density and other drag forces are lumped together since it is convenient to consider variations in drag as resulting from density variations, although they may actually arise from electromagnetic effects, ionospheric winds, etc. In any case, they are important because they are not necessarily constant with time. The rate of change of the period of a circular orbit with respect to time is directly proportional to the density as given by

$$\frac{dT}{dt} = \frac{-3\rho T C_d A V}{2m}$$

where τ = period, seconds
ρ = density, slugs/ft^3
C_d = drag coefficient
A = area, square feet
V = velocity, feet per second
m = vehicle mass, slugs

The relative uncertainty in knowledge of rate of change of period is the same as the relative uncertainty in the density. Let us call this relative uncertainty $\Delta\rho$ and the corresponding uncertainty in period change $\Delta(d\tau/dt)$; then

$$\Delta\tau = \int_0^t \Delta\left(\frac{d\tau}{dt}\right) dt$$

when $\Delta\tau$ is the accumulated uncertainty in period at time (t). The in-track error is approximately

$$E = V \int_0^t \Delta\tau \, d\tau = \frac{V}{\tau} \Delta\left(\frac{d\tau}{dt}\right)\frac{t^2}{2}$$

for V = 25,400, t = 6 hours = 21,600 seconds, and τ = 5400 seconds, with an allowable E of 200 feet.

$$\Delta\left(\frac{d\tau}{dt}\right) = \frac{2 \times 200 \times 5400}{25,409 \times (21,600)^2} = 1.8 \times 10^{-7} \text{ sec/sec}$$

At an altitude of 160 nautical miles, $d\tau/dt$ computed using the TRACE program and the Lockheed atmosphere is about 6×10^{-6}. Thus, the allowable relative uncertainty in $d\tau/dt$ and thus in density is about 3 percent at this altitude. Since the allowable error in density remains constant but the actual density decreases rapidly with altitude, the allowable relative uncertainty while small in the 150- to 180-nautical mile region becomes large at slightly greater altitudes, as shown in Figure 4-39.

The atmospheric density at orbital altitudes can be correlated with a number of variables. These include time of day, with an increased density at high altitudes during the day; solar flux as measured at 10.7 and 20 centimeters, with drag increasing as flux increases (and thus exhibiting a period corresponding to the 27 to 28 day solar rotation period, as well as periodic effects from solar flares); and geomagnetic activity, with minimal activity leading to minimal drag. However, even when all these variables are taken into account, it is difficult to attain consistent accuracies of better than about 10 percent in predicted density. (See for example, Reference 5.) This is another reason for increasing operational altitudes if possible.

4.10.2.6 Tracking Considerations

One of the stringent tests of the calculational techniques and physical model adequacy of the system would be its capability to project accurate orbital positions four orbits ahead. While such a test of the system, if successful, would certainly be confidence-inspiring, it is questionable whether it is necessary for successful accomplishment of the mission. This appears to be true since the satellite will be seen about one time per orbit on the average by the extended seven-station Satellite Control Facility (SCF/SGLS) and about three times per revolution by a typical 16-station TRANSIT network, as described in Section 4.2.4.

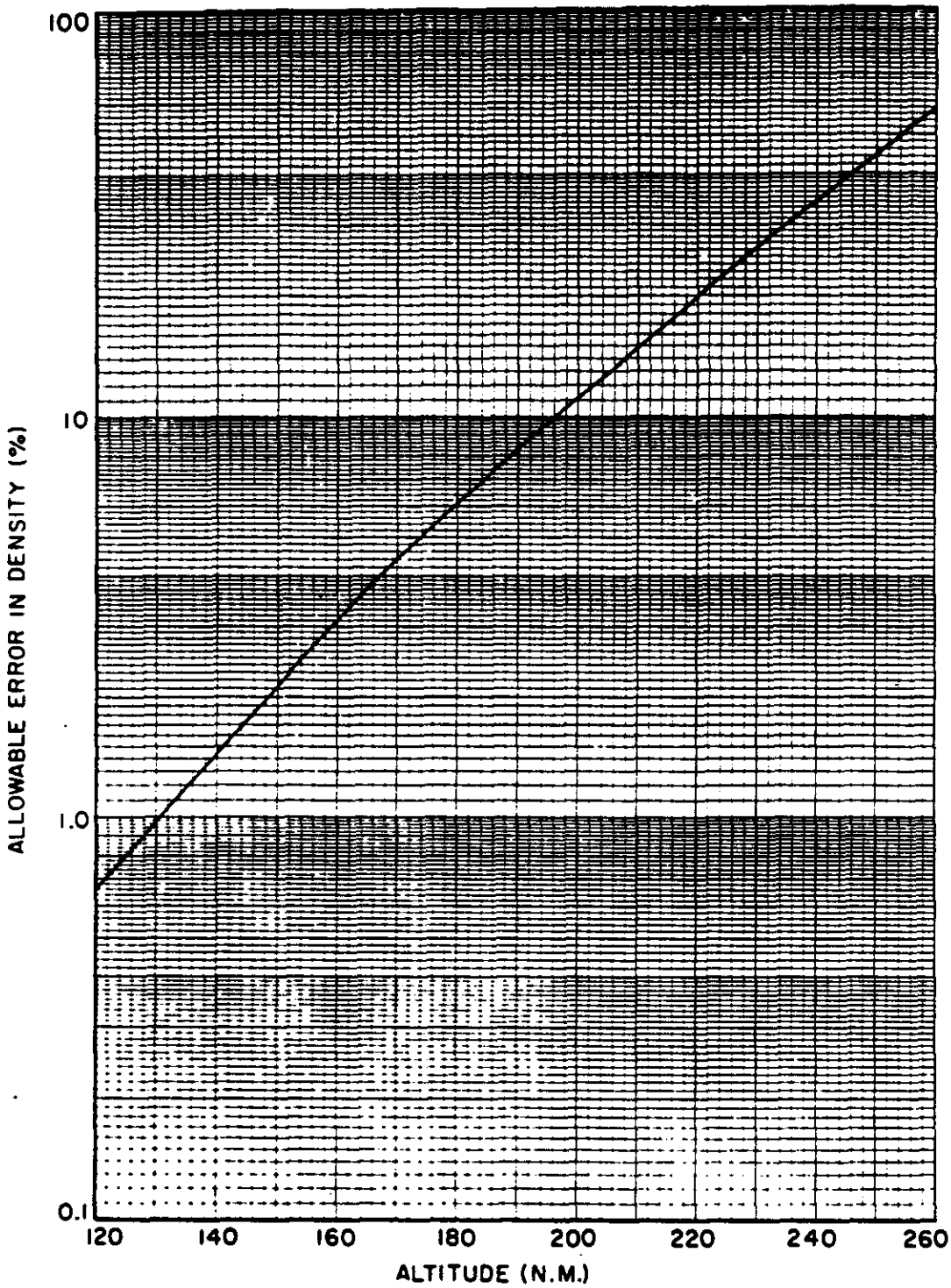

Fig. 4-39 — Density error allowed as a function of altitude

In order to obtain some ideas concerning acquisition patterns, a sighting run was made using the TRACE program under the following conditions.

Altitude—160 nautical miles on equator at 120-degree west longitude
Orbit inclination—95 degrees southward launch
W/C_DA—75
Earth model—unpublished Guier sixth-degree model obtained by private communication by Aerospace Corporation
Atmospheric model—Lockheed-Jacchia quasi-dynamical model

The sighting condition imposed for the radar (SCF/SGLS) and for TRANSIT was the intersection of a cone having an 80-degree semiapex angle from the station. The satellite was tested every 30 seconds to see if it were in the cone view. It is therefore possible that the satellite could have been in a cone of view for 29 seconds and still be missed. The frequencies with which the satellite was acquired by TRANSIT and SCF/SGLS are shown in the Tables 4-10 and 4-11, respectively. The satellite is ordinarily seen four times per revolution.

On statistical grounds, the probability of a given station acquiring a satellite in a polar orbit should be proportional to the cosine of the latitude. Thus, if P (o) is the number of times the satellite is acquired by an equatorial station and if P (λ) is the number of times for a station at latitude λ, we have

$$P(\lambda) = \frac{P(o)}{\cos \lambda}$$

This variation is plotted in Figure 4-40, which shows the frequency of acquisition by both the radar and TRANSIT stations as a function of latitude. Both networks show the same correlation as a function of latitude, and both closely follow the statistical theory. [At the pole where $P(\lambda)$ is infinite, the theory is not valid.]

It is important to know how long the satellite can go without being acquired by a network, the so-called "dead time." In order to obtain quantitative data on this question, an analysis was made of the sighting computation to obtain a frequency distribution of the dead time for both the SCF/SGLS and the TRANSIT network. The results for TRANSIT are shown in Figure 4-41 and for SCF/SGLS in Figure 4-42. For the TRANSIT network, the dead time was less than one-half hour about 65 percent of the time and over an hour only about 2 percent of the time. The maximum dead times for the second and eighth days were 137 minutes and 94 minutes, respectively. It should be noted that the dead time is a function of the minimum elevation and altitude, which here were 10 degrees and 160 nautical miles, respectively.

For the SCF/SGLS network, Figure 4-42 shows that the dead time is less than 1 hour about half the time. The maximum dead times for the second and eighth days were 166 minutes and 255 minutes, respectively.

It turns out that the dead times for TRANSIT calculated here are longer than those obtained from a corresponding Applied Physics Laboratory calculation. In our calculation, we have assumed that acquisition can be obtained only within 10 degrees of the horizon. The Applied Physics Laboratory results are based on a lower angle.

Table 4-10 — Frequency of Acquisition by TRANSIT Network

Day / Station	XA	XB	XC	XD	XE	XF	XG	XH	XI	XJ	XK	XL	XM	XN	XO	XP	Total
1	1	1	1	1	2	1	1	1	3	2	6	2	2	6	1	1	32
2	2	2	3	1	2	1	2	3	4	2	10	2	2	10	2	2	50
3	2	2	3	1	1	1	2	3	3	2	10	2	2	10	2	2	48
4	2	2	3	2	1	2	2	2	4	1	10	2	1	10	2	2	48
5	2	2	3	2	2	2	2	2	4	1	10	2	1	10	1	2	48
6	2	2	4	2	1	2	2	2	4	2	10	2	2	10	1	2	50
7	2	2	3	2	1	2	2	2	4	2	10	2	2	9	2	1	48
8	2	2	3	2	2	2	2	2	4	2	10	2	2	10	2	1	50
9	2	2	3	2	2	2	2	2	4	1	10	1	1	10	2	2	48
10	2	2	3	2	2	2	2	2	4	1	10	2	1	10	2	2	49
11	3	2	3	2	2	1	2	2	4	1	10	1	1	10	1	1	46
12	2	2	3	2	2	1	3	2	4	2	10	2	2	10	1	1	49
13	2	2	2	2	2	1	2	2	4	2	10	2	2	10	1	2	48
14	2	2	2	1	2	2	2	2	3	2	10	2	2	11	2	2	49
15	2	2	2	2	2	2	2	2	3	2	9	2	2	11	2	2	49
Total	30	29	41	26	26	24	30	31	56	25	145	28	25	147	24	25	712

Table 4-11 — Frequency of Acquisition by Satellite Control Facility

Day \ Station	RA	RB	RC	RD	RE	RF	RG	Total
1	2	1	3	1	6	1	2	16
2	2	2	3	2	10	1	2	22
3	2	2	3	2	10	1	2	22
4	2	2	3	2	10	1	1	21
5	2	2	3	2	10	2	1	22
6	1	2	3	2	10	2	2	22
7	2	2	3	3	10	2	2	24
8	1	2	3	3	10	2	2	23
9	2	2	3	2	10	2	1	22
10	2	2	4	3	10	2	1	24
11	2	3	4	3	10	2	1	25
12	2	3	4	2	10	1	2	24
13	2	2	3	2	10	1	2	22
14	2	2	3	2	10	2	2	23
15	2	2	3	2	9	2	2	22
Total	28	31	48	33	145	24	25	334

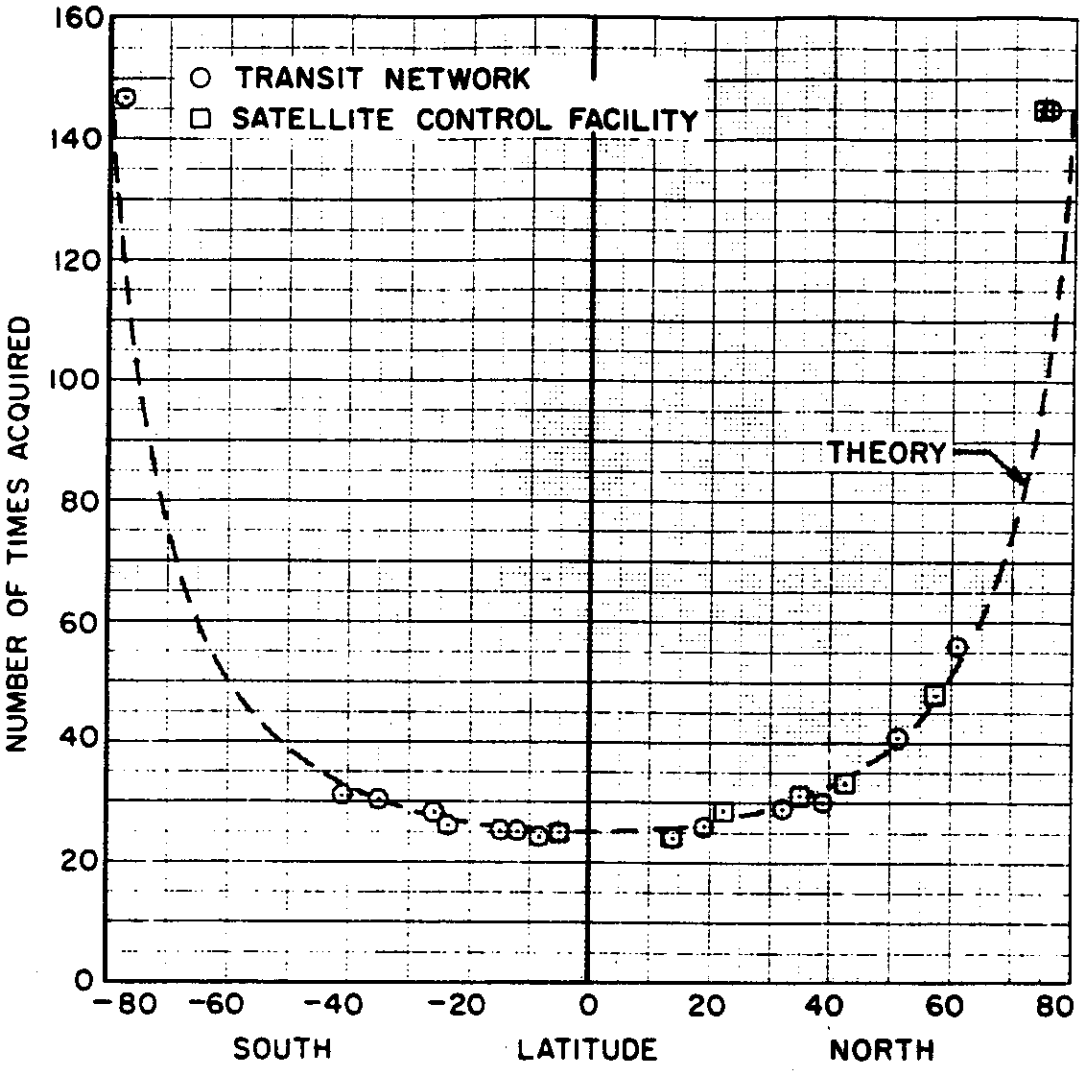

Fig. 4-40 — Frequency of acquisition as a function of latitude for a 15-day period

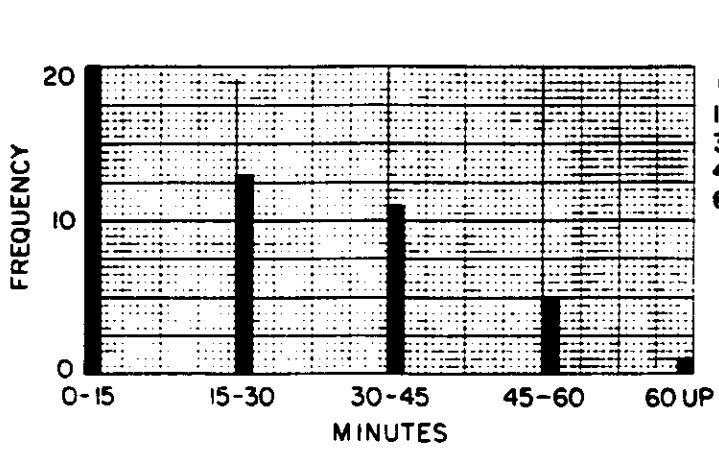

	NO. OF POINTS	%
0 – 15	20	40
15 – 30	13	26
30 – 45	11	22
45 – 60	5	10
60 UP	1	2
	50	100%

(a) SECOND DAY

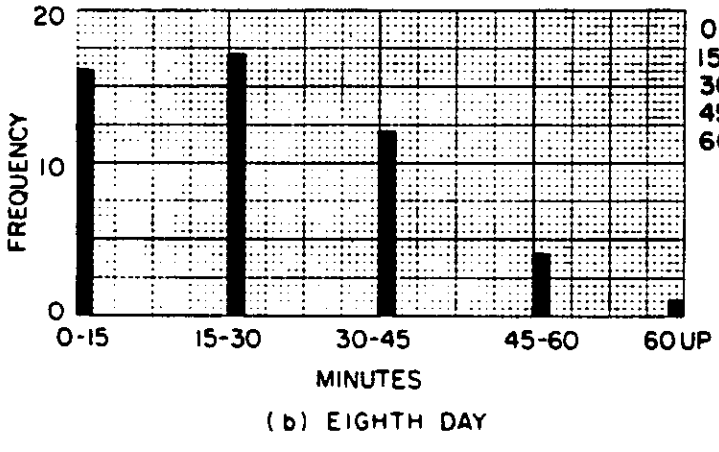

0 – 15	16	36
15 – 30	17	34
30 – 45	12	24
45 – 60	4	8
60 UP	1	2
	50	100%

(b) EIGHTH DAY

Fig. 4-41 — Frequency distribution of "dead time" of the TRANSIT network for two separate days

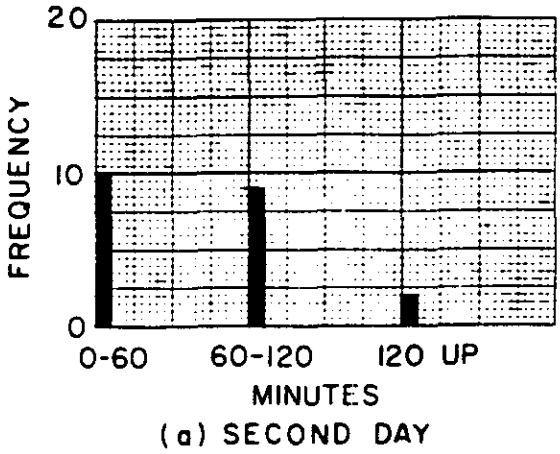

(a) SECOND DAY

	NO. OF PTS.	%
0-60	10	48
60-120	9	43
120 UP	2	9
	21	100%

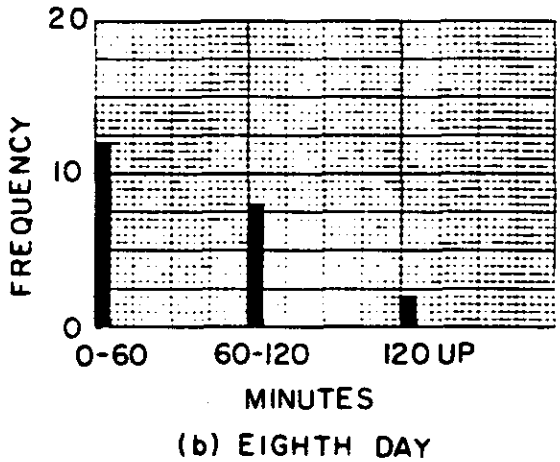

(b) EIGHTH DAY

	NO. OF PTS.	%
0-60	12	55
60-120	8	36
120 UP	2	9
	22	100%

Fig. 4-42 — Frequency distribution of "dead time" of the Satellite Control Facility for two separate days

4.10.3 Operational Considerations

Certain operational problems put constriants on the orbital plan. Certain of these constraints are discussed in this section.

4.10.3.1 Launch

The time of launch can presumably be chosen night or day. However, it appears that daylight southerly launches are probably best. Among other advantages, they provide daylight recovery on southgoing passes as required. With regard to orbital inclinations, any southerly retrograde launch can be made. Direct (eastward) launches must be southerly and, with azimuth, no less than 170 degrees east of north. This essentially rules out use of direct orbits for Vandenberg launches unless a "dog leg" trajectory can be used. No necessity for direct launches is foreseen at this time.

With regard to the accuracy of the injection parameters, three-sigma injection errors are assumed to be ±0.3 degree in flightpath angle with + velocity correlated with - altitude and flightpath angle and - velocity with - altitude and flightpath angle. Period errors are as great as 8 seconds, eccentricity errors as great as 0.006 second.

4.10.3.2 Orbit Adjust

The determination of orbit elements is complicated by outgassing, which will introduce unpredictable thrusts. This outgassing will decay exponentially, but will be large enough to have an observable effect for 10 to 15 orbits. During this time, however, orbit elements can be determined, if necessary, based on an extrapolated outgassing curve.

The orbit adjust maneuvers should probably wait until after at least 15 orbits. It will take approximately 15 to 20 orbits for the camera to come to thermal equilibrium so photography can not be initiated before then in any case. It is assumed that the orbit period can be corrected to about 10 percent or 0.8 second, that eccentricity can be corrected to less than 0.001, that the position of apogee can be corrected to within less than 10 degrees, but that no appreciable change can be made in orbit inclination.

4.10.3.3 Recovery

Recovery will be made in the area of Hawaii on a southgoing pass in the daylight at least two hours before sunset. The recovery area is wide enough to ensure at least one appropriate pass in the area each day. One recovery package will be recovered on each of two successive days if the two-package configuration is utilized.

4.10.4 Reliability Considerations

The orbit plans must be sufficiently flexible to allow for overall system reliability. For instance, if the first launch in a given orbit is unsuccessful, it would be desirable to repeat it at a later appropriate date. This is especially true for the polar orbits, which will obtain coverage not obtained by orbits of low inclinations. Thus, it will be desirable to schedule polar launches about 21 May for northern polar region coverage and 22 November for antarctic coverage. These launches are the earliest possible giving 20-degree sun altitude at the poles; a second launch two months later will give approximately the same sun angles there.

4.10.5 Solar Activity Considerations

4.10.5.1 Introduction

Solar activity may influence the GOPSS mission in two ways. In the first case, a major solar flare may produce an intense flux of high energy penetrating radiation in the vehicle vicinity, such that the absorbed radiation dosage in the photographic film is sufficient to induce serious fogging. Second, solar activity may affect the amount and types of energy fluxes incident on the earth's atmosphere, thus affecting the density distribution in the atmosphere and hence the drag forces acting on the vehicle. As discussed in the following section, it is not believed that solar flare-induced fogging of the film will be a serious consideration, but it is believed that the prediction of the drag forces acting on the vehicle can be seriously influenced by fluctuations in solar activity.

We are now entering cycle 20, a period of increasing solar activity in the 11-year solar cycle, which may peak in 1968-1970 era. It appears that solar activity should be considered as a factor in orbital planning.

4.10.5.2 Penetrating Radiation Effects

For films similar to those proposed for this mission, the absorbed dosage which will produce fogging densitites of 0.5 are in the range of about 100 to 300 rads, corresponding to x-ray dosages of 24 and 71 roentgens. Ragent[6] has summarized the expected radiation hazards to photographic film in space missions. With the exception of artifically injected radiation belt electrons,[7] solar flare protons are shown to constitute the greatest potential hazard. The following discussion is extracted in part from Reference 6.

Excellent discussions of the intense proton radiation associated with solar flares and dosage calculations for these events have been given in References 8, 9, and 10, (see Section 4.10.9). Reference 11 contains the most complete compilation and summary of data about solar flares through the middle of 1963. The solar flare of maximum integral intensity recorded through the end of 1961 was the event of 10 May 1959. for which total energy-and-time integrated particle fluxes of more than 10^{10} particles of energy greater than 30 mev were recorded. In all, for the period from 1956 through 1961, about 30 major solar flare events (class 3 or 3+) were recorded. Of these, the statistics relating to the frequency of occurrence of the largest events are very limited. Estimates, as given in Reference 11, suggest that extreme major solar flare events will occur on the average about once every 18 months and that the occurrence of these events is not correlated with the peaks in the 11-year cycle of solar flare activity. In fact, the frequency of potentially dangerous solar cosmic-ray bursts may be greater than once per 18 months during periods of increasing or decreasing solar activity and, in period near maximum or minimum, less than one per 18 months.

From a statistical analysis of the probability of encountering a major solar-flare event in a 10-day trip, Foelsche (Reference 8) obtained a value of somewhat more than 10 percent, assuming four major events per year. The results of another study reported in Reference 8 predict the probability of occurrence of two major events in 10 days as 1.2 percent.

These results, while obviously very unsatisfactory, are high enough to dictate sufficient shielding to protect the film from at least one extreme event per 10-day trip.

Figure 4-43 (taken from Reference 11) gives the proton flux and energy spectrum at the outer edge of the earth's atmosphere as functions of time for the solar flare event of 10 May 1959,

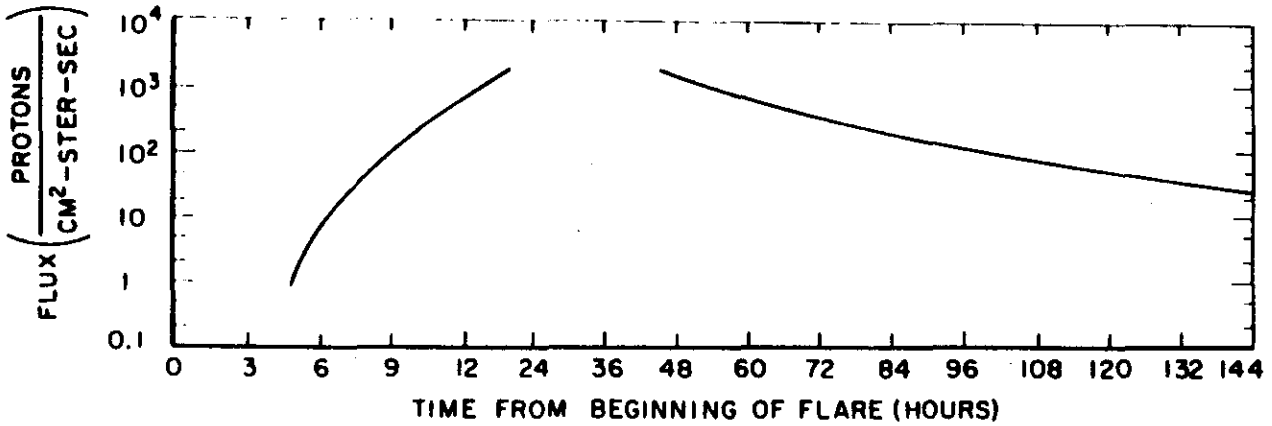

(a) TIME HISTORY

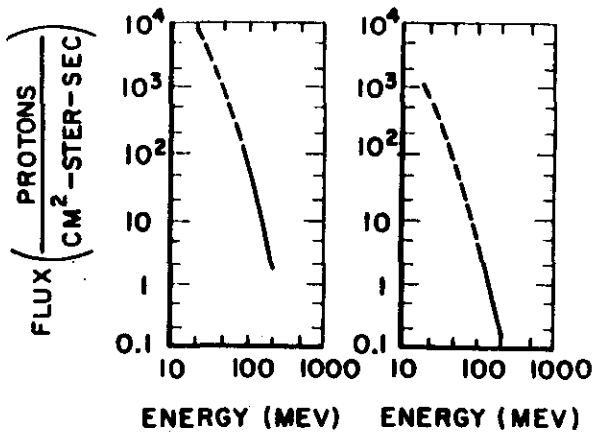

(b) ENERGY SPECTRA OF 0640 UT, MAY 12 (+34 HOURS) AND 2101 UT (+42-2/3 HOURS).

Fig. 4-43 — The May 10, 1959 event, plot of fluxes and spectra for the giant solar flare of May 10, 1959

The energy-integrated fluxes of protons are given as more than 10^{10} particles/square centimeter of protons of energy greater than 30 mev in energy and more than 3×10^{8} particles of energy greater than 100 mev. Using these numbers, McDonald (Reference 11) calculates, for the total event, a skin does of 440 rads for protons with energies greater than 30 mev and 10 rads for protons with energies greater than 100 mev. (These calculations were for tissue; the doses for emulsion will be somewhat less by about 30 to 40 percent.) A shield of 5 grams/square centimeter eliminates all primary protons with energies less than 70 mev so that the dose drops to less than 20 rads.

Wilson (Reference 9) has pointed out practical difficulties in defining the effective dosage rate in an actual geometry. These arise from considerations of self shielding for the sensitive elements. For the above event, he obtained 40 rads per hour, or 400 rads total (see Reference 11) behind a 5-gram/square centimeter aluminum shield for a dosage based on the differential energy loss rate at a point. He found a dosage almost two orders of magnitude lower in a 5-gram/square centimeter aluminum shielded "body phamtom" (52-centimeter diameter sphere of water) evaluated 5 centimeters below the surface of the phantom.

Similarly, Foelsche (Reference 8) has computed upper and lower dosage limits for this event. Behind 5 grams/square centimeter of H_2O for a spherical shield, he obtains doses extending from about 400 to 3000 rps (370 to 2800 rads).

The principal uncertainties in all these calculations involve the duration and energy spectrum as a function of time for the event. The upper limits calculated by the last two authors are probably high by an undetermined factor because of these uncertainties, whereas those calculated in Reference 11 are probably somewhat low. It should also be remembered that this event is the largest ever recorded and that a much more typical major event is that of 12 November 1960, for which Foelsche (Reference 8) calculates dose rates at least an order of magnitude lower than the previously mentioned figures. In addition, Reference 11 notes that the proton energy spectrum and time history may vary substantially from event to event, making predictions of required shielding uncertain. Thus, for example, Foelsche (Reference 8) has calculated that doubling shielding from 5 to 10 grams square centimeter for the high-energy event of 26 February 1956 would reduce the dose received by a factor of about only two while the weight of the shield increases by a factor of about six for typical film package dimensions.

Webber (Reference 10) has also considered the cumulative probability dose from solar flare protons for solar cycle 19. His analysis is somewhat phenomenological, but is based upon almost all of the available data on solar flare activity. His results are shown in Figure 4-44. Predictions of sunspot and solar flare activity through 1974 are shown in Figure 4-45 (also from Reference 10).

Based upon the above considerations and the maximum allowable film absorbed dosages, a minimum film shielding thickness of about 5 grams/square centimeter of a low atomic number element such as beryllium should be considered for the film supply casette as a minimum.

It does not appear that there are any practical orbital considerations which would appreciably influence the above result except a preflight decision to postpone the mission based upon a prediction of solar flare activity. This possibility is discussed in Section 4.10.5.4.

4.10.5.3 Atmospheric Density Fluctuations

The role of the sun in producing significant effects in atmospheric density has been discussed in other sections of this report. For most purposes these effects are, in general, regular enough

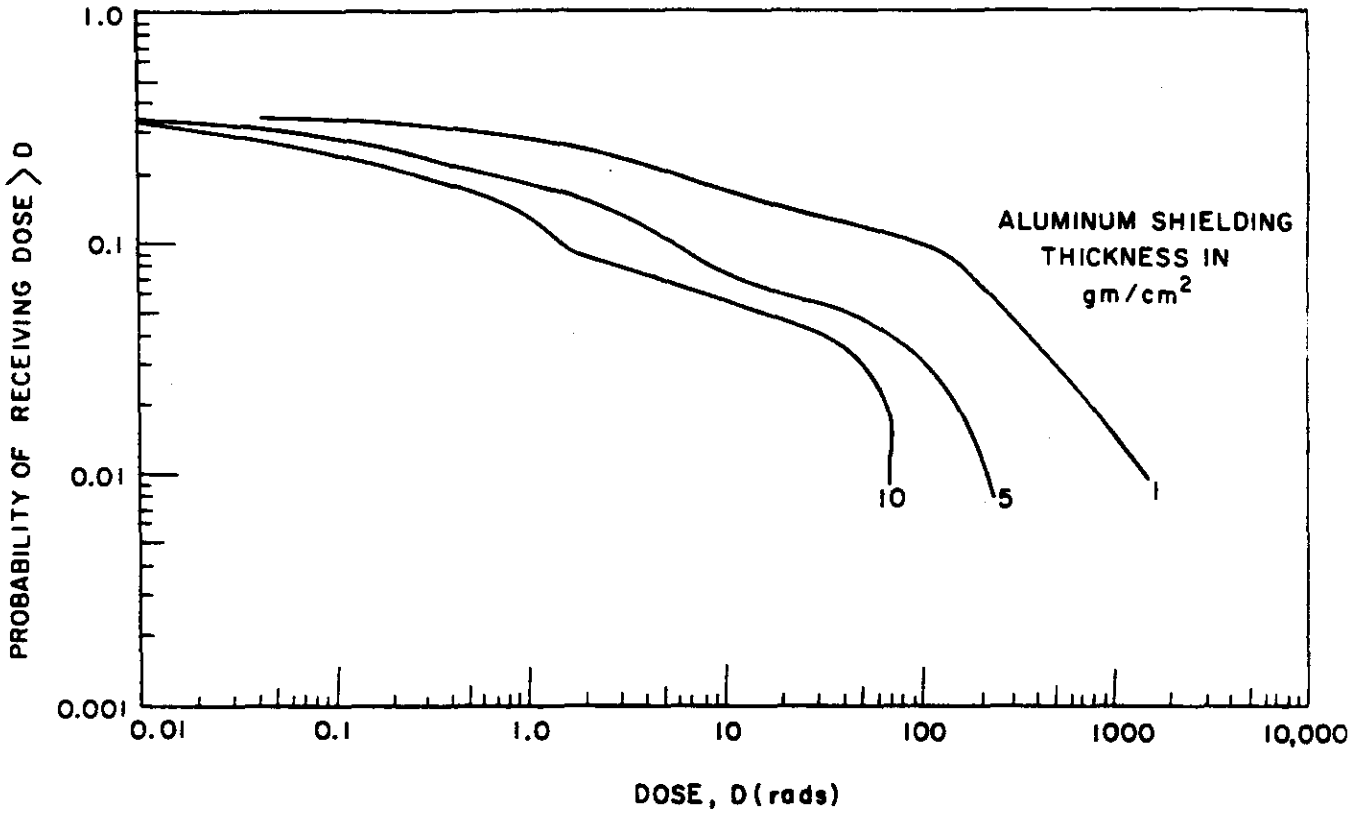

Fig. 4-44 — Cumulative probability-dose curves for 30-day mission.

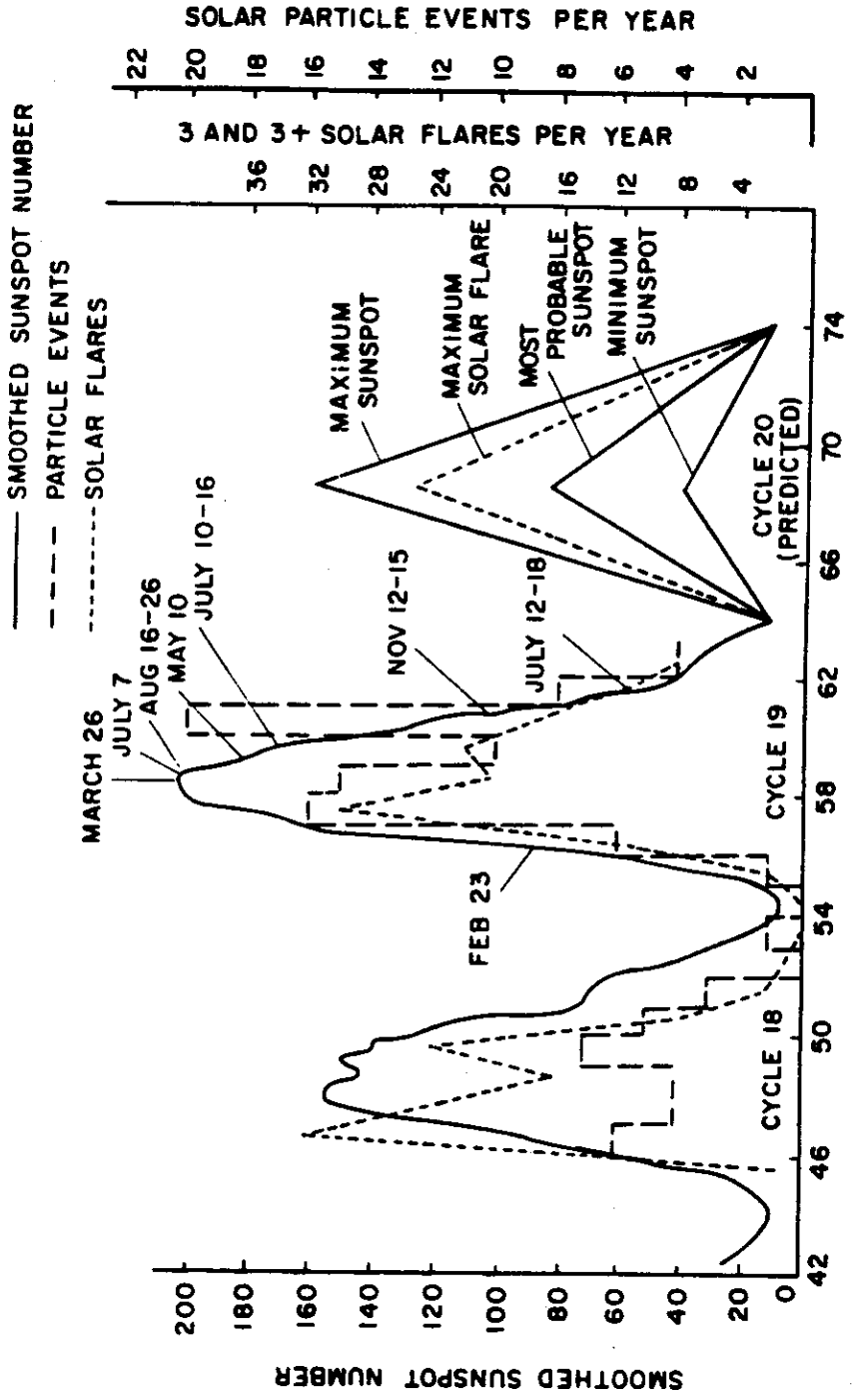

Fig. 4-45 — Solar activity

that they can be treated as predictable and characterized by parameters in an atmospheric density model which can then be used to predict drag forces acting on an orbiting vehicle. If sufficient observational data are available, and the atmospheric model is flexible enough, i.e., has enough adjustable time-dependent parameters, it has been shown to bepossible to achieve low orbital residuals for 500-mile elevation satellites (Reference 12). At the lower altitudes such as those being considered for this mission, the drag forces are much greater and must, hence, be more carefully considered. It is felt that if sufficient observations are available, it will be possible to take drag effects into account.

If, however, observational data are insufficient over part of the mission, or it is desired to predict ahead the future position of the vehicle for as much as 6 hours, then it becomes necessary to consider carefully possible rapid fluctuations in the drag forces. The principal sources of such fluctuations are solar flares and sunspot activity.

It is estimated that density fluctuations of 2 to 5 percent from the values used at the beginning of the prediction period will produce an in-track error of about 200 feet in 6 hours at 160-mile altitudes for a circular orbit. Fluctuations of this magnitude are known to exist during a 6-hour period. The rapid fluctuations of atmospheric density are not well understood in detail. Magnetic storms are known to influence the density, probably as a result of the absorption of hydromagnetic wave energy, resulting in larger effects at the poles. Energetic charged particles (e.g., from the solar flares) also probably heat the polar regions.

It is thus again desirable, from a mission planning viewpoint, to avoid, if possible, periods of enhanced solar activity. It is, of course, also desirable to have on-board accelerometers to measure any fluctuations which may occur. The prediction of solar activity is discussed in the next section.

4.10.5.4 Prediction of Solar Activity

Webber (Reference 10) has discussed the considerations involved in prediction of solar activity tending to produce solar cosmic-ray events as well as solar activity itself. He divides the desired advance warning periods into (1) a few hours, (2) a few weeks, and (3) months to years. Summarizing, Webber's conclusions follow.

Few hours. By correlating integrated 3-centimeter microwave emission from the sun with cosmic-ray activity, the integrated cosmic-ray intensity may be predicted within a factor of three. The source flare which emits the microwave radiation precedes the cosmic rays by several hours so that this amount of time may be available.

Few weeks or less. By considering the rate of development of active centers on the sun (most of which take about two solar rotations or 54 days) and selection criteria based on east-west asymmetries, it is possible to decrease the probability of encounter by a factor of five for intervals of 1- to 2-weeks duration at the expense of reducing the available launch time by about 50 percent. These predictions can be made up to 30 days in advance, using as criteria development time, location, and size of flare-producing active centers.

Months to Years. Based on phenomenological correlations and extrapolations, we may expect five to six solar cosmic-ray events per year in 1967 and 1968. The hazard during the forthcoming sunspot maximum in the 11-year cycle 20 "appears to be substantially reduced from the hazard during the previous maximum," (cycle 19). Webber's long-term predictions are shown in Figure 4-45.

4.10.6 Specific Orbit Plans

4.10.6.1 Introductory Remarks

Three orbital plans will now be presented for illustrative purposes. The plans as presently conceived have three elements: (1) orbital plan objective, (2) sequence of operations, and (3) technical data. The third element can be quite lengthy since it could contain a complete mission trajectory calculation using the TRACE program. Also, complete sighting runs for the trajectory could be given together with the camera off-on times as well as with other supplementary information.

4.10.6.2 Orbital Plan Number 1

4.10.6.2.1 Orbital Plan Objective

The particular objective of this plan is to provide photographic coverage of the northern polar regions during the summer solstice, the only time when illumination conditions permit such coverage. A secondary objective is to provide general photographic coverage of those latitudes for which the illumination is adequate. To achieve these objectives, the satellite will be launched southerly near noon into a slightly retrograde orbit from Vandenberg. Total coverage of the earth's surface at least once between the latitudes of +90 degrees north(North Pole) and -47.5-degree south will be obtained in 15 days. Recovery will be made in the Hawaiian recovery area (on successive days for the case of multiple capsule recovery).

4.10.6.2.2 Sequence of Operations

1. Launch (n = 0.5)

The satellite is to be launched from Vandenberg in order to achieve the following nominal orbital elements at the equator:

Date—22 May to 21 July 1967
Longitude—120 ± 1-degree W
Time—local noon ± one-half hour
Nominal altitude—160 nautical miles
Nominal flight path angle— zero
Orbital inclination—95 ± 1-degree retrograde
Nominal velocity—25,354 feet per second
Orbital nodal period—90.37864 minutes ± 0.8 second
Launch direction—south

The revolution number (n) is taken as 0.5 at the above condition so that n = 1.25, 2.25, 3.25,... indicates satellite positions near the North Pole and n = 1.75, 2.75, 3.75, ... indicates satellite position near the South Pole.

2. Preliminary Adjustments (n = 0.5 to n = 19)

For the first twenty revolutions, the following operations are to be carried out before commencing photographic operation:

a. Agena outgassing and fuel dumping
b. Camera thermal soaking $0 < n < 19.69$
c. Optical axis calibration $19.69 < n < 20.19$

While the Agena is outgassing, the camera can be developing its equilibrium thermal cycle. It is important to subject the camera to the same thermal loads during the preliminary period as during the photographic period although it is not necessary to expose the film continuously. Therefore, the objective should be subjected to the same thermal loading during the first 20 revolutions as during normal photographic conditions.

Before the 20th revolution, the following operations should be performed. Leaving the light side of the earth (n = 19.69) at -66.5 degrees south latitude, the Agena should be rolled about 120 degrees, and one stellar camera and the ground camera should take simultaneous pictures. The Agena should be rolled another 120 degrees, and the other stellar camera and the ground camera should take simultaneous stellar pictures. The Agena should then be rolled to its equilibrium position. When the Agena is nearing the light side of the earth (n = 20.19) near 66.5 degrees north latitude, the same optical axis calibration procedure should be performed.

3. Orbit Adjust $15 \leq n \leq 20$

After sufficient time has elapsed to obtain an accurate determination of orbital period, an orbital adjustment should be made to correct the orbital nodal period to within ± 0.8 second of its specified value. This adjustment should be made after the outgassing has proceeded far enough that its effect on orbital period is known within the specified accuracy. The adjustment would take place between n = 15 and n = 20.

4. Photographic Operation $20.24 \leq n \leq 20.63$, $2124 \leq n \leq 21.63$, etc.

The photographic operation is conducted for the next 235 orbits between (n + 0.24) and (n + 0.63) since the sun angle will equal or exceed 19 degrees above the horizon during these periods. If the sun angle equals or exceeds 19 degrees and the camera is over land, pictures are taken. The precise photographic coverage at the equator is best described by means of a figure. In Figure 4-46, the equatorial swaths are plotted for a series of adjacent swaths 16 revolutions apart, starting at n = 20.5. It is noted that 15 days later the swath width for n = 243.5 closes on that for n = 20.5. However, the overlap is very small and does not continue all the way around the earth. The actual overlaps between the adjacent swath pairs 15 days apart starting at the 20.5/243.5 pair are shown in Table 4-12. It is seen that to obtain absolute overlap on the equator, we must operate the cameras up to n = 274.5. However, such operation is considered unnecessary since there will only be small areas near the equator which are not seen. Accordingly, we will perform the camera thermal calibration and initiate recovery the next time the camera is in position.

5. Final Camera Calibration

The final camera calibration will be made about two orbits before the initiation of the recovery sequence for the first capsule. It is necessary to know when the satellite is in position for the recovery of the first capsule (in the case of multiple capsules) to know when to start the optical axis calibration. Figure 4-47 shows the equatorial crossings preceding which the satellite will be in the proper position to initiate a recovery operation. It is planned that the recovery of the first capsule will take place on the 257th revolution. Camera calibration is to be started at n = 255.63 as the satellite goes into the dark two orbits before recovery. This will permit a second calibration between 256.69 and 257.19 to obtain two sets of data for the final optical axis calibration. The calibration is to be conducted in exactly the same manner as the preliminary calibration.

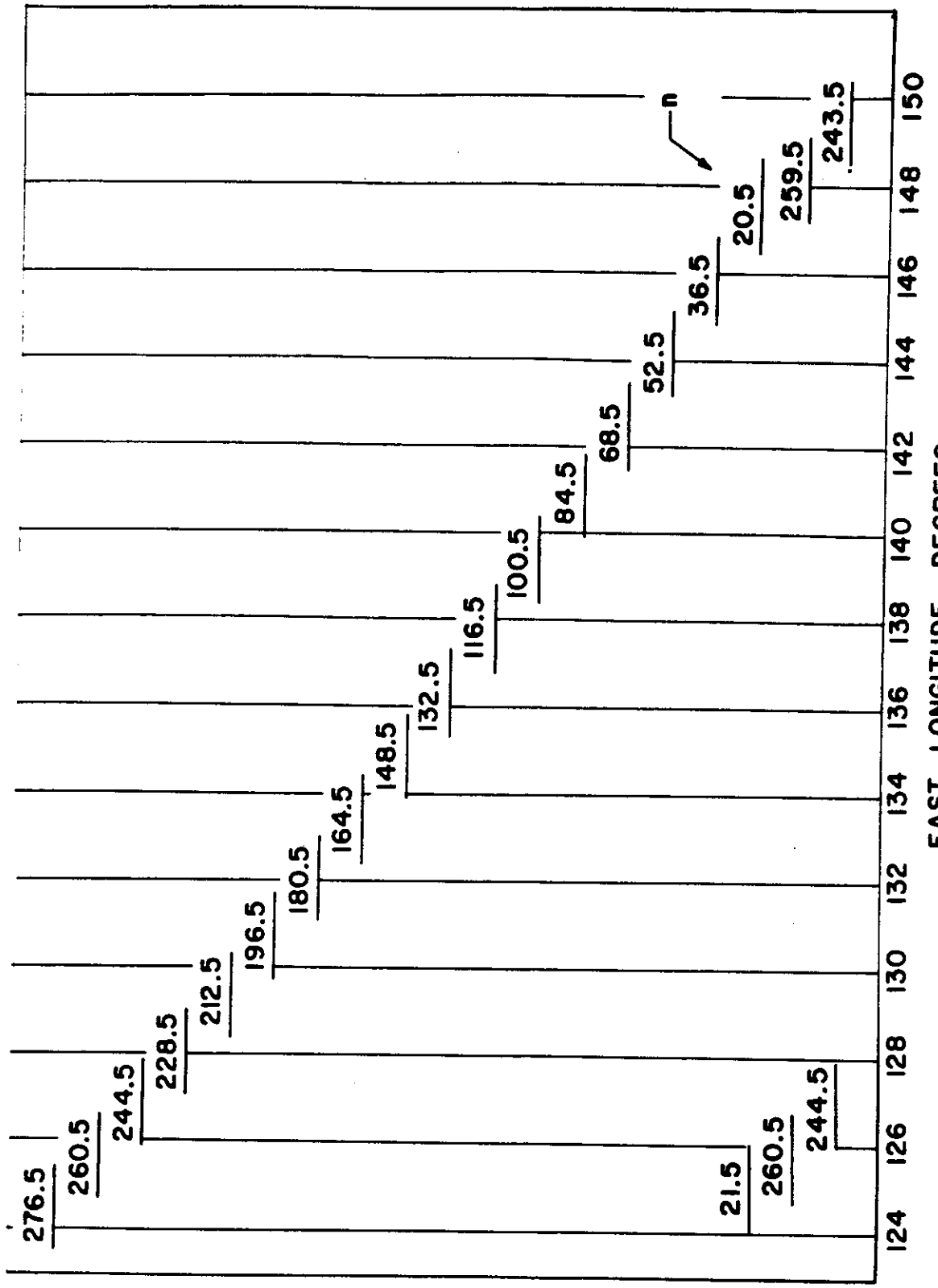

Fig. 4-46 — Equatorial photographic coverage for orbit plan number 1 starting at n = 20.5

Table 4-12 — Overlap Between Various Swath Paths Near Completion of Mission, Orbit Plan Number 1

Swath	Overlap, nautical miles	Swath	Overlap, nautical miles
20.5/243.5	6.48	20.5/259.5	79.02
21.5/244.5	4.68	21.5/260.5	77.04
22.5/245.5	2.88	22.5/261.5	75.06
23.5/246.5	1.02	23.5/262.5	73.08
24.5/247.5	-0.84	24.5/263.5	71.10
25.5/248.5	-2.82	25.5/264.5	69.12
26.5/249.5	-4.50	26.5/265.5	67.14
27.5/250.5	-6.48	27.5/266.5	65.04
28.5/251.5	-8.34	28.5/267.5	62.94
29.5/252.5	-10.26	29.5/268.5	60.96
30.5/253.5	-12.12	30.5/269.5	58.92
		31.5/270.5	56.94
		32.5/271.5	54.96
		33.5/272.5	52.98
		34.5/273.5	50.88
		35.5/274.5	48.84

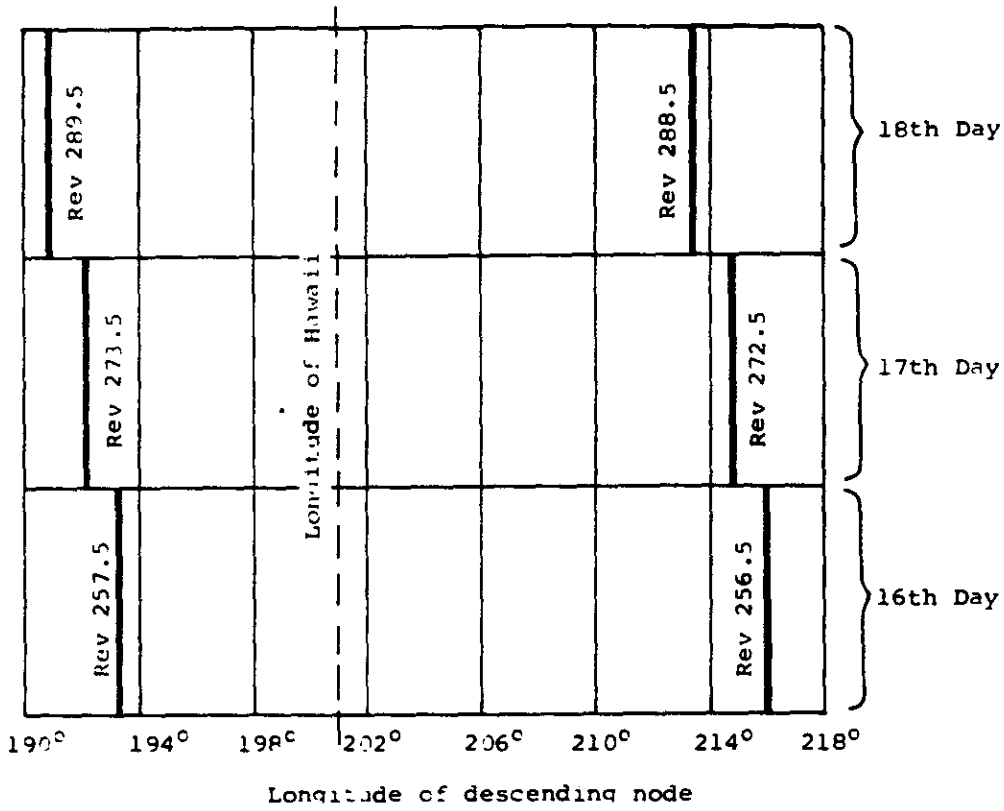

Fig. 4-47 — Equatorial crossing preceding which the satellite is in position for capsule recovery

6. Recovery Operation

The recoveries are to be accomplished during southward movement of the satellite in the area of Hawaii on successive days forthe case of multiple capsules. In this plan, the precise sequence of recovery operations will not be described except that satellite times and positions in the neighborhood of Hawaii favorable for the start of the recovery sequence will be given. In this regard, reference is made to Figure 4-48 which is a chart of the neighborhood of the SCF station in Hawaii. Time zones measured west of Greenwich are shown. Local time is Greenwich time minus the time zone number in hours. Special deviations of the time-zone boundaries are not considered.

In the figure, the satellite ground traces are shown for three successive days and two orbits per day which are suitable for recovery. We might desire to recover on the 256th revolution, but the 257th revolution is preferable because of its proximity to Honolulu. It is therefore planned to recover the first capsule on the 257th revolution and if necessary the second capsule on the 273rd revolution.

Some explanation of the local satellite times is helpful. The satellite was originally launched into an orbit which crosses the Vandenburg meridian approximately at noon. Fifteen days later, the sun has moved 15 degrees to the east, and the local time would be earlier if the orbital plane had remained fixed. The orbital plane for a retrograde orbit with i = 95 degrees precesses 11 degrees east in 15 days so that the sun has moved east 4 degrees with respect to the orbital plane. This reduces the local time by 16 minutes. Revolution 255 passes to the west of Vandenburg at about 11:45 a.m. local Vendenburg time in time zone 8. In the next pass, revolution 256, the satellite passes to the east of Hawaii at about 1:15 p.m. Vandenburg time. However, in time zone 9, the local time is about 12:15 p.m. as shown in Figure 4-48. One revolution later at n = 257.44, the satellite has moved from time zone 9 to time zone 11, thereby gaining two hours. Since a revolution requires close to 90 minutes, local time for n = 257.44 is one-half hour earlier than for n = 256.44.

The only information really required for the recovery operation from the orbital plan is the orbit number for recovery and the approximate longitude at which the satellite will cross the chosen recovery latitude. From operational experience, the distance from retrorocket firing to air snatch will be known. The time for the satellite to appear at the position for retrorocket firing will then be specified. A final correction to the satellite time can be made as it is acquired by the last SCF tracking station at [redacted]

It is suggested that the first capsule be recovered at about n = 257.44 (see Figure 4-48), with retrorocket firing a short time prior to 11 hours, 45 minutes, 0 seconds local time and if necessary that the second capsule be recovered on the n = 289.44 orbit with retrorocket firing slightly before 11 hours, 52 minutes, 30 seconds local time in the eleventh time zone west of Greenwich.

4.10.6.2.3 Technical Data

The following technical data for this orbit plan have been used throughout the report for illustrative purposes.

1. Camera duty cycle—duty cycle, 13 percent; lineal coverage per revolution, 2810 nautical miles; additional data to be found in Section 4.10.2.2.2.

2. Frequency of acquisition by Satellite Control Facility (Table 4-11).

3. Frequency of acquisition by TRANSIT network (Table 4-10).

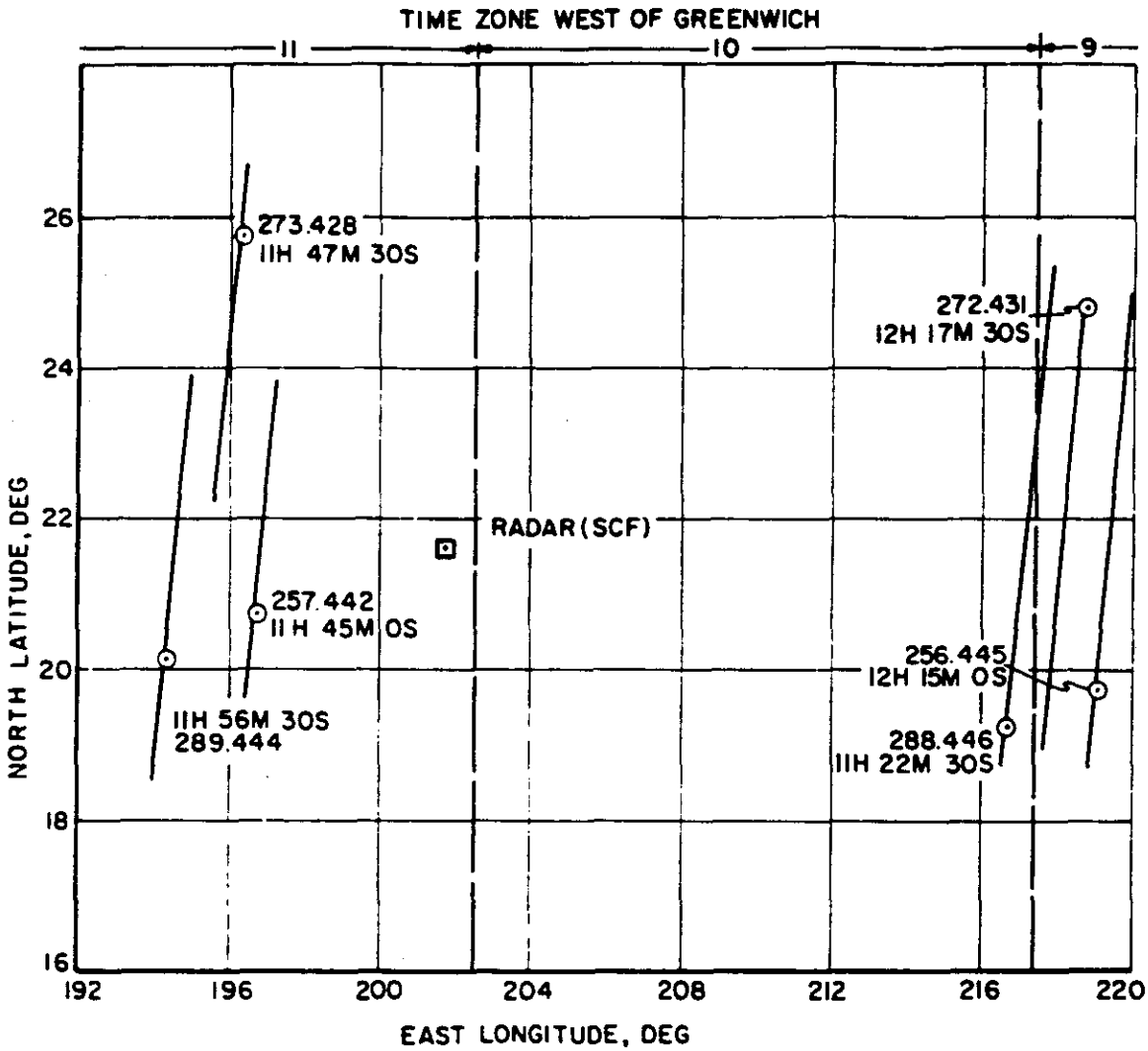

Fig. 4-48 — Satellite positions and local times in the neighborhood of Hawaii

4. Frequency distribution of dead time of Satellite Control Facility for two separate days (Figure 4-42).

5. Frequency distribution of dead time of the TRANSIT network for two separate days (Figure 4-41).

6. Equatorial photographic coverage for orbit plane number 1 starting at n = 20.5 (Figure 4-46).

7. Equatorial crossing preceding which the satellite is in position for capsule recovery (Figure 4-47).

8. Satellite positions and local times in neighborhood of Hawaii (Figure 4-48).

9. A complete trajectory calculation is available for orbit number 1 with printouts every $2\frac{1}{2}$ minutes.

10. A complete sighting run is available for orbit number 1 listing the times when the satellite is acquired by the SCF and TRANSIT network stations.

11. Q points—Figure 4-49 illustrates 16 Q points in the neighborhood of the north pole. The orbital paths are tangent to the 85-degree parallel as shown. The Q points for which the orbital paths cross at right anlges lie along the 82.9-degree parallel. The orbital trace for n = 21 is intersected at right angles four revolutions later by the orbital trace for n = 25 to form Q point Q_1. New Q points are generated each successive orbit thereafter. The figure shows 16 Q points in 360 degrees. Because of overlap requirements and of regression of the orbital plane, the Q points will not be exactly $22\frac{1}{2}$ degrees apart.

Film Weight

It is possible to obtain a good estimate of the amount of film required for a given mission if no attempts are made to reduce film weight by avoiding redundancy at the high latitudes. The number of frames per orbit is simply

$$\text{frames/orbit} = \frac{21{,}600\ (d)}{(1 - x)\ \ell}$$

where d = camera duty cycle

21,600 = number of nautical miles of ground trace per orbit

x = overlap along direction of flight (0.67)

ℓ = length of ground trace per frame, $\ell = h\ \frac{46}{30}$

h = mean altitude of satellite

This numerical value yields

$$\text{frames/orbit} = 42{,}700\ \frac{d}{h}$$

The nominal film weight is 224 pounds per bucket which contains 7100 frames. Accordingly, the film weight per mission is

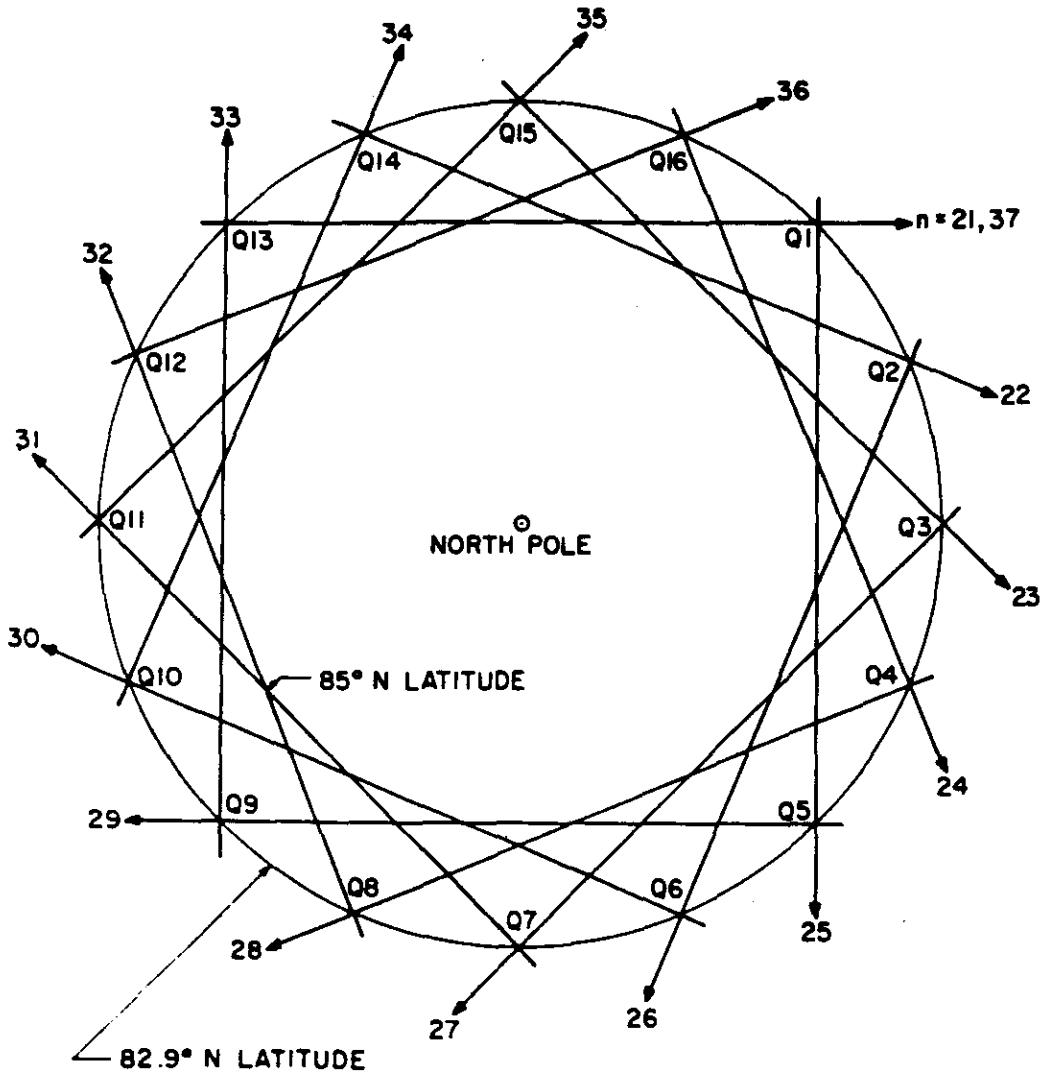

Fig. 4-49 — Q points for orbit plan number 1

$$\text{film weight (pounds)} = \frac{224\ N \cdot (42,700)}{7100} \frac{d}{h}$$

$$= 1350\ N \frac{d}{h}$$

where N = number of photographic orbits

For the present orbit plan,

N = 254 orbits

d = 0.13

h = 160 nautical miles

frames/orbit = 34.7

film weight = 279 pounds

4.10.6.3 Orbit Plan Number 2

4.10.6.3.1 Orbit Plan Objectives

This orbit is designed to take advantage of orbital inclination to give greater redundancy to the coverage of the northern temperate zone and to eliminate the highly redundant coverage of the poles. It also provides data for inclined orbits necessary to evaluate the geopotential model of the earth and may provide the capability for stronger east-west photogrammetric and orbit distance ties.

4.10.6.3.2 Sequence of Operations

1. Launch (n = 0.5)

The satellite is to be launched from Vandenburg in order to achieve the following nominal orbital elements at the equator.

Date—22 May to 21 July 1967 (We will use the date 18 June 1967 for illustrative purposes.)

Longitude—120 ± 1 degree West

Time—Local noon ± ½ hour

Nominal altitude—184.57 nautical miles

Flight-path angle—zero

Orbital inclination—115 degrees (25-degree retrograde)

Nominal Velocity—25268.15 foot/second

Orbital nodal period—91.24458 minutes. It is assumed that this value can be achieved within 0.8 second.

Launch direction—south and west

2. Preliminary Adjustments (0.5 < n < 19)

This operation is the same as for orbit plan number 1.

3. Orbit Adjust ($15 \leq n \leq 20$)

This operation is the same as for orbit plan number 1.

4. Photographic Operations ($20.245 < n < 178.652$)

This operation will be somewhat different from the first orbital plan because complete coverage will be achieved in fewer days. With reference to Figure 4-50, it is seen that the n = 163.5 revolution closes on the first photographic revolution (n = 20.5). Also n = 164.5 closes on n = 21.5. In this orbit plan, unlike orbit plan number 1, closure is maintained all the way around. This closure is shown in Table 4-13 where the overlap between n = 20.5 and n = 163.5 is seen to be about 25 nautical miles. For an altitude of 180 miles, this overlap amounts to 18 percent of the swath width. For the final overlap between n = 35.5 and n = 178.5, the overlap is 13.02 miles and corresponds to about 9 percent of the swath width. The program shows that coverage is complete at n = 178.652 with a sun elevation of 19 degrees at 48-degree south latitude and 134.6-degree east longitude.

Complete coverage for this orbit plan has taken 158 revolutions compared to 254 revolutions for orbit plan number 1. This reduction has been achieved by the wider swaths which resulted from inclining the orbit and from the higher satellite altitudes accompanying retrograde orbits. Also, closure for every swath pair of Table 4-13 has saved a day compared with the partial closure shown in Table 4-12 for orbit plan number 1.

5. Final Camera Calibration

This calibration is to be performed in the same manner as in orbit plan number 1. The only question concerns the orbit number on which recovery is to be accomplished so that the calibration can be made two orbits before. The initial capsule will be recovered on the n = 193 revolution so that calibration can be accomplished on the n = 191 or n = 192 revolution.

6. Recovery Operation n = 193.4, n = 209.4

Ground traces of the satellite in the neighborhood of the Hawaiian recovery area suitable for the recovery are shown in Figure 4-51. It was noted that the photography was completed at

Table 4-13 — Overlap Between Various Swath Pairs Near Completion of Mission Orbit Plan Number 2

Swath	Overlap, nautical miles	Swath	Overlap, nautical miles
20.5/163.5	25.44	28.5/171.5	19.08
21.5/164.5	24.60	29.5/172.5	18.12
22.5/165.5	23.94	30.5/173.5	17.34
23.5/166.5	23.10	31.5/174.5	16.56
24.5/167.5	22.32	32.5/175.5	15.66
25.5/168.5	21.54	33.5/176.5	14.76
26.5/169.5	20.70	34.5/177.5	13.86
27.5/170.5	19.86	35.5/178.5	13.02
		36.5/179.5	12.30

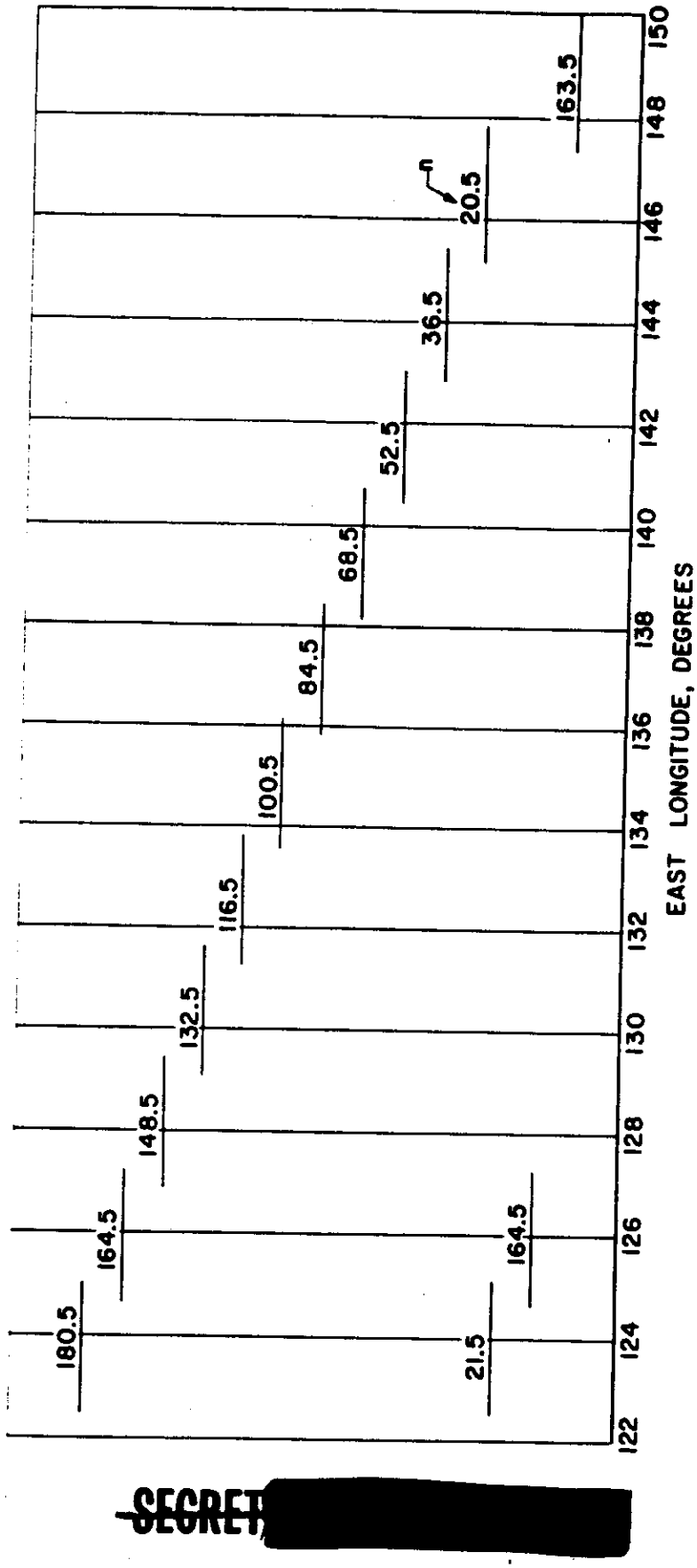

Fig. 4-50 — Equatorial photographic coverage for orbit plan number 2 starting at n = 20.5

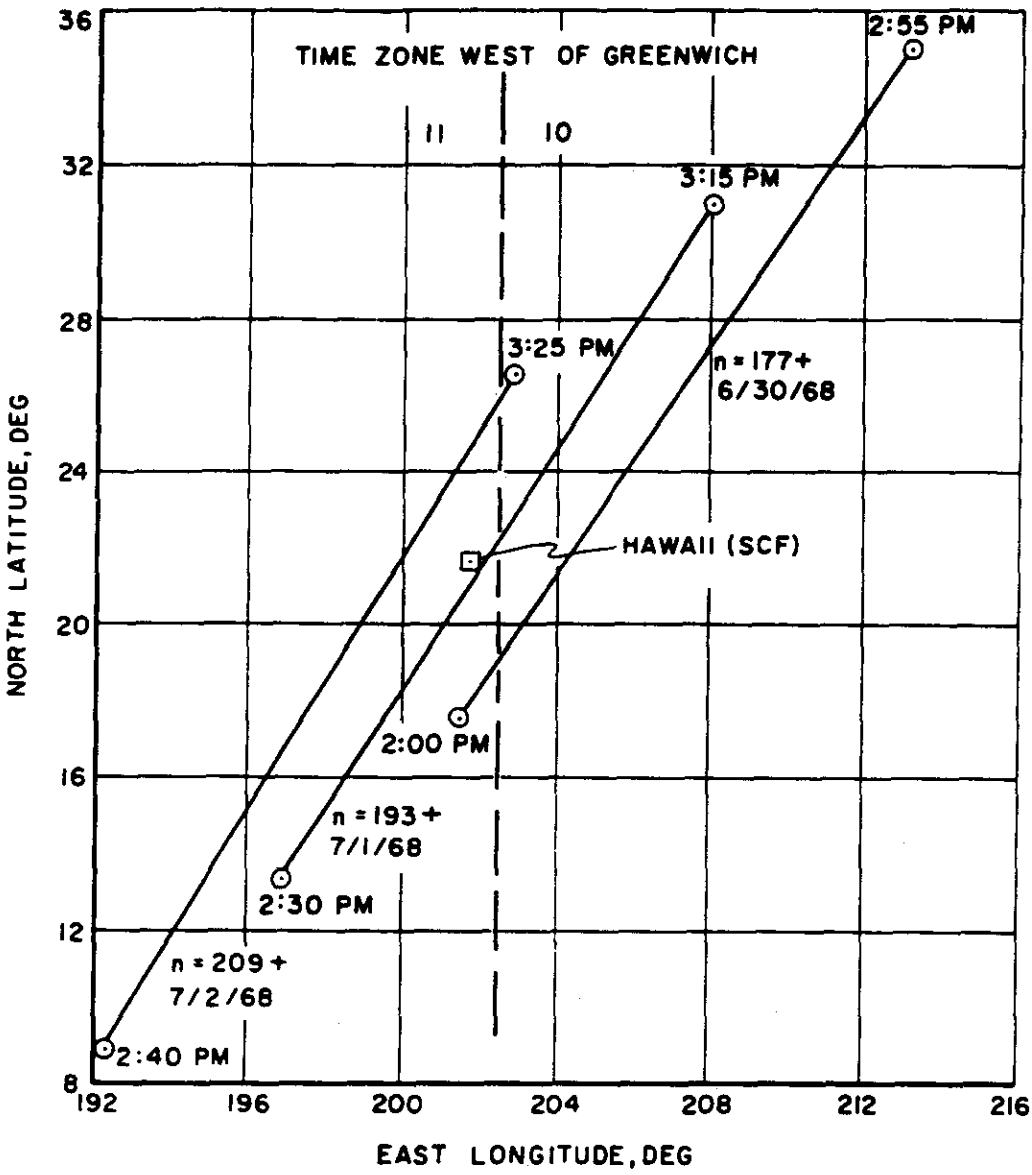

Fig. 4-51 — Ground traces of orbits suitable for recovery operations, orbital plan number 2

n = 178.65. We could recover on the n = 177 orbit and miss just one swath. (Alternately, we might start photography about two orbits sooner if the camera thermal condition and the Agena outgassing permit.)

In this case, in order to obtain complete coverage, recovery of the first capsule will be made on the n = 193 revolution and, if necessary, of the second on the n = 209 revolution. Both of these ground traces pass within about 2 degrees of longitude of the SCF station at Hawaii.

It is noted that the local times are between 2 and 3 p.m., even though we launched into a local noon orbit at n = 0.5. In 209 revolutions, the line of nodes has precessed about 46.6 degrees eastward while the sun moves only 13 degrees eastward. The orbital plane has thus moved 33.6 degrees eastward or about 2 hours and 15 minutes. In a refinement of this orbital plan, it would probably be desirable to launch about 1 hour and 12 minutes before noon to improve illumination conditions at the extreme latitudes during the last half of the mission.

4.10.6.3.3 Technical Data

1. Camera Duty Cycle

The trajectory was sampled every 5 minutes during the first and fifth days to see whether the camera was over land or sea and whether the illumination was adequate for photography; Table 4-14 summarizes the results. The cameraduty cycle of 16 percent on the first day is significantly greater than the 13 percent duty cycle for orbit plan number 1. However, the lower duty cycle for the fifth day is noteworthy. About half the reduction in the duty cycle is due to illumination and half to an increase in sea to land area.

2. Frequency of Acquisition by Satellite Control Facility

Table 4-15 shows several stations, because of their extreme latitudes do not acquire the satellite at all. The frequencies of acquisition for both the SCF and TRANSIT networks follow closely the theoretical variation as shown in Figure 4-52. This theoretical variation is given by

$$R = \frac{\sqrt{1 - \cos^2 i}}{\sqrt{\cos^2 \lambda - \cos^2 i}}$$

where R = frequency of acquisition normalized to unity at equator
i = orbital inclination
λ = latitude

The theory if $\lambda = i$ since R becomes infinite.

3. Frequency of Acquisition by TRANSIT Network

(See Table 4-16 and Figure 4-53.)

4. Distribution of Dead Time of Satellite Control Facility for Two Separate Days

Figure 4-54 shows this distribution and is to be compared with Figure 4-42 for the first orbital plan. It is noted that the dead time is greater than 2 hours, 10 to 20 percent of the time for orbit plan number 2 with 9 percent for orbit plan number 1.

Table 4-14 — Camera Duty Cycle, Statistical Analysis, Orbit Plan Number 2

	First Day		Fifth Day	
	Times	Percent	Times	Percent
In dark	176	61	180	62.5
Over land	46	16	38	13.2
Over sea	66	23	70	24.3
	288	100	288	100.0

Table 4-15 — Frequency of Acquisition by Satellite Control Facility, Orbit Plan Number 2

Day \ Station	RA	RB	RC	RD	RE	RF	RG	Total
June								
18	1	1	0	0	0	0	1	3
19	2	3	6	2	0	3	2	18
20	3	3	6	2	0	2	2	18
21	2	2	7	2	0	2	3	18
22	1	3	6	4	0	2	2	18
23	2	3	6	4	0	2	2	19
24	2	3	7	4	0	2	3	21
25	3	2	7	4	0	2	2	20
26	2	2	7	4	0	2	2	19
27	2	3	6	3	0	3	2	19
28	2	3	6	2	0	2	2	17
29	3	3	6	2	0	3	2	19
30	3	3	6	2	0	2	2	18
July								
1	2	3	6	2	0	2	3	18
2	2	2	6	4	0	2	2	18
Total	32	39	88	41	0	31	32	263

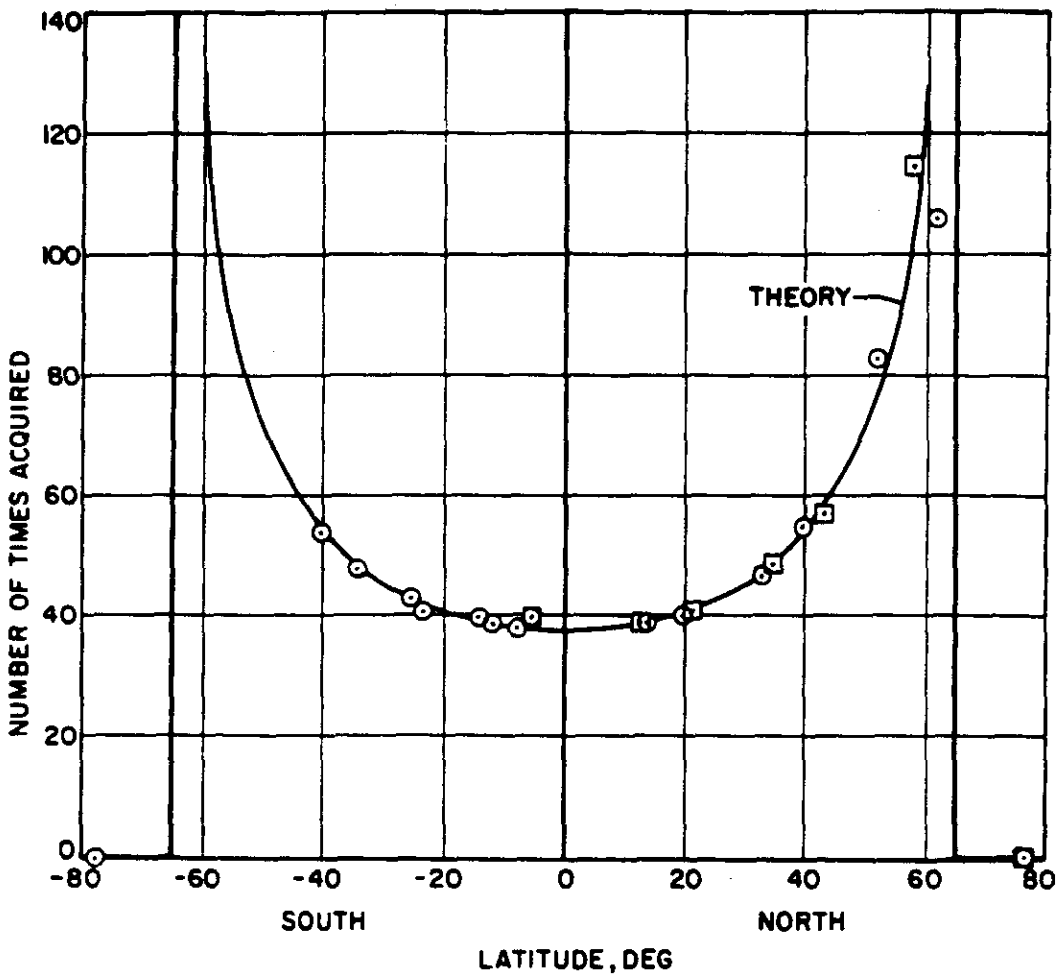

Fig. 4-52 — Frequency of acquisition as a function of latitude, orbit plan number 2

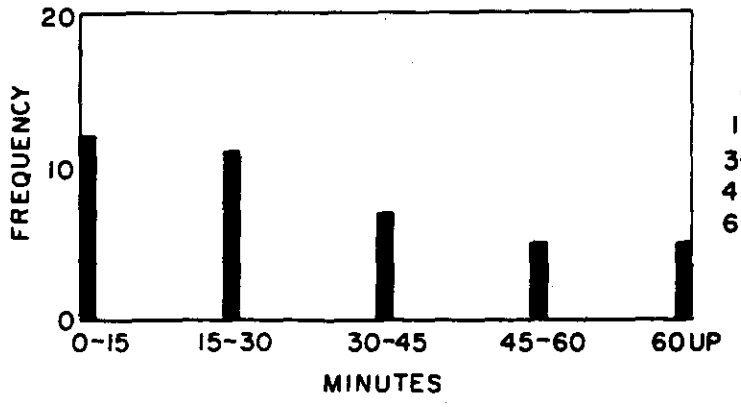

	NO. OF POINTS	%
0 – 15	12	30
15 – 30	11	27.5
30 – 45	7	17.5
45 – 60	5	12.5
60 UP	5	12.5
	40	100%

(a) FIRST DAY

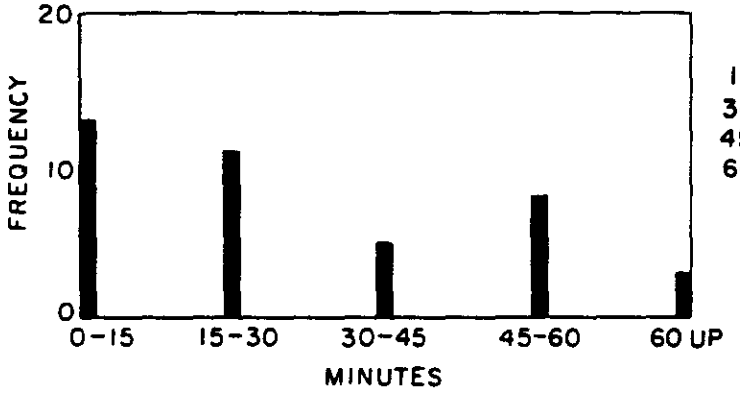

0 – 15	13	32.5
15 – 30	11	27.5
30 – 45	5	12.5
45 – 60	8	20
60 UP	3	7.5
	40	100%

(b) FIFTH DAY

Fig. 4-53 — Frequency distribution of "dead time" of the TRANSIT network for two separate days, orbit plan number 2

Table 4-16 — Frequency of Acquisition by TRANSIT Network, Orbit Plan Number 2

Day	Station	XA	XB	XC	XD	XE	XF	XG	XH	XI	XJ	XK	XL	XM	XN	XO	XP	Total
June																		
18		0	0	2	0	1	0	0	0	0	1	0	2	1	0	0	0	7
19		2	2	5	2	3	3	3	4	6	2	0	3	2	0	2	2	41
20		2	2	5	2	2	2	3	4	6	2	0	3	2	0	2	2	39
21		3	2	4	2	2	2	3	4	6	2	0	3	3	0	3	2	41
22		3	3	4	3	1	2	3	3	6	3	0	1	2	0	1	2	37
23		3	3	5	2	3	2	3	2	6	3	0	2	2	0	3	2	41
24		4	4	5	3	3	2	3	2	5	3	0	1	3	0	3	4	45
25		4	3	4	3	2	2	2	2	6	2	0	2	2	0	2	2	38
26		3	3	4	2	1	3	2	2	6	1	0	2	2	0	2	2	35
27		3	2	4	2	2	2	2	3	6	2	0	2	2	0	2	2	36
28		3	2	3	2	2	2	3	4	6	2	0	3	2	0	2	2	38
29		2	2	5	2	3	3	3	4	6	2	0	2	2	0	2	2	40
30		2	2	5	2	2	2	3	4	6	2	0	4	2	0	2	2	40
July																		
1		3	2	5	2	2	2	2	4	6	2	0	3	3	0	2	2	40
2		3	2	4	2	2	2	3	4	6	2	0	2	2	0	2	2	38
Total		40	34	64	31	31	31	38	46	83	31	0	35	32	0	30	30	556

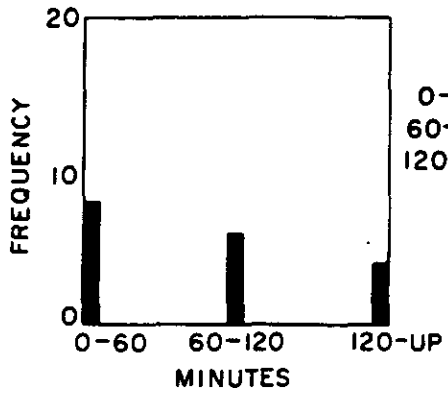

	NO. OF POINTS	%
0-60	8	44.4
60-120	6	33.3
120-UP	4	20.3
	18	100%

(a) FIRST DAY

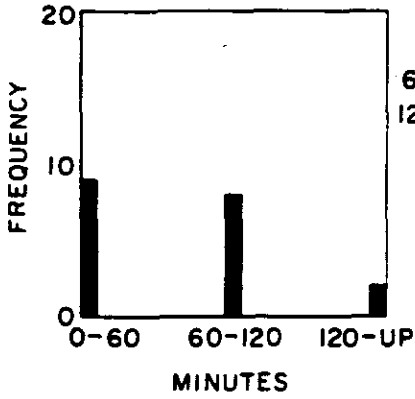

0-60	9	47.4
60-120	8	42.1
120-UP	2	10.5
	19	100%

(b) FIFTH DAY

Fig. 4-54 — Frequency distribution of "dead time" of Satellite Control Facility for two separate days, orbit plan number 2

5. Distribution of Dead Time for TRANSIT Network on Two Separate Days

Figure 4-53 shows the distribution and is comparable with Figure 4-41 for the first orbital plan. It is noted that the dead time is now greater than an hour, 7.5 to 12.5 percent of the time compared to 2 percent for orbit plan number 1.

6. Equatorial Photographic Coverage for Orbit Plan Number 2 Starting at n = 20.5

(See Figure 4-50.)

7. Ground Traces of Orbits Suitable for Recovery Operations

(See Figure 4-51.)

8. Trajectory Program

A complete trajectory program is available for orbit number 2 with printouts every 5 minutes.

9. Sighting Run

A complete sighting run is available for orbit number 1, listing the times when the satellite is acquired by the SCF and TRANSIT networks.

10. Film Weight

Using the following inputs:

N = 158 revolutions

h = 184 nautical miles

d = 0.16

it is found that

frames/orbit = 37.1

film weight = 185 pounds

4.10.6.4 Orbit Plan Number 3

4.10.6.4.1 Orbit Plan Objective

This orbit is designed to operate in between the 150- and 300-nautical mile levels to gain some of the advantages of higher altitude on coverage without taxing the launch capability. This turns out to be feasible using side-by-side swaths two days apart.

4.10.6.4.2 Sequence of Operations

1. Launch (n = 0.5)

The following quantities are assumed for equatorial launch:

Date—18 June 1968
Longitude—120 ± 1-degree West
Time—local noon
Nominal altitude—234.14 nautical miles
Nominal flight path angle—zero
Orbital inclination—5 ± 1-degree retrograde
Nominal velocity—25,001.82 feet/second
Orbital nodal period—93.1815 minutes ± 0.8 second
Launch direction—southward

2. Preliminary Adjustments (n = 0.5 to n = 19)

As in orbital plan number 1 (Section 4.10.6.2.2).

3. Orbit Adjust 15 ≤ n ≤ 20

As in orbital plane number 1 (Section 4.10.6.2.2).

4. Photographic Operation n = 20.5 to n = 158.5

The photographic coverage of this orbital plan is its distinctive feature as shown in Figure 4-55. The first equatorial swath occurs at n = 20.5. At n = 36.5, the swath lies about half way between n = 20.5 and n = 21.5. Swath 50.5 is the last swath laid down before sidelapping begins. Swath 51.5 is laid down alongside 20.5, 31 orbits or 2 days later. The first closure is of orbit 128.5 on 20.5, n = 129.5 on 21.5 until n = 158.5 makes final closure on n = 50.5. We have, in effect, carved up the equator into 31 pieces and laid down adjacent swaths in each piece every 31 revolutions. It is noted that the pieces are alternately 4 and 5 swath-widths wide.

Since complete photographic coverage is obtained by n = 159, the next sequence of operations can begin.

5. Final Camera Calibration n = 169

As in orbital plan number 1 (Section 4.10.6.2.2).

6. Recovery Operations n = 171 or 172

Photographic coverage is complete with n = 158.5. It is necessary to wait until n = 171 before initiating recovery. Some ground traces in the general area of the Hawaiian SCF station are shown in Figure 4-56. Recovery can be initiated on one of several orbits near local noon.

4.10.6.4.3 Technical Data

1. Camera Duty Cycle

The trajectory was sampled every 5 minutes on the first and fifth days to determine whether the camera was over land or sea and whether illumination was adequate for photography. The results are listed in Table 4-17.

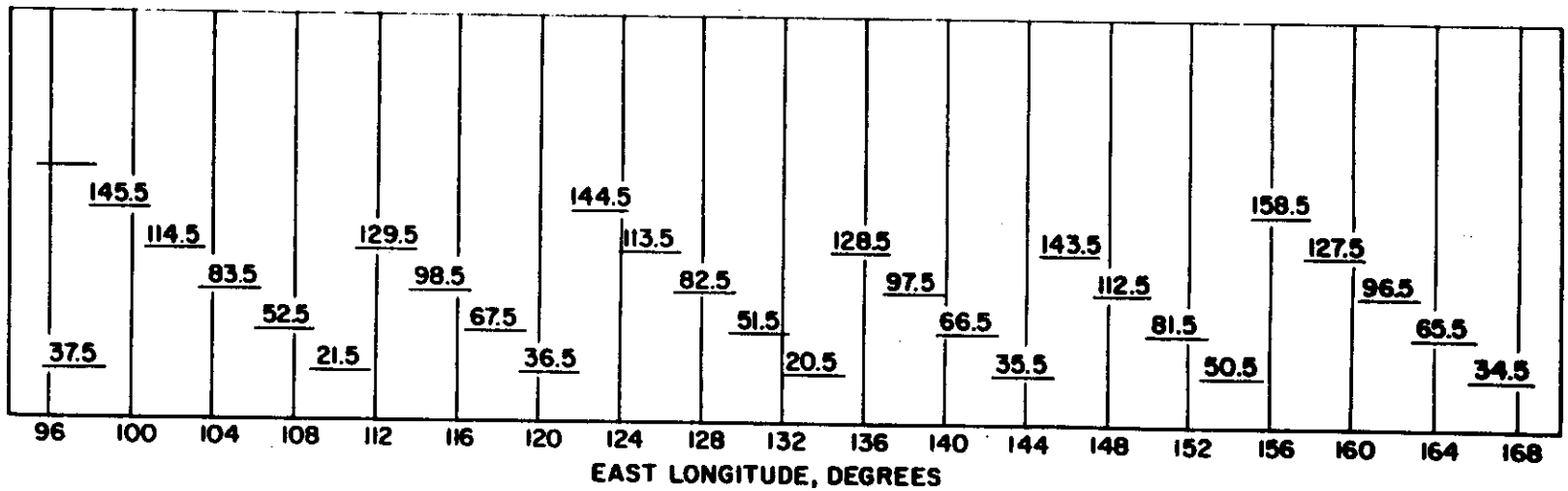

Fig. 4-55 — Equatorial photographic coverage for orbit plan number 3 starting at n = 20.5

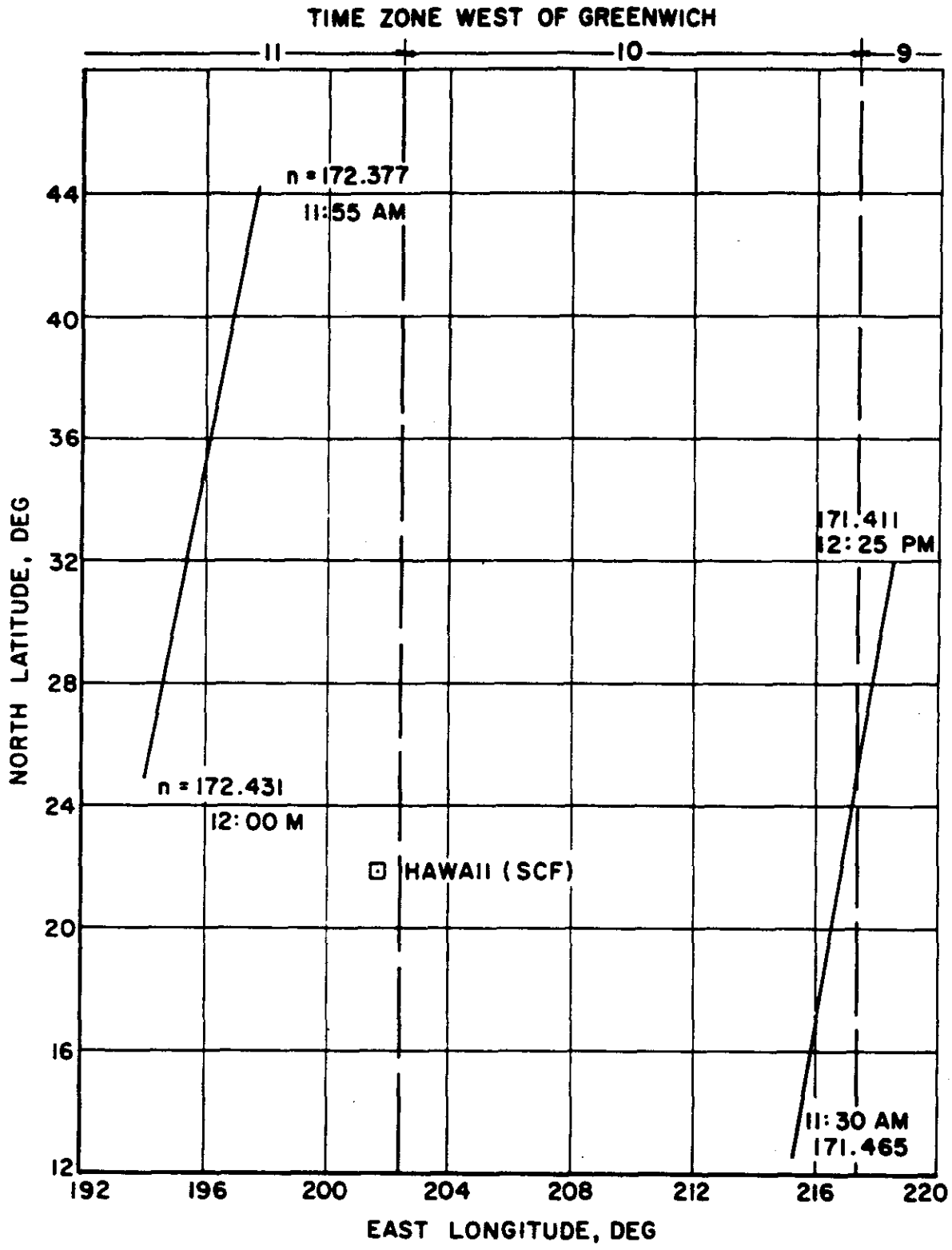

Fig. 4-56 — Ground traces of orbits suitable for recovery operations on June 29, 1968

Table 4-17 — Camera Duty Cycle, Statistical Analysis, Orbit Plan Number 3

	First Day		Fifth Day	
	Times	Percent	Times	Percent
In dark	175	60.7	172	59.7
Over land	36	12.5	34	11.8
Over sea	77	26.8	82	28.5
	288	100.0	288	100.0

The camera duty cycle is less than the 13 percent found for the same orbital inclination in orbit plan number 1.

2. Frequency of Acquisition by Satellite Control Facility

All stations of the Satellite Control Facility acquire the satellite as shown in Table 4-18. The average frequency of acquisition is 27 to 28 times per day in constrast to 22 to 23 times per day for orbit plan number 1. The difference is probably the result of higher altitudes in the present case.

3. Frequency of Acquisition by TRANSIT Network

The frequency of acquisition by the TRANSIT network is shown in Table 4-19. The average number of acquisitions per day is 59 to 60 contrasted with an average of 47 to 48 for orbit plan number 1 and 39 to 40 for orbit plan number 2.

4. Distribution of Dead Time of Satellite Control Facility for Two Separate Days

Figure 4-57 shows this frequency distribution for the second and fifth days. By comparison, the dead time for orbit plan number 3 exceeds 2 hours, only 3 to 4 percent of the time in contrast to 9 percent for orbit plan number 1. The maximum dead times are 262 and 180 minutes on the second and fifth days, respectively.

5. Distribution of Dead Time for TRANSIT Network on Two Separate Days

Figure 4-58 shows this distribution for the second and fifth days. The dead time exceeds 1 hour, once on the fifth day and not at all on the first day. These results are about the same as for orbit plan number 1. The maximum dead times are 55 and 86 minutes for the second and fifth days, respectively.

6. Equatorial Photographic Coverage for Orbit Plan Number 3, Starting at n = 20.5

(See Figure 4-55.)

7. Ground Traces of Orbits Suitable for Recovery

(See Figure 4-56.)

8. Trajectory Program

A complete trajectory program is available for oribt plan number 3 with prinouts every 5 minutes.

9. Sighting Run

A sighting run corresponding to Item (8) above is available for the SCF and TRANSIT networks.

Table 4-18 — Frequency of Acquisition by Satellite Control Facility, Orbit Plan Number 3

Day / Station	RA	RB	RC	RD	RE	RF	RG	Total
June								
18	1	0	2	0	2	0	1	6
19	2	2	4	3	12	2	2	27
20	2	3	4	3	10	2	2	26
21	2	3	4	4	12	2	2	29
22	3	2	4	2	10	4	3	28
23	3	3	3	4	12	2	2	29
24	3	2	4	2	10	2	2	25
25	2	4	4	4	12	2	3	31
26	2	2	5	2	10	2	2	25
27	2	3	4	3	10	2	2	26
28	2	2	5	3	12	2	2	28
29	2	3	4	2	10	2	2	25
30	3	3	5	4	12	2	2	31
Total	29	32	52	36	134	26	27	336

Table 4-19 — Frequency of Acquisition by TRANSIT Network, Orbit Plan Number 3

Day	Station	XA	XB	XC	XD	XE	XF	XG	XH	XI	XJ	XK	XL	XM	XN	XO	XP	Total
June																		
18		0	0	1	0	1	0	0	0	2	1	2	1	1	3	0	0	12
19		3	3	4	2	2	2	2	3	5	4	12	3	2	11	2	2	62
20		3	3	3	3	3	3	3	3	4	2	10	2	2	12	2	3	61
21		3	2	4	2	3	2	2	3	4	2	12	2	2	11	2	2	58
22		2	3	2	4	3	3	3	3	4	2	10	2	3	11	2	2	59
23		4	2	5	2	2	2	3	2	6	2	12	2	2	11	3	2	62
24		2	3	2	3	2	2	2	3	5	2	10	2	2	11	2	2	55
25		4	2	5	2	2	2	3	2	4	2	12	3	3	11	3	2	62
26		2	3	3	2	2	2	2	3	6	2	10	3	2	12	2	3	59
27		3	3	5	2	2	2	4	3	4	2	10	3	2	11	2	2	60
28		3	3	3	2	2	2	2	3	6	4	12	3	2	11	2	2	62
29		3	3	3	3	3	4	3	3	4	2	10	2	2	11	2	3	61
30		3	2	4	2	3	2	2	3	4	2	12	2	2	11	2	2	58
Total		35	32	44	29	30	28	31	34	58	29	134	30	27	137	26	27	731

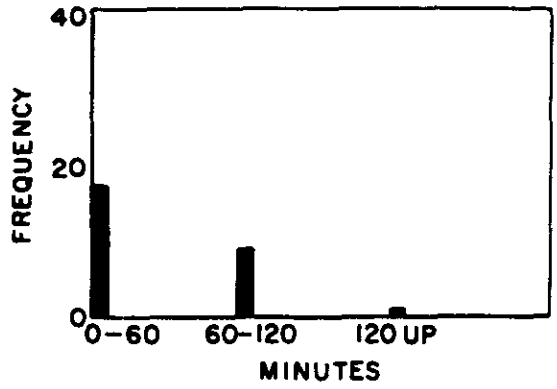

	NO. OF POINTS	%
0-60	17	63
60-120	9	33
120 UP	1	4
	27	100%

(a) SECOND DAY

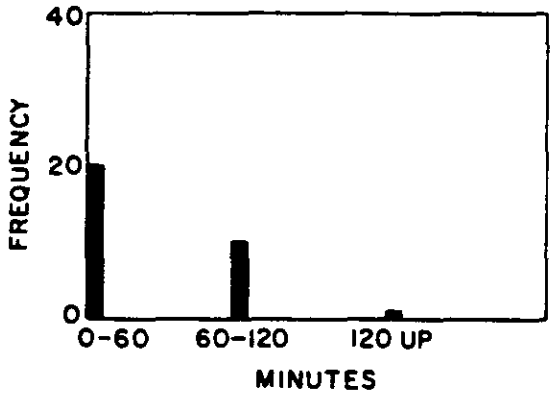

0-60	20	65
60-120	10	32
120 UP	1	3
	31	100%

(b) FIFTH DAY

Fig. 4-57 — Frequency distribution of "dead time" of Satellite Control Facility for two separate days, orbit plan number 3

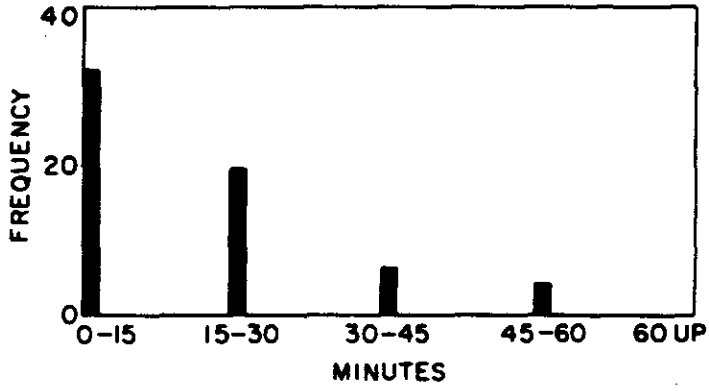

	NO. OF POINTS	%
0-15	32	52
15-30	19	31
30-45	6	10
45-60	4	7
60 UP	0	0
	61	100%

(a) SECOND DAY

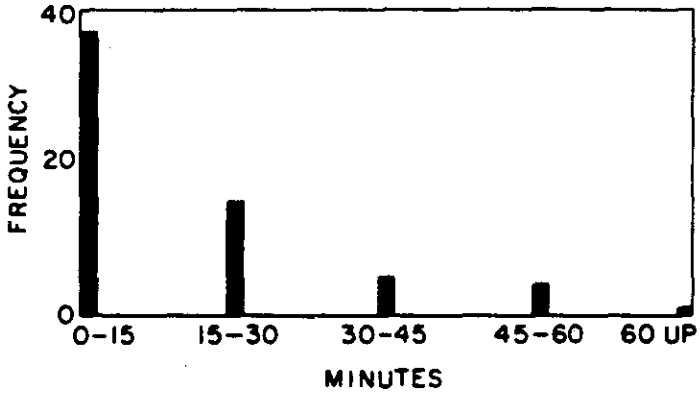

0-15	37	60
15-30	15	24
30-45	5	8
45-60	4	6
60 UP	1	2
	62	100%

(b) FIFTH DAY

Fig. 4-58 — Frequency distribution of "dead time" of the TRANSIT network for two separate days, orbit plan number 3

10. Film Weight

Using the following inputs,

N = 138 orbits

h = 234 nautical miles

d = 0.125

it is found that

frames/orbit = 22.8

film weight = 100 pounds

4.10.7 Concluding Remarks

4.10.7.1 Specific Use of Two Satellites

As a result of the study of orbit plans to date, it can be concluded that at least two of the five projected satellites should be launched into nearly polar orbits in a southerly direction, one about a month before the summer and one about a month before the winter solstice because (1) general earth coverage is desired, and only near the solstices is there sufficient illumination to obtain photographic coverage near the poles, and (2) this launch date will permit a second launch into the same orbit within a 2-month period in case of failure. Orbit plan number 1 describes the plan for the summer solstice.

4.10.7.2 Use of Remaining Satellites

The remaining satellites will probably be utilized using inclined orbits for photographic coverage or geodynamic parameter determination. Orbit plan number 2 describes a well-inclined oribt. It appears that if precise determination of the geodynamic parameters is required, a total of five satellites will be insufficient for the purpose. This statement follows from the fact that removing correlation among the geodynamic parameters may require operation near the several pertinent resonances as well as varying inclinations.

4.10.7.3 Factors Influencing Altitude and Orbital Inclination

An altitude of 300 miles is better than a lower altitude from the standpoints of drag uncertainty, film weight, and interlace. Since however, such an altitude is probably precluded because of camera considerations, operation will be in the 150 to 190-nautical mile altitude range. At 150 to 190-nautical mile altitudes, uncertainties in orbital period after orbit adjust, and orbit period change due to drag do not permit interlace. Accordingly, adjacent ground traces one day apart will be used. This means operating close to the m = 16 resonance altitude with about 100 miles movement of the ground trace per 16 orbits. It is better to operate above the resonance point than below to obtain the benefits of the slightly higher altitude and to provide westward movement of trace against the eastward movement of clouds associated with storms. For inclined orbits, retrograde launch is best because of higher operating altitudes, reduced cloud cover, and launch azimuth limitations.

4.10.7.4 Calibration of Camera and Optical Axes Orientation

The camera should be calibrated against a star background to make sure that thermal or other effects do not cause optical axis misalignments and changes in the metric. This should be done before and after the photographic part of the mission when just entering and just leaving the daylight. About 15 to 20 orbits must elapse before the initial calibration to achieve thermal equilibrium.

4.10.7.5 Probable Effect of Solar Fluxes

Surface solar activity and solar flares can fog the film and introduce transient heating effects into the earth's atmosphere, affecting the air density and the uncertainty in the prediction of air-drag effects. Fogging effects are minor for most solar events assuming nominal ($\sim 5 g/cm^2$) shielding of the film cassettes, but extreme solar flares may cause serious fogging. Prediction techniques are crude but indicate that appreciable reduction (a factor of about five) in the probability of encountering a major solar event during a mission can be obtained for prediction periods of 1 to 2 months at a cost of reducing available launching time by about 50 percent.

4.10.7.6 Orbit Plan Number 1

Three complete orbit plans have been analyzed. Orbit plan number 1 uses a nearly polar orbit (5-degree-retrograde) with launch at 160 nautical miles. Orbit plan number 2 uses retrograde launch at 184 nautical miles with an orbital inclination of 115 degrees. Orbit plan number 3 uses the same orbital inclination as orbit plan number 1 but with launch at 234 nautical miles. Based on an analysis of orbit plan number 1, the following data are presented.

Linear coverage per revolution was calculated for a noon polar orbit at the winter solstice. The illumination will be inadequate for photography 64 percent of the time. The camera will be over water about 70 percent of the remaining time. This leaves about 10 to 11 percent of the total time available for photography. The linear coverage is thus about 2200 nautical miles per orbit.

For the actual mission, a polar orbit at approximately 10 a.m. will probably be superior because of better photographic conditions near the latitude of the sun, and because of lower cloud cover in the tropics.

The TRANSIT network will acquire the satellite an average of 2 to 3 times per orbit although dead times of 169 minutes were found. The Satellite Control Facility will acquire the satellite about 1 time per orbit although dead times as long as 246 minutes were found. The frequency of acquisitions follows the theoretical variation with latitude for both networks.

The decrease in satellite period from the first to the fifthteenth day near 160-mile altitude is enough to increase the overlap from the beginning to the end of the mission by about 30 miles. This effect results in a film weight penalty of about 10 percent.

4.10.7.7 Orbit Plan Number 2

The second orbit was chosen at 115-degree inclination to provide greater redundancy of coverage in the higher latitudes up to 65 degrees. It also will provide data from a substantially inclined orbit to assess geodynamic parameters and improve east-west photogrammetric and orbit distance ties. In contrast with orbit plan number 1, coverage is achieved in 158 revolutions rather than 254 revolutions. The camera duty cycle also appears to be defintiely greater. Because the

inclination of the orbit does not permit acquisition by TRANSIT or SCF stations at extreme latitudes nearly every revolution, the maximum dead times for orbit plan number 2 are substantially greater than those for orbit plan number 1 for the SCF network, but are not greatly different for the TRANSIT network as Table 4-20 shows.

4.10.7.8 Orbit Plan Number 3

Calculations have been made to establish a new type of orbit designed to operate in the 225-nautical mile altitude range. The equator is broken up into 31 sectors and the swaths are laid down side by side without interlace. Adjacent swaths are, however, laid down two days apart rather than one day apart. The calculations show very regular coverage and very small effects of drag on overlap for a 5-degree retrograde orbit at 234 nautical miles launch altitude. Complete coverage is obtained in 138 revolutions compared with 254 revolutions for orbit plan number 1 and 158 revolutions for orbit plan number 2.

4.10.7.9 Orbit "Tuning"

As a result of detailed study of three orbital plans, it appears that small changes in orbit parameters can sometimes save up to a day of orbit time. These small adjustments come to light only after a detailed study of the orbital plan. For instance, in orbit plan number 1, it was found that closure of the overlap first occurred between ths swaths for n = 60.5 and n = 243.5, but the overlap did not continue past n = 247.5, requiring another day of operation. Some slight adjustment of the initial parameters such as the use of slight eccentricity with apogee over the equator may have solved the problem. Also, the use of 20 orbits for thermal soaking usually places the satellite too far west of Hawaii at the end of photography to effect immediate recovery. Reduction of the thermal soaking time to about 16 orbits could also save a day of satellite time.

4.10.7.10 Cloud Cover

Studies indicate that the following conditions are desirable to minimize the effects of cloud cover:

1. Redundant coverage in the higher latitudes, (a condition which is automatically fulfilled by orbital inclinations near 90 degrees)
2. Summer rather than winter flights
3. Westward diurnal motion of the ground swath to prevent observing clouds from a given storm for several days
4. Orbit crossing the equator before noon and higher latitudes around noon

4.10.8 Recommendations for Further Work

Further work in orbit planning can profitably be pursued along the following lines.

1. A type of orbit using side-by-side swaths every 2 days and operating in the 235-mile nautical altitude range was found to give excellent coverage and short periods for complete photographic coverage for near polar orbits. This type of orbit should be studied for inclined orbits with and without small eccentricity for tuning.

2. Orbit plans using interlace should be prepared for their altitude range of application where minimized drag effects permit such operation.

Table 4-20 — Maximum Dead Times, TRANSIT and SCF Networks, Orbit Plan Numbers 1 and 2

	TRANSIT Time, minutes	SCF Time, minutes
Orbit Plan Number 1		
Second day	94	166
Eighth day	137	255
Orbit Plan Number 2		
First day	93	298
Fifth day	85	265

3. Refinements of orbit plan numbers 1 and 2 appear possible to reduce the length of the mission. The use of eccentricity to "tune" orbit number 1 appears to be worthy of investigation. The possibility of reducing the camera soak period from 20 to 16 revolutions could reduce mission time by a day. A better estimate of the number of revolutions required for thermal soaking may, therefore, be worthwhile.

4. All orbits have been started at the equator on the meridian passing through Vandenburg regardless of inclination. It is not clear that such launches from Vandenburg are always feasible. It not, then the longitudes given in the orbit plans must be increased by a constant. This change could change by one the orbit number for which recovery is to be initiated as well as the recovery location. A study of this question should be conducted before final orbital plans are prepared.

5. Much of the orbital planning is capable of being automatically calculated. In particular, the camera duty cycle can be automated if a table of the latitude and longitude limits of the Earth's land area is prepared for use in the TRACE program.

6. At the present time, no account is taken of weather in the determination of camera duty cycle. The camera will be taking pictures of clouds a large percentage of the time. Some means for avoiding this difficulty could lead to substantial reductions in film weight.

7. While some preliminary studies on cloud cover have been made, further study of the problem based on existing data not yet analyzed seems warranted.

8. If certain specific orbital inclinations are required for geodynamic parameter analysis, orbital plans for such inclinations should be prepared. No positive specification for orbit inclinations has yet emerged from the geodynamic study.

9. It is recommended that the decision on when to launch include updated standard cloud cover information available from the Tiros program and other information-gathering media.

10. A systematic study of elliptical orbits seems desirable to see if increased efficiency of photographic coverage can be attained.

4.10.9 References for Section 4.10

1. [redacted]
2. Yionoulis, S. M., A Study of the Resonance Effects Due to the Earth's Potential Functions, Applied Physics Laboratory Report TG-708, Johns Hopkins University.
3. Jensen, J., Townsend, J., Cork, J., and Kraft, D., "Design Guide to Orbital Flight," McGraw-Hill Book Company, Inc., New York, 1962, p. 138.
4. Haurwitz, B. and Austin, J. M., "Climatology," McGraw-Hill Book Company, Inc., New York, 1944.
5. Rossoni, J. P., Sconzo, P., Greenfield, R. J., and Champion, K. S., "Atmosphere Density Determination from Satellite Observations, Celestial Mechanics and Astrodynamics," V. G. Szebhely, Ed., Academic Press, 1964, p. 157.
6. Ragent, B., Particle Radiation Consideration and Shielding Requirements for Space Borne Film, Vidya Technical Note No. 3642-TN-1 (Oct. 16, 1963).
7. Hess, Wilmot N., The Bomb-Produced Radiation Belt, IEEE Transactions on Nuclear Science, NS-10(1):6 (Jan. 1963).
8. Foelche, T., Current Estimates of Radiation Doses in Space, NASA TN D-1267 (July 1962).

9. Wilson, R. K., Shielding Problems for Manned Space Missions, IEEE Transactions on Nuclear Science, NS-10(1):17 (Jan. 1963).
10. Webber, W. R., An Evaluation of the Radiation Hazard Due to Solar Particle Events, The Boeing Company, Seattle, Washington, Report No. D2-90469, (Dec. 1963).
11. McDonald, F. B., Solar Proton Manual, NASA TR R-169 (Sept, 1963).
12. Anderle, R. J., Computational Methods Employed in Deriving Geodetic Results from Doppler Observations of Artificial Earth Satellites, Naval Weapons Laboratory, Dahlgren, Va., NWL Report 1977 (Apr. 1965).

4.11 CONCLUSIONS AND RECOMMENDATIONS

This study has been conducted to investigate the feasibility of achieving the orbital positioning accuracies required for the GOPSS concept. Although limitations in the available computational programs and real observational data restricted some of the analyses, it can be concluded that the goals are realistic and that present day technology is adequate to fulfill the required specifications. The principal existing difficulties involve particularly the handling of physical models and the accurate determination of the parameters characterizing these models from the data to be derived from this program. The techniques for resolving these difficulties are clear, involving primarily proper data analysis procedures, the collection of sufficient, accurate, appropriate data from a variety of orbital inclinations, and the proper utilization of auxiliary on-board sensors such as accelerometers.

It is concluded that the GOPSS concept is valid for the determination of landmark location and geodynamic parameters to high accuracy based only upon information gathered by on-board sensors (Section 4.9.1). However, substantial difficulties which exist due to ill-conditioning of data caused by sun angles, cloud cover, and the orbital distribution of geodetically controlled areas of the world can be mitigated by the useful application of supplemental sensors and minimal supplementary data. The dependency on other sensing systems, previous results, or measurements involves primarily the desirability of using the TRANSIT tracking network, the need for utilizing previous determinations for a minimum number of geodynamic parameters, and the need for observing geodetically controlled areas of the world.

A very appreciable strengthening of the system and reduction of difficulties is effected by the incorporation of the TRANSIT tracking network to aid especially in orbit determination (Section 4.9.1). Because of the limited number and duration of missions, it will be necessary to use fixed values for certain geodynamic parameters, especially, for example, zonal harmonics, obtained from other programs, or to incorporate long duration observational data from higher altitude satellites (Section 4.2.2.2.3).

It will be necessary to obtain as much photogrammetric information as possible over geodetically controlled areas of the world. In this regard, the incorporation of the tightened primary geodetic controls which may result from the PAGEOS program would prove useful, but not essential. It is expected that the GOPSS will complement PAGEOS data by reducing the uncertainties in datum positions relative to the center of the earth and each other, and provide a sufficiently dense geodetic control network for locating cultural targets and compiling large scale maps.

Discussions of the particular conclusions and recommendations relating to the objectives outlined in Section 4.2 follow.

4.11.1 Satellite Positioning

With a reasonable geographical distribution of observational data of realistic quality and density, statistical considerations indicate that the satellite positioning accuracy required for precise landmark location should be easily attained, assuming that atmospheric drag effects and uncertainties will be minimized by the use of accelerometers and proper analytical procedures, and that the gravitational potential is adequately treated. The analysis was conducted for altitudes of approximately 160 and 225 nautical miles and indicated that, for both of these altitudes, satellite positioning requirements could be satisfied (Sections 4.9.1 through 4.9.4).

It has been found that the principal result of integrating the photogrammetric data with data derived from the TRANSIT observational network is to appreciably reduce cross-track uncertainties in satellite position. The use of photogrammetric data over strongly geodetically controlled areas, together with auxiliary sensor data, is therefore recommended.

4.11.2 Tests of Calculational Techniques and Adequacy of Physical Models Using 6-Hour Prediction Criteria

There will be no orbital prediction requirements for long period prediction since the density of observations will be sufficient to preclude such a necessity. Simulation of such predictions is, however, useful in evaluating the adequacy of the calculational techniques and physical models.

Statistical analyses indicate that, although the uncertainties in satellite position are larger and growing during a 6-hour period of no observational data than during a data-taking period, the calculational techniques will certainly be adequate to meet the positioning requirements. Air-drag uncertainties again must be minimized, and the gravitational potential must be well determined (Sections 4.9.1 through 4.9.4).

4.11.3 Evaluation of Geodynamic Parameters

The data collected in this program will make it possible to obtain much better values for many critical parameters than previously obtained. For example, improved values of many of the coefficients in the gravitational potential expansion will be obtained, as will much improved formulations and evaluations of air-drag models. In particular, high degree tesseral harmonics and resonance terms peculiar to low altitude satellites should be best evaluated from the observational data of the GOPSS. An analysis of the sensitivity of the determination of these higher tesseral harmonics to orbital inclination, as suggested by Kaula, should be performed to optimize the specified orbital inclinations. Zonal harmonics and low degree tesseral harmonics should be taken either from the results of other programs, or observational data from other satellites capable of furnishing such data should be incorporated into the data reduction scheme. For example, it may be possible to use data from the Syn-Com satellite to better define $J_{2,2}$ and $J_{3,3}$.

A variety of orbital inclinations and high accuracies (retaining perhaps up to 30 or more digits) in the numerical processing will remove the high degree of correlation among various model coefficients, especially among those gravity terms which differ in degree by an even number, and among selected gravity coefficients and air-drag parameters. In addition, the proposed tracking network will overcome the difficulties arising from poor geographic distributions of data or poor quality or density of data, all of which add to ill-conditioning of the problem. It is recommended that numerical analyses be performed to optimize the determination of physical model parameters, and that well distributed tracking facilities (especially TRANSIT) be used, even, if necessary, to the extent of activating sites specifically for this program.

Ephemeris differencing techniques have indicated the need for including tesseral harmonics of degrees beyond the seventh as well as appropriate resonance terms. It is recommended that, at a minimum, eighth degree terms be included in the analyses, and, preferably, capability for handling much larger gravitational models (out to perhaps $J_{12,\ 12}$) as well as ten or more resonance terms be provided (see Section 4.9.5.).

The inclusion of on-board accelerometers to measure non-gravitational accelerations is recommended to aid in improving and refining the descriptions of atmospheric densities as functions of altitude, latitude, time of day, year, and solar and geomagnetic activity, as well as to aid in removing possible uncertainties in ballistic coefficients. In addition, it is recommended that the satellite mission not be flown during periods of predicted solar activity (as forecast by sunspot development and growth rates) and that the satellite orbit be as high as is consistent with other requirements (see Section 4.9.4).

It is also recommended that provision be made for the most sophisticated available air-drag models in the data analysis scheme, and that, in addition, a number of adjustable parameters be provided. Correlation of solar activity and geomagnetic indices is essential. Minimization of "residuals" for computed air-drag accelerations when compared with accelerometer readings will lead to better evaluations of air-drag model coefficients and to better models. One suggested model adjustment technique, for example, would use observation of orbital decay over a long period (approximately 15 days) to deduce low frequency drag effects and the data from accelerometers to specify diurnal or short term effects such as geomagnetic phenomena.

4.11.4 Datum Ties and Station Locations

Orbital analyses indicate that utilizing a partially integrated photogrammetric and TRANSIT observational network will define the orbit well enough that the accuracies required for the location of datums and major landmarks will be easily attained, subject to the comments of Section 4.11.1 (see Section 4.9.7). The photogrammetric input considered in this analysis consisted of data taken over geodetically well controlled areas.

It is obvious that the fully integrated analysis of all data—photogrammetric resection, Doppler, radar, etc.—simultaneously, including the constraints introduced, for example, by photogrammetric relative intersection data, will strengthen the landmark location capability as well as the satellite orbital position determination. It has been found in this analysis, however, because of the strength of the TRANSIT system, that, to a large extent, the orbital analysis may be considered as independent of the complete photogrammetric analysis, and as such, the orbit may be used with minor loss of accuracy as a fixed constraint on the photogrammetry. This is essentially the "long arc" concept in which the orbit is determined for all of the available observational data involving many passes. Any orbital position between period of observational data is determined by interpolation. The "short arc" concept, by contrast, involves extrapolation from one pass over a region of observation.

Within the limitations of the data handling capacity of the data reduction program, it is also desirable to utilize the results of measurements made on high altitude satellites such as Midas in order to reduce the uncertainties in tracking station locations. The principle uncertainties in physical models involve the high degree terms in the gravitational potential expansion and air-effects. At high altitudes, satellites are only weakly influenced by these terms so that it should be possible to obtain better tracking station locations using tracking data for these satellites in the final data adjustment.

4.11.5 Input Data Requirements

It has been determined that an observational data network consisting of a geographically well distributed set of TRANSIT stations and photogrammetric sighting over geodetically well controlled areas will be sufficient to establish the orbit to within the desired accuracies (see Sections 4.9.1, 4.9.2, and 4.9.3). The proposed seven-station SGLS radar network will serve as a substitute for seven of the TRANSIT stations and will, in addition, provide data for initial orbit fitting and orbit adjust or calibration maneuvers. The principal utility of the photogrammetric observations for orbit determination is in reducing the uncertainties in satellite cross-track position. The typical quoted accuracies and density of data acquisition of TRANSIT and the specified accuracies of the photogrammetry described in Volume 3 will suffice for the purposes here. It is proposed that a minimum of 14 TRANSIT stations be used (seven SGLS stations may be substituted for TRANSIT stations) of which seven are well distributed in the southern hemisphere and seven in the northern. At least one in each hemisphere should be located at very high latitudes (e.g., Thule and McMurdo). The TRANSIT stations should be located, when possible, near regions of strong geodetic control so as to minimize station location biases. Thus, for example. TRANSIT data could be used to minimize biases in the photogrammetrically derived points, and photogrammetrically derived data could be used to reduce biases in the TRANSIT station locations. Although multiple long-arc data from a single sensor type may provide sufficient data for removing biases in that data, by using a multiplicity of data types and redundant data, biases in the data of each of the individual data sensors may be better determined and minimized. Use of a multiplicity of data types also adds greater confidence in establishing landmark locations.

Altimeter data serves a minor function in orbit determination and is most useful in providing data on the undulation of the geoid in ocean areas, and in providing a constraint on the photogrammetry over land areas (see Volume 3, "Concluding Analysis"). If these latter two functions are not paramount, it is possible to dispense with the altimeter with minor consequences as far as orbit determination is concerned.

4.11.6 Physical Models and Computational Techniques

Differences in the orbital ephemerides obtained between various gravity models indicate the need for elaborate models. For spherical harmonic expansions of the gravitational potential, harmonics out through a minimum 8th order and preferably up to 10th or 12th order are necessary, plus selected resonance coefficients as determined from an analysis for the particular orbit under consideration (Sections 4.9.5 and 4.9.6).

It is recommended that equations for the computational program be formulated to include provision for both the spherical harmonic expansion for the earth's potential, and the "mass point" approach being formulated at present in order to take advantage of this latter technique if it proves tractable (Section 4.3).

Uncertainties in air drag models are sufficient to preclude fixing the models completely, especially since the tracking and accelerometer data will be extremely valuable as aids in establishing these models. It is recommended that the most sophisticated models now available be included in the data reduction scheme, but that allowance be made for sufficient adjustable parameters to take up the uncertainties in any given calculation. This portion of the program should be capable of being readily modified as new information becomes available. In addition, provision should be made for incorporating accelerometer data into the air drag model, either directly or to adjust the parameters in the air drag model in a least-squares procedure along

with the overall least-squares adjustment (including solving for biases) in the final computational scheme.

It is recommended that a numerical analysis be performed to investigate the relative improvement in landmark location and orbital position determination to be derived from (1) a complete integration of the orbital analyses and photogrammetric data in the data reduction program involving all of the relative intersection and resection data as well as all of the auxiliary sensor observational data, (2) a partial integration involving auxiliary sensor observational data photogrammetric resection data over geodetically well controlled areas, and selected relative intersection data, the so-called Q points, or (3) completely independent orbit determination from auxiliary sensor data and photogrammetric resection data. This orbit is then used as a fixed constraint on photogrammetric landmark determination. Such an investigation will yield valuable information for programming the final data analysis computation and may result in substantial advantages in computation time and cost.

Modern computer developments involving improved speeds and greatly increased memory capacities have reduced the importance of the choice of computational scheme for the orbital analysis; however, a combined analytical-empirical method is suggested for the present. The TRACE programs used in the present investigation are limited by memory capacity and computer speed; however, the proposed data reduction program should take full advantage of modern computer capabilities and should not have such limitations.

The final data reduction should ideally be performed in an integrated procedure utilizing all of the pertinent data in a minimum variance (least-squares) approach. Although this is essentially a long-arc technique, there may be expeditious applications involving analyses of shorter arcs or less complete analyses, as mentioned above. For example, it is possible, using the short-arc approach, to establish relative landmark locations within any one continent very accurately and to adjust the less accurately known intercontinental biases (datum locations) from the long-arc approach.

In addition, it is possible to obtain better first approximations to various geodynamic parameters by using data for varying arc lengths. For example, the separation of various drag parameters from high degree gravity coefficients may be enhanced by considering medium-to-long single arcs for drag determination and multiple-mission, and multiple long arcs for the gravity model parameters.

The long-arc approach involving quick access data should always be used first to attempt to solve for constant errors or biases. Redundant data from multiple data types is of great utility for this purpose. These biases can then be eliminated in the short-arc application. As indicated previously, in applying the short arc to landmark determination, account must be taken of the high degree terms in the gravity potential in the specification of the constraining orbit, since otherwise, large discrepancies may appear.

Time limitations precluded analyses which included pass points (Q data) in the photogrammetric data. However, experience indicates that relative intersection data (Q data) are very effective in constraining the long-arc orbit, especially in geographical regions such as the Sino-Soviet region where there are no observational stations. Where TRANSIT data are available, the utility of photogrammetric relative intersection data is reduced but not eliminated.

4.11.7 Auxiliary Sensors or Other Requirements

Based on the results of this investigation, it is recommended that, in addition to the main camera sensor and two stellar camera sensors, the following auxiliary apparatus be included on board the vehicle.

1. Stable TRANSIT-type oscillator and transmitter.

2. Stable clock and timing device, accurate to at least 1 millisecond and preferably 0.1 millisecond over the mission period. The timing signal may be derived from the standard TRANSIT oscillator packages.

3. Accelerometers. For the first mission, three-axis accelerometers should be used as close to the center of mass as possible. Dual, overlapping range, in-track accelerometers are desirable. Data received may indicate that, for later missions, only a single accelerometer, the in-track accelerometer, is necessary. Auxiliary data recording must be obtained from several standard outputs from Agena guidance and attitude control units aboard the vehicle.

4. Altimeter. This apparatus, while not essential for orbital analysis, will be useful in determining the undulations of the geoid and for constraining the photogrammetry.

The use of other auxiliary equipment or other techniques involving, for example, flashing lights, [redacted] transponders, range/range rate transponders, laser corner reflectors, and illuminated targets for night photography over controlled areas, have been considered and discarded primarily on the basis of lack of availability of observational facilities during the proposed mission periods, paucity or poor distribution of observational stations, or because the techniques have not been developed sufficiently to ensure reliability for these missions. Furthermore, the added complication of incorporating these systems does not lend sufficient additional strength to justify their inclusion.

4.11.8 Orbit Planning

Detailed conclusions and recommendations on orbit planning have been given in Section 4.10.7. These conclusions are summarized here.

1. It is recommended that all orbits be near circular except for minor eccentricity "tuning" needed to adjust periods for complete overlap and photographic coverage (apogee over equator over the maximum of the atmospheric bulge).

2. At least two orbits should be in slightly retrograde near-polar orbits, launched near the summer and winter solstices.

3. The remaining satellite orbits should be distributed among a variety of retrograde inclinations extending from the largest inclinations of perhaps 145 degrees (considering the allowable sacrifice in photographic coverage at the higher latitudes) to near-polar. These inclined orbits are necessary to aid in determining geodynamic parameters and also in providing stronger east-west ties to landmarks and datums. In order to determine gravity coefficients, J_{nm}, having high values of nm, low inclination orbits should be used and vice versa.

4. The highest altitudes consistent with camera resolution capabilities are essential.

5. Both cloud cover forecasts and solar activity forecasts should be considered in determining exact launch dates. Cloud cover considerations indicate that multiple missions will be required to obtain a high probability of seeing many landmarks. Solar activity considerations indicate the need for nominal shielding (5 grams square centimeter) of sensitive elements such as film and avoiding periods of high solar activity within a given month.

6. Three detailed typical orbit plans are presented, all with nominally circular orbits—at inclinations of 95 degrees retrograde and 160-nautical mile altitude, 115 degrees retrograde at 184-nautical mile altitude, and at 95 degrees retrograde at 225-nautical mile altitude.

Section F

DATA REDUCTION

4.12 DATA REDUCTION

The purpose of the data reduction section is to show how the output of the various sensors will be employed to calculate and catalog the positions of landmarks. The computation of landmark positions will involve: the determination of the mathematical expression of the orbital positions as functions of time, the interpolation of these functions for the exact locations in space of the required camera stations, and finally, the photogrammetric intersection of desired landmarks. Included in the mathematical expression of the orbit will be certain physical constants, such as the gravitational harmonic coefficients and atmospheric drag parameters. In order to meet the accuracy specifications on the landmark locations, these physical constants must be improved in the orbit adjustment process.

The data reduction program could be treated as two independent calculating schemes. The utilization of radar and Doppler tracking data as well as the onboard accelerometer and radar altimeter to determine the orbit and geodynamic parameters would be the first step. Subsequently, the orbit would be used to position the camera stations from which the landmarks are to be located. However, the treatment of the two data types by independent data reduction schemes could lead to complications because functional relationships exist between the various data types despite the fact that they are independently acquired. Therefore, the data reduction program herein described is designed for the capability of performing a total adjustment of data from all sensors. The generality of this program in no way precludes adjusting the orbit from tracking data alone, but the capability for the more rigorous simultaneous adjustment is present.

The data reduction program description will show how the data from the various sensors employed in the GOPSS supplement one another in determining the orbit and, ultimately, the precise locations of points entered in the landmark catalog. The sensors used in gathering these data have already been described in Volume 2 of this report, except for the accelerometer which is more thoroughly discussed in Volume 4. The corrections that must be applied to these data in order to remove systematic errors are, for the most part, described in existing publications by the agencies presently using these data. The specific details of the processing involved in putting the raw data from each sensor in the form required for the adjustment program will depend on the computer and other data processing hardware to be employed. It suffices to say that these processes, at least in the case of Doppler and photogrammetric observations, are state-of-the-art and the details of the preprocessing of these and all other types of outputs should be worked out in the next phase of the project. Here, all data will be assumed to be in its final form for the data reduction program.

4.12.1 Description of the Data

The Navy's TRANSIT tracking network consists of 14 (as of October 1965) tracking sites well distributed over the surface of the earth. From these stations, Doppler frequency shift measurements are obtained every 4 seconds during the time that the vehicle is above the tracking

station's horizon. From these data, the vehicle's topocentric range rate can be extracted with a standard error of 0.5 foot per second. By the time the GOPSS is ready to be orbited, a substantial improvement in range rate accuracy should be realized and the Air Force SGLS radar network should be operational. The seven stations of this network will be capable of measuring the topocentric range, azimuth, elevation angle, and range rate of the vehicle with standard errors of 60 feet for range, 0.05 degree in both angles, and 0.1 foot per second in range rate. The combined output from these two tracking nets will constitute the primary input to the orbit determination problem.

The onboard accelerometer will be capable of measuring the nongravitational acceleration, i.e., the retarding force due primarily to atmospheric drag, with a precision of 10^{-10} g. These measurements may be obtained at a rate which varies with the magnitude of the force being measured, but in any event, the sampling rate will be at least as great as two readings per minute. These data will provide the means for separating the gravitational perturbations from the perturbations arising from all nongravitational forces.

Measurements of the altitude of the satellite above the surface of the geoid can be accomplished by the operation of the onboard radar altimeter over the ocean surfaces of the earth. This instrument will measure the elevation of the vehicle at a very high sampling rate with a precision of approximately ± 15 meters. These data acquired over the ocean surface will be used in determining the field coefficients, at least through the fifth degree and order. Taken over the land surface, these data will provide additional constraints on the height of the orbiting vehicle in areas where flat terrain of known elevation is available, e.g., large inland bodies of water.

Altimeter data, acquired over the oceans, provide a distance along the geocentric vector between the satellite and the sea level surface. The removal of tidal effects and the influences of the sea state from these measurements determine the distance from the satellite to the geoid.

If this distance is denoted h, and the geocentric distance to the satellite is R, then one may write the condition that

$$R = N + h + r$$

where N is the geoid undulation at the calculable longitude and latitude at which the geocentric satellite vector intersects the reference ellipsoid, at which point the ellipsoidal radius is r.

$$Y_n = a_n P_n + a_{n1} P_n^1 \cos \lambda + \ldots + a_{np} P_n^p \cos p\lambda + \ldots + a_{nn} P_n^p \cos n\lambda$$

$$+ b_{n1} P_n^1 \sin \lambda + \ldots + b_{np} P_n^p \sin p\lambda + \ldots + b_{nn} P_n^n \sin n\lambda$$

according to

$$N_\rho = \frac{\rho}{g} \sum Y_n \cdot \rho^{-(n+2)}$$

where ρ and g are mean values of r and of the gravitational force over the equipotential surface of the earth's field.

Since in the orbit determination, the geocentric vector R is expressed in terms of the same spherical harmonics, there is no reason why the previous condition equation cannot be used to strengthen the determination of the geopotential terms.

The 12-inch metric terrain camera with simultaneous stellar exposures for orientation determination comprises the landmark sensor. The terrain exposures with 67 percent overlap and a sidelap which increases with latitude will provide multiple high resolution exposures of all land areas of the earth. Although many of these photographs will not be usable because of cloud cover, the probability of obtaining at least two photographs of any landmark of interest is quite high. From these data, a photogrammetric intersection can be accomplished to provide the landmark coordinates.

Since the position of the orbiting vehicle is to be expressed as a function of time, the precise correlation of this fundamental variable with each observation regardless of type is imperative. Each tracking station will have its own clock which has been calibrated to the time standard. The onboard clock which will record the time of each exposure will undergo an inflight calibration to determine the magnitude of corrections to be made in order to correct this instrument to the time standard. These corrections will be applied to the recorded exposure times on a postflight basis.

4.12.2 Concept

It has been pointed out that the concept to be employed in this data reduction scheme is that of simultaneously adjusting data from all sensors. This approach may not appear to be justified when the precision of orbital positions obtained from Doppler data alone is considered. These data indicate that the orbit determination can be effected with only range rate data within the position tolerances specified in this program. For this reason the Doppler tracking data is considered to be the prime sensor for orbit determination. The analyses which are reported in this volume, however, did not include simultaneous adjustment of all possible sources of error. These results may therefore be somewhat optimistic since they require that air drag and higher degree gravitational harmonic coefficient uncertainties be almost negligible. These assumptions were based on a sufficiently sensitive and highly reliable accelerometer and a sufficient distribution and density of high quality observations for a variety of inclined orbits. It is therefore desirable to obtain further insurance from a computer program which permits simultaneous adjustment of data from all sensors.

Actual orbit determinations which have been completed to date utilizing Doppler alone have been obtained with orbits of 600-mile or higher perigee points. The accuracy obtained by Doppler tracking will be reduced when the altitude is dropped to the neighborhood of 160 nautical miles. The radius of the circle about a Doppler station in which the satellite can be observed will be reduced to approximately a half, and hence the area within which observations can be made will be only 25 percent as large. Figure 4-2, shown previously in this volume, shows the resultant geographic distribution of observable areas when the reduced orbital altitude is taken into account.

Another factor which takes on increasing importance at this lower altitude is air drag. The present higher altitude Doppler accuracies are obtainable because the orbits are so designed as to make air drag insignificant. The errors introduced by the inability of any presently available model of the atmosphere to correctly describe the perturbations encountered at this low altitude will further degrade the results. An accelerometer is proposed to account for the drag forces, but this instrument has not undergone extensive operational testing and could prove to be a serious disappointment if found to be less than optimum. The observations obtained from the accelerometer, when incorporated in the adjustment should be a valuable tool for separating the drag and gravitational forces, but the residual errors introduced by the difficulty of predicting drag in the increased atmospheric density will remain a serious problem.

One contribution that photogrammetric data can make to the orbit adjustment is the improved geometric distribution of observations. Many points along the orbit are unobservable by the tracking network, because they are not within range of even a future Doppler station. No tracking sites are available, for example, in the Sino-Soviet Bloc. Other portions of the orbit will go unobserved, because of the lack of sufficient Doppler tracking instruments to provide anything near total coverage at this proposed altitude. The unavoidable result will be an increase in the expected value of the random errors of the orbit determination in these unobserved areas and, much worse, the increased probability of an undetectable systematic error affecting the computations of orbital position over the very areas where landmark positioning may be most critical, i.e., the U.S.S.R. and the Chinese mainland.

Inclusion of photogrammetric data in the orbit adjustment will increase the overall geometric strength. While there are numerous geodetic control points in the Sino-Soviet Area, few if any of them in the U.S.S.R. east of the Ural Mountains are available to the United States. Many more in China have been poorly surveyed and are of little use in this program. Therefore, a large area of Eastern Asia will provide no conventional photogrammetric control. However, since the orientation of each exposure is independently determined from the stellar frames and a set of at least seven and at most 15 orbital parameters substituted for the several thousand camera station positions, there are only three parameters to be computed for each landmark, i.e., the coordinates of the landmark itself. If this landmark is imaged on at least two photographs (which it must be), there will be four independent geometric conditions relating the images and object—an x and a y equation from each photograph. Only three equations are needed for an explicit solution for the landmark coordinate, so one degree of freedom is available to enhance the accuracy of the orbit determination. Of course, in practice there will be at least three successive exposures of the landmark and coverage from other passes of the same satellite as well as from other satellites of the same series, each new exposure adding three more equations to the orbit determination.

The effect of adding degrees of freedom to the orbit determination may not be very obvious. The geometric significance of these observations varies with the certainty that can be placed on the estimate of the geocentric coordinates of the ground point. If this point is a part of the proposed PAGEOS net of super control points, the weighting factor applied to this point will be such that the orbit, or several orbits, will be forced to coincide exactly with the computed points in space from which the station was observed. At the other end of the scale, this point may be known only from its relationship to nearby features that can be located on very small scale maps. The observed point is known only to within a few kilometers and its contribution to the adjustment would be to force the several exposure stations from which it was observed (preferably camera stations on two different passes or even from two different satellites) to conform to a fixed relative geometry. In areas where no geodetic control is available, such relative control points will provide an additional constraint in areas where it is needed most.

Since Doppler and acceleromenter data are immediately available, this program is so designed that a preliminary orbit determination can be accomplished long before any photogrammetric data is available. Altimeter data could then be added on a limited scale and its contribution to the total adjustment evaluated. As photogrammetric data becomes available it could also be added and its worth appraised. If it happens that Doppler observations supplemented only by accelerometer measurements are sufficient to solve the problem, there is no need to spend the additional computer time required to include the photogrammetric observations. The only loss then would be the extra programming required to develop the more general simultaneous adjustment. If, on the other hand, the program were not capable of using photogrammetric data and such data

were found to be necessary, a serious delay in the data reduction would result. The cost of programming unnecessary generality and never using it appears to be a good investment in light of the possible consequences of relying too heavily on one or two kinds of data.

4.12.3 Description

There are three basic approaches to the problem of orbit determination: analytical, empirical, and numerical integration. The data reduction program herein described used that portion of each of the basic approaches which best suits the problem to be solved, namely, the simultaneous solution for geodynamic parameters and precise orbital ephemerides. An explicit solution is borrowed from the analysts, inadequacies of the explicit solution are compensated by using the enormous mass of data available to determine empirical corrections, and numerical techniques are used in determining the effects of perturbing forces that do not lend themselves to explicit expression.

While a large computer, both in terms of core storage capacity and word length, is very desirable, this program is not aimed at a particular computer. New developments in computer hardware which may be obtained in the near future could greatly increase the speed with which this program could solve a particular problem, but the magnitude of the problems that can be solved will not be changed materially. This program is based on a computer word size that is compatible with the problem being solved. If a computer with a much larger word size becomes available, double precision may be dropped from many operations where it is not required. Likewise, the indicated use of magnetic tape as an intermediate storage device could be eliminated if a computer with a greatly expanded core storage capacity should become available.

The program performs a rigorous least squares adjustment of observation data from all system sensors—range, range rate, altitude, retarding force, and photogrammetric. The parameters to be adjusted are of five types:

1. Orbital elements
2. Geodynamic parameters
3. Bias parameters
4. Landmark positions
5. Datum shifts

The first two types of parameters fall into the group that are not dependent on a particular station. In this case, the term "station" means any identifiable point on the surface of the earth whose position enters into all observations of or from the station. Hence all tracking stations and all landmarks imaged on the terrain photographs, whether of known position or not, are called by the general term station. All landmark positions are, of course, station-dependent parameters and some, though not all, of the bias parameters are station-dependent. The reason for making this distinction between parameters which are station-dependent and those which are not is that the two types will be handled differently in the formation, solution, and inversion of the system normal equations.

For purposes of illustration, the coefficient matrix of the normal equations of a typical multiple-mission adjustment is illustrated in Figure 4-59. The shaded areas are elements of the matrix which are expected to contain non-zero entries while unshaded blocks are known to contain all zeros. The upper left block contains the entries pertaining to geodynamic parameters:

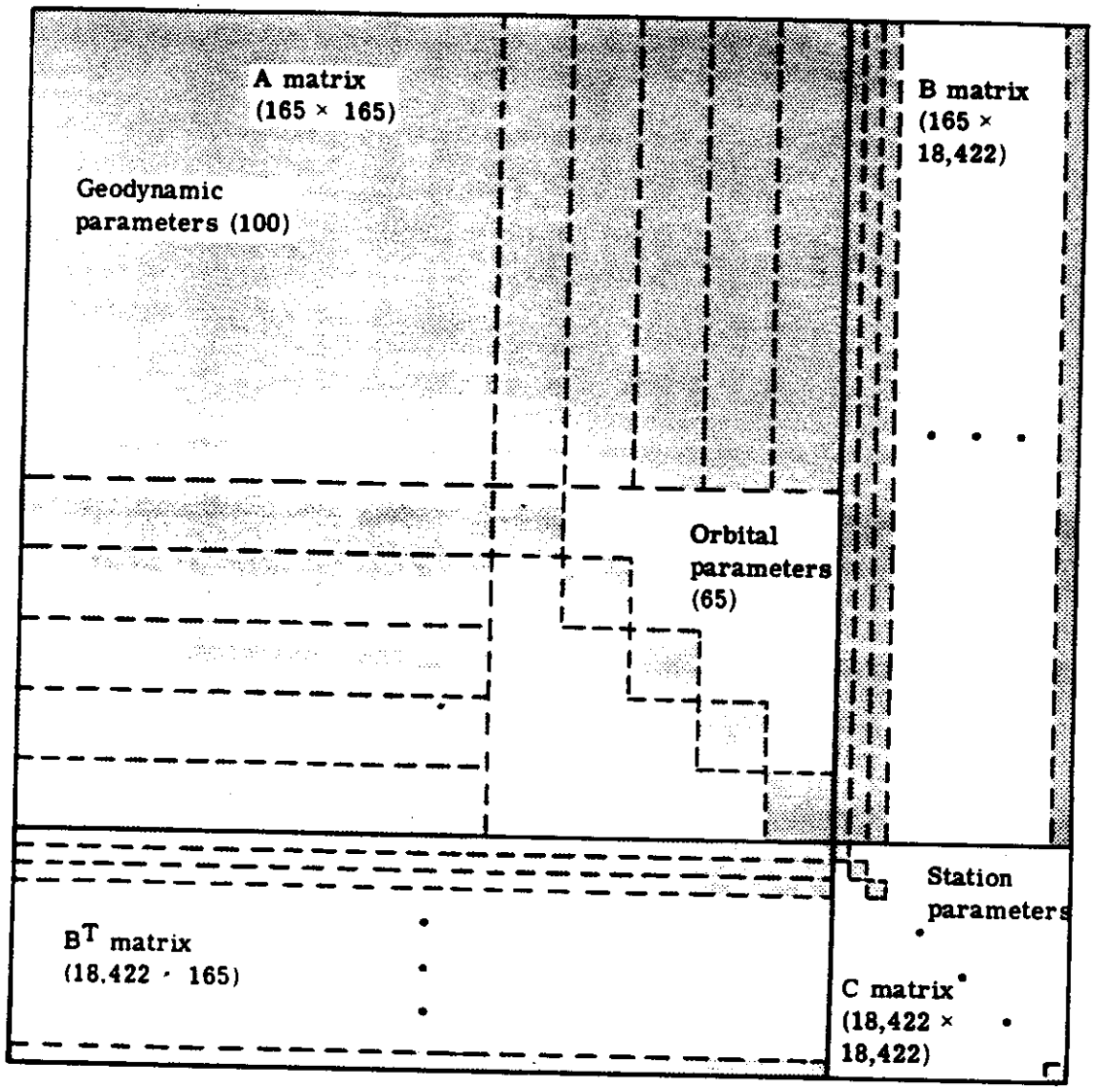

Fig. 4-59 — Coefficient matrix of normal equations

Coefficients of 35 gravitational harmonics	70 parameters
Coefficients of 6 resonant harmonics	12 parameters
18 atmospheric drag parameters	18 parameters
Total geometric parameters	100

This list included non-zonal gravitational harmonics from 2,1 through 8,8. The 2,1 harmonic is included as a check on the adjustment since this harmonic is known to be of insignificant magnitude. The resonance harmonics are limited to six on the assumption that all of the satellites included in this adjustment are at near enough the same altitude to be affected by the same resonant terms.

The next block of matrix elements, continuing down the principal diagonal will contain the orbital and bias parameters associated with each of the five satellite missions. Six orbital elements and seven bias parameters have been assumed for each mission. The orbital parameters are the usual six osculating elements. The bias parameters include three terms for the camera and two each for the acceleromenter and radar altimeter. The number of these bias parameters is based on the use of data that has already been corrected for systematic errors as well as those which can be described mathematically. Hence, the bias parameters serve to correct only residual systematic errors.

The next and last block contains the matrix entries pertaining to:

3 translation parameters for each 10 major geodetic datums	30 parameters
3 coordinate corrections for each of 14 tracking stations	42 parameters
25 bias parameters associated with each of the 14 tracking stations	350 parameters
3 coordinate corrections for each of 6000 landmarks	18,000 parameters

All of these parameters are station-dependent except the datum shifts which are dependent on many stations. The 25 bias parameters, five for each mission observed, associated with each tracking station is again based on the assumption that all data has been corrected for all known biases before entering this program. The assumed number of 6000 landmarks includes all points used in the photogrammetric condition equation whether it is assumed known to a high degree of certainty or essentially unknown. This number allows a landmark every 100 miles over the entire land surface of the earth.

Counting total parameters yields 18,587 of which 165 are nonstation-dependent. As will be shown, the maximum matrix which must be stored in the computer at any time during the formation of the normal equations is this 165 × 165 (of which only the triangular part must be stored since it is symmetric), a 28 × 165 matrix corresponding to the off-diagonal portion associated with both the 28 tracking station parameters (25 bias and 3 coordinate parameters) and the 165 nonstation-dependent parameters, and a 28 × 28 matrix of the tracking station parameters. The maximum matrix which must be inverted by conventional methods is 165 × 165. The formation of the normal equation matrix is based on the assumption that the observation data has been

ordered by station. All observations from/of a particular station are processed before any observations from/of the next station. It is thereby possible to let one area of computer storage be used for the station-dependent parameters of a single station and re-use this area for the parameters of like kind associated with the next station. This procedure is illustrated in the flow chart, Figure 4-60.

A new station record read from the data tape signals the program to form and add the contribution of the previous station's observations to the nonstation-dependent portion of the normal equations. The data from this new station is then processed through the appropriate condition equations until another station record is encountered.

To illustrate this process, let the normal equation coefficient matrix illustrated in Figure 4-59 be partitioned in the following manner. Let the upper left 165 × 165 submatrix be labeled A. A contains the matrix elements pertaining to all parameters that are not station-dependent. Call the submatrix on the lower right C. C will be of order 18,000+, but will be quasi-diagonal, having as its only non-zero elements the set of 3 × 3's (or 28 × 28's in the case of tracking stations) which pertain to the station coordinates down the main diagonal. B then is the 165 × 18,000+ submatrix on the upper right. The system normal equations can now be written symbolically as

$$\begin{bmatrix} A & B \\ B^T & C \end{bmatrix} \begin{bmatrix} \Delta_o \\ \Delta_s \end{bmatrix} = \begin{bmatrix} D_o \\ D_s \end{bmatrix} \tag{4.1}$$

where Δ_o = the vector of corrections to the 165 parameters that are not station dependent

Δ_s = the vector of corrections to the 18,000+ station-dependent parameters

The solution of equation (4.1) can be written

$$\begin{bmatrix} \Delta_o \\ \Delta_s \end{bmatrix} = \begin{bmatrix} L & M \\ M^T & N \end{bmatrix} \begin{bmatrix} D_o \\ D_s \end{bmatrix} \tag{4.2}$$

By standard formulas for inverting a matrix by partitioning, it is found that

$$L = (A - BC^{-1}B^T)^{-1} \tag{4.3}$$

$$M = LBC^{-1} \tag{4.4}$$

$$N = C^{-1} + C^{-1}B^T LBC^{-1} \tag{4.5}$$

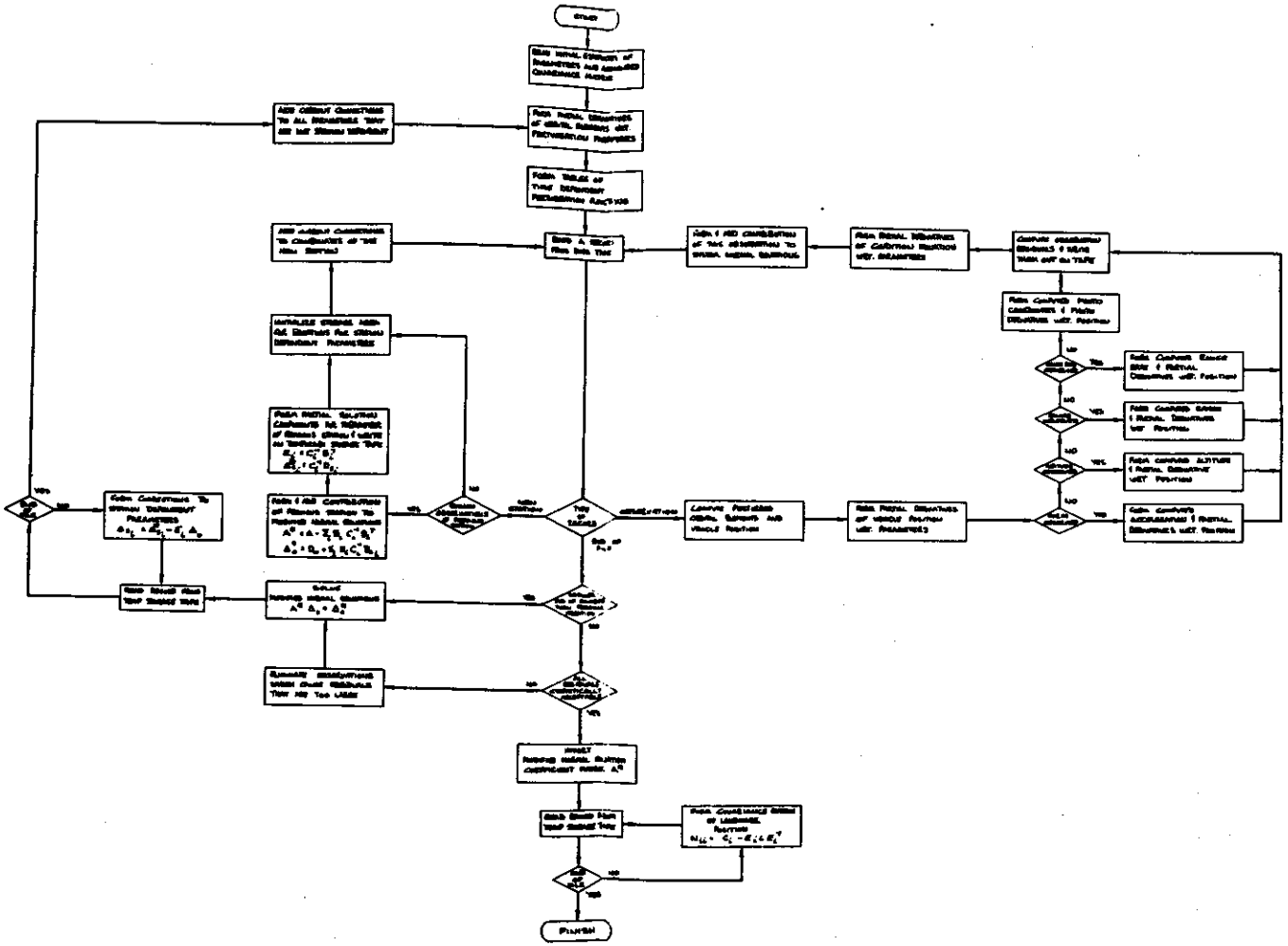

Fig. 4-60 — Data reduction, flow diagram

$$L = (A^*)^{-1} \tag{4.14}$$

should be easily obtained by standard matrix inversion techniques and M can be formed a station at a time from

$$M_i = LB_iC_i^{-1} = LE_i^T \tag{4.15}$$

The matrix N which is the covariance matrix of the station positions can also be formed as 3 × 3 submatrix at a time, but the form of N,

$$N = \begin{bmatrix} C_1 - E_1LE_1^T & -E_1LE_2^T & \cdots & -E_1LE_{6,024}^T \\ -E_2LE_1^T & C_2 - E_2LE_2^T & \cdots & -E_2LE_{6,024}^T \\ \vdots & \vdots & & \vdots \\ -E_{6,024}LE_1^T & -E_{6,024}LE_2^T & \cdots & C_{6,024} - E_{6,024}LE_{6,024}^T \end{bmatrix} \tag{4.16}$$

requires that the temporary storage tape be read and rewound in the computations of each row or column which means reading the tape 6024 times, once for each submatrix of C. This does not appear to be a practical undertaking. Instead, the individual covariance matrices of the station positions and associated bias parameters will be formed and all other off-diagonal terms will be dropped. Hence, in one reading of the temporary storage tape, the covariance matrices of all stations can be formed using

$$N_{ii} = C_i - E_iLE_i^T \tag{4.17}$$

The temporary storage tape can be saved and the covariance between specific stations computed when the need arises.

The adjustment phase of the data reduction program has now been described in some detail while the processing of individual observations has been nearly neglected. It has been mentioned that all observations of or from a particular station must be grouped together on the data tape. These will be preceded by a station record which contains data pertaining to the station itself, and the end of such data can be recognized by the presence of a new station record. Each observation record will contain:

1. The time of the observation
2. The observed data
3. A covariance matrix of the observation
4. Any required auxiliary data

The observing time is used to compute the position of the vehicle which is a function of time. Various computed perturbations are applied to the vehicle position and the partial derivatives of

The parameter corrections are then given by

$$\Delta_O = L(D_O - BC^{-1}D_S) \tag{4.6}$$

$$\Delta_S = C^{-1}D_S + C^{-1}B^T\Delta_O \tag{4.7}$$

Since the inverse of C is obtained by replacing each 3 × 3, or 28 × 28 in the case of tracking stations, by its inverse, formulas (4.3) through (4.6) can be applied a station at a time. Let C be an individual 3 × 3 from the main diagonal of the C submatrix and B the corresponding 165 × 3 from the submatrix B. Then

$$A^* = A - \sum_i B_i C_i^{-1} B_i^T \tag{4.8}$$

$$\Delta_O^* = D_O \sum_i B_i C_i^{-1} D_{Si} \tag{4.9}$$

can be formed by processing data from one station at a time, storing only A^* and Δ_O^* and providing temporary storage for B_i, C_i, and D_{Si}. At the same time it is convenient to form the vector

$$\Delta_{Si}^* = c_i^{-1} D_{Si} \tag{4.10}$$

and the matrix

$$E_i = C_i^{-1} B_i^T \tag{4.11}$$

and to write them out on magnetic tape or some other off-line storage area. Once all data has been processed, the station-independent parameter corrections can be obtained by solving the modified normal equations

$$A^*\Delta_O = \Delta_O^* \tag{4.12}$$

Then the corrections to the station coordinates can be computed a station at a time by bringing back into core the Δ_S^* and E_i and evaluating

$$\Delta_{Si} = \Delta_{Si}^* - E_i\Delta_O \tag{4.13}$$

It should be noted that the flow diagram of the program shows that the system of equations is solved at each iteration, the inversion being performed only once, after the final solution has been completed. The time consumed in solving a system of equations is proportional to the square of the order while the time consumed in inversion is proportional to the cube of the order. For Equation (4.12), which is of order 165, the computer time required to invert A^* is approximately equal to the time required to execute 165 solutions. Therefore, the inversion is only performed in order to obtain the covariance matrix associated with the final parameter values.

vehicle position with respect to orbital parameters, geodynamic parameters, and some of the bias parameters are computed in exactly the same manner irrespective of the type of observation being processed. The partial derivatives of the observation equation with respect to the vehicle position, station position, and remaining bias parameters are then formed according to observation type. The product of these two matrices of partial derivatives is the set of partials of observation equations with respect to parameters. It is this product that is required for the formation of the system normal equations.

To illustrate this process, consider a range observation. Given the time of the observation, the elements of the osculating ellipse are computed:

$$\vec{K} = f(\vec{P}, \vec{G}, t) \tag{4.18}$$

where $\vec{K}$ = a vector of Keplerian elements
$\vec{P}$ = a vector of orbital parameters which include $\vec{K}$ and express the change in $\vec{K}$ as a function of time (t)
$\vec{G}$ = a vector of geodynamic parameters which cause perturbations of the elements.

The vehicle position vector $\vec{V}$ is a function of $\vec{K}$ alone or

$$\vec{V} = g(\vec{K}) \tag{4.19}$$

Knowing these functional relationships it is easy to compute the partial derivatives

$$\frac{\partial \vec{V}}{\partial \vec{P}} = \frac{\partial \vec{V}}{\partial \vec{K}} \frac{\partial \vec{K}}{\partial \vec{P}} \tag{4.20}$$

and

$$\frac{\partial \vec{V}}{\partial \vec{G}} = \frac{\partial \vec{V}}{\partial \vec{K}} \frac{\partial \vec{K}}{\partial \vec{G}} \tag{4.21}$$

It should be noted at this point that the derivative of an n-dimensional vector with respect to an m-dimensional vector is an n × m matrix. This definition is compatible with: (1) the derivative of an n-dimensional vector with respect to a scaler is an n-dimensional vector, and (2) the derivative of a scaler with respect to an n-dimensional vector is a row vector of dimension n.

The condition equation for topocentric range expresses the relationship between the vehicle position $\vec{V}$ and the station position $\vec{S}$.

$$R = h(\vec{V}, \vec{S}) \tag{4.22}$$

The partial derivatives $\partial R/\partial \vec{V}$ and $\partial R/\partial \vec{S}$ can now be computed and the partial derivatives of the range observation with respect to the parameters to be adjusted are:

$$\left[\frac{\partial R}{\partial \vec{G}} \frac{\partial R}{\partial \vec{P}} \frac{\partial R}{\partial \vec{S}}\right] = \frac{\partial R}{\partial \vec{V}} \left[\frac{\partial \vec{V}}{\partial \vec{G}} \frac{\partial \vec{V}}{\partial \vec{P}} - I\right] \tag{4.23}$$

The identity matrix on the right hand side of Equation (4.23) occurs because

$$\frac{\partial R}{\partial \vec{S}} = -\frac{\partial R}{\partial \vec{V}} \tag{4.24}$$

which holds for all of the condition equations which involve the station position.

Given the weight matrix (W_R) which in this case is just the reciprocal of the assumed variance in the range measurement, then the contribution to the system normal equations is formed by

$$\begin{bmatrix} A'_{11} & A'_{12} & B'_1 \\ A'_{21} & A'_{22} & B'_2 \\ B'^{T}_1 & B'^{T}_2 & C' \end{bmatrix} = \begin{bmatrix} \frac{\partial \vec{V}^T}{\partial \vec{G}} \\ \frac{\partial \vec{V}^T}{\partial \vec{P}} \\ -I \end{bmatrix} \frac{\partial R^T}{\partial \vec{V}} W_R \begin{bmatrix} \frac{\partial R}{\partial \vec{V}} & \frac{\partial \vec{V}}{\partial \vec{G}} & \frac{\partial \vec{V}}{\partial \vec{P}} & I \end{bmatrix} \tag{4.25}$$

and

$$\begin{bmatrix} D'_{01} \\ D'_{02} \\ D'_S \end{bmatrix} = \begin{bmatrix} \frac{\partial \vec{V}^T}{\partial \vec{G}} \\ \frac{\partial \vec{V}^T}{\partial \vec{P}} \\ -I \end{bmatrix} \frac{\partial R^T}{\partial \vec{V}} W_R E_R \tag{4.26}$$

where E_R = the discrepancy between the observed and computed topocentric range

It must be remembered that this is only the contribution of a single observation. Similar contributions of many more observations, even from this single station must be added to the above before a set of normal equations like Figure 4-59 is obtained. To emphasize this fact, the quantities on the left in Equations (4.25) and (4.26) have been primed.

Much emphasis has been placed on the capability in this program of adjusting as parameters as many quantities as possible. However, it is necessary to enforce certain values in order to obtain a solution. Among these are the various physical constants such as the radius and mass of the Earth, the universal gravitational constant, the speed of light, etc., which have already been measured numerous times by systems designed specifically for this purpose. To this list should probably be added the coefficients of the zonal harmonics in the Earth's potential field. Good values for these coefficients have already been obtained from observations of a single satellite over a period of several months. Since the principal perturbations due to the zonal harmonics are secular in the case of even degree and very long period periodic in the case of odd degree terms, it seems doubtful that observations covering only 15 days could improve these values.

In summary, the data reduction program herein described is designed to utilize the vast amounts of observation data available to compute the most precise orbital ephemerides, geodynamic parameters, and landmark positions possible. Data from all vehicles in this series and

all observing systems employed will be combined in a rigorous least squares adjustment for the above parameters. A special partitioning is then applied in order to take advantage of the zeros in this matrix so that the formation, the solution, and finally the inversion can be accomplished by present day computers.